Ulm University

Institute of Medical Systems Biology

Prof. Dr. Hans A. Kestler

MODELLING PATHWAY CROSSTALK AND DYNAMICS WITH QUALITATIVE MODELS

Dissertation submitted in partial fulfilment of the requirements for the degree of „Doctor rerum naturalium“ (Dr. rer. nat.) of the International Graduate School in Molecular Medicine Ulm

Silke Daniela Kühlwein
born in Offenbach am Main

Ulm, 2020

1. Current dean of the medical faculty: Prof. Dr. Thomas Wirth

2. Chairman of the Graduate School: Prof. Dr. Bernd Knöll

3. Thesis Advisory Committee:

    - First supervisor: Prof. Dr. Hans A. Kestler

    - Second supervisor: Prof. Dr. Michael Kühl

    - Third supervisor: Prof. Dr. Malte Buchholz

4. External reviewer:

    - Prof. Dr. Dr. Melanie Börries

    - Prof. Dr. Tim Friede

5. Day doctorate awarded: 22.02.2021

Some results gained in this thesis have previously been published in the following publications:

- Schwab, J. D.*, **Kühlwein, S. D.***, Ikonomi Nensi, Kühl, M., Kestler, H. A. (2020). Concepts in Boolean network modeling: What do they all mean? *Computational and Structural Biotechnology Journal*, 18: 571-582.
  doi: 10.1016/j.csbj.2020.03.001

- Siegle, L.*, Schwab, J. D.*, **Kühlwein, S. D.***, Lausser, L., Tümpel, S., Pfister, A. S., Kühl, M., Kestler, H. A. (2018). A Boolean network of the crosstalk between IGF and Wnt signaling in aging satellite cells. *PLOS ONE*, 13(3): e0195126.
  doi: 10.1371/journal.pone.0195126

- Schwab, J. D.*, Siegle, L.*, **Kühlwein, S. D.***, Kühl, M., Kestler, H. A. (2017). Stability of signaling pathways during aging—a Boolean network approach. *MDPI Biology*, 6(4): 46.
  doi: 10.3390/biology6040046

- Groß, A., Kracher, B., Kraus, J. M., **Kühlwein, S. D.**, Pfister, A. S., Wiese, S., Luckert, K., Pötz, O., Joos, T., Van Daele, D., De Raedt, L., Kühl, M., Kestler, H. A. (2019). Representing dynamic biological networks with multi-scale probabilistic models. *Communications Biology*, 2(21).
  doi: 10.1038/s42003-018-0268-3

  ∗ **equally contributed**

Currently in revision/preparation:

- **Kühlwein, S. D.***, Schwab, J. D.*, Tatura, M.*, Kreider, R., Sipos, B., Sperveslage, J., Gress, T. M., Buchholz, M., Kestler, H. A. Comprehensive Boolean network-based modeling of molecular interactions mediating tumor-promoting functions of cofilin-1 in pancreatic cancer.

- **Kühlwein, S. D.***, Ikonomi, I.*, Schwab, J. D.*, Kraus, J. M., Pfister, A. S., Schuler, R., Kühl, M., Kestler, H. A. Implicants: dynamic analysis unravels molecular intervention targets.

  ∗ **equally contributed**

TABLE OF CONTENTS

List of abbreviations VI

1 Introduction 1
- 1.1 Systems biology - the necessity of changing points of view 2
- 1.2 Dynamic modelling 4
  - 1.2.1 Boolean network models 6
- 1.3 Network dynamics 10
- 1.4 Use cases 13
  - 1.4.1 Ageing 13
  - 1.4.2 Cancer 15
- 1.5 Aims of the thesis 18

2 Materials and Methods 19
- 2.1 Boolean network models 19
  - 2.1.1 Simulation of Boolean network models 20
  - 2.1.2 Intervention screening for treatable targets in Boolean network models 21
  - 2.1.3 Robustness analysis within Boolean network models 21
- 2.2 Model setup 22
  - 2.2.1 Literature-based Boolean network models 22
  - 2.2.2 Data-driven Boolean network models 24
- 2.3 Model validation 27
  - 2.3.1 Laboratory experiments 27
  - 2.3.2 Attractor comparison to gene expression data 31
- 2.4 Analyses for dynamic-influencing nodes 32
  - 2.4.1 Heuristic approach 33
  - 2.4.2 Exhaustive approach 33
  - 2.4.3 Collection of Boolean network models 35
  - 2.4.4 Identification of network hubs 36
- 2.5 Statistics and visualisation 37

3 Results 38
- 3.1 Modelling ageing 38
  - 3.1.1 IGF-1/Wnt crosstalk during ageing 38
  - 3.1.2 Discussion – IGF-1/ Wnt crosstalk 53
  - 3.1.3 NF-κB signalling during ageing 55

3.1.4 Discussion – Modelling ageing 60
3.2 Predicting the behaviour of cofilin-1 in pancreatic cancer 64
3.2.1 A Boolean network model of CFL1 in pancreatic cancer 64
3.2.2 Discussion – Cofilin-1 in pancreatic cancer 93
3.3 Dynamic characteristics in biological networks 99
3.3.1 Biologically motivated Boolean network models differ in size 99
3.3.2 Boolean network models of biological pathways show a scale-free topology 102
3.3.3 Removal of redundant nodes accelerates running time 102
3.3.4 Small sets of nodes determine the dynamic behaviour 103
3.3.5 Stable attractors are observable from the implicant sets 104
3.3.6 The majority of implicant nodes is low connected but behaves like hub nodes 106
3.3.7 Lowly connected implicants are suitable for targeted interventions 108
3.3.8 Intervention screening for treatment of colorectal cancer patients 109
3.3.9 Discussion – Dynamic characteristics in biological networks 123

4 General Discussion 126
4.1 Mathematical models for gene regulatory networks and the choice of the right model 126
4.2 Data-driven versus literature-based modelling 127
4.3 Is there a loss of information by binarization? 129

5 Summary 130

6 References 132

7 Appendix 144

LIST OF ABBREVIATIONS

&; $\wedge$ and

|; $\vee$ or

!; $\neg$ not

$\subseteq$ is a subset of

$\in$ is member of

$\cup$ set union

$\propto$ is proportional to

$\mathbb{N}$ set of natural numbers

$\mathbb{R}$ set of real numbers

ADP adenosine diphosphate

AKT protein kinase B

AP1 activator protein 1

Apaf-1 apoptotic protease-activating factor 1

APC adenomatous polyposis coli protein

ARP 2/3 actin-related protein-2/3

AUC area under the curve

AURKA aurora kinase A

AXIN2 axis inhibition protein 2

BAD Bcl-2-antagonist of cell death

BASC binarization across multiple scales

BAX Bcl-2-associated X protein

β-TRCP β-transducin repeat-containing protein

BCL2L1 Bcl-2-like 1

CD44 CD44 antigen

CDKN1A cyclin-dependent kinase inhibitor 1A

CDKN1B cyclin-dependent kinase inhibitor 1B

DNA desoxyribonucleic acid

CDH1 E-cadherin

CCND1 cyclin D1

CCNE1 cyclin E1

CDK4/6 cyclin dependent kinase 4/6

C. elegans Caenorhabditis elegans

CFL1 cofilin-1

cFOS Fos proto-oncogene

CIP2A cancerous inhibitor of PP2A

cJun Jun proto-oncogene

CK1 casein kinase 1

COX2 cyclooxygenase-2

CRAF raf-1 proto-oncogene

CTNNB1 β-catenin

CYCS cytochrome C

daf-2 dauer formation protein 2

DC destruction complex

DAG diacylglycerol

DIA diaphanous-related formin

DOCK dedicator of cytokinesis

Dvl dishevelled

E2F transcription factor E2F

EBP1 Erb3-binding protein 1

EGFR epidermal growth factor receptor

eIF4F eukaryotic initiation factor 4F

EMT epithelial to mesenchymal transition

ERBB1 epdiermal growth factor receptor gene

ERK extracellulat signal-regulated protein kinase

f function

F-actin filamentous actin

F-actin$_{new}$ new branched actin fiber

F-actin$_{old}$ prolonged actin fiber

FAP familial adenomatous polyposis

FAS Fas cell surface death receptor gene

FBS fetal bovine serum

FOXO forkhead Box-O

FZD Frizzled

GEO Gene Expression Omnibus

GRN gene regulatory network

GSK3β glycogen synthase kinase 3 beta

HDAC2 histone deacetylase 2

Hd Hamming distance

hub higly connected component

IGF-1 insulin-like growth factor 1

IGFR1 insulin-like growth factor 1 receptor

IQGAP1 IQ motif-containing GTPase-activating protein 1

IIS insulin/insuline-like growth factor signalling

IRS insulin receptor substrate

JNK c-Jun-N-terminal kinase

kDa kilo dalton

KRAS kirsten rat sarcoma

KEGG Kyoto Encyclopedia of Genes and Genomes

LIMK LIM domain kinase

LRP5/6 low-density lipoprotein receptor-related protein 5/6

MAPK mitogen-activated protein kinase

MCL1 induced myeloid leukemia cell differentiation protein

MEK mitogen-activated kinase kinase

MEKK1 mitogen-activated kinase kinase kinase 1

mRNA messenger RNA

mTORC1 mammalian target of rapamycin complex 1

mTORC2 mammalian target of rapamycin complex 2

MYC Myc proto-oncogene

NP complexity class nondeterministic polynomial time

n number of nodes in a network

NF-κB nuclear factor kappa-light-chain-enhancer of activated B-cells

$\mathcal{O}$ big O notation for time complexity

ODE ordinary differential equation

P complexity class polynomial time

p21 cyclin-dependent kinase inhibitor 1A

p27 cyclin-dependent kinase inhibitor 1B

PAK1 p21-activated kinase 1

PAK4 p21-activated kinase 4

PanIN pancreatic intraepithelial neoplasia lesions

PBS phosphate-buffered saline

PDAC pancreatic ductal adenocarcinoma

pdBf partially defined Boolean function

PDK1 pyruvate dehydrogenase kinase 1

PGE2 prostaglandin E_2

PI3K phosphoinositide 3-kinase

PIP2 phosphatidylinositol 4,5-bisphosphate

PIP3 phosphatidylinositol-3,4,5-triphosphate

PKC protein kinase C

PLC phospholipase C

PRKD1 protein kinase D1

PP2A protein phosphatase 2A

PLD1 phospholipase D1

ProbRules probabilistic rule-based model

PTEN phosphatase and tensin homolog

RAC1 Ras-related C_3 botulinum toxin substrate 1

RAF rapidly accelerated fibrosarcoma

RAS rat sarcoma

RB retinoblastom

RHOA Ras homolog gene family member A

rpm rounds per minute

ROC receiver operating characteristic

ROCK RHOA associated protein kinase

RNA ribonucleic acid

RSK1/2 90-kDa ribosomal S6 kinase

S6K ribosomal protein S6 kinase

SAT satisfiability problem for classical propositional logic

SCF scaffolding

SDE stochastic differential equation

SDS-PAGE sodium dodecyl sulfate polyacrylamide gel electrophoresis

siRNA small interfering RNA

SSH1L slingshot protein phosphatase 1L

SNAIL1 snail family transcriptional repressor 1

STAT3 signal transducer and activator of transcription 3

t point in time

TBS-T Tris-buffered saline with Tween20

TCF7L2 transcription factor 7-like 2

TCF T-cell specific transcription factor

TCF/LEF T-cell factor/lymphoid enhancer-binding factor

TIAM1 T-lymphoma invasion and mestastasis-inducing protein

TSC2 tuberous sclerosis complex 2

TWIST1 twist-related protein 1

WASP Wiskott-Adrich syndrome protein

WAVE Verplin-homologous protein

WHO World Health Organisation

Wnt wingless

x Boolean variable of gene

$x(t)$ state at time t

$x'(t)$ perturbed state at point in time t

1

INTRODUCTION

This work aims to explore new relationships in signalling pathways through systems biology. We begin by briefly describing gene regulation followed by systems biological approaches that allow for dynamic modelling of these regulations. Subsequently, Boolean network models and network dynamics are introduced. Finally, use cases from ageing to cancer are explored in more detail with these mathematical models. See Figure 1 for an overview of this thesis.

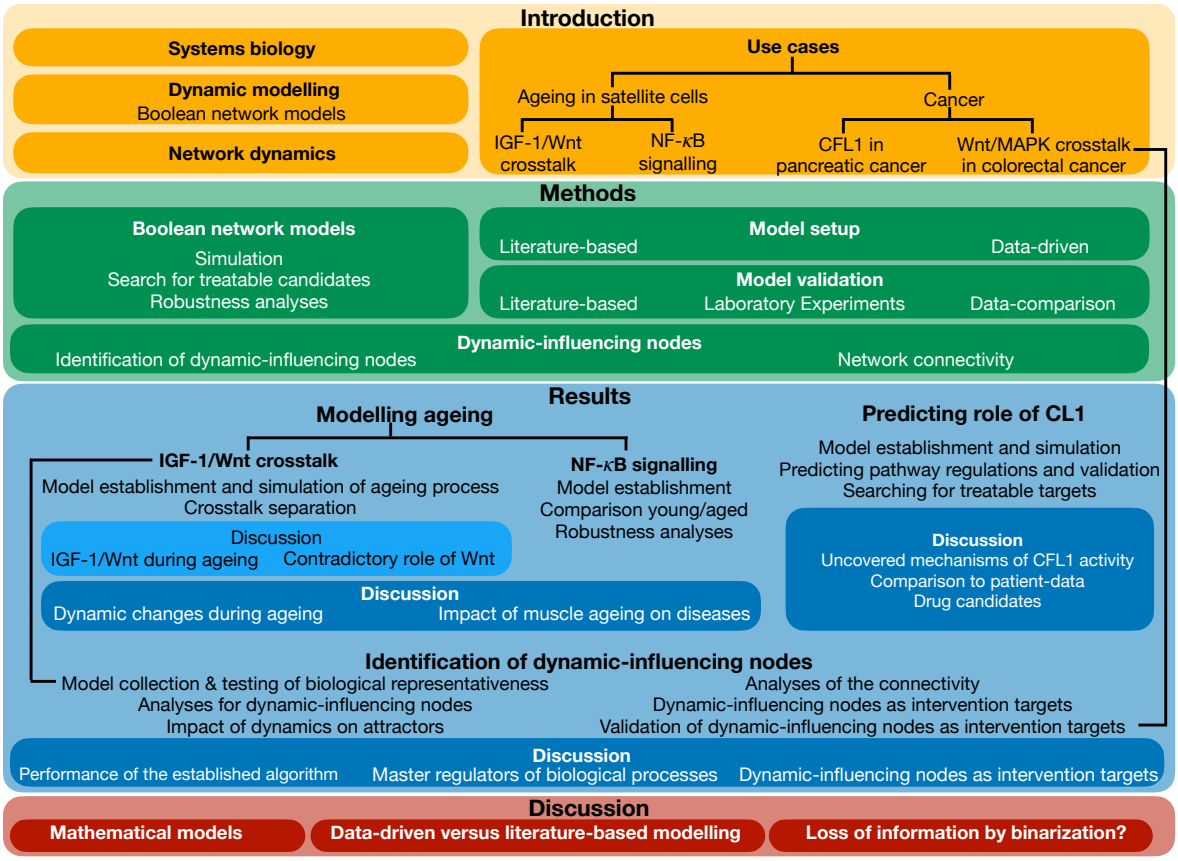

Figure 1: **Overview of this thesis.**

1.1 Systems biology - the necessity of changing points of view

Biology on its basic level is the interaction between deoxyribonucleic acid (DNA), ribonucleic acid (RNA) and proteins [77]. The source of information of an organism is encoded in its DNA in the form of genes (RNA viruses are neglected). These genes can be transcribed into messenger RNAs (mRNAs) which can be further translated into proteins [77, 176]. Each of these modules has different functions that can influence the others and thereby create a large interaction network or gene regulatory network (GRN) [176] (Figure 2).

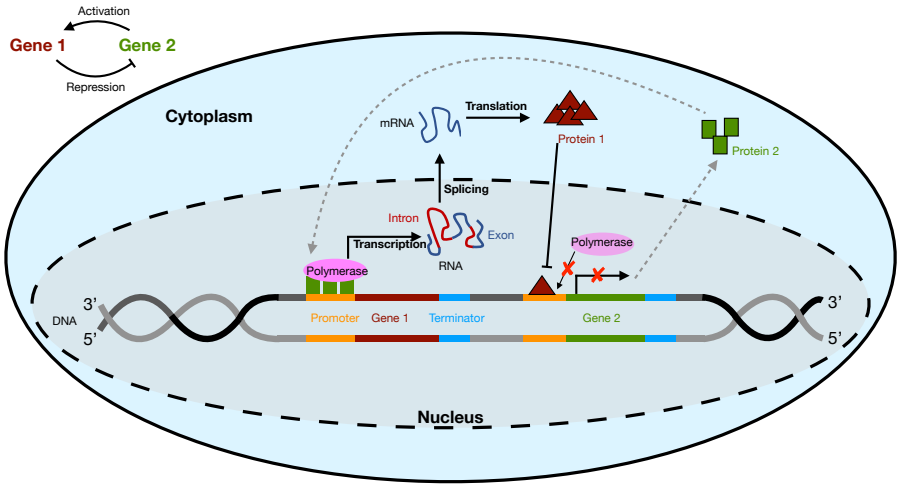

Figure 2: **Gene regulatory network.** Genes are encoded on deoxyribonucleic acid (DNA). Binding of transcription factors to the DNA allows (=enhancer) or prohibit (=silencer) the polymerase to bind the DNA to induce the transcription of preliminary RNA including introns and exons. The processed ribonucleic acid (RNA= mRNA) is translated into proteins. Here, both proteins act as transcription factors. While protein 1 is a repressor of gene 2, protein 2 acts as an activator of gene 1. Thereby building a small gene regulatory network.

In the past, molecular biology has focused on studying single interactions by collecting plenty of information about DNA sequences, protein interactions, expression profiles or cellular localisation [176, 212]. However, the development of diseases or cancer is rarely a process induced by the change of a single module in the interaction network. Rather it is an interplay between deregulated pathways [82, 454]. Thus, studying isolated interactions is not sufficient to understand complex biological behaviour [212, 454, 462].
Systems biology tries to address this problem and considers systems in their entirety. The idea is to collect existing information and combine it into a global often mathematical model [462]. These models can then be used to generate

hypotheses and guide laboratory experiments [176, 242] (Figure 3).

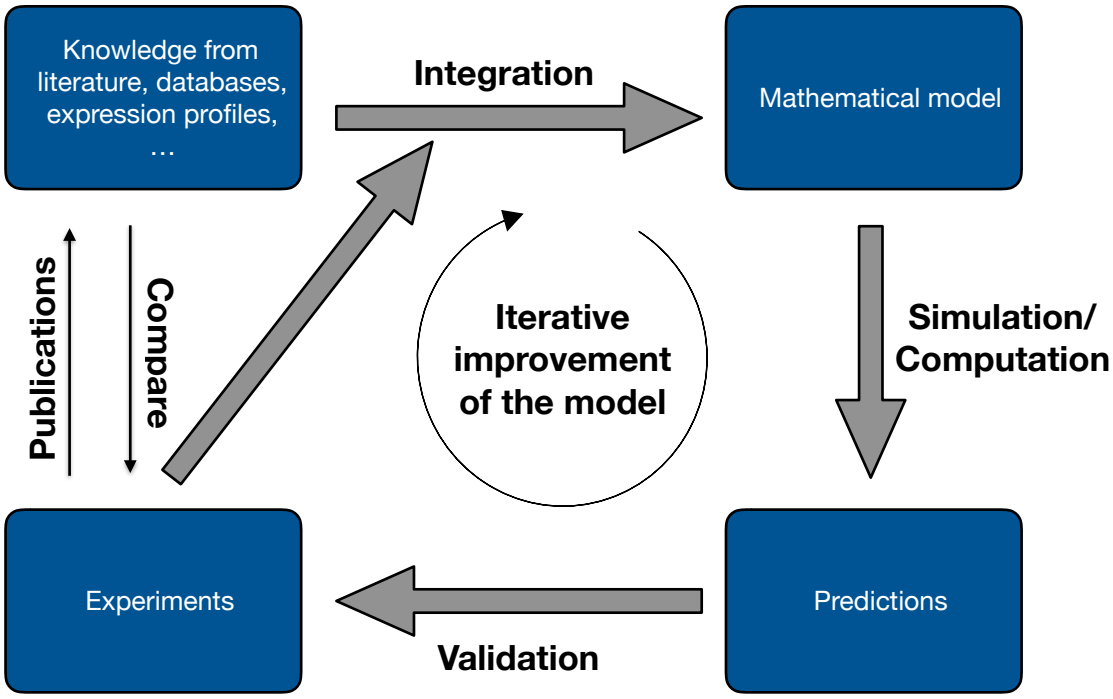

Figure 3: **Systems biology pipeline.** Systems biology is an interdisciplinary approach that covers biological, clinical, chemical, physical, and computational research. Wet lab experiments create new datasets and contradictory issues that can be processed, analysed or integrated into models. Predictions generated from simulations can then be tested by targeted wet-lab experiments. Thus, there is an iterative cycle between the single parts of systems biology.

In general, mathematical models used in systems biology can be divided into two categories: static and dynamic models. Static models search for dependencies like diagnostic markers in gene expression profiles. Here, diverse clustering techniques are applied frequently to analyse the models[213, 341]. However, the data on which these analyses are performed only represents a snapshot of the general behaviour e.g. altered gene expression. In contrast, dynamic models also incorporate temporal changes of the system [45].

1.2 Dynamic modelling

Biological networks consist of regulatory interactions that can influence the expression level of genes or the activity of proteins. Different factors interact simultaneously and influence each other in a positively or negatively manner. Here, feedback or feedforward regulations are a common motif that can be found in biological networks [10, 352]. Such regulatory interactions are frequently displayed in interaction graphs where directed edges between nodes represent genes or proteins [352] (Figure 4A). However, such static representations cannot display dynamic behaviour (Figure 4B) evolving from crosstalk interactions.

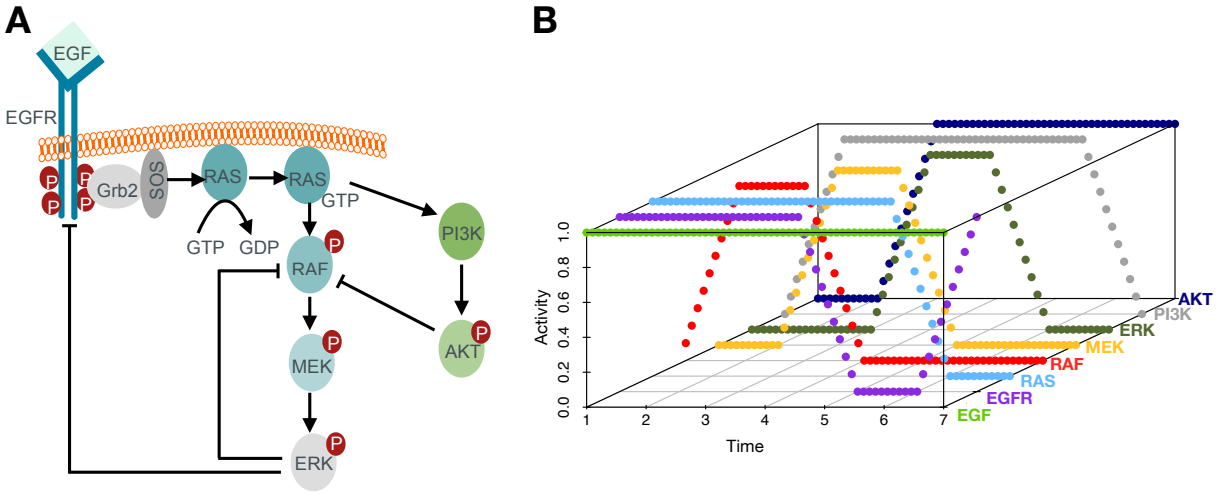

Figure 4: **Static interactions graphs are not able to depict temporal behaviour.** (A) The static interaction graph of the mitogen-activated protein kinase (MAPK) cascade depicts regulatory interactions by directed edges between the proteins. However, based on this representation, it is impossible to assess the temporal changes in activity depending on multiple regulators. (B) However, transferring this knowledge about interactions into dynamic mathematical models allows the depiction of alternating activity rates (y-axis) of each network protein (z-axis) over time (x-axis).

Dynamical changes are time-dependent and can only be mapped by model types that take time into account [45]. A variety of dynamic models have been proposed to describe GRNs. They differ in terms of complexity and abstraction (Figure 5) and can be either qualitative or quantitative nature. Thus, the choice of a suitable model depends on the issue to be tackled and the available information. Although continuous models such as ordinary differential equation (ODE) or stochastic differential equation (SDE) models can describe dynamical changes in more detail,

their creation requires precise knowledge about kinetic parameters which is often not available [344, 352]. In contrast, logical models such as Boolean network models [195] or probabilistic rule-based (ProbRules) models [137] are primarily based on the description of interactions and require few or no kinetic parameters (figure 5) [344]. Thus, they are suitable to investigate lesser-known systems or signalling pathways [344].

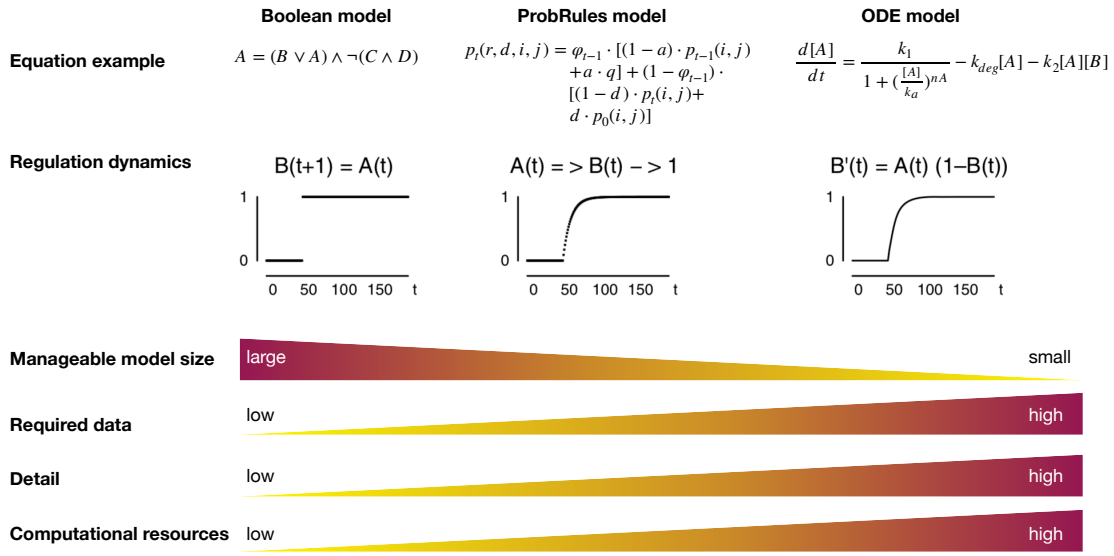

Figure 5: **The complexity of dynamic models.** Three dynamic model types that differ in complexity are depicted. Differences can already be recognised in the exemplary functions. While Boolean functions are sufficiently described by the logical connectives AND ($\wedge$), OR ($\vee$) and NOT ($\neg$), probabilistic rule-based (ProbRules) models already require attack rates (a) and decay rates (d). Ordinary differential equation (ODE) models require additional parameters about kinetics and concentrations. The dynamic comparison is shown below for an input A that activates B. Before time t=50 input A is not present but fully present afterwards. Dynamic representations are taken from Groß et al. [137], licensed under CC BY 4.0, https://creativecommons.org/licenses/by/4.0/.

1.2.1 *Boolean network models*

Boolean network models are simple dynamic models [5]. Nevertheless, they are able to describe complex biological behaviour ranging from development [159] to ageing [387] and cancer [83, 280].
In Boolean network models, all biological components of the network (n in total) are treated as Boolean variables $x_i, i \subseteq \{1, ..., n\}$. Dependencies (regulatory interactions) between them are described by the three logical connections AND (&; $\wedge$), OR (| ; $\vee$) and NOT (!; $\neg$) and summarised in a set of Boolean functions $f_i, i \subseteq \{1, ..., n\}$ [195] (Figure 6). The simplicity of Boolean network models arises from the assumption that variables can be represented in binary states [195]. Thus, nodes are either active (1) or inactive (0). This results in a total state space of 2^n states [195]. The state of the complete network is defined by a binary vector containing the state of each node at a specific point in time $X(t) = \{x_1(t), ..., x_n(t)\}, x_i \in \{0, 1\}$.

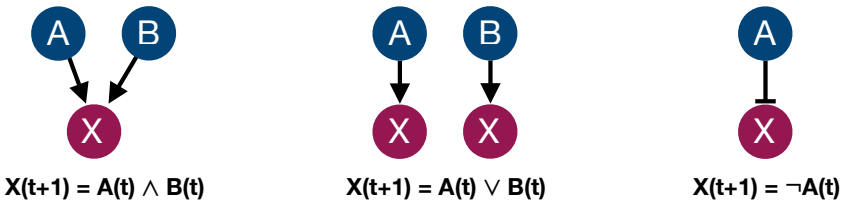

AND

A	B	X
0	0	0
1	0	0
0	1	0
1	1	1

OR

A	B	X
0	0	0
1	0	1
0	1	1
1	1	1

NOT

A	X
0	1
1	0
0	1
1	0

Figure 6: **Logical connections.** Logical connections AND; $\wedge$, OR;$\vee$, and NOT;$\neg$ are used to summarise regulatory interactions in Boolean network models. Boolean functions as well as truth tables are representatives of Boolean network models. Both representatives are able to describe temporal behaviours.

Dynamic characteristics can be achieved by applying Boolean functions to create state transitions [195]. Depending on the updating scheme of Boolean functions, Boolean network models can be divided into three categories - synchronous [195, 196], asynchronous [149] and probabilistic Boolean networks [383]. In synchronous Boolean network models, all Boolean functions are updated simultaneously while in asynchronous Boolean network models one function is randomly

chosen and updated at each point in time. In contrast to synchronous and asynchronous Boolean network models, in probabilistic Boolean network models, each node of the model can have multiple Boolean functions with different probabilities assigned to them. Here, the state transition is achieved by randomly choosing one of the possible functions of each variable and then synchronously updating the model (Figure 7) [3, 365].

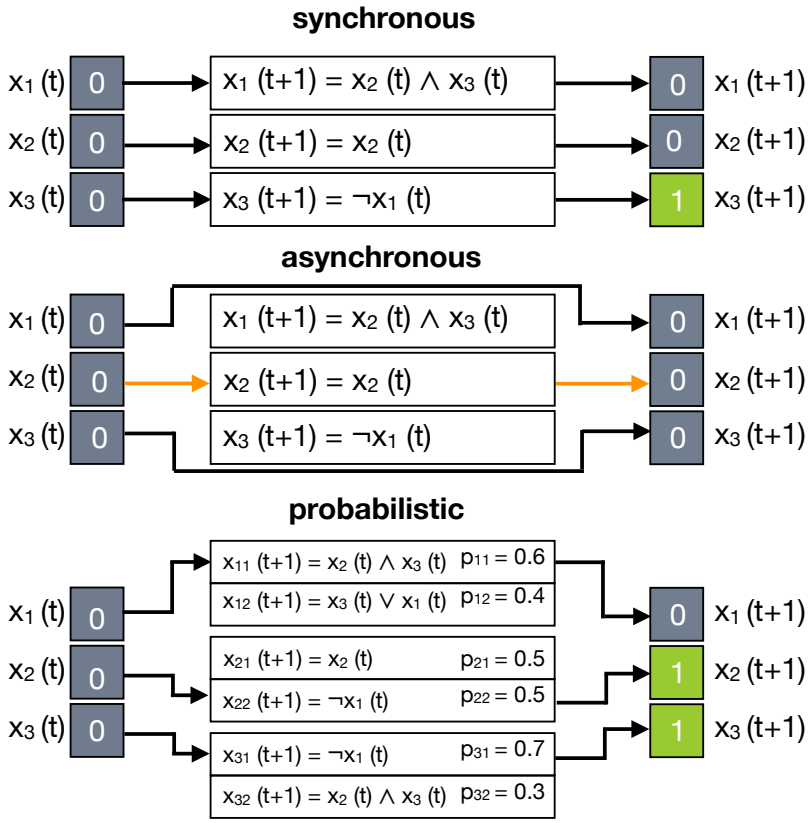

Figure 7: **Update schemes of Boolean network models.** In synchronous Boolean network models, all Boolean functions are updated synchronously. Contrary, in asynchronous Boolean network models one randomly chosen function (marked in orange) is updated per step in time. Probabilistic Boolean network models can have multiple Boolean functions with different probabilities $(p_{i1}, p_{i2}), i \subseteq \{1, ..., n\}$. When updating, one of these functions is chosen randomly per variable x_i and all functions are updated synchronously [3, 365]. The initial state of the nodes x_i at time t is listed on the left in coloured squares. The corresponding Boolean function is represented inside the rectangles. The arrows represent the updating of the model from time t to its successor state at time $t+1$. This figure has been modified from Schwab, Kühlwein et al. [367], licensed under CC BY 4.0, https://creativecommons.org/licenses/by/4.0/.

Comparable to an interaction graph, the dynamics of a network can be displayed in a state transition graph. Here, nodes represent the states of the network while edges show the transition from one state to its successor [3, 471]. Note, that in the state transition graph of synchronous Boolean network models each state of the network has only one unique successor state. In contrast, in asynchronous Boolean network models a state may have multiple successor states (Figure 8) [345]. Due to their finite number of states (in total 2^n) Boolean network models eventually converge to recurrent sequences of states, called attractors. Attractors describe the long-term behaviour of the model and are associated with biological phenotypes [196, 421]. Depending on the sequence of recurrent states, there are single state and multiple state attractors. Since all states that lead into the same attractor are part of its basin of attraction [345], attractors with a large basin of attraction are more plausible [471]. Recall that attractors of synchronous models have disjoint basins of attraction while in asynchronous models or probabilistic models these basins of attraction may overlap [345] (Figure 8).
In general, there are two major ways to create Boolean network models. Either they are based on intensive literature search or on the reconstruction of time series of gene expression data [168, 365, 387]. However, since few time series of gene expression data with more than three points in time are available, most Boolean network models are based on literature searches sometimes combined with individual laboratory experiments [365].

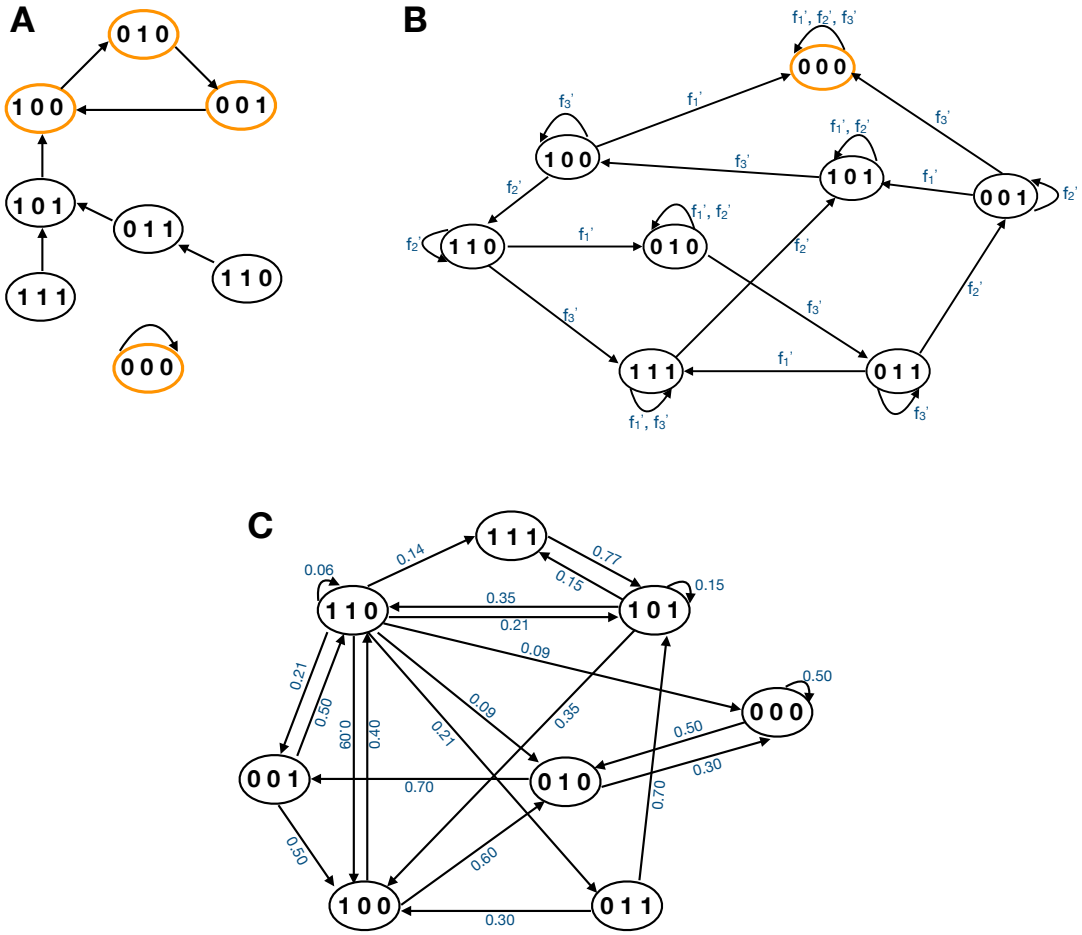

Figure 8: **State transition graphs.** Dynamics of Boolean network models can be displayed as a state transition graph. Here, states of the network are represented by nodes and edges between them describe state transitions. A state in a synchronous Boolean network (A) has only one unique successor state while a state in an asynchronous Boolean network model (B) or probabilistic Boolean network model (C) can have multiple successor states. The updated Boolean function (either f_1' or f_2' or f_3') for each state transition of the asynchronous model are depicted above the corresponding edges. For the probabilistic state graph (C) the p-values showing the probability for the corresponding transition are depicted. Attractors (marked in orange) represent the long-term behaviour of the network. All states that lead into the same attractor are part of its basin of attraction. This figure has been modified from Schwab, Kühlwein et al. [367], licensed under CC BY 4.0, https://creativecommons.org/licenses/by/4.0/.

1.3 Network dynamics

Boolean network models can reveal network dynamics. Generally, these simulations can be performed on the entire state space [83, 159] or on initial states that correspond to known situations of interest [280, 387]. In this perspective, simulations including the whole state space are applied to study general long-term behaviour, while simulations starting with certain initial states are used to reveal mechanistic regulation leading to a certain attractor and thus biological phenotype [280, 387]. However, no matter how simulations are performed, at the end the model should be able to reproduce expected behaviours known from laboratory experiments, otherwise, the model has to be improved [213].
Robustness is an essential feature of biological systems [212, 213]. Robust systems are assumed to be relatively insensitive to both internal alterations and environmental changes [212]. However, considering cancer cells which are often highly resistant to therapy, it seems that robustness is not always to an organism's advantage [212]. Network stability is achieved in biology by feedback regulation as well as by multiple pathways regulating the same node. [22, 128, 212]. This can be used for the concept of modelling. Here, robustness measurements can be taken into account to identify biologically meaningful attractors [196]. In order to assess the robustness of Boolean network models, they can be perturbed on structural or dynamic levels [471]. The latter refers to spontaneous state changes leading to temporal perturbations. Such alterations can be performed by randomly bit-flipping one or more states [3, 365]. In contrast, structural alterations refer to changes in the network wiring (alterations of inputs or operators) [7, 471]. Regarding the robustness of a network, it could be shown that the network architecture plays an important role [365]. In directed networks, each component has several in- and out-going edges which can be summarised as an in-degree and an out-degree [7, 22]. While all components in random networks have comparable average degrees the majority of components in scale-free networks have few connections and only a small number of components is highly connected [22] (Figure 9A). Comparable studies with these two types of networks showed that scale-free networks are more robust against arbitrary perturbations than random networks. However, these networks are more susceptible to alterations of highly connected components called hubs [6, 212].
The probability to find components with a certain degree ($P(x)$) can be described by a power-law distribution ($P(x) \propto x^{-\alpha}$) for scale-free networks while the degree distribution of random networks is better described by a Poisson distribution ($P(x) = \frac{\alpha^x}{x!}e^{-\alpha}$) [22, 182] (Figure 9B-C). Barabási and colleagues [22] compared the behaviour of protein-interaction networks to these findings and stated that they are scale-free. Since that time and because the removal of highly connected

components is more related to lethal phenotypes [181], hub nodes are considered as master regulators of biological processes [34]. However, some behaviours of these scale-free networks are discussed controversially [212, 258, 396].

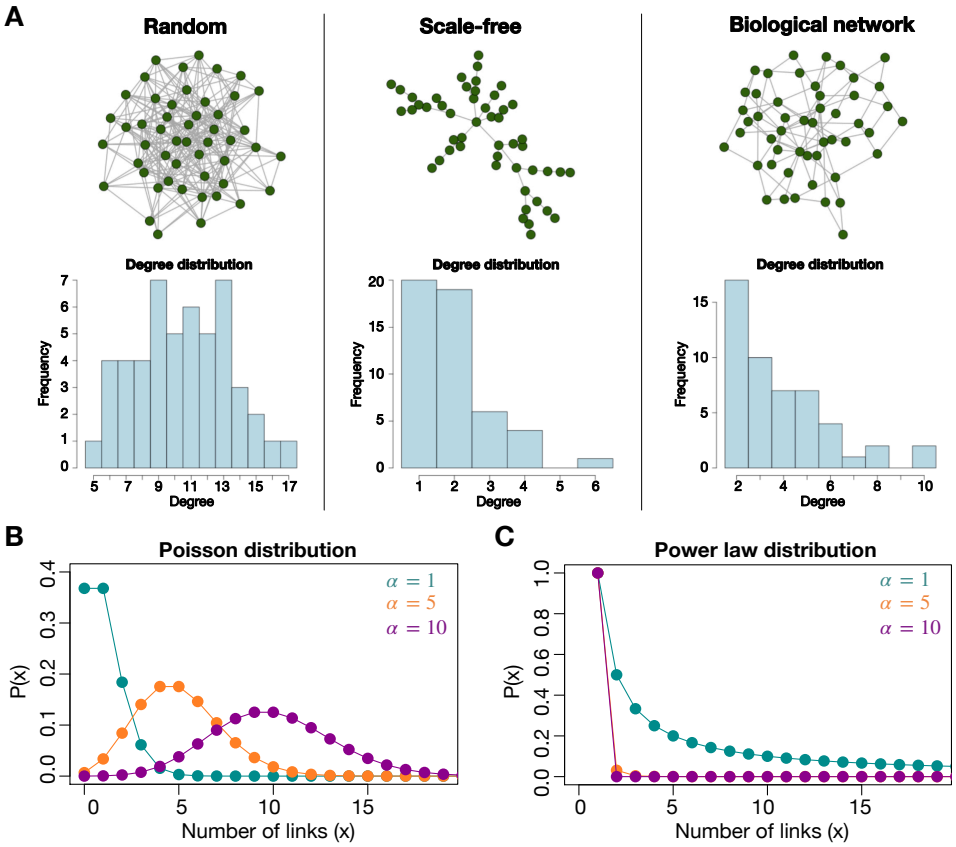

Figure 9: **Network topology.** (A) Network topology of a random, a scale-free and a biological network with 50 nodes are depicted. The corresponding degree-distribution is shown below. Models were calculated with the web tool ELIXIR [1]. (B) The probability distribution P(x) to find nodes with x connections to other nodes can be described by Poisson distribution ($P(x) = \frac{\alpha^x}{x!}e^{-\alpha}$) for random networks or (C) by power-law distribution $P(x) \propto x^{-\alpha}$ for scale-free networks [22].

Besides assessing the biological representativeness of an established network model, perturbation studies can also be used to search for promising intervention targets [280]. This can be achieved by fixing the state of a node. Similar procedures are the performances of laboratory overexpression or knockout experiment [343]. Automatic *in silico* screening can be performed to systematically test all possible intervention targets (Figure 10). Promising targets can later be tested in laboratory experiments [364, 366].

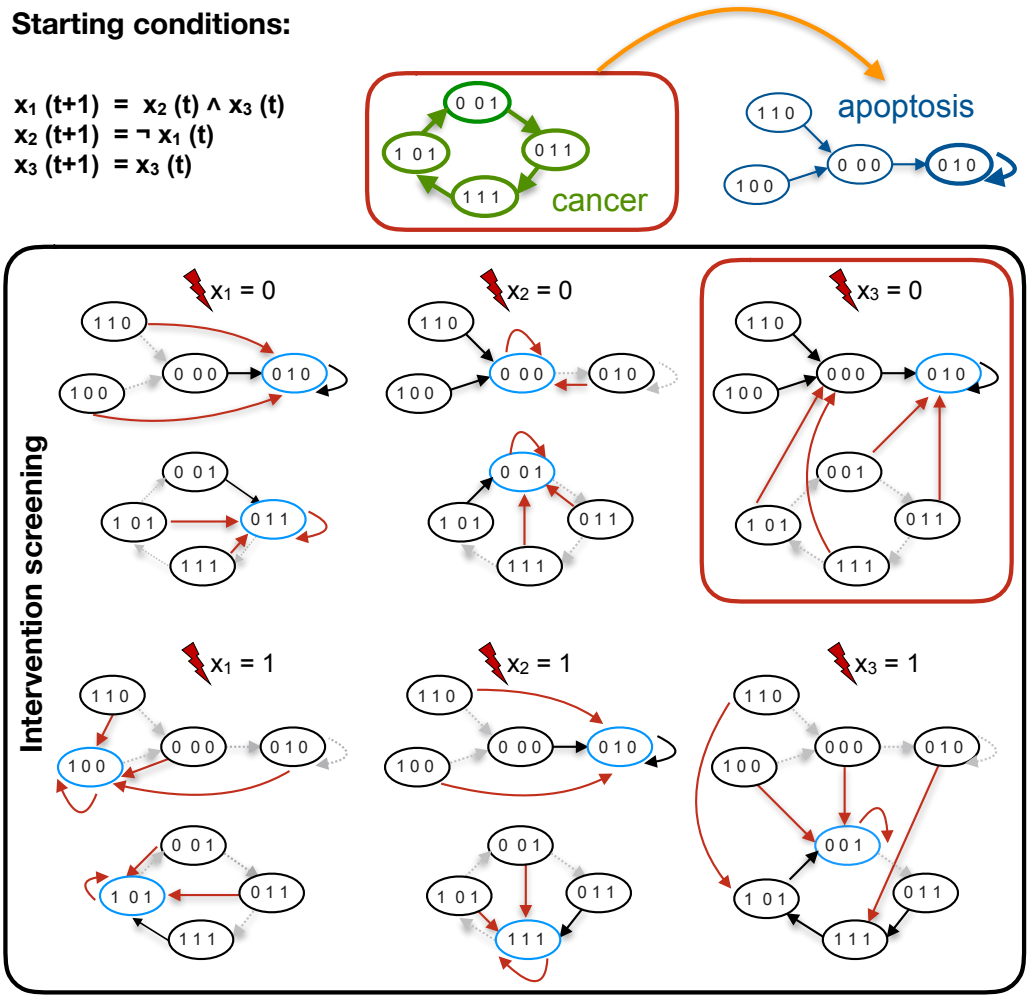

Figure 10: **Searching for intervention targets.** Systematic *in silico* testing of intervention outcomes by successively fixing single states of all components of a Boolean network model allows the prediction of promising intervention targets. The toy example includes three genes (x_1, x_2, x_3) whose Boolean functions are depicted on the top left. The corresponding state transition graph is shown on the right side. Attractors representing cancer and apoptosis are highlighted in boldface. Here, the intervention screening aimed to identify genes whose intervention switches the cancer attractor to apoptosis without the development of new attractors (orange arrow). Performed intervention screening indicates this shift for a knockout of gene x_3. Altered state transitions in comparison to the unperturbed network are emphasised by red arrows and corresponding attractors in blue.

1.4 Use cases

Within this work, Boolean network approaches were applied to different use cases such as ageing or cancer, which are described in the following sections. Ageing-related pathways such as insulin-like growth factor 1 (IGF-1)/wingless (Wnt) crosstalk or nuclear factor kappa-light-chain-enhancer of activated B-cell (NF-κB) signalling were studied in the context of healthy muscle stem cells (satellite cells) while cofilin-1 (CFL1) signalling or the Wnt/MAPK crosstalk were examined in the context of pancreatic and colorectal cancer, respectively.

1.4.1 *Ageing*

Ageing is a biological process that seems to affect the majority of higher organisms [151]. In contrast to any disease, ageing occurs in these organisms after they have completed a certain stage of development [151]. Here, the ageing process is often characterized by a decline in fertility and regeneration, a decrease in fitness, as well as an increase in pathological processes [359, 426]. However, few counter-examples seem less affected by ageing. Hydra, for example, a small freshwater cnidarian polyp, is able to regenerate any part of its body after loss or damage independent of the age [426]. Likewise, the fertility of naked mole-rats seems to be maintained until old age [48]. These controversies between organisms indicate that mechanisms behind ageing are far from being understood. The life expectancy of humans in developed countries has increased in recent decades [151, 315]. Nevertheless, the maximum life span of humans stagnated at 122 years [98, 334]. Reasons for the increase in life expectancy of humans are improvements in medical care as well as improved hygiene conditions [299, 315]. Therefore, the probability to develop age-related diseases increases [315]. Typical diseases associated with ageing are cardiovascular diseases, cancer or neurodegeneration [299, 315].
Several ageing-associated processes from puberty to menopause are regulated by endocrine levels and not on a genetic level [139, 151, 315]. For this reason, it is not surprising that some hormone concentrations change with age [88, 223]. One major investigated pathway in this context is the insulin/insulin-like growth factor (IIS) signalling pathway [139, 201, 299, 315]. Here, it was discovered that a mutation lowering dauer formation protein 2 (*daf-2*) expression more than doubles the life span of *Caenorhabditis elegans* (*C. elegans)* [139, 200, 201, 210]. The gene *daf-2* in *C. elegans* encodes a hormone receptor which is a homologue to the insulin-like growth factor receptor (IGFR1) in humans [139, 201, 315]. Besides *daf-2*, there are also other mutations which are able to influence the life span of model organisms [88].
Although the regulation of ageing is not clear in detail, ageing is frequently described as an accumulation of damage [256, 315, 371]. This accumulation of damage

is provoked for instance by disruption of DNA repair mechanisms, altered intercellular communications or protein aggregation [256].
The reasons for cancer development are manifold but ageing is one of the main highly associated risk factors [42, 88]. However, ageing and cancer are not directly linked [119]. Rather it seems that the accumulation of damage or the changes in metabolic or endocrine signalling during ageing are factors that promote the development of cancer [88, 119, 256, 371]. So, it is not surprising that pathways regulating ageing are also involved in cancer development.

1.4.1.1 *Satellite cell ageing*

One effect of ageing is a reshaping of body composition [223]. Affected by this body transformation are, among others, muscle cells which decrease in mass and strength [133, 223, 228, 433]. This process is called sarcopenia [133, 228, 433]. Based on this age-related reshaping muscle cells are believed to be good model systems to study ageing [76]. Adult skeletal muscles are composed of myofibers that differentiate from satellite cells [228, 484]. Normally, satellite cells are quiescent in adult muscles, however, after injury or for muscle regeneration they can enter mitosis [228, 484]. Indeed, this regeneration potential of muscle cells declines with age which is associated with reduced satellite cell activity [228].
The mechanisms of sarcopenia are not fully understood, but influences like reduced hormone concentrations or inadequate nutrition are assumed [133, 228, 433, 484]. One of the most studied pathways in ageing research is the insulin-like growth factor 1 (IGF-1) signalling cascade [139, 201, 299, 315]. This cascade is also assumed to be a master regulator of satellite cell ageing [133, 433].

1.4.1.2 *IGF-1/Wnt crosstalk*

Wnt and IGF-1 signalling are two evolutionary conserved pathways across multiple species [138, 210, 254, 270]. Since the Wnt signalling pathway is attributed to a major role in early development, it has been studied in the context of development or in connection with the onset of cancer [138]. Little is known about its influence later in life [138]. In contrast, since the discovery of *daf*-2 mutations that extend the life span of *C. elegans* [139, 200, 201, 210], IGF-1 signalling is one of the most studied pathways in ageing research [139, 201, 299, 315]. However, recent studies also indicate the role of Wnt signalling in the process of ageing [38, 117, 249, 417]. For example, Brack et al. [38] were able to show that treating young skeletal muscles with Wnt converts these cells into an aged phenotype while blocking Wnt abolishes this change [38]. In the same year, Liu et al. [249] discovered that in the Klotho mouse model of accelerated ageing which lacks the Wnt antagonist Klotho [221] chronic Wnt stimulation leads to premature ageing [249]. All these

studies point to increased Wnt activity during the process of ageing. But the role of Wnt during ageing seems to be more complex. For example, it was shown that a reduction of Wnt signalling is associated with a decline of neural stem cell function [308] and ageing of intestinal [417] and haematopoietic stem cells [117]. One reason for this complex and contradictory behaviour may be the overlapping functions of multiple pathways. Numerous crosstalk interactions can be identified between IGF-1 and Wnt signalling. For instance, the canonical Wnt mediator β-catenin (CTNNB1) is able to activate the longevity-related protein Forkhead Box-O (FOXO) [109, 167, 266, 270], one of the most important transcriptional effectors of IGF-1 signalling [200, 270]. However, in contrast to Wnt IGF-1 signalling mediates phosphorylation of FOXO via the phosphoinositide 3-kinases (PI3K) - protein kinase B (AKT) pathway activation and thus nuclear exclusion of FOXO and transcriptional inhibition of FOXO target genes [143, 270, 498]. Another example of this crosstalk interaction is the regulation of axis inhibition protein 2 (AXIN2). AXIN2 is a well-known feedback inhibitor of Wnt signalling [184] but it can also be activated by IGF-1 [361]. Thereby IGF-1 signalling antagonises the activity of the canonical Wnt cascade [361].

1.4.1.3 *NF-κB signalling*

Another hallmark of ageing is an increase in the activity of NF-κB signalling [256, 423]. As for the IGF-1 signalling pathway [139, 201, 315], several mutations were found that can suppress NF-κB signalling and increase the life span of several model organisms [350]. First assumptions that NF-κB is involved in ageing arose in the wake of electrophoretic mobility shift assays, showing enhanced DNA binding of NF-κB complex [155, 312] and thus activation of downstream targets [423]. Besides, Magalhães et al. [89] performed a meta-analysis of ageing-related datasets. This analysis indicated overexpression of genes involved in immune response and inflammation during ageing [89, 350]. Interestingly, NF-κB signalling is involved in immune response and inflammation [350].
Sarcopenia is a major problem during ageing and studies showed that NF-κB signalling is increased in myofibers taken from elderly in comparison to myofibers taken from younger people [80, 236].

1.4.2 *Cancer*

Cancer diseases are characterised by abnormal cell growth with the possibility of infiltrating other tissues [148]. Today, there are more than 100 different cancers and subtypes of cancers known [148]. Based on estimations of the World Health Or-

ganisation (WHO), cancer is classified as the leading cause of death in the 21st century [42]. Cancer is frequently considered as an age-associated disease since the incidence of developing cancer increases with age. However, the type of cancer diagnosed varies widely depending on the person's age [459]. Additionally, the probability of developing cancer or to die based on a cancer disease decreases considerably with an age above 90 years [459]. One characteristic of cancer cells is their ability to alter signalling pathways [148]. Common characteristics are increased proliferation and inhibition of apoptotic cascades [148].

1.4.2.1 *Pancreatic cancer*

Pancreatic cancer is a kind of cancer that mainly occurs in an elderly population. It has the highest incidence rate in the group of people above 70 years [170]. Once pancreatic cancer has been diagnosed, it proceeds fast in comparison to other cancers [42]. With an incidence rate (458,918 new cases [42]) nearly equal to the mortality rate (432,242 cases [42]) and a 5-year survival rate of less than 5% [385], pancreatic cancer is one of the most lethal cancers in developed countries. With an occurrence of 80% pancreatic ductal adenocarcinomas (PDACs) is the most common subtype of pancreatic cancer [372]. Based on genetic studies it is assumed that PDAC can develop from three precursor lesions. These are called pancreatic intraepithelial neoplasias (PanINs), intraductal papillary mucinous neoplasms and mucinous cystic neoplasms [161]. However, PDAC mainly develops from PanINs [161].
As opposed to other cancers, treating pancreatic cancer is still challenging [298]. Reasons for this are the late diagnosis of pancreatic cancer due to a lack of characteristic symptoms as well as the remarkable resistance to chemotherapeutic treatment [372]. Hence, surgery combined with adjuvant chemotherapy offers chances for long-term survival [298, 372].
In order to improve the treatment of pancreatic cancer patients, it is important to understand the mechanisms of the disease. This will enable a more specific treatment of patients and hopefully an improved prognosis.

1.4.2.2 *Cofilin-1 in pancreatic cancer*

High-throughput screenings of pancreatic tissue identified cofilin-1 (CFL1) as a potential biomarker for pancreatic cancer [47, 134, 446]. Within pancreatic cancer tissue, there is an elevated abundance of CFL1 on the mRNA as well as on the protein level [211, 355]. CFL1 is a small (19 kDa) and ubiquitously expressed protein that is mainly described in terms of its involvement in actin dynamics [30, 442]. In line with this, cancerous characteristics like migration and invasion could be associated with an increased expression of CFL1 [264, 442, 443, 479]. Besides its support in migration, high expression of CFL1 often seen together with

a decreased overall survival of patients [264, 303, 318, 443] including pancreatic cancer patients [355]. Furthermore, an elevated CFL1 expression can be associated with increased proliferation rates [211, 438].
Recently, it was described in bladder cancer that a knockdown of CFL1 leads to gap 1 phase (G1)-cell cycle arrest accompanied by a raised apoptosis rate [438]. In contrast to this study, Tsai et al. reported that an increase in CFL1 expression is associated with a G1-cell cycle arrest in lung cancer cells [429]. So there might be different regulation mechanisms for the cell cycle regulation downstream of CFL1. While Tsai et al. proposed a mechanism based on cyclin-dependent kinase inhibitor 1B (p27) regulated by CFL1 [429], there is no mechanistic explanation for the cell cycle regulation downstream of CFL1 in bladder cancer. Similarly to a knockdown of CFL1 in bladder cancer, it leads to attenuation of the G1- to S-phase transition in pancreatic cancer [211]. However, as opposed to previous findings, there is no induction of apoptosis [211]. Furthermore, a knockdown of CFL1 in pancreatic cancer cells results in a decelerated migration velocity and reduced migration potential [211, 355]. This might be interesting since metastases account for more than 90% of cancer-related deaths [58].

1.4.2.3 *Colorectal cancer*

Colorectal cancer is the third most common cancer and accounts for 5.8% of cancer-related deaths [42]. Similar to pancreatic cancer, the incidence of colorectal cancer increases in elderly populations [118]. Often, it develops from a polyp into an adenoma and further into an adenocarcinoma that is able to infiltrate distinct tissues. This progression is effected by a stepwise-accumulation of mutations. One of the earliest mutations that are present in 90% of colorectal cancer patients is a functional loss of adenomatous polyposis coli (APC) [14]. This is followed by aberrant activation of Kirsten rat sarcoma (KRAS) [183] that takes place in 50% of colorectal cancer patients [233]. Interestingly, both alterations alone are not sufficient to induce severe phenotype. However, if present together they lead to increased proliferation and invasion [233]. Interaction of the involved canonical Wnt signalling and the mitogen-activated protein kinase (MAPK) cascade can be observed on different regulatory levels leading to a stabilisation of both CTNNB1 and KRAS [183]. Although the importance of Wnt and MAPK crosstalk for the development of colorectal cancer is well known, its dynamics are still poorly understood [183].

1.5 Aims of the thesis

This thesis aims to explore new relationships between signalling pathways that play a role in the context of ageing and cancer by a holistic approach. For this purpose, different strategies to establish Boolean network models will be used and compared. Additionally, dynamic properties of biological networks will be studied using Boolean network models to identify factors that determine the dynamics and to test their usability for therapeutic approaches. In general, dynamic analyses will be restricted to synchronous and asynchronous updating. Besides, the established approaches and models will be used to elucidate the molecular mechanisms responsible for ageing-related diseases and cancer.

2

MATERIALS AND METHODS

This thesis deals with Boolean models, which serve as a basis to answer biological questions. Therefore, the materials and methods section first includes a short mathematical explanation of these models and explains how they were simulated in this thesis. Afterwards, it is explained how to search for intervention targets within the models to be established and how perturbation studies can be used for network comparisons. Subsequently, the establishment process of the Boolean models developed in this thesis is discussed. First, the development of literature-based models is described. This includes the models for Wnt/IGF-1 crosstalk during ageing, CFL1 signalling in pancreatic cancer and Wnt/MAPK crosstalk in colorectal cancer. In addition to literature-based models, data-driven models of age-dependent alterations within the NF-κB pathway were developed in this thesis. For the reconstruction of these models from time series of gene expression data, a binarization of the data is required first, which will be discussed before the model reconstruction. Subsequently, the *in vitro* investigations and data-based analyses used in this work will be discussed to support the model-generated hypotheses on therapeutic targets and mechanistic regulations. The methods section concludes with the implementations for the dynamic analysis of Boolean networks, the collection of published models used for this purpose and the comparison of dynamic-influencing nodes and network hubs.

2.1 Boolean network models

Boolean network models are comprised of a set $X = \{x_1, ..., x_n\}$ of variables $x_i, i \subseteq \{1, ..., n\}$ that represent n genes or proteins [3, 195]. Each variable x_i can be either active or inactive. Thus, they can acquire two states $x_i \in \{0, 1\}$ [195]. Regulatory interactions within the model can be summarised in a set of Boolean functions $F = \{f_1, ..., f_n\}$ with Boolean functions $f_i, i \subseteq \{1, ..., n\}$ by three logical connectives AND (&, $\wedge$), OR (|, $\vee$) and NOT (!, $\neg$).
Since Boolean network models have a finite number of nodes, they can assume 2^n states [195]. A state x(t) is defined by the value $\{0, 1\}$ of each component at

a specific point in time t. The dynamics within these models are achieved by applying Boolean functions f_i and thereby creating state transition from state $x(t) = (x_1(t), ..., x_n(t))$ to its successor state $x(t+1) = (f_1(x_1(t)), ..., f_n(x_n(t)))$ [195]. Boolean network models can be divided into three main groups depending on the updating scheme of their functions, namely synchronous [195, 196], asynchronous [149] and probabilistic [383] Boolean network models. Within the scope of this work, only synchronous and asynchronous updating schemes were considered. The difference between these two updating schemes is that in synchronous Boolean network models all Boolean functions are updated at the same time while in asynchronous Boolean network models only one function is randomly chosen and updated at each point in time [3].
Simulations were performed using the R-package BoolNet [289].

2.1.1 *Simulation of Boolean network models*

Independent of the updating scheme, simulations of Boolean network models can be performed on the entire state space to study the long-term behaviour of the model [83, 159]. Another possibility is to use initial states that correspond to known situations of interest [280, 387]. In this case, the mechanistic regulation leading to this behaviour can be investigated by examining the state transitions towards an attractor [280, 387].
Note that an exhaustive search for attractors by analysing the whole state space is demanding in terms of memory and runtime (both are $\mathcal{O}(2^n)$) [168]. To circumvent these limitations that only allow for an analysis of smaller networks up to 29 nodes [289] it is possible to start simulations from a reduced set of randomly drawn initial states or to apply Boolean satisfiability problem (SAT) algorithms. Dubrova and Teslenko [102] proposed such a mapping to SAT for synchronous Boolean network models. The idea behind this 'sat.exhaustive' algorithm is simple. It searches for trajectories and checks if the last state of this path is present at least twice. If a path does not contain a loop, the path length is doubled. To accelerate this procedure, the algorithm searches only for paths whose last state is not included and terminates if all path lengths fulfil the criteria [102]. Note, that SAT is known to be NP-complete [3]. Hence, SAT can be solved in $\mathcal{O}(2^n \mathrm{poly}(m, n))$ time where m denotes the number of clauses [3].
Intervention studies like knockout or overexpression of proteins can be simulated by fixing the state $x_i \in \{0, 1\}$ of a node i and running the simulation [343].

2.1.2 *Intervention screening for treatable targets in Boolean network models*

Biological networks are considered to be stable against random perturbations [6, 212]. Nevertheless, targeted interventions can change the dynamic of a complete network. Laboratory screening of promising interventions is cost-intensive and can be time-consuming if not even impossible [366, 501]. Therefore, automatic *in silico* screenings based on the dynamics of Boolean network models can help with the identification of meaningful intervention targets [366].
In the scope of this work, the Javascript application ViSiBooL [364, 366] was applied to screen for meaningful intervention targets in the established Boolean network models. Initially, attractors were selected into which the long-term behaviour of selected components is to change. In a next step, a set of c candidates e.g. $X' = \{x_3, x_7, x_{11}\}$ was selected for intervention screening as well as the maximum number of these combinations m [366]. Based on these specifications, a SAT-solver performs all possible intervention combinations parallel, in total $\sum_{i=1}^{m} \binom{c}{i} \cdot 2^i$, and returned a list of interventions that show the desired long-term behaviour of the simulations [366].

2.1.3 *Robustness analysis within Boolean network models*

Scale-free networks, including biological networks, display a high error tolerance [6, 212]. This characteristic can be used to identify biologically meaningful networks [196]. Under the assumption that perturbation hardly influences biologically meaningful network attractors while randomly generated suffer more from perturbations in general the characteristic of error tolerance can be used for computer-intensive tests [501].
Robustness measurements through random state changes by single bit-flip mutations and comparison of the transition behaviour from the original state x(t) to its successor state x(t+1) and the perturbed state x'(t) to its successor state x'(t+1) by using the normalised Hamming distance (Hd, Equation 1) have been suggested previously [128].

$$Hd(x, x') = \frac{1}{n} \sum_{i=1}^{n} | x_i - x'_i | \tag{1}$$

In total, p network states are perturbed and the mean Hamming distance of a network is considered. To assess the effect of the perturbations in the original network, a set of randomly generated networks R of the equal number of genes compared to the original network is created. Here, also p bit flip mutations are performed for each network $\in$ R. The mean Hamming distance is considered as significant if

the 95% confidence interval of all random networks is greater than the Hamming distance of the original network [365, 501]. If there is no change in the transition between the perturbed network state and the original state, the Hamming distance is zero [128].
The Hamming distance cannot only be calculated to compare successor states after perturbations. It can also be applied to analyse the effect of perturbations after several time steps, e.g. five time steps x(t+5) or the effect of perturbing an attractor state [365].

2.2 Model setup

Within the scope of this work, Boolean network models were created using a literature search or time series of gene expression data. The following sections describe the individual model setups.

2.2.1 *Literature-based Boolean network models*

Three Boolean network models considering pathway dysregulation in ageing and cancer were built based on literature statements within the scope of this thesis. These models include the IGF-1/Wnt crosstalk, the regulation of CFL1 and downstream effects in pancreatic cancer as well as the Wnt/MAPK crosstalk in colorectal cancer. The following sections describe the literature search for their establishment.

2.2.1.1 *IGF-1/Wnt crosstalk*

The first signalling pathway investigated in this thesis concerning age-related changes is the IGF-1/Wnt crosstalk. Since it could already be shown that the Wnt signalling pathway influences the ageing of muscle cells [38], the crosstalk of IGF-1 and Wnt was studied in satellite cells (muscle stem cells). For this reason, the considered literature was restricted to studies in the context of satellite or muscle cells. First, general reviews of both signalling pathways were screened to identify nodes that are regulated by both signalling cascades or regulate both pathways. Subsequently, the search was specified using search terms such as "IGF-1 ageing satellite" and "Wnt ageing satellite". Besides, it was searched for interaction partners of previously identified crosstalk regulators in muscle cells. Although canonical and non-canonical Wnt signalling exists that distinguishes in the binding of Wnt ligands and receptors [205], these ligands and receptors were combined in this model.
The initial Boolean network model of the IGF-1/Wnt crosstalk was developed in

the context of Lea Siegle's bachelor thesis [386] and further extended with regard to ageing.

2.2.1.2 *Cofilin-1 in pancreatic cancer*

The second literature-based model that was created in the scope of this thesis deals with the role of CFL1 in pancreatic cancer. Since an elevated abundance of CFL1 is described for pancreatic cancer cells [211, 355], its general regulation was addressed in this model. Besides, it could be shown that a knockdown of CFL1 in pancreatic cancer cells attenuates the cell cycle transition from gap 1 phase (G1) to synthesis phase (S) and reduces the migratory potential without inducing apoptosis [211, 355]. Therefore, the model also takes into account pathways that regulate proliferation and apoptosis.
The initial model was established by searching for proteins regulating CFL1, the cell cycle transition from G1 to S phase as well as apoptosis in general. Therefore, search items like "CFL1 regulation", "CFL1 pancreatic cancer", "CFL1 cell cycle" or "apoptosis pancreatic cancer" were considered. Whenever possible, findings obtained in pancreatic cancer cells were weighted more favourably. Moreover, studies describing CFL1 knockdown experiments and their effects on downstream targets as well as studies that observed changes in CFL1 expression or protein amount were considered for the identification of crosstalk regulators within this model. Finally, the proteins included in the initial model were analysed concerning their mutual regulation.

2.2.1.3 *Wnt/MAPK crosstalk in colorectal cancer*

The third literature-based model deals with the crosstalk of Wnt and MAPK signalling in colorectal cancer. Frequently, a loss of the APC protein occurs during the development of this type of cancer [14]. A mutation of KRAS can cause a further progression of the cancer [183]. APC is at the beginning of the Wnt cascade whereas KRAS controls the MAPK cascade [183]. For this reason, the interactions between these two pathways were investigated. First, general review papers were reviewed to identify key proteins of both pathways and possible crosstalk regulators. Subsequently, the search was refined with search terms such as "Wnt colorectal cancer" and "MAPK signalling colorectal cancer". Finally, the cured databases BioGRID [403] and Metacore™ (Thomson Reuters Inc., Carlsbad, CA) were used to identify further possible interactions of components that were integrated into a first model. The initial model was created by myself and extended in the master thesis of Nensi Ikonomi [177] under my supervision.

2.2.2 *Data-driven Boolean network models*

Besides a model setup based on literature statements, Boolean models can also be reconstructed based on gene expression data. Since gene expression data consists of values $\in \mathbb{R}$ while Boolean network models work with binary values, the gene expression values first have to be binarized. In the following sections, the unsupervised binarization of gene expression data and the data-driven reconstruction of Boolean networks will be discussed. The GSE362 dataset [453] was used to reconstruct Boolean network models of the age-dependent changes of NF-κB signalling in the progression of ageing.

2.2.2.1 *Dataset for network reconstruction*

The GSE362 dataset [453] gathered on a Human Genome U133A Array chip was used for network reconstruction. It includes 15 samples of satellite cells taken from healthy human males of different ages. The age of these donors ranges from 21 to 27 years and 67 to 75 years. Within this dataset, two points in time are represented by two samples. These samples were averaged and further considered as one sample.
Since this dataset was analysed in the context of NF-κB signalling during ageing, only genes which are included in the NF-κB signalling as described in the hsa04064 Kyoto Encyclopedia of Genes and Genomes (KEGG) database [192] were considered.

2.2.2.2 *Binarization across multiple scales*

Binarization across multiple scales (BASC) algorithms as suggested by Hopfensitz et al. [169] are two methods for the binarization of gene expression data. For the network reconstruction of NF-κB signalling in the progression of ageing, the BASC A algorithm implemented in the R-package BiTrinA [290] was applied. Here, the expression values of gene a are combined in vector $a = (a_1, ..., a_N) \in \mathbb{R}^N$ according to their increasing expression values. Afterwards this vector is used to define a step function f (Equation 2) with N steps in the intervals A_i (Equation 3) with its indicator function I_A (Equation 4) [169]:

$$f(x) = \sum_{i=1}^{N} a_i \cdot I_{A_i}(x) \tag{2}$$

$$A_i = \begin{cases} (0, d_i], & \text{if} \quad i = 1 \\ (d_{i-1}, N], & \text{if} \quad i = N \\ (d_{i-1}, d_i], & \text{otherwise} \end{cases} \tag{3}$$

$$I_{A_i} = \begin{cases} 1, & \text{if} \quad x \in A \\ 0, & \text{otherwise} \end{cases} \tag{4}$$

Expression data is not continuous and exhibits certain discontinuities $d_i \in \{1, ..., N-1\}$. Therefore, the BASC A approach calculates a set of step functions $f = (f_1, ..., f_n)$ with a reduced amount of discontinuities $n \quad (n < N-1)$ so that the Euclidean distance of two step functions (e.g. f_1 and f_2, Equation 5) is minimised compared to the initial one [169]:

$$\| f_1 - f_2 \| = \sqrt{\sum_{x=1}^{N} (f_1(x) - f_2(x))^2} \tag{5}$$

Next, the the strongest discontinuity in each step function with j steps is calculated by taking into account the maximal distance (height) h between the starting point $P_i(j)$ and the terminal point $P_i(j)+1$ of the discontinuity (Equation 6) and the approximation error e (Equation 7). This results in a scoring function q (Equation 9) which can later be applied to calculate the strongest discontinuities of the optimal step functions v_j (Equation 10). To calculate the distance of the mean value between the starting point and the terminal point, y is considered (Equation 6) [169].

$$h = \begin{cases} y(P_i(j)+1, P_{i+1}(j)) - y(1, P_i(j)), & i = 1 \wedge j > 1 \\ y(P_i(j)+1, N) - y(P_{i-1}(j)+1, P_i(j)), & i = j > 1 \\ y(P_i(j)+1, N) - y(1, P_i(j)), & i = j = 1 \\ y(P_i(j)+1, P_{i+1}(j)) - y(P_{i-1}(j)+1, P_i(j)), & \text{otherwise} \end{cases} \tag{6}$$

$$e = \sum_{d=1}^{N} (f(d) - z)^2 \tag{7}$$

whereby

$$z = \frac{f(P_i(j)) + f(P_i(j)+1)}{2} \tag{8}$$

$$q = \frac{h}{e} \tag{9}$$

Based on this, the optimal step function v_j can be calculated (Equation 10):

$$v_j = \{P_i(j) : i = \operatorname{argmax}_{1,...,j} q\} \tag{10}$$

At the end, a single binarization threshold T is defined (Equation 11) [169] using the median $\tilde{v}$ of the strongest discontinuities v:

$$T = \frac{f(\lfloor \tilde{v} \rfloor + 1) + f(\lfloor \tilde{v} \rfloor)}{2}. \tag{11}$$

However, not all gene expression datasets can be binarised equally sell. To ensure that the gene expression data is clearly separable based on the defined threshold a p-value Equation 13) can be computed. First, v is normalised by division by $N - 1$ to obtain the normalised vector v'. Next, the average deviation AD (Equation 12) of sample x with N elements is computed where $\tilde{x}$ is the median [169].

$$AD(x) = \frac{1}{N} \sum_{j=1}^{N} |x_j - \tilde{x}| \tag{12}$$

In order to account for a dependency between the data in v', a moving-blocks bootstrap test is applied. Here, $v^* = (v_1^*, ..., v_{N-2}^*)$ is the bootstrap of B samples built from concatenated blocks l of replacement of $v' = (v_1', ..., v_{N-2}')$ [169]. For the BASC A approach l is $(N-2)^{\frac{1}{4}} + 1$ [169].

$$p = \frac{| \quad \{(AD(v\prime) - AD(v*)) \geqslant (\tau - AD(v\prime))\} \quad |}{B} \tag{13}$$

Here, $\tau \in (0, 1]$ is used to adjust sensitivity and specificity [169, 290]. For the binarization of the gene expression data of ageing satellite cells, $\tau = 0.01$ was used.

2.2.2.3 *Inferring Boolean network models from time-series*

In the scope of this thesis, the best-fit extension algorithm by Lähdismäki et al. [222] and implemented in the R-package BoolNet [289] was applied to infer Boolean network models of the NF-κB signalling during ageing. This algorithm has a reduced runtime complexity in comparison to the algorithm by Akutsu et al. [4] and determines the Boolean functions with a minimal error for each gene [289].
The algorithm has to define Boolean functions f which are able to distinguish between true and false examples in the given data. This can be achieved with a partially defined Boolean function (pdBf(T,F)) denoting a set T of true examples $T(f_i) = \{x_i \in \{0,1\}^n : f_i(x_i) = 1\}$ and a set F of false examples $F(f_i) = \{x_i \in \{0,1\}^n : f_i(x_i) = 0\}$. Next, the error size is defined. To achieve this positive weights $\omega(x_i) > 0$ are given to all variables $x_i \in T \cup F$ and the weights of all subsets $S \subseteq T \cup F$ are calculated (Equation 14) [222]:

$$\omega(S) = \sum_{x \in S} \omega(x) \tag{14}$$

Based on the weights of the subsets, the error size ϵ of function f_i can now be calculated (Equation 15). For the best-fit approach the minimal error size of the pdBf is of interest [222]:

$$\epsilon(f_i) = \omega(T \cup F(f_i)) + \omega(F \cup T(f_i)) \tag{15}$$

One representative of a Boolean network model is its truth table. Thus, in a further step a truth table for each Boolean function f indexed from 1 to 2^{n-1} is defined (Equation 16). Here, the i-th variable of f can either be inactive $\{0\}$, active $\{1\}$, undefined $\{?\}$ or a conflict $\{*\}$. The truth table is generated by iteratively performing the following procedure for all examples $e \in T \cup F$ and over all time steps $t = 1, ..., m$. The index m denotes the current measurement [222, 365]:

$$f_i^t = \begin{cases} 0, & \text{if} \quad e \in F \wedge f_i^{t-1} =? \\ 1, & \text{if} \quad e \in T \wedge f_i^{t-1} =? \\ *, & \text{otherwise} \end{cases} \tag{16}$$

Finally, the algorithm returns Boolean functions for all variables provided by the data which recapitulate the changes in expression of the time series.

2.3 Model validation

Model-generated hypotheses about mechanistic regulation or altered activity levels can be supported by comparing literature studies or confirmed by laboratory experiments. While the assumptions of the IGF-1/Wnt model were supported by comparisons to published studies, the assumptions of the CFL1 model and the Wnt/MAPK model were validated by laboratory experiments. The following sections describe the laboratory experiments carried out to support the model-based assumptions. Moreover, the CFL1 model was confirmed by comparisons of the attractor pattern to binarized gene expression data of pancreatic cancer tissues.

2.3.1 *Laboratory experiments*

The initial laboratory experiments, as well as the model-based predictions about CFL1 dysregulation in pancreatic cancer cells, were performed by our cooperation partners in Marburg (Department of Gastroenterology, Endocrinology and Metabolism, Philipps-University, Marburg).
The laboratory experiments with colorectal cancer cell lines were conducted by myself or from Nensi Ikonomi under my supervision.

2.3.1.1 *Cell lines and culture conditions*

Laboratory experiments supporting the CFL1 model were performed with S2-007 cells while the ones for the Wnt/MAPK model were carried out in SW480 cells.

S2-007 cells were obtained from T. Iwamura (Miyazaki Medical College, Miyazaki, Japan). Cells were cultured in Dulbecco's modified Eagle's medium supplemented with 10% fetal bovine serum (FBS) and 0.05 mg/ml Gentamicin at 37° C in a 5% CO_2 containing incubator.

SW480 cells were obtained from the American Type Culture Collection. This cell line was cultured in Dulbecco's Modified Eagle's Medium - high glucose supplemented with 10% FBS and 1% Penicillin-Streptomycin.

2.3.1.2 *CFL1 knockdown in pancreatic cancer cells*

Since many observations concerning the role of CFL1 in pancreatic cancer were made by comparing untreated cells with CFL1-silenced cells [211, 355], this CFL1-silencing was simulated in the model and the corresponding attractor pattern was compared to knockdown experiments.

To knockdown CFL1 expression in human pancreatic cancer cells, three pre-designed silencer small interfering RNAs (siRNAs) #146652 (5'-GGGAUCAAGCAUGAAUUGCtt-3'), #5455 (5'-GGAGAGCAAGAAGGAGGAUtt-3') and #5366 (5'-GGACAAGAAGAACAUCAUCtt-3') (Applied Biosystems/Ambion, Austin, TX, USA) targeting human CFL1 were used. In addition, a non-silencing siRNA construct (Thermo Fisher Scientific, Dharmacon Products, Lafayette, LA, USA) was used as control. These constructs were transfected into the cells in a concentration of 40 nmol by using the siLentFect Lipid Reagent (Bio Rad, München, Germany) according to the manufacturer's protocol.

2.3.1.3 *Drug treatment of colorectal cancer cells*

In contrast to the CFL1 model in which the role of CFL1 in cancer development was investigated, the Wnt/MAPK model was used to find proteins for a targeted therapy. For this reason, the inhibition of identified targets was performed with small molecules and not by siRNAs.

SW480 cells for drug treatment derived from a 10 cm dish that was split in a 1 : 20 ratio were seeded in six-well plates. After 24 hours cells were treated for 24 hours with 1 ml medium either containing DMSO (Sigma-Aldrich, St. Louis, Missouri, USA), 2 μM BVD-523 (# HY-15816, MedChemExpress, Monmouth Junction, NJ,

USA) diluted in DMSO, 12 μM TD52 (# SML2145, Sigma-Aldrich, St. Louis, Missouri, USA) diluted in DMSO or 2 μM BVD-523 or 12 μM TD52 diluted in DMSO.

2.3.1.4 *Cell counting*

Cell counts were performed on SW480 cells to check whether the targeted therapy with the small molecules affects proliferation or apoptosis.

Cell numbers as well as the percentage of dead cells were determined using a cell counter machine (Counter II, Invitrogen, Carlsbad, California, USA). 10 μl of cell lysate was mixed with 10 μl of trypan blue (Fluka analytical, St. Louis, Missouri, USA) and loaded on counting slides (Countess^{TM}, Invitrogen, Carlsbad, California, USA). Both the amount of living as well as dead cells were determined.

2.3.1.5 *Western blot*

Simulations with the CFL1 model as well as with the Wnt/MAPK model showed that some proteins changed in their activity state. Whether this change of state is equivalent to a reduction of their protein level was checked by western blots.

To extract proteins cells were centrifuged in culture medium at 13,000 rounds per minute (rpm) and room temperature for 5 minutes. Next, the cell pellet was resuspended in phosphate-buffered saline (PBS) (137 mM NaCl, 2.7 mM KCl, 10 mM Na_2HPO_4, 1.8 mM KH_2PO_4, pH 7.4) supplemented with proteinase inhibitor (G-Biosciences, Maryland Heights, USA) and treated with ultrasound with a Labsonic U (B.Braun, Melsungen, Germany). The protein concentration was measured using Bradford assay with the Multiskan FC photometer (Thermo Scientific, Langenselbold, Germany). Western blots were performed according to standard procedures. The sodium dodecyl sulfate polyacrylamide gel electrophoresis (SDS-PAGE) separated proteins were transferred to a nitrocellulose membrane (Whatman GmbH, Dassel, Germany) which was blocked for 4 to 6 hours at 4° C in Tris-buffered saline with Tween20 (TBS-T) (50 mM Tris, 150 mM NaCl, 0.1% Tween-20 (v/v), pH 7.6) containing 5% powdered milk. Primary antibodies CFL-1 (ab42824, Abcam, Cambridge, UK), caspase-3 (#9662, Cell Signaling Technology, Danvers, USA), cleaved caspase-3 (#9661, Cell Signaling Technology, Danvers, USA), STAT3 (#9139, Cell Signaling Technology, Danvers, USA), phospho-STAT3 (Tyr705) (#9145, Cell Signaling Technology, Danvers, USA), Cyclin D1 (#ab16663, Abcam, Cambridge, UK), and c-Myc (#sc-481, Santa Cruz Biotechnology, Santa Cruz, USA) were diluted 1 : 1,000 in blocking buffer and incubated over night at 4° C while secondary antibody anti-rabbit (#7074, Cell Signaling Technology, Danvers, USA) was diluted 1 : 10,000 and incubated for 1 to 2 hours at 4° C. As loading controls blots were probed with β-

actin (#sc-1616 HRP, Santa Cruz Biotechnology, Santa Cruz, USA) or Lamin A/C (#2032, Cell Signaling Technology, Danvers, USA). Proteins were visualised using the ECL immunoblot kit (GE Healthcare Europe GmbH, Freiburg, Germany).

2.3.1.6 *E-cadherin staining*

Simulations with the Wnt/MAPK model indicated that some interventions restore E-cadherin at the cell membrane thereby leading to reduced migratory potential. To support this model-based suggestion, E-cadherin was stained.

SW480 cells were seeded on fibronectin coverslips in a six-well plate. After 24 hours of treatment, cells were fixed with 4% paraformaldehyde (Sigma Aldrich, St. Louis, Missouri, USA) for 15 minutes. Afterwards, cells were permeabilised with 0.1% Triton X-100 (Merck, Kenilworth, New Jersey, USA) for 10 minutes and blocked in 0.5% bovine serum albumin (Sigma Aldrich, St. Louis, Missouri, USA) for 45 minutes. Antibody incubation was performed at room temperature for 2 hours (E-cadherin #610181, BD Bioscience, San Jose, CA, USA, 1 : 200) and 1 hour (anti-mouse Alexa 488, Dianova, Hamburg, Germany, 1 : 1000) respectively and cells were mounted in DAPI mounting medium (Invitrogen, Carlsbad, California, USA). Leica TCS SP5 II confocal microscope in a single plane (63-objective) using LAS AF software was used for image acquisition. Same exposure settings were used for all samples.

2.3.1.7 *Wound healing assay*

In addition to the E-cadherin staining, it was tested whether restored E-cadherin at the plasma membrane leads to a reduced migratory potential. Therefore, wound healing assays were performed.

SW480 cells were seeded in a six-well plate on fibronectin coated coverslips. After cells reached a confluent state they were treated with either BVD-523 (2 μM diluted in DMSO), TD-52 (12 μM diluted in DMSO) or a combination of both (2 μM BVD-523, 12 μM TD-52 both diluted in DMSO). DMSO and untreated cells were used as control. A wound between confluent cells was created with a 200 μl pipette tip and cells were incubated for 48 hours at 37 °C and 5% CO_2. Images of the wounds were taken after 0 hours, 24 hours and 48 hours. The closing of the gap was analysed with the Image-J tool MRI Wound Healing Tool. Statistical analyses were performed between the control group (untreated) and treated cells using Wilcoxon test with Bonferroni correction.

2.3.2 *Attractor comparison to gene expression data*

In addition to the laboratory experiments, the assumptions of the CFL1 model were checked using microarray data of normal and pancreatic cancer tissues. Here, three datasets with the accession numbers GSE15471 [18] (36 tumours, 36 healthy controls each with three replicates), GSE16515 [316] (36 tumours, 16 healthy controls) and GSE32676 [97] (25 tumours, 7 healthy controls) were considered. All these microarrays were performed on Affymetrix U133 Plus 2.0 whole-genome chips.

As for reconstruction, the gene expression data must be binarized to compare them to the attractor pattern. This time, however, the datasets include labels which can be used for binarization. For this reason, a supervised binarization method was used. Here the best binarization threshold for each individual gene of the model was determined by using a ROC curve. ROC curves are plots of sensitivity against 1-specificity [31, 146]. Thus, sensitivity (or recall) is defined as the proportion of positive results that are classified correctly [333, 31] (Equation 17) and specificity is defined as results which are correctly identified as negative results [31, 146, 333] (Equation 18).

$$\text{sensitivity} = \frac{\text{true positives}}{\text{all positives}} \tag{17}$$

$$\text{specificity} = \frac{\text{true negatives}}{\text{false positives} + \text{true negatives}} \tag{18}$$

Under optimal conditions, both sensitivity and specificity are equal to one [31]. Consequently, a threshold close to this optimum would be desirable. To judge the performance of the classifier, the area under the curve (AUC) can be calculated by the sum of the areas (Equation 19) [31, 114]. For the calculation of each trapezium the starting coordinates (x_k, y_k) and terminal coordinates (x_{k+1}, y_{k+1}) in the plot of the ROC curve are used. Here, the maximal range $m \in \mathbb{N}$ and the coordinates x_k as well as y_k are $\in [0, 1]$.

$$\text{AUC} = \sum_{k=1}^{m-1} (x_{k+1} - x_k) \cdot \frac{y_k + y_{k+1}}{2} \tag{19}$$

The determination of binarisation thresholds for gene expression data in the pancreatic cancer datatsets GSE15471 [18], GSE16515 [316] and GSE32676 [97] was performed with the R-implementation pROC [333].

2.4 Analyses for dynamic-influencing nodes

Besides exploring new relationships between signalling cascades, another aim of this thesis was to identify nodes that determine the dynamics of a regulatory network. It is assumed that a small set of nodes determines the dynamic of a complete network. Hence, if this small set of nodes receives an initial state $x_i \in \{0,1\}$ it is possible to determine the states of all nodes within the network although these other states are initially undefined {?}. This can be achieved by repeatedly applying Boolean functions. If the function of an undefined node can be uniquely determined by already defined nodes it is assigned a value. This procedure is repeated until a binary value is assigned to all nodes (Figure 11).
Nodes that are part of the minimal set of dynamic influencing nodes are defined here as implicants.

Initial occupancy				Partial assignment to defined states									
CD45	CD8	TCRlig	cCbl	CD45	CD8	TCRlig	TCRbind	cCbl	Fyn	ZAP70	Lck	TCRphos	PAGCsk
1	1	1	1	1	1	1	?	1	?	?	?	?	?
				1	1	1	0	1	?	0	?	?	?
				1	1	1	0	0	?	0	?	?	1
				1	1	1	1	0	?	0	0	?	1
				1	1	1	1	0	1	0	0	?	1
				1	1	1	1	0	1	0	0	1	1

Figure 11: **Partial assignment.** The state of a set of nodes is predefined. By applying Boolean functions to these predefined nodes the yet undefined nodes {?} are assigned a value. The procedure of partial assignment is shown exemplarily for the reduced network of Klamt et al. [214].

To identify nodes that are part of the implicant set two methods were established in the scope of this work. These two methods are described in the following sections. Exhaustively testing all possible combination of nodes until the smallest set of implicants is found can be time-consuming if not even impossible. Therefore, this strategy was used as a reference for a newly established heuristic search for implicants.

2.4.1 *Heuristic approach*

The heuristic approach chooses nodes according to a here defined significance. Based on this defined significance, the significance value of a node is maximal if it is an input. Else the significance of a node depends on the number of functions depending on this node. The heuristic approach iteratively chooses additional nodes with decreasing significance until an implicant set is defined (Algorithm 1).

Algorithm 1 : Heuristic

input : Set of Boolean functions $F = (F_1, \ldots, F_n)$
output : A minimal implicant set

$G \leftarrow \emptyset$
repeat
  $w \leftarrow$ `nodeWeight(`*F,G*`)`
  $g \leftarrow x_i$, *where* $w(x_i) = \max(w)$
  $G \leftarrow G \cup \{g\}$
  observables $\leftarrow$ `observableStates(`*F,G*`)`
until *observables*;
return G

`nodeWeight(`*F,G*`)`
  for *all nodes* x_i *in* G **do**
    remove rule F_i *and all occurrences of* x_i *from* F
  end
  for *all nodes* x_i, *where* F_i *depends only on* x_i **do**
    $w(x_i) \leftarrow n$ `// max weight`
  end
  for *all nodes* x_i, *where* F_i *depends only on* x_j, $i \neq j$ **do**
    $w(x_i) \leftarrow 0$ `// min weight`
  end
  for *all nodes* x_i, *where* $w(x_i)$ *is not already set* **do**
    $w(x_i) \leftarrow$ the number of j such that F_j depends on x_i
  end
  return w

2.4.2 *Exhaustive approach*

Heuristics are algorithms that can be applied to problems that cannot be solved in reasonable time [219]. These algorithms do not always reveal the best solution but try to find a local optimum. The implemented heuristic to search a set of implicant nodes belongs to the class of greedy-algorithms. Greedy-algorithms make

incremental decisions based on available information thereby choosing each time the local optimum [75]. In contrast to heuristic approaches, simple exhaustive algorithms test all possible solutions of a given search space revealing the best are time-consuming [219]. Thus, the worst-case time complexity to find a minimal implicant set in a given Boolean network model is $\mathcal{O}(2^n)$. Nevertheless, also an exhaustive approach was established (Algorithm 2) to search for the implicant set in order to assess the performance of the previously mentioned heuristic approach.

Algorithm 2 : Exhaustive

```
input  : Set of Boolean functions F = (f_1, ..., f_n)
output : Minimal implicant sets

success ← false
implicants ← ∅
for increasing values of k do
    for all possible selections G = {x_{i_1}, ..., x_{i_k}} of k nodes do
        observables ← observableStates(F,G)
        if observables then
            success ← true
            implicants ← implicants ∪ {G}
        end
    end
    if success then
        return implicants
    end
end

observableStates(F,G)
    for every assignment a to the k nodes of G do
        let the assignment a be undefined for all remaining n-k nodes
        evaluate F until an attractor A_a ist found
        if A_a is undefined on some node then
            return false
        end
    end
    return true
```

2.4.2.1 *Network size reduction*

The time complexity of exhaustive search approaches increases with each additional node. For this reason, a network size reduction approach was implemented to accelerate the exhaustive search approach. Therefore, Boolean functions of nodes

that are regulated by others but do not regulate other nodes themselves were removed from the set of Boolean functions (Algorithm 3)

Algorithm 3 : Reducing network size

input : Set of Boolean functions $F = (F_1, \ldots, F_n)$
output : Set of reduced network functions

$In \leftarrow \{x_i \mid F_i(x) = x_i\}$
while $\exists x_l \in F, x_{i_1}, \ldots, x_{i_k} \in In : F_l(x) = f(x_{i_1}, \ldots, x_{i_k})$ **do**
  remove F_l *from rule set* F
  substitute all occurrences of x_l *in* F *by* $f(x_{i_1}, \ldots, x_{i_k})$
end
while $\exists x_l \in F : x_l$ *is not contained in any rule* F_i **do**
  remove F_l *from ruleset* F
end

2.4.3 *Collection of Boolean network models*

To study the dynamics of signalling in biology, several biologically motivated Boolean network models were extracted from the interactive modelling of the biological networks database (Cell Collective) [157]. Additionally, a literature search was performed in PubMed with the search item "Boolean network model" including works up to May 24th 2017. Networks that could not be simulated in a feasible time, networks with too many attractors and networks in which nearly all nodes are input nodes were excluded from this collection.

2.4.3.1 *Testing scale-freeness*

Biological networks are error-tolerant. One reason for this behaviour is their scale-free network structure [6, 212]. The connectivity of scale-free networks can be described by the power-law distribution (Equation 20). In order to perform the dynamic analyses on Boolean network models that show biological characteristics, it was tested if the connectivity of the literature collected Boolean network models can be described by the power-law distribution.

$$P(x) \propto x^{-\alpha} \tag{20}$$

The scaling parameter α of the power law distribution was obtained by estimating the minimal distance x_{min} between the cumulative distribution function of the data S(x) and the fitted model P(x) (Equation 21) [69]:

$$D = \max_{x \geqslant x_{min}} |S(x) - P(x)| \tag{21}$$

Due to the uncertainty of x_{min}, a bootstrap procedure can be used to define the final x_{min}. Afterwards, the scaling parameter α is calculated (Equation 22) with x_{min} and the data values x_i by approximating the maximum likelihood estimator:

$$\alpha \simeq 1 + n \left[\sum_{i=1}^{n} \ln \frac{x_i}{x_{min} - 0.5} \right]^{-1} \tag{22}$$

In the end, a goodness-of-fit test can be applied to test if the data of the Boolean model can be plausibly fitted by a power-law distribution. This can be done with a Kolmogorov-Smirnov statistic [68]. As defined by Clauset et al. [68], the connectivity of the corresponding Boolean network model cannot be described by the power-law distribution if the resulting p-value is $\leqslant 0.1$.
The poweRlaw package [130] was used to discern if the connectivity of nodes within the chosen Boolean network models could be described by the power-law distribution.

2.4.4 *Identification of network hubs*

Highly connected nodes (hubs) within the network structure of biological processes are frequently regarded as master regulators [34]. To test whether there is an overlap of implicants and hub nodes, the general connectivity of the nodes within the Boolean network models was analysed.
The degree of a node within a Boolean network model is defined by its interactions with other network components. Similar to this the degree of proteins is based on their interaction partners. While the information about the connection of nodes in the Boolean network model can be extracted by counting edges, connections of biological partners can be extracted from protein-protein interaction databases such as BioGRID [403]. For this project, protein-protein interactions were extracted from BioGRID Version 3.5.168. These interactions were compared to the ones within the Boolean network models. Some nodes within the collected Boolean network models represent protein complexes or multiple isoforms. In these cases, the interactions of all these proteins in the complexes or of both isoforms were summarised and their average of them was used to define network hubs.
To identify hubs within the network structure, Guimera et al. [141] proposed to determine a z-score (Equation 23). This z-score is calculated based on the connections to interaction partners x_i as well as with the average number of interactions of all nodes in the network x_n and their standard deviation σ.

$$Z = \frac{x_i - x_n}{\sigma} \tag{23}$$

Nodes with a z-score > 2.5 are considered hub nodes according to the definition by Guimera et al. [141]. Wilcoxon test with Bonferroni correction was applied to

analyse differences between implicant nodes, hubs and the rest of the nodes. This test was also applied to compare the degree of nodes within the Boolean network models with biological interactions. To achieve this the R-package RVAideMemoire [160] was used.

2.5 Statistics and visualisation

R [324] (www.r-project.org) was used for statistical analyses and visualisation. Experimental data was analysed by Wilcoxon test.

3

RESULTS

The results are divided into individual sections that specifically address individual signalling pathways. Each specific result section is followed by a short discussion that only comprises this part of the work.
For the model-based investigation of ageing, a literature-based and a data-driven approach were chosen. Here, IGF-1/Wnt crosstalk, as well as NF-κB signalling, were studied and parallels between the pathways and the power between both establishment-strategies were compared. The studies in regard to ageing are followed by a Boolean network model that tries to elucidate the role of CFL1 in pancreatic cancer and possible treatment options. The results are concluded by an investigation of nodes that determine the overall dynamic properties of a network. Here, a method to identify these nodes and validate their role with a newly established Boolean network of Wnt/MAPK crosstalk in colorectal cancer is presented.

3.1 Modelling ageing

Ageing is a biological process that limits most organisms in their regeneration potential [359, 426]. However, not all organisms seem to be equally affected [48, 359]. Hence, the comprehension of the mechanisms behind ageing is far from being understood. Two signalling pathways, IGF-1 and NF-κB, are known to be involved in ageing [139, 201, 256, 299, 315, 423] and both vary in their activity during this process [172, 256, 423]. In order to get a better understanding of their regulation, they were studied based on Boolean network models was studied. This was done in the context of muscle cell ageing.

3.1.1 *IGF-1/Wnt crosstalk during ageing*

One of the best-studied pathways in the context of ageing is the IIS pathway [139, 201, 299, 315]. During ageing IGF-1 concentration declines in satellite cells. In contrast, the Wnt signalling and its downstream targets increase during ageing of satellite cells and can even accelerate this process [38, 249]. Besides changes in

their activity, both signalling pathways have even more in common: They partially regulate the same downstream targets [8, 206, 361, 486].
The protein Axin-2, a direct target of the Wnt signalling pathway, is often used to test for Wnt activity. However, it can also be regulated by IGF-1 signalling [361]. But the IGF-1/Wnt crosstalk is not unilateral. For example, Dvl which is part of Wnt signalling can activate the typically IGF-1 assigned MAPK cascade [8, 206, 486]. Consequently, there is intensive crosstalk between IGF-1 and Wnt signalling (Figure 12). In the scope of this work, the effect of this crosstalk is being investigated in more detail with regard to ageing by a Boolean network model. The established model (Table 1) includes the most important key players of IGF-1 and Wnt signalling as well as their common downstream targets (Figure 12). Note that both signalling molecules can act in a paracrine manner as they are secreted by surrounded cells [326]. Thus, IGF-1 and Wnt are considered as input nodes of the model and are not regulated from within the network.

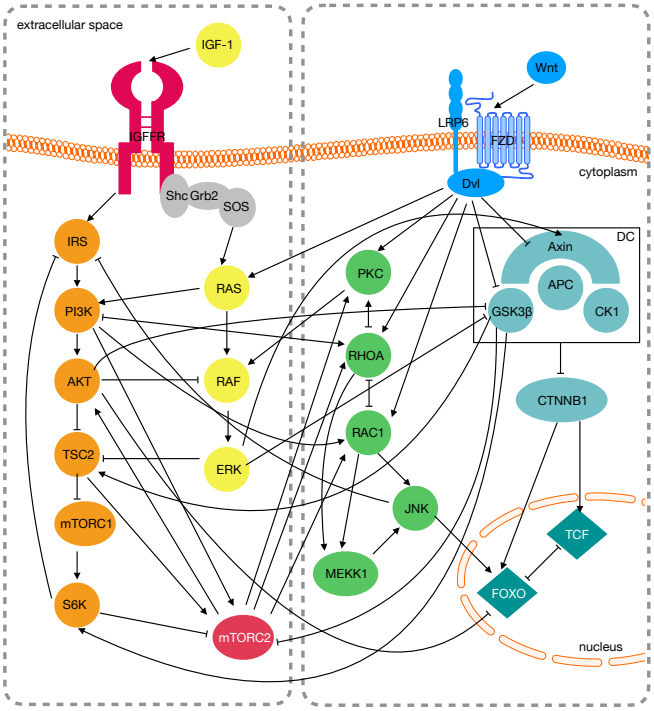

Figure 12: **Interactions within the IGF-1/Wnt network model.** IGF-1 and Wnt signalling share some common downstream targets. The most important components of both pathways as well as their common targets were included in the model. To distinguish the pathways from each other they are separated by dashed boxes. Regulatory interactions are depicted by arrows for activating interactions or by bar-headed lines for inhibiting interactions. The figure has been modified from Siegle, Schwab, Kühlwein et al. [387], licensed under CC BY 4.0, https://creativecommons.org/licenses/by/4.0/.

Table 1: Boolean functions of the IGF-1/Wnt crosstalk model and their descriptions modified from Siegle, Schwab, Kühlwein et al. [387], licensed under CC BY 4.0, https://creativecommons.org/licenses/by/4.0/. All proteins are abbreviated in accordance with the current nomenclature. Logical connectives are depicted by & (=AND), | (=OR), and ! (=NOT).

	Node; $t+1$	**Boolean network function;** t	**Description**
IGF-1 subnetwork	IGF-1	IGF-1	IGF-1 is a paracrine signalling molecule which binds to its receptor and activates the cascade [331, 509]
	IRS	IGF-1 & !(S6K & JNK)	The activated IGFR1 (here IGF-1) activates insulin receptor substrate (IRS) when it is not inhibited by ribosomal protein S6 kinase (S6K) or c-Jun N-terminal kinase (JNK) [94, 174, 207, 274, 331, 351, 380, 381, 469, 509]
	PI3K	(IRS | RAS) & !RHOA	PI3K binds to IRS and gets activated. Otherwise it can be activated by rat sarcoma (RAS). Both activations can be inhibited by phosphatase and tensin homolog (PTEN). PTEN is activated by RHOA associated protein kinase (ROCK) downstream of the small GTPase Ras homolog gene family member A (RHOA) (here RHOA inhibits PI3K) [44, 62, 123, 247, 274, 285, 369, 469, 478]
	AKT	PI3K | mTORC2	AKT is phosphorylated and thus activated by PI3K or mammalian target of rapamycin complex 2 (mTORC2) [37, 62, 174, 243, 380, 469]

Table 1: Boolean functions of the IGF-1/Wnt crosstalk model and their descriptions modified from Siegle, Schwab, Kühlwein et al. [387], licensed under CC BY 4.0, https://creativecommons.org/licenses/by/4.0/. All proteins are abbreviated in accordance with the current nomenclature. Logical connectives are depicted by & (=AND), | (=OR), and ! (=NOT).

	Node; $t+1$	**Boolean network function;** t	**Description**
IGF-1 subnetwork	TSC2	!(AKT | ERK) | GSK3β	AKT as well as extracellular signal-regulated kinases (ERK) inhibit tuberous sclerosis complex 2 (TSC2). In contrast, if cellular energy is sparse, an adenosine monophosphate-activated protein reduces mTROC2 activity and in combination with glycogen synthase kinase 3 beta (GSK3β) TSC2 gets activated (here GSK3β activates TSC2) [62, 175, 178, 380, 469]
	mTORC1	!TSC2	TSC2 inhibits mammalian target of rapamycin complex 1 (mTORC1) [37, 174, 175, 380, 469]
	S6K	mTORC1 | GSK3β	S6K can be activated either by mTORC1 or GSK3β [37, 62, 174, 380, 381, 470, 469, 502]
	RAS	IGF-1 | Wnt	RAS can either be activated by binding of Src homology 1 which is activated downstream of IGF-1 (here directly by IGF-1) or based on non-canonical Wnt signalling activating Dishevelled (Dvl, here directly via Wnt) [8, 92, 206, 273, 274, 331, 486, 490]
	RAF	(RAS | PKC) & !AKT	Rapidly accelerated fibrosarcoma (RAF) can be activated either by RAS or protein kinase C (PKC) if not inhibited by AKT [15, 92, 208, 232, 237, 273, 274, 282, 339, 418, 469]

Table 1: Boolean functions of the IGF-1/Wnt crosstalk model and their descriptions modified from Siegle, Schwab, Kühlwein et al. [387], licensed under CC BY 4.0, https://creativecommons.org/licenses/by/4.0/. All proteins are abbreviated in accordance with the current nomenclature. Logical connectives are depicted by & (=AND), | (=OR), and ! (=NOT).

	Node; t + 1	**Boolean network function; t**	**Description**
IGF-1 subnetwork	ERK	RAF	RAF activates ERK [92, 224, 273, 288, 404]
	mTORC2	!(S6K | GSK3β) & (PI3K | TSC2)	mTORC2 is inhibited by S6K. GSK3β acts negatively on an adenosine monophasphate-activated protein thereby lowering mTORC2 activity (here GSK3β inhibits mTORC2). Although the mechanism is not yet fully elucidated, TSC2 as well as PI3K activity seems to be important for mTORC2 activation [37, 65, 94, 174, 175, 274, 347, 469, 472, 510]
Wnt subnetwork	Wnt	Wnt	Wnt ligands are glycoproteins which are able to act in a paracrine fashion. They bind to a frizzeled receptor (FZD) and its co-receptor lipoprotein receptor-related protein 5/6 (LRP5/6) thereby activating Dvl (here Wnt is self-activating) [203, 326, 463]
	Axin	ERK | !Wnt	Axin is activated by ERK or inhibited by Wnt [326, 361]
	GSK3β	!(Wnt | ERK | AKT)	Dvl activated by Wnt inhibits GSK3β. Additionally, GSK3β is inhibited by ERK or AKT [62, 96, 167, 203, 207, 208, 274, 326, 363, 430, 483]
	DC	Axin & GSK3β	Together, Axin and GSK3β form the destruction complex (DC) [203, 326, 463]

Table 1: Boolean functions of the IGF-1/Wnt crosstalk model and their descriptions modified from Siegle, Schwab, Kühlwein et al. [387], licensed under CC BY 4.0, https://creativecommons.org/licenses/by/4.0/. All proteins are abbreviated in accordance with the current nomenclature. Logical connectives are depicted by & (=AND), | (=OR), and ! (=NOT).

	Node; t + 1	**Boolean network function; t**	**Description**
Wnt subnetwork	CTNNB1	!DC	The DC targets CTNNB1 for proteasomal degradation [203, 326, 463]
	TCF	CTNNB1 & !(JNK & FOXO)	T-cell specific transcription factor (TCF) and FOXO compete for binding to CTNNB1 which activates both. In the presence of JNK, a further activator of FOXO there is an imbalance in the binding of TCF and FOXO in favour to FOXO, thus inhibiting TCF [167, 186, 266, 282, 330, 391, 483, 498]
	FOXO	!AKT & CTNNB1	Phosphorylation by AKT inhibits FOXO. To function as a transcription factor FOXO is dependent on CTNNB1 [44, 62, 167, 243, 335, 470, 498]
	RHOA	(Wnt | PI3K | mTORC2) & !(RAC1 | PKC)	Wnt molecules as well as PI3K or mTORC2 can activate RHOA. Ras-releated C3 botulinum toxin substrate 1 (RAC1) and RHOA are responsible for different functions on the actin cytoskeleton, causing them to inhibit each other. RHOA-activated PKC forms a negative feedback loop and inhibits RHOA [36, 37, 41, 65, 123, 140, 150, 158, 203, 207, 252, 285, 329, 337, 347, 356, 363, 430, 493, 502, 508, 509]

Table 1: Boolean functions of the IGF-1/Wnt crosstalk model and their descriptions modified from Siegle, Schwab, Kühlwein et al. [387], licensed under CC BY 4.0, https://creativecommons.org/licenses/by/4.0/. All proteins are abbreviated in accordance with the current nomenclature. Logical connectives are depicted by & (=AND), | (=OR), and ! (=NOT).

	Node; $t+1$	**Boolean network function;** t	**Description**
Wnt subnetwork	RAC1	(Wnt | PI3K | mTORC2) & !RHOA	Wnt molecules as well as PI3K or mTORC2 can activate RHOA. RAC1 and RHOA are responsible for different functions on the actin cytoskeleton causing them to inhibit each other [36, 37, 65, 123, 140, 150, 158, 203, 207, 252, 285, 329, 337, 347, 356, 363, 430, 493, 502, 508]
	MEKK1	RAC1 | RHOA	Both RAC1 and RHOA are able to activate mitogen activated protein kinase kinase kinase 1 (MEKK1) [92, 237]
	PKC	RHOA | Wnt | mTORC2	Activated Dvl (here Wnt) stimulates phospholipase C (PLC) that hydrolyses phosphatidylinositol-(4,5)-bisphosphate (PIP2) into diacylglycerol (DAG) leading to further activation of PKC. Furthermore, PKC can be activated by RHOA or mTORC2 [37, 94, 203, 207, 244, 430, 469, 498]

Simulations with all state combinations (exhaustive simulation) of the IGF-1/Wnt crosstalk model revealed five attractors with different frequencies of occurrence (Figure 13). Having two input nodes, there are four possible input combinations for the model. First, all external inputs are absent. This condition would correspond to an unstimulated cell. Another possibility is that both external inputs, IGF-1 and Wnt, are present. However, IGF-1 concentration drops during ageing while Wnt concentration increases [172]. Thus, a period during which both are active would be consistent with a mid-aged phenotype. Instead, the two combinations of either IGF-1 or Wnt active represent a young and aged phenotype respectively.
Based on these input combinations, attractor 1 (Figure 13) can be assigned to an unstimulated cell. Moreover, attractor 2 and 5 (Figure 13) with only IGF-1 as input are assigned to a young phenotype. Attractor 3 (Figure 13) shows both inputs in an active state. Therefore, it can be matched to the mid-aged phenotype. Finally attractor 4 (Figure 13) in which only Wnt as external input is active can be assigned to an aged-phenotype.

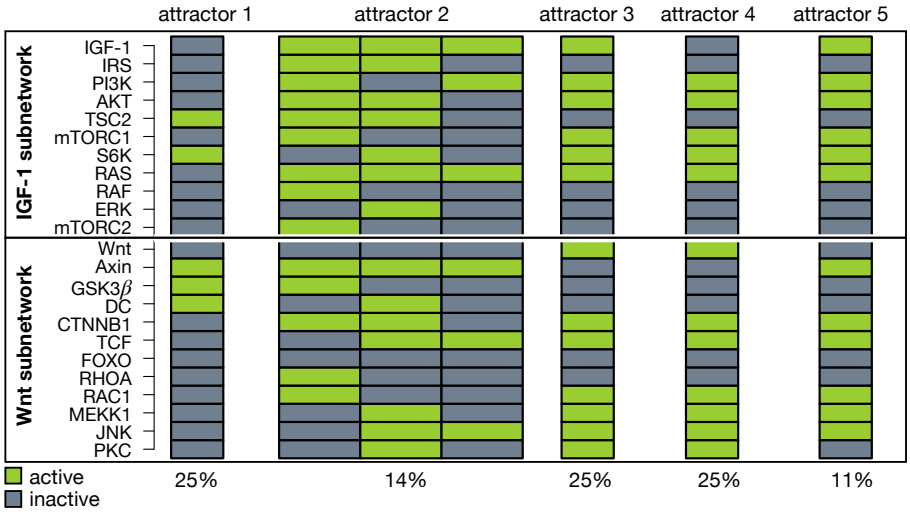

Figure 13: **Attractors of the IGF-1/Wnt crosstalk.** An exhaustive attractor search was performed to reveal the long-term behaviour of the IGF-1/Wnt crosstalk model. It yields four single state and one three-state attractors with different frequencies of appearance (percentage below). The nodes in the attractors were separated by boxes to show their pathway affiliation. The activity of each node listed on the left side is depicted by coloured rectangles. Here, green represents an active state while grey represents an inactive state. The figure has been modified from Siegle, Schwab, Kühlwein et al. [387], licensed under CC BY 4.0, https://creativecommons.org/licenses/by/4.0/.

3.1.1.1 *From young to old - modelling the process of ageing*

A good model depicts reality as closely as possible. In order to test the temporal behaviour of the IGF-1/Wnt crosstalk model and whether it is able to depict ageing, the simulation was started from a completely inactive state of the network. Subsequently, IGF-1 and Wnt were regulated according to their temporal changes during ageing by fixing their state constantly to 1 [38, 249] (Figure 14). The first part of the simulation ends after four steps in time in a single state attractor. This attractor could be matched to attractor 1 (Figure 13). As defined before, it represents an unstimulated cell since both external inputs are inactive.

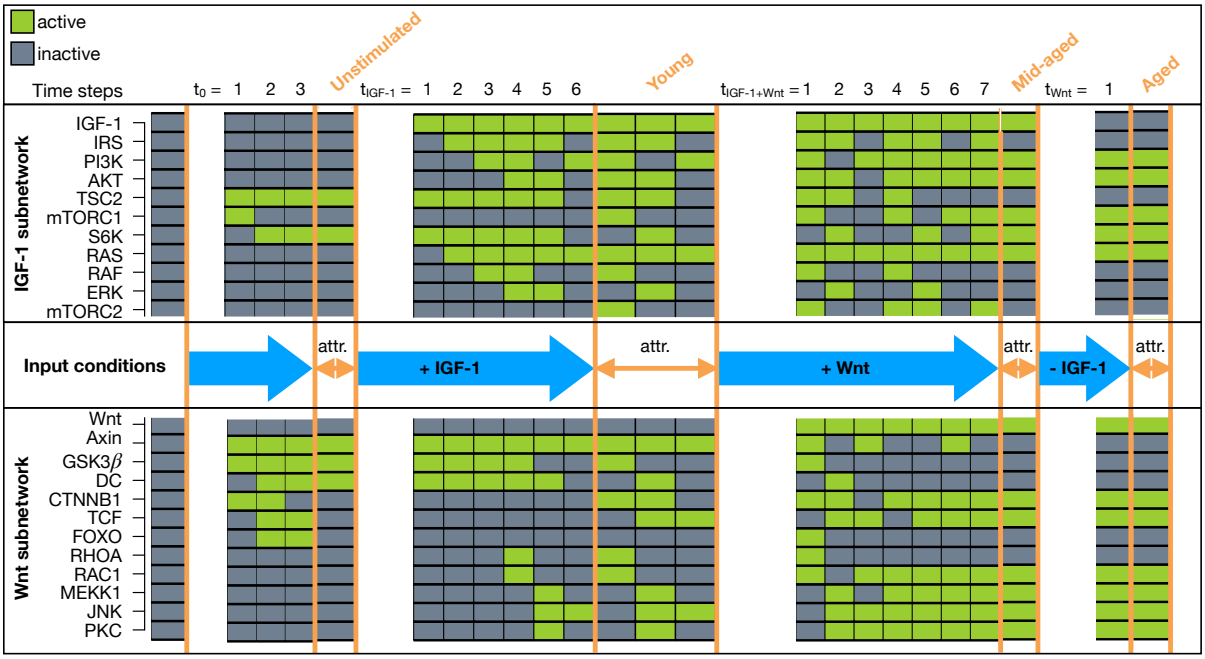

Figure 14: **Progression of ageing.** During ageing IGF-1 signalling declines while Wnt signalling increases in satellite cells [172]. This can be simulated by inhibiting IGF-1 and activating Wnt respectively in a cascade (switch is depicted by blue arrows). The simulation of ageing was performed starting from a state with completely inactive components and a synchronous updating scheme. After an attractor (orange arrow separated by orange lines) has been reached, a new input condition was introduced into the states of the attractor and the simulation was continued. The components of the network are listed on the left and separated into the two subnetworks. The state of each component is represented by green (=active) and grey (=inactive) rectangles. The time steps from one attractor into another are listed above. The figure has been modified from Siegle, Schwab, Kühlwein et al. [387], licensed under CC BY 4.0, https://creativecommons.org/licenses/by/4.0/.

Starting the simulation from a completly inactive state, the model first activates CTNNB1. Based on the initial condition, CTNNB1 is not inhibited by the DC. However, in consideration of the missing Wnt activation, Axin and GSK3β are also active and build the DC that further inhibits CTNNB1 [203, 326, 463] and its downstream targets TCF and FOXO [266]. The IGF-1 pathway with its associated proteins is not activated during the whole cascade. Because TSC2 is not inhibited downstream of IGF-1 signalling, it is active and inhibits mTORC1 [178]. In addition, TSC2 is activated by GSK3β as well as S6K [178, 380].
During youth and at the beginning of life, IGF-1 is present. Therefore, to simulate a young phenotype, IGF-1 was activated in the attractor of an unstimulated cell and the model progressed from the single state attractor towards a three-state attractor (Figure 14). This attractor is the same as the one previously found to represent the young phenotype (attractor 2 in Figure 13). Within this attractor, nearly all components are highly regulated and crosstalk between IGF-1 and Wnt can be observed. Even without external activation of Wnt molecules CTNNB1 and its downstream targets are partially active.
Activation of IGF-1 in an unstimulated cell immediately activates the two downstream cascades RAS-RAF-ERK and PI3K/AKT [44]. Due to crosstalk ERK as well as AKT inhibit GSK3β and hence activate CTNNB1 [272]. Under physiological conditions everything is regulated and, therefore, S6K inhibits IGF-1 by inhibiting IRS and mTORC2 [469]. The observed activation of AKT, ERK as well as S6K by IGF-1 is supported by the findings of Rommel et al. [336].
In the process of ageing, Wnt starts to increase. Hence, there is a time when both IGF-1 and Wnt are active. To simulate this condition Wnt was activated in the attractor of a young phenotype. No matter from which state of the young attractor the simulation starts, it ends in one single state attractor. This attractor can be matched to attractor 3 (Figure 13).
Induced by the activity of Wnt, the DC gets inhibited leading to activation of canonical Wnt signalling [203]. Thereby CTNNB1 or TCF are activated as described by Naito et al. [292] or Watanabe et al. [448] for satellite cell ageing. In addition, Wnt further activates non-canonical signalling [203] (activation of PKC). During the progression from young to mid-aged components of the IGF-1 cascade are still regulated while Wnt signalling starts to stabilise. Thus, the RAS-PI3K-AKT cascade is constitutively active leading to inhibition of RAF and activation of S6K. These findings are in line with the observations by J. von Maltzahn et al. [435] which were not used for network construction. Here, the authors could show that cross-activation of the IGF-1 cascade is induced by Wnt7a [435]. Based on the active proteins within this attractor, there exists an imbalance between IGF-1 and Wnt signalling. IGF-1 signalling is now reduced since S6K constitutively inhibits IRS [469] and also its downstream target ERK is inhibited due to constitutively active AKT [92].

Since activation of Wnt already reduced the effect of IGF-1 while stabilising some crosstalk components, the additional removal of IGF-1 in the simulation of ageing did not show any further effects on the attractor. The resulting attractor can be matched to attractor 4 (Figure 13).
In summary, it was possible to model ageing in a stepwise manner based on a temporal ageing-related regulation of the two inputs IGF-1 and Wnt. Consequently, the model seems to be able to depict the progression of ageing in this context. It should be noted that the simulation starting from an unstimulated cell with activity changes of IGF-1 and Wnt never passed or resulted in attractor 5. Therefore, this attractor was excluded from further analyses.

3.1.1.2 *The aged-phenotype is prone to develop ageing associated diseases*

Ageing is not the cause for the development of diseases and cancer, but alterations in signalling cascades can promote their initiation [151]. The comparison of the mid-aged attractor with the aged attractor already showed an imbalance between IGF-1 and Wnt signalling. Here, both attractors show the same long-term behaviour even if IGF-1 signalling is present as input. These two attractors depict symptoms of cancer or characteristics prone to develop age-associated diseases.
On the one hand, both attractors show constitutively active mTORC1. This protein can be related to the induction of diabetes mellitus type II [145]. Furthermore, mTORC1 is able to inhibit autophagy thus contributing to possible accumulation of damaged cells [57, 340]. Two other characteristics in these attractors that can be associated with cancer development are the constitutive activation of AKT and TCF. AKT which is frequently active in cancers [121, 147] regulates further downstream targets whose activity also supports cancer development. Here, AKT's activity suppresses GSK3β [121]. This inhibition of GSK3β further enhances the activity of canonical Wnt signalling. In addition, AKT inhibits pro-apoptotic proteins like BAD or caspase-9 [147, 457]. Thereby it prevents the induction of apoptosis which is a common rescue mechanism of healthy cells [100, 147]. Furthermore, AKT is responsible for the relocalisation of cell cycle inhibitors into the cytoplasm which supports cell cycle progression and accelerates proliferation [100, 107]. The increased cell cycle progression is further supported by the activity of TCF inducing the expression of cyclin D [379, 419]. Hence, based on their impact on downstream targets both proteins promote high proliferation rates and formation of cancer.
Another characteristic of the attractors with increased Wnt signalling is the activity of S6K. However, S6K stimulates the development of diabetes mellitus type II, a common ageing-associated disease by inhibiting IRS [74, 495].

3.1.1.3 *Only IGF-1/Wnt crosstalk is able to model ageing*

As shown by the Boolean network approach, changes in the IGF-1 and Wnt concentration can promote age-associated diseases. This seems to be because IGF-1 decreases in concentration while Wnt increases. To further substantiate the presumption that IGF-1/Wnt crosstalk promotes ageing the crosstalk model was divided into its single pathways (Tables 2, 3) and IGF-1 and Wnt signalling pathways were simulated separately.

Table 2: Boolean functions of the IGF-1 subnetwork taken from Siegle, Schwab, Kühlwein et al. [387], licensed under CC BY 4.0, https://creativecommons.org/licenses/by/4.0/. All proteins are abbreviated in accordance with the current nomenclature. Logical connectives are depicted by & (=AND), | (=OR), and ! (=NOT).

Node; $t+1$	**Boolean network function;** t
IGF-1	IGF-1
IRS	IGF & !S6K
PI3K	(IRS | RAS)
AKT	PI3K | mTORC2
TSC2	! (AKT | ERK)
mTORC1	!TSC2
S6K	mTORC1
RAS	IGF-1
RAF	RAS & !AKT
ERK	RAF
mTORC2	!S6K & (PI3K | TSC2)

Table 3: Boolean functions of the Wnt subnetwork taken from Siegle, Schwab, Kühlwein et al. [387], licensed under CC BY 4.0, https://creativecommons.org/licenses/by/4.0/. All proteins are abbreviated in accordance with the current nomenclature. Logical connectives are depicted by & (=AND), | (=OR), and ! (=NOT).

Node, t + 1	**Boolean network function; t**
Wnt	Wnt
Axin	!Wnt
GSK3β	!Wnt
DC	Axin & GSK3β
CTNNB1	!DC
TCF	CTNNB1 & !(JNK & FOXO)
FOXO	JNK
RHOA	Wnt & !(RAC1 | PKC)
RAC1	Wnt & !RHOA
MEKK1	RAC1 | RHOA
JNK	MEKK1 | RAC1
PKC	RHOA | Wnt

The separated simulation of the IGF-1 network (Figure 15 IGF-1 subnetwork) revealed three attractors A-C with different lengths and percentages of occurrences. In comparison to the attractor patterns of the crosstalk simulation (Figure 13), only the pattern of attractor A could be matched to the patterns of the IGF-1 part of attractor 3 and 5 in the crosstalk model. The other two attractors B and C of the IGF-1 subnetwork simulation did not match.
The same behaviour as noted for the IGF-1 subnetwork simulation can be observed by simulating the Wnt cascade by itself. Simulating Wnt signalling revealed two single state attractors D and E (Figure 15 Wnt subnetwork). Likewise, only attractor D of the Wnt subnetwork simulation could be matched to the pattern of the Wnt part in the crosstalk model (Figure 13).

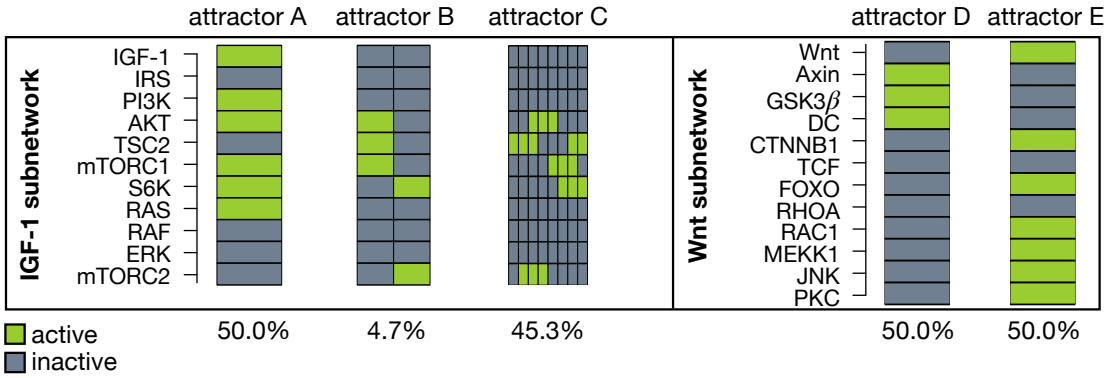

Figure 15: **Dynamics of subnetworks.** The crosstalk regulations were removed from the model and the long-term behaviour of both signalling pathways without crosstalk was simulated. The simulation of the IGF-1 subnetwork revealed three attractors A-C while the simulation of the Wnt subnetwork showed two attractors D-E. The state of each component in the subnetworks listed on the left side is represented by green (=active) and grey (=inactive) rectangles. The frequency of appearance is depicted in percentage below each attractor. The figure has been modified from Siegle, Schwab, Kühlwein et al. [387], licensed under CC BY 4.0, https://creativecommons.org/licenses/by/4.0/.

In total, three attractor patterns of the simulation without crosstalk could not be matched to the attractor patterns of the corresponding crosstalk simulation. Thus, the crosstalk seems to stabilise the individual signalling pathways leading to the disappearance of some attractor patterns. In contrast, there was no overlap to the attractor patterns of young- (attractor 2) and aged-phenotype (attractor 4) in the simulation of each signalling cascade by itself. Consequently, modelling of ageing appears to be possible only if the crosstalk between IGF-1 and Wnt exists.

3.1.1.4 *Only IGF-1/Wnt crosstalk shows superior robustness*

Each organism is daily exposed to environmental changes. Nevertheless, biological systems are considered to be robust and are able to adapt to changes [212]. In order to investigate if this behaviour can also be found in the IGF-1/Wnt crosstalk model, random state changes were performed. Next, the successor state of the original state and the perturbed state were compared using the normalised Hamming distance. The Hamming distance takes all proteins into account which differ from the original network. A small Hamming distance is desirable because it supports that the model is able to adapt to changes [128]. In order to judge model robustness as challenged by 100 random performed state changes, its behaviour was compared to 1000 randomly generated Boolean network models of the same

size (Figure 16). Here, it could be shown that the IGF-1/Wnt crosstalk model (mean normalised Hamming distance = 0.043) is significantly more robust ($p < 10^6$) to randomly performed state changes in comparison to randomly generated Boolean network models.
Unlike the IGF-1/Wnt crosstalk model, the robustness analysis of the subnetworks against randomly state changes revealed a mean normalised Hamming distance of 0.05 and 0.09, respectively. These results are not significantly better ($p_{IGF-1} = 0.5$, $p_{Wnt} = 0.2$) than the performance of randomly generated networks. Thus, it cannot be excluded that the observed effect is based on chance.

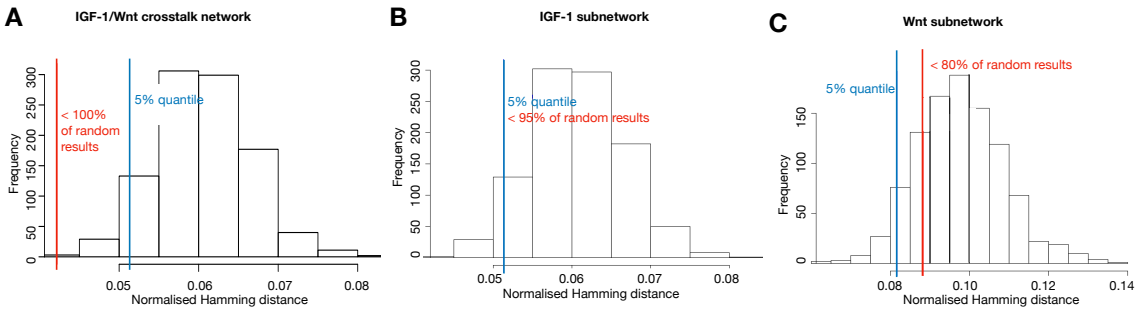

Figure 16: **The crosstalk model is more robust.** Model robustness can be judged by calculating the mean normalised Hamming distance of the model in comparison to randomly generated models. This was done for (A) the IGF-1/Wnt crosstalk model as well as for (B) the IGF-1 subnetwork and (C) the Wnt subnetwork. The histogram depicts the performance of the established crosstalk model (red line) in comparison to 1000 randomly generated Boolean network models (blue line = 5% quantile). The figure has been modified from Siegle, Schwab, Kühlwein et al. [387], licensed under CC BY 4.0, https://creativecommons.org/licenses/by/4.0/.

3.1.2 *Discussion – IGF-1/ Wnt crosstalk*

3.1.2.1 *Importance of the IGF-1/Wnt crosstalk during ageing*

Each day an organism has to adapt to environmental changes or has to sustain external alterations induced by for example UV-light. Assuming that biological systems are robust against random changes, a comparison to randomly generated ones of similar structures can be made [22, 212, 501]. If the generated Boolean network model is not significantly more stable than randomly generated models of the same size biological relevance may be doubted [196, 501].
The IGF-1/Wnt crosstalk model shows significantly increased stability compared to randomly generated networks as long as the crosstalk between IGF-1 and Wnt exists (Figure 16). In fact, as soon as crosstalk interactions are removed from the model the subnetworks do not perform better than random networks ($p_{IGF-1} = 0.5$, $p_{Wnt} = 0.2$). This fact supports the importance of crosstalk between both pathways since crosstalk stabilises both pathways leading to the disappearance of oscillating attractors (Figure 15).
In the course of ageing IGF-1 decreases while Wnt signalling increases in concentration [172]. For this reason, the simulations are based on the assumption that IGF-1 is active initially. This ratio shifts over time from an equilibrium towards active Wnt only. These assumptions are supported by descriptions of high Wnt activity in aged satellite cells [38, 249]. Furthermore, another report shows enhanced muscle mass after IGF-1 overexpression [25] which is the opposite of sarcopenia [133, 223, 228, 433]. However, neither simulations with IGF-1 alone nor simulations with only Wnt were able to maintain the young and aged phenotype achieved by crosstalk simulations (Figure 15). This fact supports the hypothesis that common objectives which are regulated by crosstalk are important for the process of ageing. However, structural changes in the signalling pathway due to the omission of regulations can be excluded. Independent studies could show that the ageing phenotype of satellite cells can be accelerated by increasing Wnt concentrations [38, 249].
Ageing is a complex process [151]. Thus, it is obvious that IGF-1 and Wnt are not the sole key players responsible for ageing. A multitude of other growth factors exists that can influence one of the two signalling pathways too [133]. These regulations are most likely responsible for alterations in the concentrations of IGF-1 and Wnt during ageing. A direct influence of Wnt on IGF-1 via miRNA-29 may also be possible [172]. The focus of this network was limited to a core network describing IGF-1 and Wnt crosstalk. Since this model was established based on literature search all possible interactions had to be examined manually. For this reason, this type of modelling reaches the limits of feasibility according to the model size at some point. Despite these limitations, the model has proven its biological rele-

vance. In the future, it can be extended by including further signalling pathways and components.

3.1.2.2 *Dealing with the contradictory role of Wnt signalling during ageing*

The capacity of stem cell self-renewal declines during ageing [251, 417]. Numerous studies associate alterations in canonical Wnt signalling with the process of ageing [38, 249, 330, 430]. However, its impact seems to be contradictory and differs between populations of stem cells. While Wnt signalling increases in concentration during satellite cell ageing, its decrease is reported to be responsible for neural stem cell dysfunction [308] as well as intestinal [417] and hematopoietic stem cell ageing [117]. One reason for this complex and contradictory behaviour of Wnt in different stem cell populations may be the overlapping functions of multiple pathways. In contrast to satellite cells where the balance between IGF-1 and Wnt is responsible for maintaining stem cell functions, in intestinal stem cells this process is regulated by Wnt and Notch [422].
In addition, it is not fully understood which receptors and co-receptors of the Wnt signalling pathway and which Wnt molecules are involved [205]. In mammals there are 19 Wnt ligands [205] known to bind to one or more of the 15 Wnt-receptors and co-receptors [301]. Receptor binding induces activation of canonical and non-canonical signalling cascades. However, the combination of ligands and receptors that impact different downstream cascades are not fully elucidated. In order to overcome this limitation of knowledge the model simplifies this by considering only one Wnt-ligand and one receptor and having their interactions be enough to activate both canonical and non-canonical Wnt signalling (Figure 12).

3.1.3 *NF-κB signalling during ageing*

Sarcopenia, the loss of skeletal muscle, is a major problem during healthy ageing and NF-κB signalling seems to have a leading part in this process [236]. Similar to Wnt signalling, NF-κB signalling intensifies with age [38, 256, 423]. It has been shown that NF-κB signalling has an influence on the ageing phenotype of myofibers [80, 236]. Therefore, these cells have been proven to be a suitable model system to study NF-κB signalling in ageing.
Boolean network models can be constructed based on intensive literature search or on the basis of expression data taken from time series. The GSE362 dataset [453] is one of few datasets containing time series of gene expression data. For this reason, it was used to study NF-κB signalling based on a data-driven approach. In order to get insights into the temporal changes of NF-κB signalling during ageing, the GSE362 dataset containing expression data of young and aged human muscle samples was considered [453]. This dataset includes 15 samples ranging in age between 21 years and 75 years which could be divided into two groups young (21 - 27 years old) and aged (67 - 75 years old). Based on these two groups separate Boolean network models were reconstructed representing young and aged phenotypes.

3.1.3.1 *Fewer Boolean functions can be found for the aged phenotype*

The complexity and computational time to simulate Boolean network models increase exponentially with every additional node. To overcome this limitation initially only genes assigned to NF-κB signalling according to the KEGG database [192] were considered for the network reconstruction. The gene set consists of 95 genes in total but only 86 out of these genes were available in the considered dataset [365]. In order to further reduce the number of genes for the reconstruction only significantly binarizable genes according to BASC's significance test ($p < 0.05$) [169, 290] were considered. This procedure reduces the number of genes to 22. All genes that were used for network reconstruction are listed in Table 4 with their Entrez IDs.

Table 4: Genes with their corresponding Entrez IDs that were used for network reconstruction.

Gene	Entrez ID	Gene	Entrez ID
TAB1	10454	PRKCQ	5588
CHUK	1147	PTGS2	5743
CSNK2A2	1459	BTK	695

Table 4: Genes with their corresponding Entrez IDs that were used for network reconstruction.

Gene	Entrez ID	Gene	Entrez ID
ERC1	23085	TNF	7124
CARD10	29775	TRAF1	7185
IRAK1	3654	TRAF3	7187
LBP	3929	TRAF5	7188
LTA	4049	TNFSF11	8600
LTBR	4055	BCL10	8915
PLCG2	5336	CD14	929
PRKCB	5579	CD40	958

Using the best-fit algorithm [222] multiple possible Boolean function variants were reconstructed for each protein (Table 4) which reflected the proteins' behaviour in the time series. In total it was possible to identify up to 59 (mean 17) and up to 39 (mean 7) Boolean functions for each protein of the young phenotype and the aged phenotype, respectively. Despite these huge variations, the input degree per function differed barely between both age groups (Figure 17A). Four proteins of the aged phenotype (TRAF5, PLCG2, IRAK1 and CARD10) were constantly reconstructed with a Boolean function set to zero (Figure 17C). The mean input degree of the aged phenotype was 1.27 while the one for the young phenotype was 1.32 (Figure 17A). To confirm that the reconstructed interactions represent real biological regulations, identified interactions were verified based on the protein interaction database STRING [392]. Although database search was limited to data from experiments or curated databases all reconstructed dependencies could be found as either direct or indirect connections (data not shown, see Schwab, Siegle, Kühlwein et al. [365] Supplement S2).
On the basis of the identified Boolean functions, 1000 synchronous Boolean network models were created for each phenotype by randomly choosing one of the reconstructed Boolean functions per protein. Two of these networks are exemplarily represented in Figure 17B and 17C. Both networks show comparable inputs which are in line with the initial finding of equally input degrees.

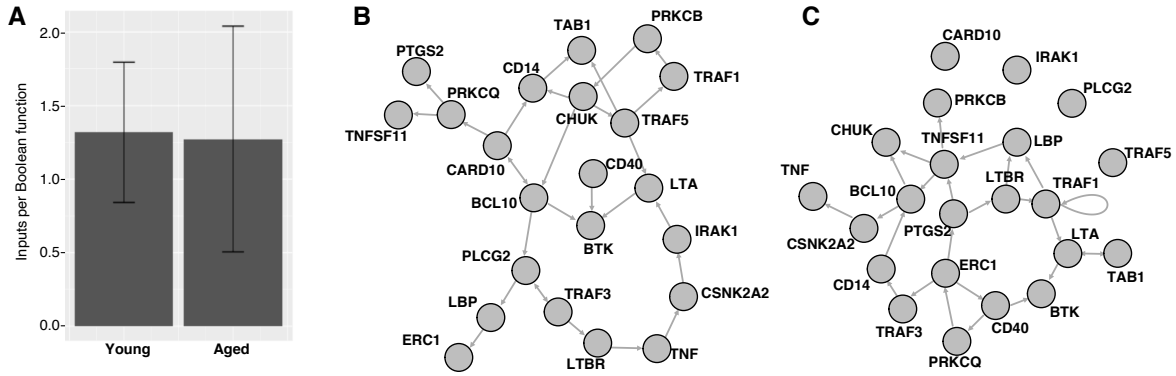

Figure 17: **Reconstructed network interactions.** (A) Mean number of inputs per Boolean function based on the network reconstruction with error bars showing the standard deviation. Regulatory interactions in an exemplarily young (B) and aged (C) reconstructed Boolean network. Arrows represent the direction of regulation. This figure has been modified from Schwab, Siegle, Kühlwein et al. [365], licensed under CC BY 4.0, https://creativecommons.org/licenses/by/4.0/.

3.1.3.2 *Aged phenotype is more prone to alterations*

As further support of the biological representativeness of the reconstructed networks, their stability against perturbation was examined. Biological networks are considered to be robust and withstand external alterations. In order to confirm this behaviour for the reconstructed networks, random bitflip alterations were simulated on the state x(t) and their effects were studied on the long-term behaviour of the complete networks. To compare the impact of the perturbation the normalised Hamming distance was calculated between the direct successor state of the perturbed network $x'(t+1)$ and the successor state of the original state $x(t+1)$. The same procedure was performed after five state transitions. In total, 1000 random start states were drawn and the perturbation of these states, their successor states and their attractor states were studied for each of the 1000 reconstructed networks of the young and aged phenotypes (Figure 18).

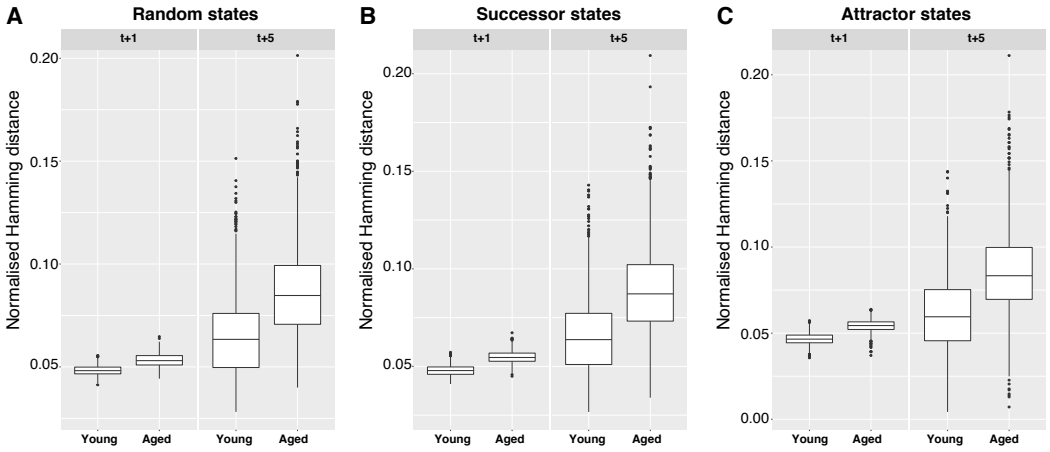

Figure 18: **Aged phenotype is more prone to perturbations.** (A) 1000 random start states were created and the normalised Hamming distance was calculated between the perturbed states and their original states after one and five state transitions. Additionally, the long-term effect of the perturbation was studied on the successor states (B) and the corresponding attractor states (C) of these randomly chosen states. The average normalised Hamming distance is shown with significant differences between young and aged phenotype (Wilcoxon rank sum test $p < 2.2 \cdot 10^{-16}$). This figure has been modified from Schwab, Siegle, Kühlwein et al. [365], licensed under CC BY 4.0, https://creativecommons.org/licenses/by/4.0/.

Table 5: Normalised Hamming distance was taken into account to examine the effect of bit flip alterations on 1000 random start states, their successor states as well as their attractor states. The table was modified from Schwab, Siegle, Kühlwein et al. [365], licensed under CC BY 4.0, https://creativecommons.org/licenses/by/4.0/.

one state transition	Young phenotype			Aged phenotype		
	min	max	mean	min	max	mean
random initial state	0.041	0.056	0.048	0.044	0.065	0.053
random successor state	0.041	0.057	0.048	0.045	0.067	0.055
random attractor state	0.036	0.057	0.047	0.037	0.064	0.054
five state transitions	**Young phenotype**			**Aged phenotype**		
	min	max	mean	min	max	mean
random initial state	0.028	0.151	0.063	0.040	0.201	0.085
random successor state	0.027	0.143	0.064	0.034	0.209	0.087
random attractor state	0.004	0.144	0.060	0.007	0.211	0.083

This analysis shows that for both ageing phenotypes the deviations increase by seven to eight fold with a rising number of transitions (Figure 18, Table 5). Further conclusion can be drawn from the analysis of the normalised Hamming distance by comparing the mean normalised Hamming distances. A smaller normalised Hamming distance can be associated with a more robust network which is more plausible biologically. The comparison to the networks of the ageing phenotypes showed that the networks of the young phenotype are more robust against state perturbations compared to networks of the aged phenotype. After one state transition the mean normalised Hamming distance of the aged phenotype already increased by between 10% and 15% compared to the young phenotype. This behaviour increased again to 35% - 38% after five state transitions (Figure 18, Table 5).

3.1.3.3 *Loss of compensatory pathways with age*

The analysis of the normalised Hamming distance showed that there are differences in the stability of the young and aged phenotype networks. The next question that arises from this observation is what causes the differences in stability. A reduced number of regulatory factors per gene can already be excluded since the mean input degrees per Boolean function of 1.32 and 1.27 respectively were nearly the same for both ageing phenotypes (Figure 17). However, during the network reconstruction, it became apparent that less possible Boolean functions per gene could be found for the aged phenotype. On the basis of this observation, the gene dependencies in young and aged networks were examined in more detail. Therefore, all directed interactions found by the best-fit algorithm were summarised in an adjacency matrix (Appendix Table 10, 11). While for the young phenotype 158 different dependencies could be found altogether, only 125 dependencies were found for the aged phenotype. This observation leads to the conclusion that some compensatory signalling pathways disappear in the process of ageing. The lack of compensation can cause damage to spread which is correlated with the larger Hamming distance previously found in the old phenotype (Section 3.1.3.2). Besides, the accumulation of damage can be associated with age-associated diseases.

3.1.4 *Discussion – Modelling ageing*

3.1.4.1 *Dynamical changes during ageing*

Many ageing-associated processes are caused by concentration changes of endocrine factors [139, 151, 315]. Two well-studied pathways in the process of ageing are IGF-1 and NF-κB [139, 201, 256, 299, 315, 423] both playing a role in satellite cell ageing [80, 172, 236]. Although IGF-1 and NF-κB signalling are regulated in opposite directions in the course of ageing [80, 172, 236] both have parallels in the dynamics of their networks.
First differences between the young and aged phenotype could be observed when gene expression values were binarised. While all 22 significantly binarizable genes of the young phenotype change their activity level, four genes of the old phenotype were constantly switched off. Similar changes could also be observed in the IGF-1/Wnt crosstalk model compared to NF-κB signalling with regard to ageing. Here, exhaustive simulations indicate that a regulated multi-state attractor can only be reached when IGF-1 alone is active. The corresponding attractor could be assigned to a young phenotype. However, IGF-1 signalling drops while Wnt signalling steadily increases with age [172]. Thus, simulations with additional Wnt activity lead to attractors which show states with constant active or inactive components. Epigenetic changes that lead to the silencing of a majority of genes only required during initial embryonic development are well-known [51]. But gene silencing by DNA methylation, chromatin remodelling or histone modifications proceeds during ageing [51, 256]. In line with this, 57% of genes that are altered in an aged phenotype show reduced expression levels [53]. Continuous silencing of genes is associated with progressive ageing, in particular, cell cycle regulators, as well as tumour suppressors or inflammatory regulators, are affected [51, 256]. Thus, it is not surprising that four genes of the reconstructed NF-κB signalling are found to be constitutively inactive.
Furthermore, stability analyses showed clear differences between the young and aged phenotypes. It was shown that the young phenotype was much more robust against different types of internally induced stresses than the old phenotype. However, the reduced network connectivity of all nodes can be excluded. Both phenotypes had approximately the same number of regulators per Boolean function. On the other hand, the networks of both phenotypes showed large differences in the number of Boolean functions found per component. This suggests that the lower robustness of the old phenotype to disturbances is due to a decrease in redundant regulations. In general, redundancy is considered as an important criterion for stability in network theory [213]. Nevertheless, biological observations also support the assumption that lack of redundancy is responsible for the loss of stability. For example, several comparative studies found that longer-living mammals have a

higher abundance of redundant essential genes than short-living species [81, 275]. All these studies support the assumption of stability reduction due to the loss of redundancy.

3.1.4.2 *Alterations during muscle ageing support development of diseases*

Skeletal muscle mass accounts for the majority of the body mass (40% of lean body mass) [267]. For this reason, muscles are the main regulators of metabolic and inflammatory signalling pathways that are also associated with immune functions [73]. A decrease in muscle mass takes place in normal, healthy ageing. However, once this decline in muscle mass becomes pathogenic (sarcopenia) it is associated with an increased risk of cancer development, increased toxicity with medication and a lower survival prognosis [73]. Evidence of pathogenic pathway alterations also found in the analyses of the IGF-1/Wnt crosstalk model as well as in the reconstructed Boolean network models of the NF-κB pathway.
An augmentation of the Wnt pathway is associated with many age-related diseases, including diabetes mellitus type II [185], cancer [494] and atherosclerosis [120]. Simulations of ageing with the IGF-1/Wnt crosstalk model highlight that Wnt stimulation dominates IGF-1 stimulation (Figure 14). Thereby, pathogenic signalling pathways are activated. Insulin resistance of muscle cells is the primary trigger for diabetes [267]. Here, the mTOR signalling pathway which regulates the response to nutrients plays an important role [267]. It has already been shown in mouse models that the activation of mTORC1 by deletion of its inhibitor TSC1 leads to insulin resistance [145]. In addition, increased mTORC1 activity was observed in sarcopenic muscles [188]. Likewise, induced activation of mTORC1 resulted in muscle atrophy in young mice [57]. Furthermore, mTORC1 activity is described with inhibition of autophagy [188]. Autophagy decreases with age whereby damage can accumulate and contribute to age-associated diseases [340]. Based on these facts, it seems that an increase of mTORC1 which is already permanently active in the simulation of the mid-aged phenotype (Figure 14) is related to a pathogenic phenotype.
Besides, mTORC1 influences the activity of S6K and AKT [267]. Both become constitutively active in the simulation (Figure 14) and can be associated with the development of cancers by inhibiting apoptosis [100, 147] or inducing insulin resistance [74, 495]. Moreover, AKT is responsible for the relocalisation of cell cycle inhibitors and thus affects enhanced proliferation [100, 107] that contributes to cancer development.
On the basis of these comparisons, it can be concluded that not only Wnt dysregulation itself can be associated with ageing-associated diseases. This imbalance of Wnt in aged muscle cells has a further negative impact on other signalling pathways like mTORC1 or AK which also favour the development of ageing-related

diseases.
Results comparable to the IGF-1/Wnt crosstalk analysis were obtained from the analysis of reconstructed Boolean network models of NF-κB signalling. Similar to Wnt signalling, NF-κB levels rise during ageing and are reported to play a role in numerous ageing-associated diseases including Alzheimer's, sarcopenia, diabetes mellitus type II or atherosclerosis [423]. In contrast to the analysis performed with the IGF-1/Wnt crosstalk model the focus of the analysis of the NF-κB signalling networks was on static alterations.
During the reconstruction of various models for the young as well as the old phenotype, it has already been observed that fewer dependencies between proteins could be found for the aged phenotype. These results indicate, as mentioned before, a decrease in redundancy with age. Consequently, it is more likely that accidental damage to individual proteins will have more far-reaching consequences as they cannot be compensated. In this way, damage accumulates which is considered to be the main cause of cancer [88, 119, 256, 371].
Furthermore, the reconstruction of NF-κB signalling revealed that four proteins within the network, CARD10, IRAK1, PLCG2 and TRAF5, are not regulated in the aged model (Figure 17). Binarization of these proteins showed that they can be considered as inactive. It is possible to associate the inhibition of some of these proteins with the development of ageing-related diseases. CARD10, for example, regulates NF-κB signalling by inhibiting nuclear translocation of p65, thereby reducing angiogenesis [327]. However, in contrast to tumour development angiogenesis in muscle cells is linked to functional improvements. A clinical study could even show that patients with limited walking capacity were able to increase their walking performance after administration of angiogenic growth factors over a certain time [230]. Intensive pathway analyses indicate that normally regulated NF-κB signalling builds a negative feedback loop thereby inhibiting its own activity. Here, NF-κB activates miR-146a that induces the expression of the NF-κB inhibitor CARD10 [327]. Since CARD10 seems to be lost during ageing (Figure 17), NF-κB levels are not reduced anymore and inhibit angiogenesis [327] thus, leading to reduced muscle functionality, a phenomenon that is known to take place in the elderly [309].
Similar conclusions can be drawn for the inhibition of TRAF5 during ageing. Initially, inhibition of TRAF5 appears to be a positive event since the NF-κB pathway is the main cascade that can be activated downstream of TRAF5 [293]. However, it could be shown that TRAF5 deficient endothelial cells favour the adhesion of inflammatory cells and thus loss of TRAF5 contributes to the development of arteriosclerosis [283]. In addition, TRAF5 knockout is associated with lower antibody production of B cells [294] contributing to the decrease in the inflammatory response that can be observed with ageing [350]. Furthermore, it is assumed that

TRAF2 and TRAF5 are functionally the most similar proteins within the TRAF family members [293]. It has been shown that mice with a loss of TRAF2 suffer from impaired viability of skeletal muscle tissue [261]. Similar effects could also be caused by inhibition of TRAF5 due to the functional similarities of both proteins.
To sum up, both the dynamic as well as the static network analyses corroborate that alterations affecting the dynamics of the network contribute to the development of ageing-associated diseases.

3.2 Predicting the behaviour of cofilin-1 in pancreatic cancer

High-throughput screenings of pancreatic tissues identified CFL1 as a potential biomarker for pancreatic cancer [47, 134, 446]. Its role in actin-dynamics is well described [30, 442] and increased CFL1 expression is associated with migration and invasion of cancer cells [264, 442, 443, 479]. In contrast, less information is available on the involvement of CFL1 in cell cycle regulation and apoptosis induction.
Understanding the influences of CFL1 on the development of pancreatic cancer requires knowledge about its signalling pathways. Currently, it is known that CFL1 is overexpressed in pancreatic cancer [211, 355]. However, signalling pathways leading to this overexpression are unknown. The same applies to the regulation of proliferation downstream of CFL1. Additionally, the mechanisms of apoptosis inhibition and induction in pancreatic cancer cells still remain unresolved [211]. To reveal the impact of CFL1 on pancreatic cancer a Boolean network model was established whose simulation should address the behaviour of CFL1 in pancreatic cancer.

3.2.1 *A Boolean network model of CFL1 in pancreatic cancer*

Initially, the model was set up by collecting literature information about regulators of CFL1, actin-dynamics, proteins involved in the progression of G1- to S-phase transition and proteins involved in the induction of apoptosis with a focus on pancreatic cancer. Next, studies of CFL1-knockdown or overexpression experiments and their effects on downstream targets were considered. Finally, protein changes that play a major role in pancreatic cancer development and progression were considered and reciprocal regulations between all proteins involved in the model were taken into account.
During model setup, the most controversial information about a regulatory mechanism could be found for proliferation downstream of CFL1. On the one hand, it may be possible that CFL1 influences the cell cycle by inducing the expression of cell cycle inhibitors p21 and p27 as proposed by Tsai et al. [429] for lung cancer cells. However, overexpression of cell cycle inhibitors would lead to cell cycle arrest [91], if they are not transported out of the nucleus. A protein that is able to translocate cell cycle inhibitors to the cytoplasm is AKT [225, 226, 436]. AKT is considered to be highly active in pancreatic cancer [147]. Furthermore, p21 and p27 have a cytoplasmic role. Here, they inhibit RHOA and RAC1, thereby influencing actin dynamics [91]. On the other hand, CFL1 may affect proliferation by its activity on STAT3 expression as described by Wu et al. [464] in bladder cancer. Since STAT3 on its own is not involved in cell cycle regulation, its downstream targets may mediate its regulatory effects [162]. Both regulations may occur in

pancreatic cancer. Thus, two independent models were established and their performance was compared (Figure 19).

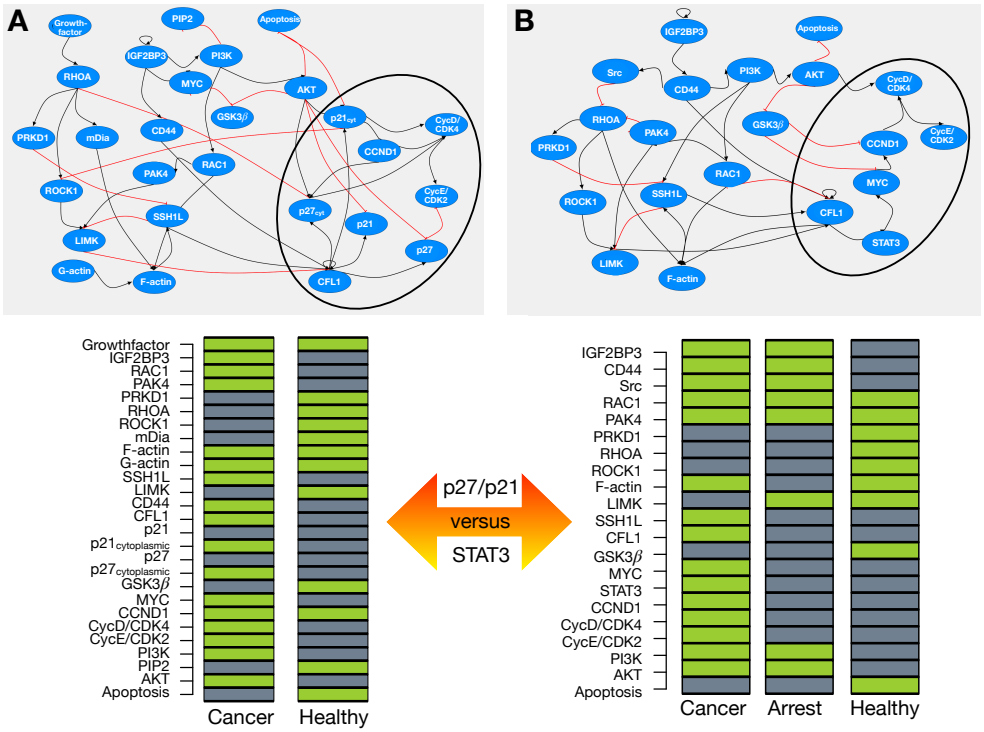

Figure 19: **Uncover cell cycle regulation downstream of CFL1 by simulation.** There are indications that cell cycle is regulated downstream of CFL1 by p21 and p27 (A) or by influences on STAT3 (B). In order to be able to support one theory, both possible regulations were included in separate initial Boolean network models and simulations were performed. Depicted are the interaction graphs and their corresponding attractors. Cell cycle regulation is highlighted in the interaction graph (black circle). Interactions are represented by edges between nodes. In the attractors, proteins are listed on the left while the activity of each protein is depicted by green (=active) and grey (=inactive) rectangles.

Model simulation including cell cycle inhibitors results in two single state attractors (Figure 19A). One of the two attractors shows a proliferative phenotype (active CycE/CDK2) without apoptosis and active CFL1. Based on the description of CFL1 in pancreatic cancer, this attractor is assigned to cancer. The other attractor shows induction of apoptosis without active CFL1. This represents a healthy phenotype because even without CFL1 the induction of apoptosis is possible.
In contrast, the simulation with the initial Boolean network model containing a cell cycle regulation influenced by STAT3 ends in three single state attractors (Figure 19B). As before, two of the attractor patterns could be matched to cancer and

healthy conditions respectively. One attractor shows active CFL1 with proliferation but no induction of apoptosis while the other attractor has inactive CFL1 and inhibition of G1-to S-phase transition in combination with induction of apoptosis. Interestingly, the third attractor also shows no active CFL1 and inhibition of cell cycle but this time without induction of apoptosis. Thus, reproducing known behaviour from CFL1 knockdown experiments [211].

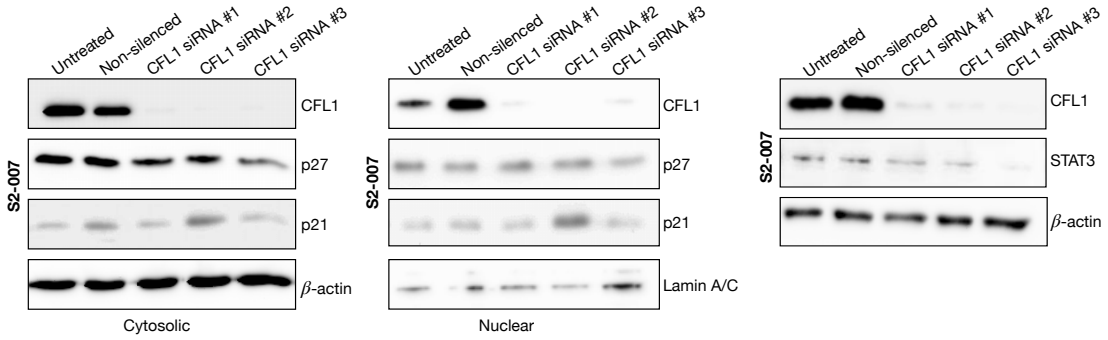

Figure 20: **Uncover cell cycle regulation downstream of CFL1 by *in vitro* experiments.** There are indications that cell cycle is regulated downstream of CFL1 by the cell cycle inhibitors p21 and p27 [429] or by influences on STAT3 [464]. Western blots show that CFL1 silencing by three independent siRNAs does not affect the protein levels of cell cycle inhibitors p21 and p27 nor their cellular localisation. Instead, CFL1 silencing further reduced STAT3 protein levels. β-actin, as well as Lamin A/C, were used to confirm equal loading. A non-silenced construct as well as untreated cells were used as controls. Western blot results were kindly provided by M. Buchholz.

The comparison of the simulations of the initial models with respect to the effect of CFL1 on proliferation supports both model variants. However, the variant with STAT3 is also able to represent the behaviour of a CFL1 knockdown making the model more interesting concerning CFL1 status in pancreatic cancer cell lines. In order to further support the theory that CFL1 impacts the cell cycle via STAT3, western blot analyses were performed to assess the influence of CFL1 on cell cycle inhibitors and STAT3 (Figure 20). Here, it could be shown that changes in CFL1 expression have no effect on cell cycle inhibitor expression levels nor on their cellular localisation. Instead, protein levels of STAT3 were reduced after silencing of CFL1. The *in vitro* findings exclude a regulation of cell cycle by an effect of CFL1 on cell cycle inhibitors in pancreatic cancer cells. Therefore, influences of STAT3 and its downstream targets were included in the final model (Table 6).
The final model of CFL1 in pancreatic cancer consists of 33 nodes. To my best knowledge, it is the first model that captures all mechanisms in which an involvement of

CFL1 is assumed. Thus, CFL1 regulation on its own as well as actin remodelling, cell cycle regulation and apoptosis are included (Figure 21).

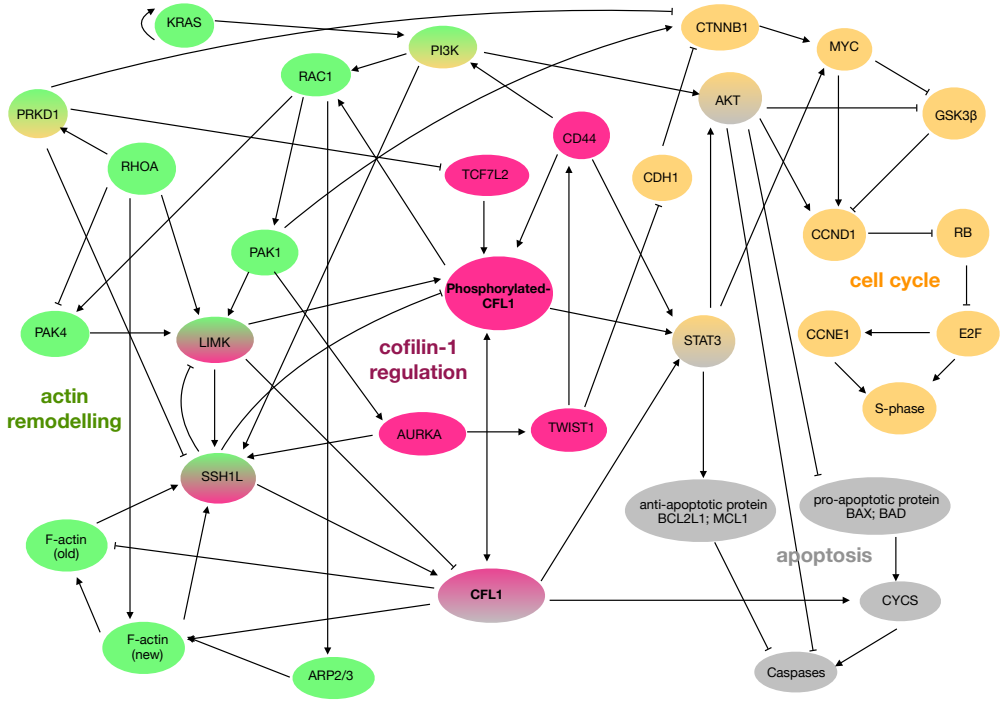

Figure 21: **Regulatory interactions of the CFL1 Boolean network model.** Directed interaction graph with all 33 proteins comprised in the model in coloured circles. The model connects actin remodelling (green circles) with CFL1 regulation (pink circles) as well as downstream effects of CFL1 with impacts on the cell cycle (yellow circles) and the induction of apoptosis (grey circles). Activating interactions are depicted by arrows and inhibiting interactions by bar-headed lines.

Table 6: Boolean functions of the model about cofilin-1 in pancreatic cancer. All proteins are abbreviated in accordance with the current nomenclature. Logical connectives are depicted by & (=AND), | (=OR), and ! (=NOT).

	Node; $t+1$	**Boolean network function;** t	**References**
Actin remodelling	F-actin$_{new}$	(CFL1 & ARP 2/3) | (RHOA[-3] & !CFL1)	CFL1 and actin-related protein-2/3 (ARP 2/3) work in synergy to create new branched actin fibers (F-actin$_{new}$) [64, 72, 93, 328, 382, 416, 504]. The RHOA/ROCK/DIA (diaphanous-related formin) pathway mediates filamentous actin (F-actin) polymerisation [101, 296, 321, 390]. Since this is a linear connection, only RHOA is considered.
	F-actin$_{old}$	(F-actin$_{old}$ & !CFL1) | F-actin$_{new}$	CFL1 is involved in actin dynamics by severing F-actin [72, 99, 104]. Here, it prefers to sever old adenosine diphosphate (ADP)-F-actin [33, 64, 322, 416]. Newly formed actin fibers are build, prolonged and thus converted into old ones (F-actin$_{old}$).
	ARP 2/3	RAC1[-2]	The RAC1/WAVE (Verplin-homologous protein) or WASP (Wiskott-Adrich syndrome protein) axes activate the ARP 2/3 complex [64, 390, 504].
	KRAS	1	Activating KRAS mutations are one of the earliest mutations and present in more than 90% of PDAC patients [108, 215, 255, 476].

Table 6: Boolean functions of the model about cofilin-1 in pancreatic cancer. All proteins are abbreviated in accordance with the current nomenclature. Logical connectives are depicted by & (=AND), | (=OR), and ! (=NOT).

	Node; $t+1$	**Boolean network function;** t	**References**
Actin remodelling	PI3K	KRAS | CD44	The PI3K-pathway is one of the main effector pathways downstream of RAS [56]. PI3K, but not CRAF (Raf-1 proto-oncogene) is the effector on oncogenic KRAS in PDAC [107, 108]. Binding of hyaluronan to its receptor CD44 antigen (CD44) activates the PI3K/AKT pathway [26, 61, 257].
	PRKD1	RHOA	RHOA mediates the activation of protein kinase D1 (PRKD1) [99, 104, 399, 438].
	RHOA	!PAK4	p21-activated kinase 4 (PAK4) but not p21-activated kinase 1 (PAK1) inhibits the activity of RHOA [300].
	RAC1	PI3K | phospho-CFL1[-3]	The production of phosphatidylinositol-3,4,5-triphosphate (PIP3) downstream of PI3K activates RAC1 [56, 107, 304]. Phosphorylated CFL1 activates phospholipase D1 (PLD1) which subsequently increases the membrane phosphatidic acid and thus activates dedicator of cytokinesis (DOCK) - an activator of RAC1 [21]. Since this is a linear connection, only a delay from phosphorylated CFL1 is included.

Table 6: Boolean functions of the model about cofilin-1 in pancreatic cancer. All proteins are abbreviated in accordance with the current nomenclature. Logical connectives are depicted by & (=AND), | (=OR), and ! (=NOT).

	Node; $t+1$	**Boolean network function;** t	**References**
Actin remodelling	PAK1	RAC1	Within the PAK family, PAK1 and PAK4 are the major regulators of cytoskeletal reorganisation downstream of RAC1 [110, 476]. PAK1 is activated by several stimuli downstream of RAC1 [54, 103, 325, 370, 482].
	PAK4	RAC1	Within the PAK family, PAK1 and PAK4 are the major regulators of cytoskeletal reorganisation downstream of RAC1 [110, 476]. PAK4 is activated by various stimuli downstream of RAC1 [103, 325, 482].
Cofilin-1 regulation	LIMK	((RHOA | PAK4 | PAK1) & !SSH1L)	PAK1, PAK4, and ROCK (downstream of RHOA) activate LIM domain kinase (LIMK) by dephosphorylation [39, 99, 110, 325, 390, 399, 445, 482]. LIMK and slingshot protein phosphatase 1L (SSH1L) can form a complex that effectively dephosphorylates both [39, 397].
	SSH1L	((F-actin$_{new}$ | F-actin$_{old}$) & !PRKD1) | (PI3K & AURKA) | (LIMK & SSH1L)	The activity of SSH1L is enhanced after binding to F-actin [104, 399, 445]. PRKD1 phosphorylates SSH1L. Aurora kinase A (AURKA) induces the expression of SSH1L but only if PI3K is present [166, 304, 441]. LIMK and SSH1L can build a complex that effectively dephosphorylates both [39, 397].

Table 6: Boolean functions of the model about cofilin-1 in pancreatic cancer. All proteins are abbreviated in accordance with the current nomenclature. Logical connectives are depicted by & (=AND), | (=OR), and ! (=NOT).

	Node; $t+1$	**Boolean network function; t**	**References**
Cofilin-1 regulation	phospho-CFL1	CD44 | TCF7L2 | (CFL1 & LIMK & !SSH1L)	Transcription factor 7-like 2 (TCF7L2) activates the transcription of CFL1 [438]. CD44 expression induces the expression of CFL1 [231, 406]. LIMK phosphorylates and thus inhibits CFL1 [104, 166, 304, 325, 399, 441]. However, in the presence of SSH1L the dephosphorylation activity of SSH1L is more pronounced than the inhibition of LIMK [64, 397].
	CFL1	(SSH1L & pCFL1) | (SSH1L & LIMK & phospho-CFL1)	SSH1L dephosphorylates CFL1 thereby activating it [64, 104, 166, 304, 399, 441, 442, 445]. Instead, LIMK phosphorylates CFL1 thus deactivating it [64, 104, 166, 399, 442]. If SSH1L and LIMK are present LIMK may restore phosphorylation but the dephosphorylation of SSH1L is more pronounced [64, 397].
	AURKA	PAK1	AURKA gets activated by PAK1 via transphosphorylation [103, 302, 482].
	CD44	TWIST1	Twist-related protein 1 (TWIST1) upregulates CD44 expression [61, 440].
	TCF7L2	!PRKD1	PRKD1 inhibits TCF7L2 expression [438].
	TWIST1	AURKA	AURKA inhibits the degradation of TWIST1 [440].

Table 6: Boolean functions of the model about cofilin-1 in pancreatic cancer. All proteins are abbreviated in accordance with the current nomenclature. Logical connectives are depicted by & (=AND), | (=OR), and ! (=NOT).

	Node; $t+1$	**Boolean network function;** t	**References**
Cell cycle regulation	CDH1	!TWIST1	E-cadherin (CDH1) expression is reduced downstream of TWIST1 [306, 373, 434, 440, 499].
	CTNNB1	PAK1 & !PRKD1 & !CDH1	PAK1 stabilises CTNNB1 [54, 325, 370, 482]. CDH1 assembles with CTNNB1 and inhibits its nuclear localisation [187, 209, 373, 461]. Overexpression of PRKD1 lower the expression of CTNNB1 [438].
	GSK3β	!AKT	AKT inactivates GSK3β by phosphorylation [19, 56, 60, 166, 427].
	MYC	(GSK3β & STAT3) | (CTNNB1 & !GSK3β)	Myc proto-oncogene (MYC) expression is reduced after signal transducer and activator of transcription 3 (STAT3) knockdown [166, 173, 191, 246, 473, 503]. GSK3β inhibition stabilises MYC which is ubiquitinated by GSK3β [412]. GSK3β is part of the DC which degrades cytoplasmic CTNNB1 thereby inhibiting its nuclear localisation and activation of downstream targets like MYC [103, 209, 259, 492].

Table 6: Boolean functions of the model about cofilin-1 in pancreatic cancer. All proteins are abbreviated in accordance with the current nomenclature. Logical connectives are depicted by & (=AND), | (=OR), and ! (=NOT).

	Node; $t+1$	**Boolean network function;** t	**References**
Cell cycle regulation	CCND1	!GSK3β & MYC & AKT	Phosphorylation of cyclin D1 (CCND1) by GSK3β leads to its destabilisation [19, 427]. AKT reduces the inhibitory function of cyclin-dependent kinase inhibitor 1A (CDKN1A or p21) and/or cyclin-dependent kinase inhibitor 1B (CDKN1B or p27) towards CCND1 and supports the assembly of CCND1 with cyclin dependent kinase 4/6 (CDK4/6) [19, 225, 226, 436, 452, 487]. MYC is involved in the transcription of CCND1 [60, 319, 452].
	RB	!CCND1	CCND1 phosphorylates retinoblastom (RB) [60, 427, 451].
	E2F	!RB	Phosphorylation of RB frees transcription factor E2F (E2F) [60, 427, 451].
	CCNE1	E2F	E2F induces the expression of cyclin E1 (CCNE1) [60, 427].
	S-phase	E2F & CCND1	The activity of CCNE1 enhances the activity of E2F thus supporting the synthesis of proteins required for S-phase transition [60, 412, 427].

Table 6: Boolean functions of the model about cofilin-1 in pancreatic cancer. All proteins are abbreviated in accordance with the current nomenclature. Logical connectives are depicted by & (=AND), | (=OR), and ! (=NOT).

	Node; $t+1$	**Boolean network function;** t	**References**
Apoptosis regulation	AKT	PI3K & STAT3	Activated PI3K transfers PIP2 to PIP3 followed by activation of downstream targets such as AKT [226, 304, 427, 447, 452]. STAT3 down-regulation decreases the phosphorylation of AKT as well as AKT expression levels [246, 250, 384, 496].
	STAT3	(CFL1 | phospho-CFL1) & CD44	Knockdown of CFL1 decreases the amount of STAT3 [464]. High levels of CD44 are enough to activate STAT3 [393].
	Anti-apoptotic proteins	STAT3	Downstream targets of STAT3 are anti-apoptotic proteins like Bcl-2-like 1 (BCL2L1) or induced myeloid leukemia cell differentiation protein (MCL1) [173, 191, 457, 473, 503].
	Pro-apoptotic proteins	!AKT	AKT phosphorylates and thus inhibits the pro-apoptotic protein Bcl-2-antagonist of cell death (BAD) [13, 147, 457].

Table 6: Boolean functions of the model about cofilin-1 in pancreatic cancer. All proteins are abbreviated in accordance with the current nomenclature. Logical connectives are depicted by & (=AND), | (=OR), and ! (=NOT).

	Node; $t+1$	**Boolean network function;** t	**References**
Apoptosis regulation	CYCS	Pro-apoptotic proteins & !Anti-apoptotic proteins & CFL1	Pancreatic cancer cells require the mitochondrial enhancing signal to induce apoptosis [147, 457]. An imbalance between pro- and anti-apoptotic proteins induces apoptosis by activating Bcl-2-associated X protein (BAX) [147, 457]. Unphosphorylated CFL1 translocates to the mitochondria after induction of apoptosis to induce the release of cytochrome C (CYCS) [67, 124, 414, 415]. Knockdown of CFL1 reduces apoptosis [67, 414, 415]. CFL1 might act as a carrier to transport BAX to the mitochondrion [323].
	Caspases	CYCS & !AKT	Pancreatic cancer cells require the mitochondrial enhancing signal to induce apoptosis [147, 457]. The released CYCS from the mitochondrion into the cytoplasm forms the apoptosome multi-protein complex together with procaspase-9 and apoptotic protease-activating factor 1 (Apaf-1). This activates caspase-9 further activating caspase-3 [67, 124, 147, 239, 378, 457, 511]. Caspase-9 can be phosphorylated and thus inhibited by AKT [147, 415, 457].

Simulations of the finally established model yield one single state attractor (figure 22). The attractor shows activity of the active form of CFL1 (unphosphorylated CFL1) which is reported to be present in many malignant cells [475]. In addition, F-actin$_{new}$ is active. In particular, the activity of F-actin$_{new}$ is a sign of migratory potential of the attractor because new actin fibres are important for cellular motility. Furthermore, all proteins responsible for the progression of the cell cycle from G1- to S-phase (CCND1, E2F, CCNE1 and S-phase) are constitutively active. This indicates a high level of proliferation, a hallmark of cancer [148]. Besides increased proliferation, another hallmark of cancer is the circumvention of apoptosis [148]. Based on the model, apoptosis is abrogated by the inactivity of caspases. Thus, the achieved attractor shows migratory as well as high proliferative potential but no induction of apoptosis. Thereby, it resembles known behaviour from pancreatic tumours with high CFL1 expression.

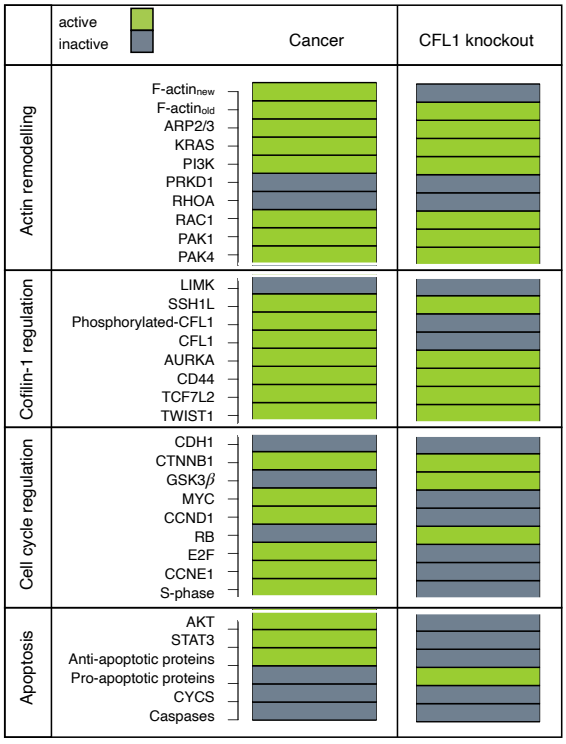

Figure 22: **Attractors of the CFL1 model.** Simulations of the unperturbed (cancer) as well as of the CFL1 knockdown model revealed a single state attractor each. The attractor plot is divided into blocks of regulation with the involved proteins listed on the left side. The activity of each model compound is depicted by green (=active) or grey (=inactive) rectangles.

Next, an *in silico* knockout of CFL1 was performed. Again, the simulation ends in a single state attractor (Figure 22). This time the attractor reveals inactive F-actin$_{new}$ and thus inhibition of migration. This behaviour is in line with decelerated migration velocity as observed in CFL1-silenced pancreatic cancer cell lines [211]. Likewise, the described attenuation of the cell cycle in the G1- to S-phase transition [211] can be depicted by this attractor (inactive CCND1, E2F1, CCNE1, S-phase). Additionally, the attractor shows no induction of apoptosis, thereby also representing findings in CFL1-silenced pancreatic cancer cell lines [211]. On the basis of the CFL1 knockout simulation, it can be concluded that the model is equally capable of depicting the behaviour of CFL1 in pancreatic cancer as well as in CFL1-silenced pancreatic cancer cell lines.
To further support the model, the achieved attractor pattern of "cancer" (Figure 22) was compared to binarised gene expression data from pancreatic cancer tissues (GSE15471 [18], GSE16515 [316], GSE32676 [97]). Since these datasets include labels, a ROC curve as supervised binarization method was applied to compare the genes involved in the model to known expression values of those genes in pancreatic cancer samples. How well each gene matches to the described activity in the attractor can be seen by its percental coverage rate (Figure 23). Most activity rates of the network's compounds are well covered by the gene expression data. Thus, a small normalised Hamming distance of 0.387 was found for the comparison of expression data from 100 tumours samples to the attractor pattern. This indicates that only a few proteins differ on the transcriptional level between the attractor pattern and the gene expression data. However, non of the 100 patients included in the datasets reflected the attractor pattern with a 100% coverage. The best match could be found for four patients who showed variations in six network compounds.

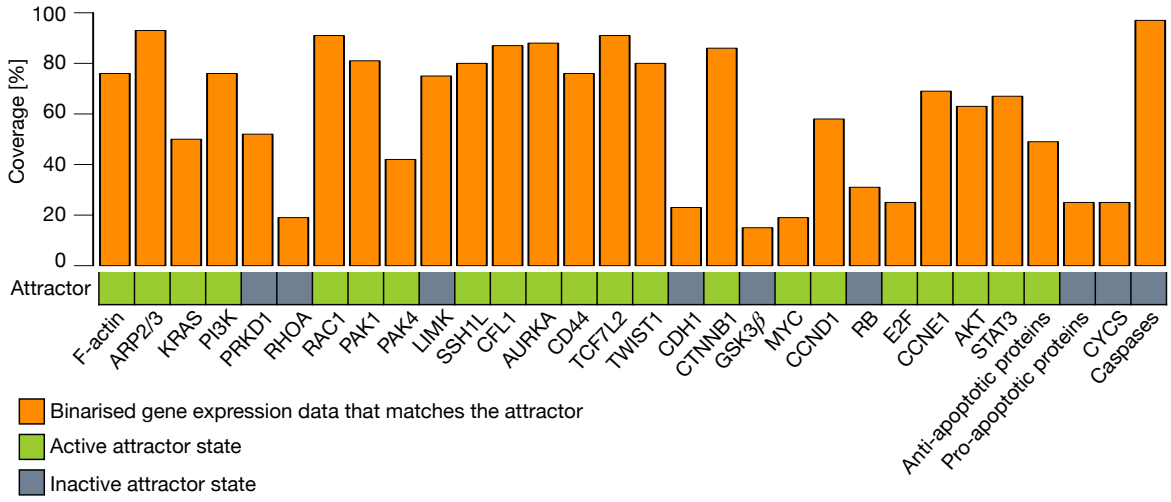

Figure 23: **Pancreatic cancer patient data covers the attractor pattern.** The attractor representing pancreatic cancer was compared to binarised gene expression data of 100 tumour samples dissected from pancreatic cancer patients. Bars represent how well the attractor could be represented by the data.

Based on the attractor comparison with *in vitro* experiments as well as with gene expression data, it can be concluded that the established model is able to reflect the behaviour of CFL1 in pancreatic cancer. Thus, in the following section, it will be used to identify the underlying regulatory mechanisms.

3.2.1.1 *Imbalance in actin remodelling leads to CFL1 overexpression*

CFL1 can be present in two states, phosphorylated on its serine 3 residue or unphosphorylated [64, 104, 166, 304, 399, 441, 442, 445]. Based on studies regarding the involvement of CFL1 in actin dynamics it was assumed that CFL1 is only active in its unphosphorylated state [72, 99, 104]. Recently, however, regulatory functions of phosphorylated CFL1 were shown [21].
Overexpression of active/unphosphorylated CFL1 is well described in different cancers including pancreatic cancer [211, 264, 303, 318, 355, 443, 475]. However, dysregulated mechanisms leading to this overexpression and dephosphorylation of CFL1 are yet unknown.
Since the established model is capable of adequately reproducing the long-term behaviour of CFL1 overexpression as well as CFL1 silencing in pancreatic cancer cells, it was used as a basis to study the signalling cascade towards cancer. Activating KRAS mutations are present in 90% of pancreatic cancer patients as one of the earliest mutations [108, 215, 255, 476]. This fact was considered in the signalling cascade by starting the simulation from an initial state in which all

proteins except KRAS are inactive (Figure 24).

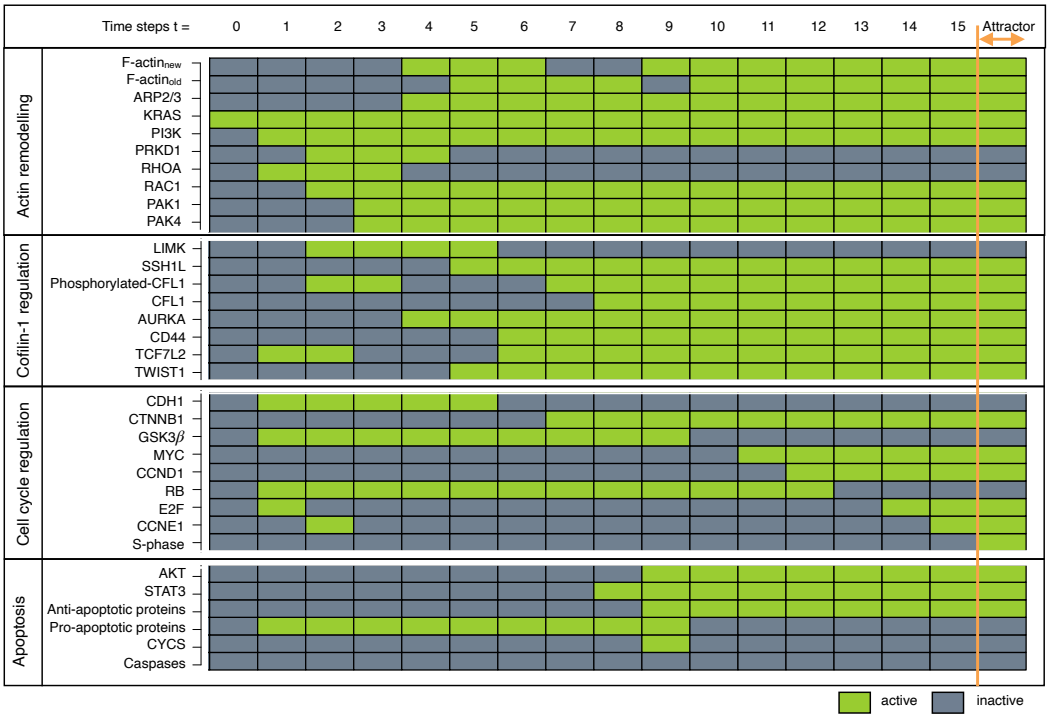

Figure 24: **Signalling cascade to pancreatic cancer.** Activating KRAS mutations are present in 90% of pancreatic cancer patients [108, 215, 255, 476]. Therefore, the signalling cascade starts from an initial state in which all components are inactive except KRAS. Simulating the model with distinct time steps (t) it proceeds into a single state attractor (orange double-headed arrow) matching the one of cancer. The plot of the signalling cascade is divided into blocks of regulation with the involved proteins listed on the left side. The activity of each component is depicted by green (=active) or grey (=inactive) rectangles.

Initially, all proteins that have KRAS as an activator and those whose inhibitors are still inactive are activated (Figure 24). Then, during time steps one and two, both actin remodellers RHOA and RAC1 are active. Indeed, both proteins are responsible for different actin dynamics. RAC1 is responsible for lamellipodia formation while RHOA regulates filopodia formation [390]. Therefore, they are opponents and inhibit each other [153]. Certainly, the signalling cascade towards cancer illustrates an imbalance in their regulation that leads to permanent activation of RAC1 while RHOA remains inactive. Interestingly, both proteins - RAC1 and RHOA - regulate downstream targets that have an impact on CFL1 (Figure 25).

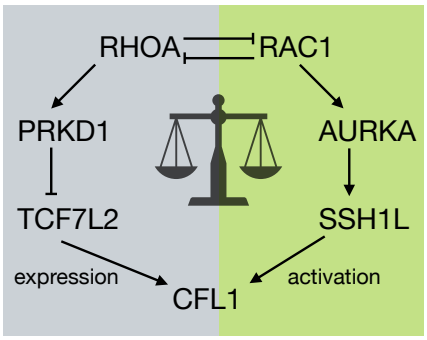

Figure 25: **Imbalance of actin remodellers.** An imbalance between RHOA and RAC1 in favour of RAC1 leads to overexpression and activation of CFL1. Depicted are two signalling cascades involved in CFL1 regulation. Activating interactions are depicted by arrows and inhibiting regulations by bar-headed lines.

RHOA mediates the activation of PRKD1 [99, 104, 399, 438], an inhibitor of TCF7L2 [438]. Consequently, permanent repression of RHOA leads to a decrease in the activity of PRKD1 (time step five, Figure 24) and subsequent activation of TCF7L2 (time step six) which is no longer inhibited by PRKD1 (Figure 24, 25). This mechanistic change may cause overexpression of CFL1 since TCF7L2 is able to induce CFL1 expression [438].
On the other hand, persistent activation of RAC1 induces the expression of AURKA via its downstream target PAK1 [103, 482] (time step two until four). AURKA in turn induces the expression of SSH1L [166, 304, 441], an activator of CFL1 [64, 104, 166, 304, 399, 441, 442, 445]. Thus leading to activation of CFL1 (Figure 25).
The signalling cascade towards cancer illustrates an imbalance of actin remodellers causing CFL1 expression and activation. In order to validate this model-based hypothesis RMA-normalised and binarised microarray data of pancreatic tissue taken from healthy donors and pancreatic cancer patients were considered (Figure 26). In contrast to the reconstruction of Boolean network models, this time a supervised binarization method was used since the datasets included tissue classes (normal, tumour). This allowed a better comparison between the attractor representing cancer and pancreatic cancer tissue.
Consequences of the assumed imbalance between RAC1 and RHOA are the overexpression of TCF7L2 and AURKA. Therefore, these two proteins were analysed concerning their expression in pancreatic cancer patients. The analysis of gene expression data demonstrated that both proteins are significantly overexpressed (AURKA $\leqslant 0.04$, TCF7L2 $\leqslant 0.001$) in pancreatic cancer tissues (Figure 26). Furthermore, the median of the expression data from pancreatic cancer tissues is above the binarization threshold for all three datasets while the median of normal

tissues is below this threshold. Therefore, both proteins AURKA and TCF7L2 are considered active in pancreatic cancer as suggested by the model (Figure 26).

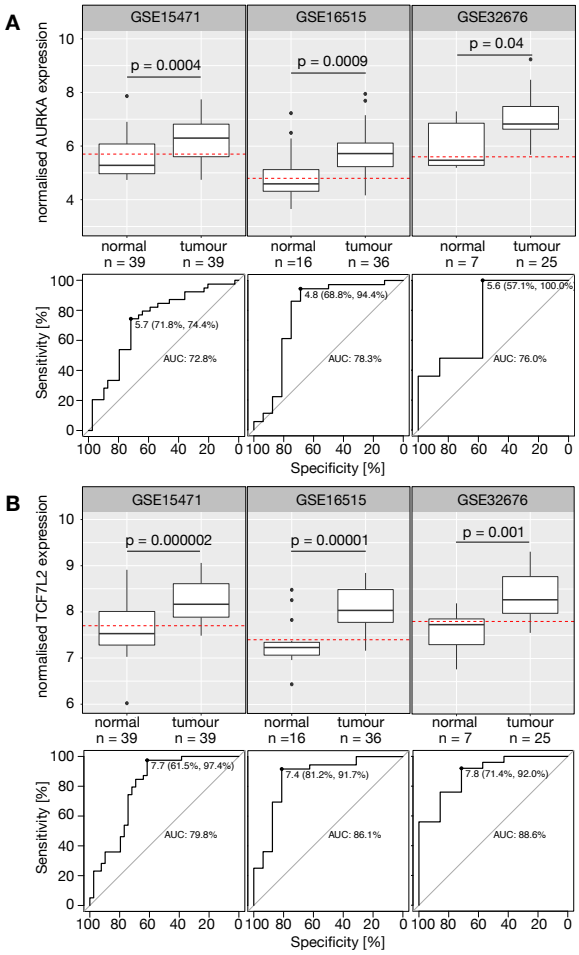

Figure 26: **Validation of model suggested overexpression of AURKA and TCF7L2.** Boxplots showing the gene expression of the CFL1 activator AURKA (A) and its inducer TCF7L2 (B) in tissue derived from healthy donors (normal) and pancreatic cancer patients (tumour). The depicted datasets are available under accession number GSE15471 [18], GSE16515 [316] and GSE32676 [97]. Statistical analyses were performed using a Wilcoxon test. p-values $\leqslant 0.05$ were considered significant. The red dashed lines represent the binarization threshold defined by the ROC curves below. Here, a supervised binarization method was used to consider the provided tissue classes in the datasets. The binarization threshold defines the value which separates the two groups, normal and tumour, with the highest sensitivity and highest specificity simultaneously. The AUC describes how well this feature predicts the classes.

Taken together, the confirmations of overexpression of AURKA and TCF7L2 in pancreatic cancer tissues are a first indication of the accuracy of the model-based assumption of an imbalance in actin dynamics.

3.2.1.2 *Migratory potential of pancreatic cancer cells is based on ARP 2/3-CFL1 synergy*

One characteristic of pancreatic cancer is its high degree of early and aggressive metastasis [215]. The driving force for this migratory potential derives from the formation of lamellipodia [260, 475] which are part of actin dynamics. The actin cytoskeleton of a cell is reshaped constantly. This process is regulated by a balance between RHOA and RAC1. However, the signalling cascade towards cancer already demonstrated an imbalance of both proteins in favour of active RAC1 (Figure 24). Similarly, as for the activation of CFL1, RAC1 may play a role for the migratory potential of pancreatic cancer cells. By acting on WASP and WAVE, RAC1 signalling is able to activate ARP 2/3 [64, 390, 504]. ARP 2/3 is described as one of the principal regulators in the assembly of lamellipodia [260].
In addition, it could be shown that CFL1 has an impact on the migratory potential of pancreatic cancer cells [211]. This finding is in line with the simulation of the signalling cascade of CFL1-silenced pancreatic cancer cells (Figure 27). Here, it was shown that the pure activity of ARP 2/3 is not sufficient to generate new lamellipodia (here F-actin$_{new}$). In contrast, the simulation of the unaffected network indicates a constant activation of F-actin$_{new}$ in the presence of CFL1 (Figure 24). The outcome of the simulation is supported by studies assuming an involvement of CFL1 in lamellipodia formation. One explanation for the requirement of ARP 2/3 and CFL1 for the formation of lamellipodia could be that CFL1 provides free barbed ends by severing old ADP ends of F-actin fibres. These fragments are then preferentially occupied by ARP 2/3 to construct new branched actin fibres known as lamellipodia [20, 93, 416]. Based on this, CFL1 and ARP 2/3 work in synergy to create new actin fibres which are necessary for cell spreading.

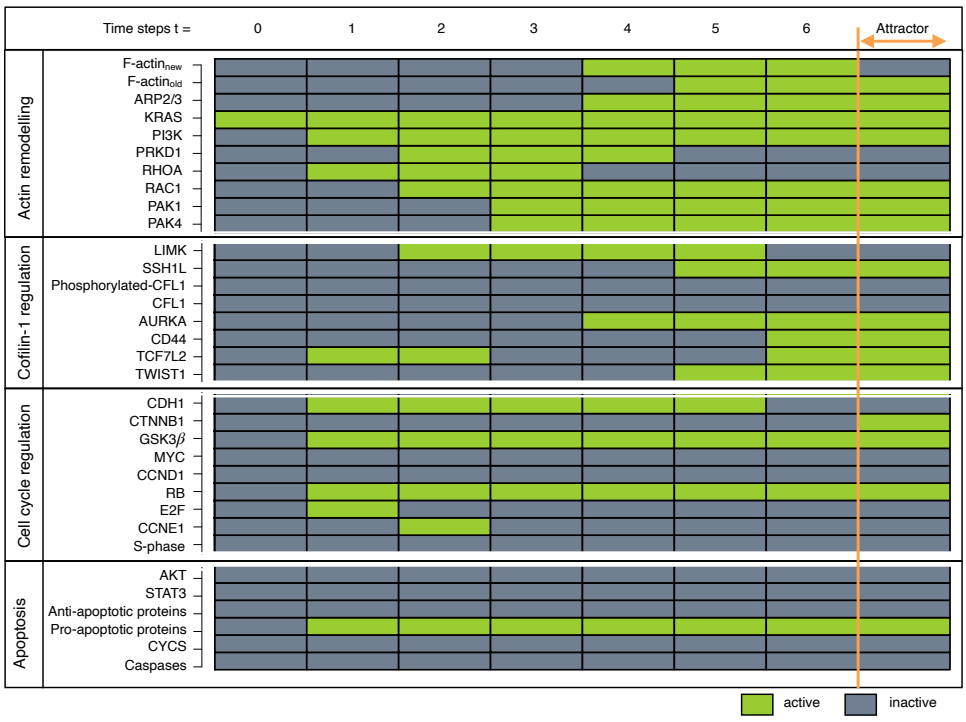

Figure 27: **Signalling cascade of CFL1-silenced pancreatic cancer cells.** Simulating the model with distinct time steps (t) from an initial state in which all components of the model are inactive except KRAS, it proceeds into a single state attractor (orange double-headed arrow). The plot of the signalling cascade is divided into blocks of regulation with the involved proteins listed on the left side. The activity of each compound is depicted by green (=active) or grey (=inactive) rectangles.

3.2.1.3 *CFL1 influences proliferation via STAT3*

A characteristic of cancer is an elevated proliferation rate [148]. In line with this description, CFL1 overexpression could be associated with increased proliferation [438] while CFL1-silencing is reported to attenuate G1- to S-phase transition [211]. Certainly, mechanistic regulation of cell cycle regulators by CFL1 in pancreatic cancer is unknown.

Looking at the signalling cascade towards cancer (Figure 24), the next protein that is activated after the induction of CFL1 expression (time step seven) is STAT3 (time step eight). But activation of STAT3 is not enough to induce CCND1 activity and thus proliferation since STAT3 is not a direct regulator of CCND1. Furthermore, to promote cell cycle progression CCND1 has to join with CDK4/6 in order to translocate into the nucleus [452]. This assembly is promoted by the activity of AKT [19, 225, 226, 436, 452, 487] whose expression level can be regulated downstream of STAT3. Therefore, AKT gets activated after STAT3 (time step nine) since its inducer of expression STAT3 [246, 250, 496] and its activa-

tor PI3K [226, 304, 384, 427, 447, 452] are active beforehand. Besides its effect on the CCND1-CDK4/6 assembly, AKT further promotes proliferation by inhibiting GSK3β [19, 56, 60, 166, 427] (time step ten). As a consequence, MYC expression is induced by CTNNB1 (time step eleven) [103, 209, 259, 492] further activating the expression of CCND1 [60, 319, 452]. The recently activated CCND1 phosphorylates (inhibits) RB and thereby releases E2F. This in turn induces the expression of CCNE1 and thus enables the progression from G1- to S-phase transition [60, 427, 451]. Opposed to that, all of these proteins involved in the described cell cycle regulation stay unchanged in the signalling cascade of CFL1 knockdown (Figure 27). The same behaviour can be observed in the model simulation with silenced STAT3 (Figure 28). However, in contrast to an *in silico* CFL1 knockout, this simulation shows no inhibition of migration but induction of apoptosis.

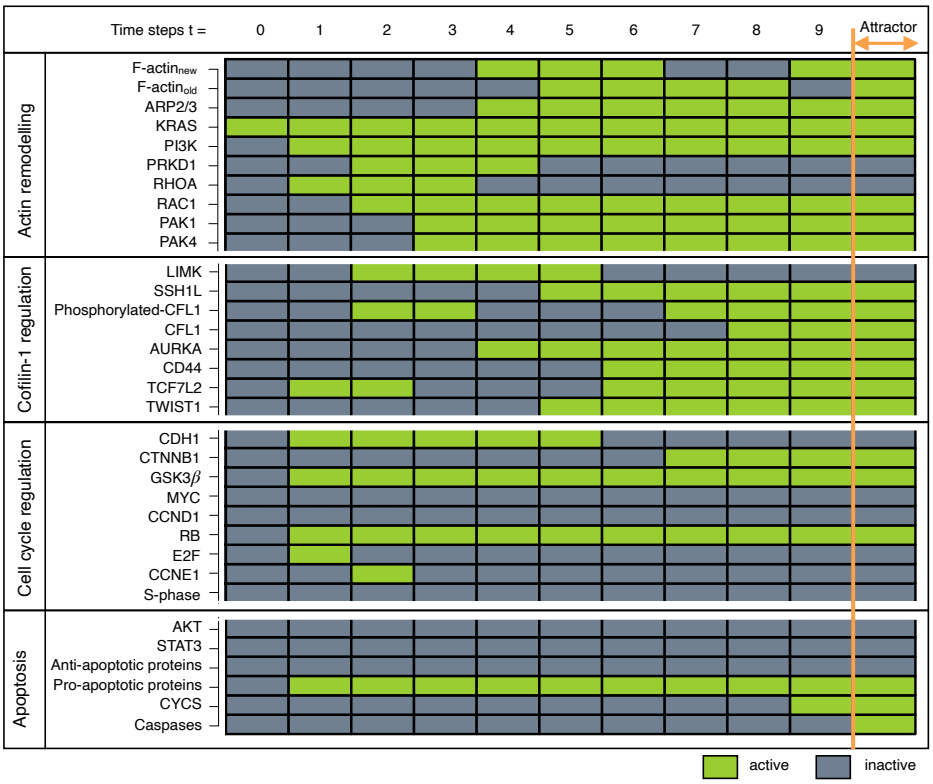

Figure 28: **Signalling cascade of STAT3 silenced pancreatic cancer cells.** Simulating the model with distinct time steps (t) from an initial state in which all components of the model are inactive except KRAS, it proceeds into a single state attractor (orange double-headed arrow). The plot of the signalling cascade is divided into blocks of regulation with the involved proteins listed on the left side. The activity of each component is depicted by green (=active) or grey (=inactive) rectangles. The simulation is performed with a synchronous updating scheme, only STAT3 is fixed to its inactive state.

On the basis of these signalling cascades (Figures 24, 27, 28), it can be concluded that the accumulation in the G1- to S-phase transition is evoked by the impact of CFL1 on STAT3. In order to confirm this hypothesis, protein levels of STAT3 and its downstream targets were investigated in CFL1 expressing and CFL1 silenced S2-007 cells (Figure 29). Here, it could be observed that the total amount of STAT3 as well as the active (phosphorylated) amount of STAT3 decrease after CFL1 knockdown. The same was true for the two STAT3 downstream targets MYC and CCND1. Hence, the performed laboratory experiments confirm the model-suggested cell cycle regulation via STAT3.

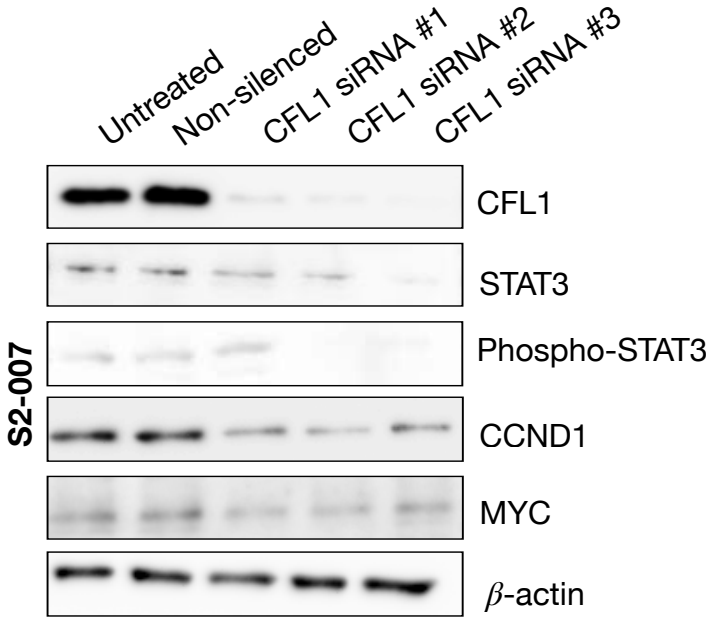

Figure 29: **Experimental validation of suggested cell cycle regulation.** Model simulations indicated that CFL1 affects the cell cycle via its downstream target STAT3. Western blots confirmed a decrease of total STAT3 and active (phospho-) STAT3 as well as its downstream targets cyclin D1 (CCND1) and MYC after silencing of CFL1. CFL1 knockdown was achieved with siRNAs. A non-silenced construct as well as untreated cells were used as controls. Actin was used as a control to ensure equal loading. Western blot results were kindly provided by M. Buchholz.

3.2.1.4 *Dual role of CFL1 in apoptosis induction*

Apart from an increase in the rate of proliferation, another hallmark of cancer is the ability to circumvent apoptosis [148]. Especially pancreatic cancer cells acquire a high degree of apoptotic resistance. Accordingly, they require a mitochondrial enhancing signal in addition to death cell receptor signals to induce apoptosis [147, 457]. By releasing CYCS into the cytoplasm, the mitochondrion triggers the induction of apoptosis [67]. Released CYCS forms a complex with Apaf1 which cleaves pro-caspase-9 into its active form [147]. Caspase-9 itself further activates caspase-3, thereby inducing apoptosis [147]. Within the model, apoptosis is assumed to be induced if caspases are active.
Although CYCS is active in the signalling cascade towards cancer for a short period of time, it is not sufficient to induce further steps towards apoptosis (Figure 24). One reason for the resistance could be the simultaneous activation of anti-apoptotic proteins. BCL2L1 is one of these anti-apoptotic proteins that is associated with inhibition of mitochondrial induced apoptosis in pancreatic cancer cells [246, 503]. Furthermore, the expression of BCL2L1 can be induced by STAT3 [503] which was activated shortly before. Thus, the activity of STAT3 which is regulated by CFL1 [464] may lead to resistance to apoptosis. In addition to STAT3, AKT is active when there is no induction of apoptosis (Figure 24). AKT is another well-known inhibitor of apoptosis which inhibits cell death through phosphorylation of caspase-9 [147].
In order to test the hypothesis that apoptosis is inhibited in pancreatic cancer cells by an unbalanced expression of anti-apoptotic proteins, the expression levels of BCL2L1 and BAD in tissue samples from pancreatic cancer patients and healthy donors of three independent datasets were studied (Figure 30). While BCL2L1 was significantly overexpressed ($\leqslant 0.0001$) in tissues taken from pancreatic cancer patients only one dataset showed significant differences in the expression of BAD. Furthermore, the medians of BCL2L1 expression in tumour tissues differ in their activity in comparison to normal tissues as defined by the binarization thresholds. In contrast, by binarization of BAX expression, the medians of tumours and normal tissues were both above the binarization threshold and thus classified as active. Hence, there are no differences between pancreatic cancer samples and normal healthy tissues regarding BAX expression while the expression of BCL2L1 is enhanced in pancreatic cancer. These findings support the model-based assumption that an increase in anti-apoptotic proteins is responsible for inhibition of apoptosis in pancreatic cancer cells with active CFL1.

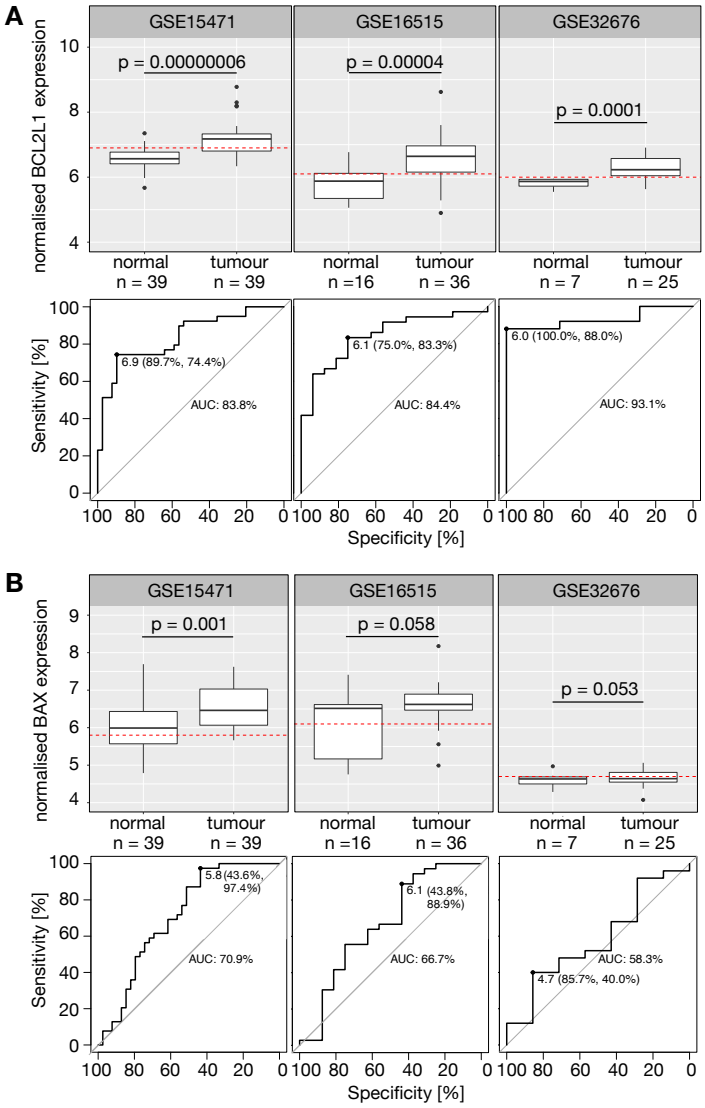

Figure 30: **Experimental validation of suggested apoptosis regulation.** Model simulations indicated that anti-apoptotic proteins are unbalanced in pancreatic cancer cells. Boxplots depict the gene expression levels of the anti-apoptotic protein BCL2L1 (A) and the pro-apoptotic protein BAX (B) in tissues derived from healthy donors (normal) and pancreatic cancer patients (tumour). The depicted data are available under the accession number GSE15471 [18], GSE16515 [316] and GSE32676 [97]. Differences in gene expression levels were evaluated using Wilcoxon test assuming results with $p \leqslant 0.05$ as significant. The dashed lines in the box plots represent the binarization thresholds as defined by a ROC curve (below). This threshold determines a value of gene expression that is able to separate the two groups (normal and tumour) with the highest sensitivity and highest specificity simultaneously. Proteins whose expression values are above the threshold are considered active while proteins with expression values below the threshold are considered inactive. The AUC describes how well this feature predicts the classes.

Besides its impact on STAT3, there might be another involvement of CFL1 in the inhibition of apoptosis. Although it has been described in other types of cancers that a knockdown of CFL1 leads to induction of apoptosis [438], this behaviour could not be observed in pancreatic cancer cells [211]. For this regulation, however, participation of STAT3 and AKT can be excluded since both proteins are inactive in the signalling cascade of CFL1-silenced pancreatic cancer cells (Figure 27). In contrast to the simulation with active CFL1 (Figure 24), CYCS is not active in the signalling cascade with CFL1 knockout (Figure 27). Thus, the mitochondrial enhancing signal fails to induce apoptosis. Active unphosphorylated CFL1 is thought to transport CYCS to the mitochondrion where it can induce apoptosis [67, 124, 414, 415]. Thus, CFL1 is assigned a dual role in the induction of apoptosis. Actually, CFL1 has an apoptosis-inducing role based on its impact on CYCS, but further dynamic changes in tumour regulation activate other targets like STAT3 that inhibit apoptosis.

3.2.1.5 *Potential therapeutically approaches to treat pancreatic cancer patients with increased CFL1 expression*

Although the presented model about CFL1 in pancreatic cancer is coarse, it was possible to support model-based assumptions about regulatory mechanisms in first laboratory experiments. In the next step, the model was applied to search for promising interventions that mediate induction of apoptosis in the unperturbed CFL1 model. As before apoptosis is deemed to be induced if the node "caspases" is active.
First, automatic screening was performed for single interventions that may induce apoptosis. Here, the model suggested a knockout of the proteins CD44, STAT3 or TWIST1 (Table 7). All these interventions work without changing the activity of CFL1 (Figure 31). Nevertheless, they all lead to inhibition of proliferation (inactive S-phase) and induction of apoptosis (active caspases). To evaluate the model-based interventions, a literature search was performed. Currently, there are 18 clinical studies involving CD44 inhibitors, 34 clinical studies involving STAT3 inhibitors and one observational study about a TWIST1 inhibitor (ClinicalTrials.gov).
The antisense oligonucleotide inhibitor AZD9150 [164] is the most commonly used STAT3 inhibitor in clinical trials (ClinicalTrials.gov) which is also used to treat pancreatic cancer patients (ClinicalTrials.gov: NCT02983578). Preclinical studies using AZD9150 describe a dose-mediated STAT3 reduction in lymphoma and lung cancer cells which is associated with anti-tumoral activity [164]. In conjunction with this, several studies report aberrant STAT3 activity in pancreatic cancer [362] while treatment of pancreatic cancer cells with benzyl isothiocyanate mediates apoptosis by targeting STAT3 activity [349], thus, supporting model-suggested induction of apoptosis by inhibition of STAT3 (Figure 31).

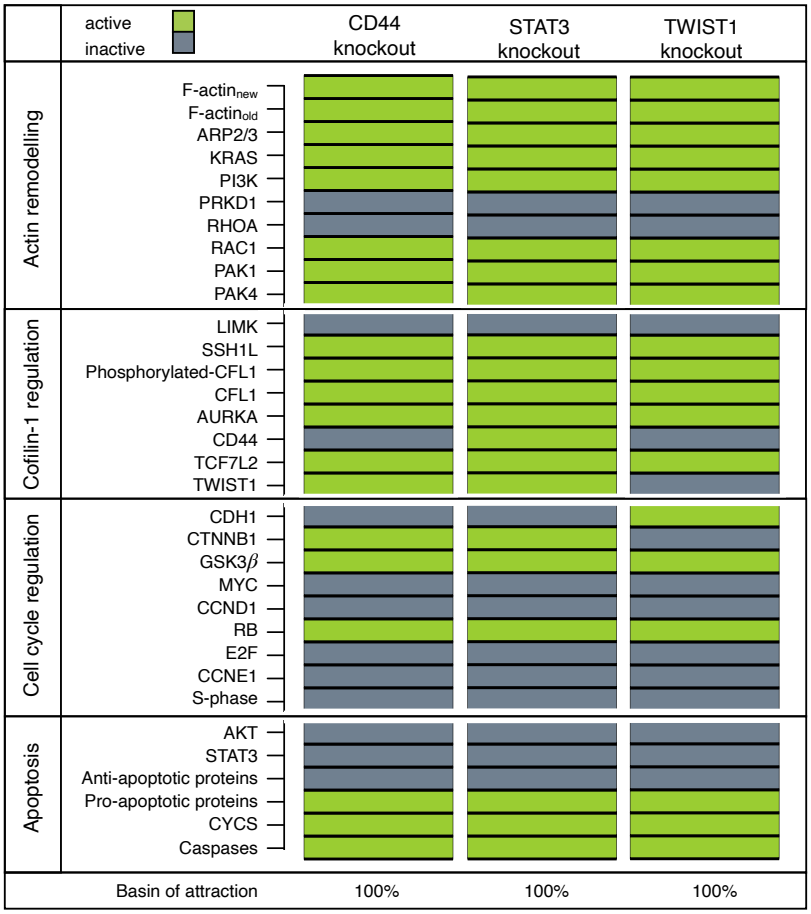

Figure 31: **Attractors of single intervention screening.** *In silico* knockouts of CD44, STAT3 or TWIST1 all result in 100% induction of apoptosis (=active caspases). Components of the network are shown on the left. The state of each component within the attractor is depicted by green (=active) and grey (=inactive) rectangles.

Several strategies have been developed to inhibit CD44 ranging from antibody treatment to ligands as carriers of chemotherapeutics or pharmacological inhibition [61]. Of these approaches, the functional monoclonal antibody RO5429083 (ClinicalTrials.gov: NCT01358903, NCT01641250), as well as the pharmacological inhibitor silibinin (ClinicalTrials.gov: NCT00487721, NCT01816490, NCT01935817), have been tested in clinical trials. Especially silibinin which showed anti-neoplastic activity in various cancer models [116, 218, 389] is able to reduce proliferation and increase the rate of apoptosis of pancreatic cancer cells [295]. While xenograft studies did not show any adverse side effect in treatment with silibinin [388] phase I clinical trials with prostate cancer patients showed the occurrence of hyperbilirubinaemia

as the most common side effect [116]. Thus, silibinin seems to be tolerated in humans [295].
Contrary to STAT3 and CD44, there are no TWIST1 inhibitors for humans. Only one observation study has been performed to assess the role of TWIST1 in the induction of EMT (ClinicalTrials.gov: NCT01927354). However, harmine the first TWIST1 inhibitor with promising anti-tumoral activity *in vivo* and *in vitro* [485], is associated with neurotoxicity in humans [63].
This initial literature search for model-suggested intervention targets indicates that it is possible to find interventions based on the proposed targets. Especially CD44 appears to be interesting in this context since CD44 inhibitors are available for humans but they are not yet tested for pancreatic cancer patients.
In addition to the individual interventions, screening was extended to combinations (Table 7). Some of these proposed interventions contain apoptosis proteins (CYCS and anti-apoptotic proteins). Therefore, they were excluded for a more detailed examination. The majority of the remaining suggestions contain either a knockout of AURKA or PAK1. The screening was performed for high infiltrating cancer cells with increased CFL1 expression. Thus, CFL1 as well as F-actin$_{new}$ and F-actin$_{old}$ can be regarded as active [264, 442, 443, 475, 479]. Based on these assumptions the effect of a single knockout of AURKA or PAK1 was studied (Figure 32). Furthermore, the impact of the other targets suggested in the combinations was tested in order to not underestimate a positive impact, even if the target is not able to induce apoptosis (Figure 32).

Table 7: Model-suggested interventions to induce apoptosis. Knockouts are marked by 0 and overexpressions by 1. Proteins are abbreviated in accordance with current nomenclature.

Single interventions	Double interventions
CD44 = 0	Phosphorylated-CFL1 = 0, CYCS = 1
STAT3 = 0	CFL1 = 1, PAK1 = 0
TWIST1 = 0	CFL1 = 1, AURKA = 0
	F-actin$_{old}$ = 1, PAK1 = 0
	F-actin$_{old}$ = 1, AURKA = 0
	F-actin$_{new}$ = 1, PAK1 = 0
	F-actin$_{new}$ = 1, AURKA = 0
	PI3K = 0, CYCS = 1
	AKT = 0, anti-apoptotic proteins = 0
	AKT= 0, CYCS = 1

Table 7: Model-suggested interventions to induce apoptosis. Knockouts are marked by 0 and overexpressions by 1. Proteins are abbreviated in accordance with current nomenclature.

Single interventions	Double interventions
	PAK1 = 0, CYCS = 1
	AURKA = 0, CYCS = 1
	SSH1L = 1, PAK1 = 0
	SSH1L = 1, AURKA = 0

Except a knockout of PI3K, all the proposed interventions yield stable single state attractors (Figure 32). Since attractors can be associated with biological phenotypes [196, 421], a treatment that can generate 34 different cell populations may not be the best for targeted treatment. Nevertheless, 97.86% of the PI3K attractors show induction of apoptosis. Opposed to that a single knockout of AKT or overexpression of SSH1L does not mediate induction of apoptosis. While AKT knockout is able to abrogate proliferation it is not able to reduce CFL1 activity and the migratory potential of pancreatic cancer cells. Therefore, there is a chance that the cells will migrate to distant tissues where other external influences affect them. This can be regarded as an external perturbation that may lead to non-assessable attractor changes. The majority of AURKA knockout or PAK1 knockout simulations conclude in an attractor showing apoptosis (98.11% or 98.69% respectively, Figure 32). In contrast to the other simulations with AKT knockout, SSH1L overexpression or PI3K knockout, the remaining states which do not lead to apoptosis conclude in an attractor that represents a quiescent cell. Here, the active form of CFL1 is repressed. Additionally, both interventions are able to abrogate the migratory potential by inhibiting F-actin and proliferation (inactive S-phase).
However, due to high sequence homology between the members of the PAK-family members, it is difficult to find specific small molecules targeting PAK1 [370]. In contrast to PAK1 inhibitors, several clinical trials are conducted using the AURKA inhibitor Alisertib (MLN8237) and its next-generation MLN8054. In total 59 clinical trials are using one of these two inhibitors and three studies include the treatment of pancreatic cancer patients (ClinicalTrials.gov: NCT00249301, NCT01677559, NCT01924260). Additionally, in preclinical studies it could be shown that treatment with MLN8237 decreases the migratory potential of cancer cells and inhibits oncogenic pathways like AKT or STAT3 [84, 194] which is in line with the attractor pattern of an AURKA knockout (Figure 32). Therefore, AURKA seems to be another interesting target for pancreatic cancer patients with high CFL1 expression.

To sum up, the fact that both AURKA and STAT3 inhibitors are already studied in clinical trials with pancreatic cancer patients can be seen as another support of the correctness of this model predictions. Additionally, the model provides three further intervention targets. Since two of them currently do not have small molecules available to treat humans the inhibition of CD44 is the most promising suggested model-based intervention target that is not yet studied in clinical trials for pancreatic cancer patients.

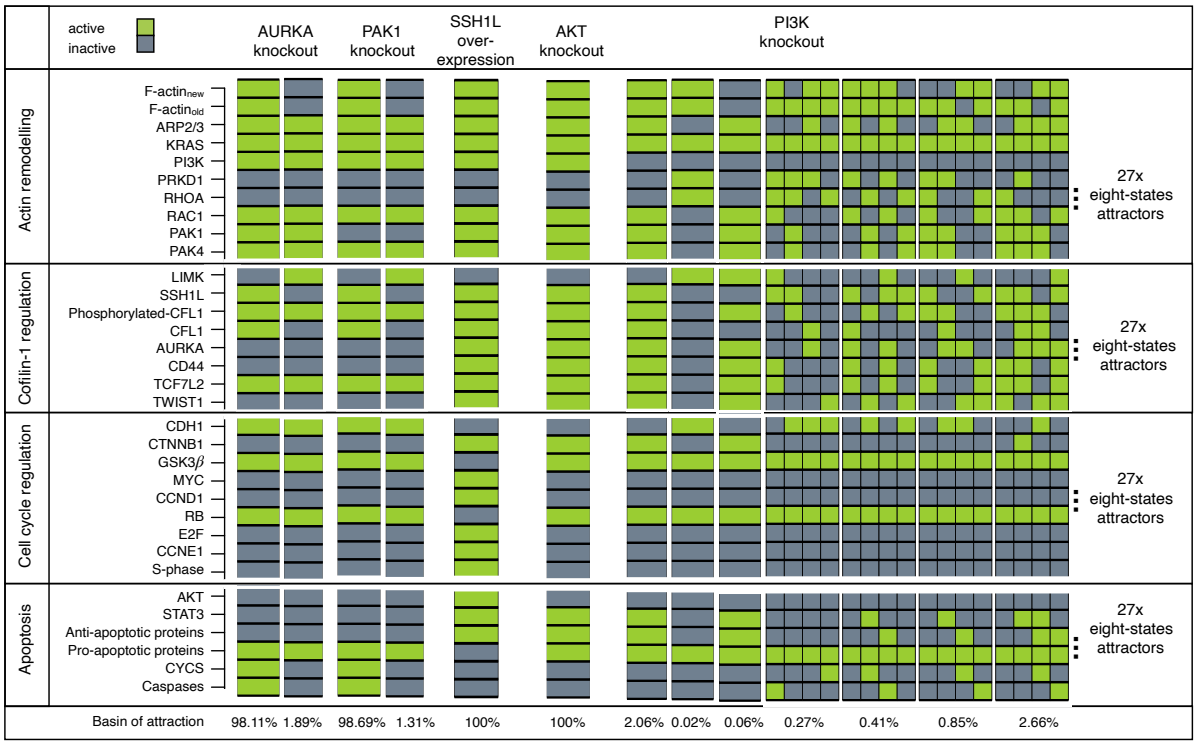

Figure 32: **Studying the impact of single knockouts of proteins suggested in combinations.** Automatic screening suggested that combinations of interventions with AURKA, PAK1, SSH1L, AKT or PI3K result in the induction of apoptosis (=active caspases). Their single intervention impact on cancer was studied. Components of the network are shown on the left. The state of each component within the attractor is depicted by green (=active) and grey (=inactive) rectangles.

3.2.2 *Discussion – Cofilin-1 in pancreatic cancer*

3.2.2.1 *Uncovering the mechanisms behind cancerous CFL1 activity*

In various types of cancer CFL1 involvement is associated with infiltration, metastasis and poorer overall survival [264, 303, 318, 442, 443, 479]. However, so far only an influence of CFL1 on the development of cancer could be described but mechanistic regulations behind it are largely unclear. Only the impact of CFL1 on actin-remodelling has been examined in more detail [72, 99, 104].
Besides actin-remodelling, the model about CFL1 in pancreatic cancer also comprises regulations of CFL1 on its own as well as regulations of cell cycle and induction of apoptosis. Thus, to the best of my knowledge, this model is the first to consider the impact of CFL1 on cancer development as a whole. For the first time, this makes it possible to check whether individual assumptions also fit into an overall picture.
Other studies have already shown that many actin regulating proteins are overexpressed in cancer [475]. Together, these studies demonstrate a change in the actin cytoskeleton composition in the development of cancer. This seems plausible since the formation of lamellipodia is a driving force for cancer migration [475]. Lamellipodia is formed downstream of RAC1 [504]. But CFL1 overexpression has been shown to increase the velocity of cell migration as well [481]. Frequently, only the depolymerizing role of CFL1 in actin remodelling is discussed [439]. Obviously, this function contributes to migration because new glomerulus actin monomers can be provided and used for new actin fibres [439]. Other studies assume that CFL1 plays a role in the formation of new actin fibres [64, 93, 382, 416]. This assumption is supported by the model simulations showing a synergistic effect of ARP 2/3 with CFL1. As long as CFL1 is inactive, new actin filaments are formed downstream of RHOA. On the other hand, activation by RAC1 with subsequent activation of ARP 2/3 is not sufficient to form new actin fibres (Figure 24). This is only possible through synergistic involvement of CFL1. Furthermore, these findings are in line with Rauhala et al. [328] showing that inhibition of ARP 2/3 subunits decreases the migratory potential of pancreatic cancer.
Silencing of CFL1 in pancreatic cancer cells is described to induce G1 arrest [211]. Similar observations are made for bladder cancer [438] and vulvar squamous cell carcinoma [464]. While Wu et al. [464] assume that the anti-tumoural effect achieved by CFL1 silencing is due to further silencing of STAT3, other studies do not go into detail about possible mechanical regulations. In contrast to these findings, CFL1 overexpression is described to induce G1 arrest in lung cancer cells [429]. Here, the authors assume an induction of p27 expression downstream of CFL1 [429]. A regulation based on cell cycle inhibitors would also be possible in pancreatic cancer cells but only if the regulators are exported from the nucleus to the cytoplasm [91].

However, this kind of regulation was excluded based on western blot results (Figure 20) showing that expression levels, as well as localisation of cell cycle inhibitors, do not change with varying of CFL1 protein levels. On the other hand, the modelling approach supports the assumption by Wu et al. [464] that CFL1 influences cell cycle regulation via its impact on STAT3. This regulatory effect was confirmed by western blots showing that the total, as well as the active STAT3 level, are dependent on CFL1 presence. Besides these findings, the model is able to propose a mechanism for cell cycle regulation. Here, STAT3 downstream of CFL1 activates AKT and MYC. They further induce CCND1 expression as well as its assembly and transport to the nucleus (Figure 24, 28). Thereby proliferation of pancreatic cancer cells may be increased. However, it should be mentioned that CFL1 alone is not responsible for the activity of STAT3. CFL1 knockdown is described to reduce the amount of STAT3 [464], but STAT3 is a kinase that requires activation to be functional. This activation can be achieved by high levels of CD44 [393] which are described for pancreatic cancer cells [241]. Based on their effect on STAT3 the interplay between CFL1 and CD44 is responsible for the high proliferation potential of pancreatic cancer cells. In line with this assumption, CFL1-independent silencing of CD44 is described to reduce the proliferation potential of pancreatic cancer cells [241]. Furthermore, inhibition of STAT3 activity by Janus kinase inhibitor AG490 is associated with reduced proliferation in pancreatic cancer cells as well [428].
The role of CFL1 in actin remodelling is well-investigated [72, 99, 104]. However, only the dynamic modelling approach that takes proteins involved in actin remodelling, as well as the activating mutation of KRAS into account, could provide a regulatory mechanism that explains how CFL1 is overexpressed and activated as described for many cancers [264, 303, 318, 443]. Based on the model, it can be suggested that CFL1 is overexpressed and activated in pancreatic cancer by an imbalance of actin remodelling. The imbalance between RAC1 and RHOA may result from permanent active KRAS present in 90% of pancreatic cancer patients [108, 215, 255, 476]. Downstream of both actin regulators AURKA expression is induced while TCF7L2 expression is no longer inhibited by PRKD1 (25, figure 27). Thus, CFL1 can be expressed and activated. This assumption is also supported by gene expression comparisons of multiple independent datasets showing a significant overexpression of AURKA as well as TCF7L2 in comparison to healthy donors (Figure 25). Another study in colorectal cancer, on the other hand, linked overexpression as well as the activation of CFL1 to the activity of CD44 [231, 406]. However, this is not necessarily a contradiction as AURKA is able to influence the expression of CD44 by stabilising TWIST1 [61, 440].
Some proteins within the CFL1 model have overlapping functions. Apart from their role in cell cycle regulation STAT3 and AKT are assigned another role. AKT is often thought to have anti-apoptotic functions and it is known that it shows enhanced

activity in pancreatic cancer cells [147, 360]. By phosphorylation of caspase-9, AKT is capable to inhibit its activation and thus arrests apoptosis [147, 415, 457]. Similar to AKT, STAT3 is associated with arresting apoptosis by inducing the expression of anti-apoptotic proteins such as MCL1 or BCL2L1 [173, 191, 457, 473, 503]. The simulation with CFL1 knockout depicts that both AKT and STAT3 are regulated in their activity by CFL1 (Figure 24). Therefore, their activity merely explains the resistance against apoptosis in CFL1 expressing cells but not in CFL1 silenced cells as shown by Kirchhoff [211]. Moreover, the simulation containing a CFL1 knockout depicts constitutively inactive CYCS which is required for activation of caspases (Figure 27). It is described that upon induction of apoptosis, CFL1 translocates to the mitochondrion to release CYCS [67, 124, 414, 415]. Thereby, CFL1 would have a positive role in the activation of apoptosis. In contrast to other types of cancer, where CFL1 knockdown is described to enhance the apoptosis rate [438, 464] a CFL1 knockdown does not induce apoptosis in pancreatic cancer cells [211]. This may be explained by the fact that the other types of cancer do not require the mitochondrial enhancing signal to induce apoptosis [147, 357].

3.2.2.2 *Attractor pattern in real patient data*

Tumour heterogeneity is a major problem in the treatment of cancer patients and contributes to therapy resistance. Especially pancreatic cancer is known for its high degree of inter-tumour heterogeneity [79, 189]. Although PDAC is the most common pancreatic cancer other types exist with distinct molecular signatures as well as clinical outcomes [79]. Samples considered to be in the single microarray datasets GSE15471 [18], GSE16515 [316] and GSE32676 [97] are described as pancreatic tumour tissues. This does not exclude different types of pancreatic cancer. For this reason and due to the immense inter-tumour heterogeneity, it is not surprising that the attractor pattern cannot be matched perfectly to the binarised expression data of tissues taken from pancreatic cancer patients (Figure 23). To assess the similarity between the patient-derived expression data and the network attractor, the normalised Hamming distance was calculated. It computes how many states of proteins in the CFL1 network are differing. Here, a mean normalised Hamming distance of 0.387 was calculated thus indicating that a mean of 38.7% of proteins differs between the attractor and the tissue-derived patient data. For a few proteins, the expression levels of tumour samples differ strongly from the attractor pattern (Figure 23). However, even those proteins do not necessarily contradict the model. RHOA, for example, is thought to be particularly important in p53 mutated tumours [424]. The CFL1 model, however, focuses on KRAS-driven tumours which are more frequent [108, 215, 255, 358, 424, 476]. In addition, active and unphosphorylated CFL1 is assumed to be overexpressed in cancer [211, 264, 303, 318, 355, 443, 475] and thus is the focus of the model. In this

respect, it could be shown that overexpression of RHOA leads to elevated phosphorylated CFL1 levels [253].
A loss of CDH1 expression occurs mainly in undifferentiated pancreatic cancer cells, which are associated with a worse prognosis [165]. The established model is supposed to represent a particularly severe phenotype. For this reason, an undifferentiated tumour was assumed whose literature description is in line with the attractor pattern.
Moreover, the expression level of GSK3β could barely be matched to the attractor pattern. GSK3β is often regarded as tumour suppressor due to its activity on CTNNB1, MYC and CCND1 [19, 103, 209, 259, 412, 427, 492]. In line with this, it could be shown that inhibition of GSK3β is responsible for growth as well as radioresistance of pancreatic cancer cells due to the resulting stabilisation of CTNNB1 [449]. However, phosphorylation of GSK3β has been described after irradiation of pancreatic cancer cells [398]. AKT is capable to inhibit GSK3β after irradiation [413]. For this reason, the behaviour of GSK3β in the expression data is also no contradiction to the CFL1 model. However, it should be mentioned that other studies assume a tumour promoting role of overexpressed GSK3β. Following this point of view, Ougolkov et al. [313] report a nuclear accumulation of GSK3β in approximately half of the analysed pancreatic cancer samples which they associate with poor differentiation. Possibly GSK3β has a different tumour-promoting function in the cell nucleus [28]. However, the CFL1 model only considers its cytoplasmic function. Thus, inactive GSK3β can be assumed as shown by the attractor of cancer (Figure 22).
In order to prevent cell cycle progression from G1 to S-phase unphosphorylated RB binds to E2F. Thereby, RB inhibits E2F's activity [60, 427, 451]. Indeed, RB is reported to be hyperphosphorylated in pancreatic cancer [135]. Hyperphosphorylation is a post-translational modification that cannot be detected on the expression level. Therefore, inactive RB is in line with the behaviour of pancreatic cancer cells. Furthermore, it also indicates that E2F is no more bound to RB and is therefore active. This further supports the attractor pattern and the biological meaning of the CFL1 model.
The behaviour of the expression levels of pro-apoptotic proteins is difficult to estimate because little is known about pro-apoptotic BCL2 proteins in pancreatic cancer [147]. However, an imbalance in favour of anti-apoptotic proteins can be assumed [353]. In line with this, overexpression of anti-apoptotic BCL2L1 is known for pancreatic cancer [173, 191, 457, 473, 503]. Additionally, some pro-apoptotic proteins such as BAD are inhibited in their activity by AKT [13, 147, 457] which is known to have increased activity [147, 360].
The explanation for the contradictory expression levels of CYCS in comparison to the attractor is similar to RB since the model assumes that CYCS is only active

when it is released into the cytoplasm. Regulatory functions like this are not determined on expression levels.
In summary, it could be shown that even the attractor states that are not consistent with the expression values have their justification and reflect the behaviour of an aggressive, undifferentiated pancreatic tumour. Given the high heterogeneity of pancreatic cancer in general, it seems impossible to find a drug that can be applied to all patients. For this reason, more targeted treatment based on tumour phenotypes could be desirable [189]. The established model focuses on pancreatic cancer showing high CFL1 expression. For this reason, the model-based treatment proposals are particularly suitable for patients with high CFL1 expression. But these suggestions may be ineffective for pancreatic cancer patients showing a completely different phenotype.

3.2.2.3 *CD44 is the most promising candidate to treat pancreatic cancer patients with high CFL1 expression*

Due to remarkable resistance, it is still challenging to treat pancreatic cancer patients [298, 372]. Hence, surgery combined with adjuvant chemotherapy offers chances for long-term survival [298, 372]. Nevertheless, cancer recurrence within one year is described for many patients [171]. Thus, the identification of new therapeutic targets is of great importance to improve the survival and therapy of pancreatic cancer patients. High-throughput screenings of pancreatic tissue identified CFL1 as a potential biomarker for pancreatic cancer [47, 134, 446]. CFL1 is described to be involved in migration and invasion of cancer [264, 442, 443, 479]. So it is not surprising that high CFL1 expression is associated with a decreased overall survival of pancreatic cancer patients [355]. For this reason, the model about CFL1 in pancreatic cancer seems to be an adequate representation of a severe phenotype. Therefore, it was used to screen for promising interventions targets.
Model screening identified a list of targets that were more closely studied concerning an application as treatment of pancreatic cancer patients (see section 3.2.1.5). Here, AKT, as well as SSH1L knockout, were excluded because they were unable to induce apoptosis by single intervention in model simulations. In addition to them, PI3K was excluded due to the high amount of resulting attractors that may represent side effects. In contrast, the simulation with PAK1 and TWIST knockout showed promising results. However, there are no specific drugs available for PAK1 [370] and only one observable study to assess the role of TWIST1 in EMT has been described so far (ClinicalTrials.gov: NCT01927354). Besides the targets already in use STAT3 (ClinicalTrials.gov: NCT0283578, NCT03382340) and AURKA (ClinicalTrials.gov: NCT00249301, NCT01924260) in the treatment of pancreatic cancer patients, CD44 seems to be interesting to study as a treatment option.
An *in silico* knockout of CD44 in the CFL1 model (Figure 31) provided promising

results. The proliferative phenotype could be blocked. More interestingly, the inhibition of CD44 lead to the induction of apoptosis. Diverse CD44 inhibitors are already being tested in clinical trials ranging from pharmacological CD44 inhibition to antibodies or aptamers [61], though none of these substances is applied to treat pancreatic cancer patients so far (ClinicalTrials.gov). However, treating pancreatic cancer patients with a CD44 inhibitor may be promising for several reasons. Firstly, the main activator of CD44 activity, hyaluronic acid, is highly expressed and secreted in pancreatic cancer cell lines such as Mia-PaCa2 leading to activation of multiple CD44 downstream targets [407]. Those include cancer-characteristic pathways such as RAS, MAPK or PI3K but also STAT3 signalling or CTNNB1 signalling are impacted by CD44 [61]. Furthermore, CD44 is described to be involved in the expression and activation of CFL1 [231, 406]. Based on these regulations, CD44 plays a role in cancer-characteristic pathways such as differentiation, adhesion or migration [241]. Secondly, chemotherapeutic treatment of pancreatic cancer cell lines with gemcitabine (a basic module of pancreatic cancer therapy [50]) induces a more invasive phenotype that shows increased CD44 expression [29]. Thus, it is not surprising that high CD44 expression correlates with an aggressive phenotype and poor survival [241]. In contrast, preclinical studies with CD44 inhibition showed reduced growth and migratory potential of pancreatic cancer cells [241, 295]. In these studies, a CD44 inhibition-associated reduction of the activity of STAT3 or p-AKT was shown[241, 393]. These findings are in line with the intervention attractor with CD44 knockout (Figure 31). Besides, AKT activity is coupled to drug resistance [305, 500] underlining more benefits of CD44 inhibition.
In summary, CD44 inhibition appears to be the most promising new target for the treatment of patients for the reasons outlined above.

3.3 Dynamic characteristics in biological networks

Many signalling pathways and their dynamic characteristics are poorly understood. Nevertheless, it is assumed that cancer or genetic diseases are rarely a consequence of a single gene mutation rather than deregulation of complex networks [23, 24]. Hence, network analysis has emerged as a powerful tool to support biological research [23]. Highly connected components (hubs) within the network structure of a biological process are frequently regarded as master regulators [34]. Since their removal is correlated with lethal phenotypes it is questionable if they are suitable targets for interventions [181]. In addition, there is evidence that hubs do not influence network dynamics [258].
As already shown above and by others (Table 8), Boolean network models are strong simplifications of biological processes but still able to depict main dynamic characteristics. Hence, they can be considered as initial models for the identification of dynamic-influencing components within biological pathways.

3.3.1 *Biologically motivated Boolean network models differ in size*

To study dynamic characteristics 40 published and biologically motivated Boolean network models describing various signalling pathways ranging from cell cycle to development to cancer were collected (Table 8). They range in size from 5 to 40 nodes and cover a large number of intermediate sizes (Figure 33). In total these Boolean network models have an average size of 19 nodes (dashed line in Figure 33A).

Table 8: Boolean network models taken from literature.

Network	Organism	Process
Azpeitia et al. 2013 [16]	*Arabidopsis thaliana*	Root stem cell niche
Brandon et al. 2015 [40]	*Aspergillus fumigatus*	Oxidative stress response
Calzone et al. 2010 [52]	*Homo sapiens*	Cell-fate decision
Cohen et al. 2015 [71]	*Homo sapiens*	Epithelial-to-mesenchymal transition (EMT)
Dahlhaus et al. 2016 [83]	*Homo sapiens*	Cancer signalling in neuroblastoma

Table 8: Boolean network models taken from literature.

Network	Organism	Process
Davila-Velderrain et al. 2015 [85]	*Arabidopsis thaliana*	Early flower development
Enciso et al. 2016 [105]	*Homo sapiens*	Lineage fate decision of haemopoietic cells
Fauré et al. 2006 [112]	*Homo sapiens*	Mammalian cell cycle
Garciá - Gómez et al. 2017 [125]	*Arabidopsis thaliana*	Root apical meristem
Giacomantonio et al. 2010 [129]	*Homo sapiens*	Cortical area development
Gupta et al. 2007 [144]	*Homo sapiens*	Neurotransmitter signalling
Herrmann et al. 2012 [159]	*Homo sapiens*	Cardiac development
Irons 2009 [179]	*Saccharomyces cerevisiae*	Cell cycle
Klamt et al. 2006 [214]	*Homo sapiens*	T-cell receptor signalling
Krumsiek et al. 2011 [220]	*Homo sapiens*	Haematopoiesis
MacLean et al. 2010 [262]	*Pseudomonas syringae*	Type III secretion system
Mai et 2009 [263]	*Homo sapiens*	Apoptosis
Marques-Pita et al. 2013 [268]	*Drosophila melanogaster*	Body segmentation
Martinez-Sanchez et al. 2015 [269]	*Homo sapiens*	CD4+ T-cell fate
Méndez et al. 2016 [276]	*Homo sapiens*	B-cell differentiation
Méndez-López et al. 2017 [277]	*Homo sapiens*	Immortalisation of epithelial cells
Mendoza et al. 2006 [278]	*Homo sapiens*	T-cell signalling
Meyer et al. 2017 [280]	*Homo sapiens*	Senescence-associated secretory phenotype
Orlando et al. 2008 [310]	*Saccharomyces cerevisiae*	Cell cycle
Ortiz-Gutiérrez et al. 2015 [311]	*Arabidopsis thaliana*	Cell cycle
Ríos et al. 2015 [332]	*Homo sapiens*	Gonadal sex determination

Table 8: Boolean network models taken from literature.

Network	Organism	Process
Saadatpour et al. 2011 [346]	*Homo sapiens*	T-cell large granular lymphocyte survival
Sahin et al. 2009 [348]	*Homo sapiens*	Cell cycle
Sankar et al. 2011 [354]	*Arabidopsis thaliana*	Hormone crosstalk
Siegle et al. 2018 [387]	*Homo sapiens*	Ageing of satellite cells
Sridharan et al. 2012 [400]	*Homo sapiens*	Oxidative stress
Sun et al. 2014 [409]	*Sea urchin*	Endomesoderm tissue specification
Thakar et al. 2012 [420]	*Homo sapiens*	Immune response against infection
Todd et al. 2012 [425]	*Saccharomyces cerevisiae*	Cell cycle
Yousefi et al. 2013 [488]	*Homo sapiens*	Metastatic melanoma

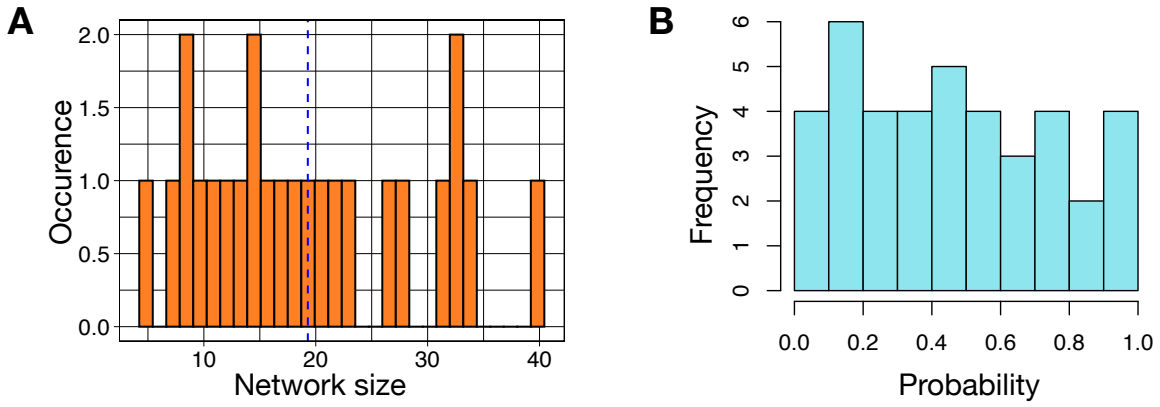

Figure 33: **Overview of chosen Boolean network models.** (A) The collected Boolean network models cover a range from 5 to 40 nodes with an average size of 19 nodes (blue dashed line). (B) The distribution of probabilities shows how plausible the connectivity of nodes within the Boolean network models can be fitted by a power-law distribution.

3.3.2 *Boolean network models of biological pathways show a scale-free topology*

The static interaction graph of biological networks consists of few highly connected nodes. The majority of nodes has only a few connections to partners [141, 152]. Such a network structure is called scale-free [24]. One characteristic of scale-free networks is that they are error-tolerant to random perturbations but sensitive to targeted interventions [6, 24]. In contrast to random networks whose degree distribution can be described by the Poisson distribution, the degree distribution of scale-free networks follows the power-law distribution [22].
To ensure that the collected 40 biologically motivated Boolean network models represent the structural characteristics of biological networks, it was tested if their connectivity follows the power-law distribution with a plausible fit [68, 130]. According to the definition by Clauset et al. [68], the hypothesis that the degree distribution of a network can be described by the power-law distribution has to be rejected if $p \leqslant 0.1$. Thus, the corresponding Boolean network models have no scale-free network topology. In total, the degree distribution of 90% (36/40) of the initially chosen Boolean network models can be described by the power-law distribution (Figure 33B) indicating a scale-free network topology. The degree distribution of the remaining Boolean network models (10%) could not be fitted to the power-law distribution. This was the case for the networks of Bauer et al. [27], Mbodj et al. [271], Thakar et al. [420] (network with *Trichostrongylus retortaeformis*) and Veliz-Cuba et al. [431]. Here, the power-law distribution fit revealed a p-value $p \leqslant 0.1$. Hence, these networks do not have a scale-free network topology and were excluded from further analyses.

3.3.3 *Removal of redundant nodes accelerates running time*

The size and complexity of Boolean network models increase rapidly with each additional node [168]. Thus, exhaustive search algorithms are currently infeasible to be applied to larger networks. One possibility to accelerate an analysis is a reduction of the search space. This can be achieved by removing redundant nodes. A node is defined as redundant if it does not influence the dynamic behaviour of any other node.
In total, the reduction strategy could reduce the network size in 21 out of the 36 collected Boolean network models. Thereby, the average network size reduced from 19 to 16.5 nodes. Interestingly, the reduction approach was able to reduce one of the Boolean network models (Kervizic et al. [202]) down to its input nodes. Since the corresponding attractors are only dependent on the input values propagated through the network and not on internal network regulation, this network was also excluded from further analyses. Since the time complexity of the exhaustive search

algorithm ($\mathcal{O}(n^k \cdot 2^k)$) to find a dynamic determining set of nodes k in a network of n nodes increases with each additional network node, the reduction approach accelerated the exhaustive search of the final 35 networks by a factor of 9.3.

3.3.4 *Small sets of nodes determine the dynamic behaviour*

The state of a node within a Boolean network model depends on the previous states of its regulators. Thus, state changes can be achieved by applying Boolean functions for each node. It is not necessarily true that all nodes in a network are involved in its dynamics. An implicant set, as defined here, is a subset of nodes that is able to determine the dynamic of a complete network. For the identification of implicant sets within the remaining 35 biologically motivated Boolean network models two strategies - a heuristic approach and an exhaustive search approach for reference - were applied.
The exhaustive search algorithm tests possible combinations of an increasingly larger set of nodes until it identifies the smallest set that is able to predefine the state of all other nodes in the network. In contrast, the applied heuristic chooses nodes according to their significance. Here, the significance of a node is maximal if its transition function depends on its own value (external input). Otherwise, the significance of a node depends on the number of nodes whose transition functions depend on that node.
Comparing both algorithms regarding their estimated running time the heuristic ($\mathcal{O}(n^2 \cdot k \cdot 2^k)$) is faster than the exhaustive approach ($\mathcal{O}(n^k \cdot 2^k)$) especially for increasingly larger implicant sets k.
If the performance of both algorithms is compared, the heuristic identified a minimal set of implicants only for 54.3% of all networks. Taking into account that the heuristic approach tries to find a solution close to the optimum [75], it was checked if the heuristic was able to identify a minimal set or a superset of implicants compared to the exhaustive algorithm (Appendix Table 12, Figure 34A). The former was the case for 32 implicant sets out of 35 supporting the good performance of the heuristic. In total, the analysis of the implicant sets demonstrated that the typical set size of nodes determining the dynamic behaviour in biologically motivated Boolean network models is small ranging from one to nine nodes (exhaustive algorithm, Figure 34B). Only a poor relation between the size of the implicant set and network size could be found. Neither Pearson correlation (0.32 for the exhaustive approach and 0.39 for the heuristic), nor a regression line ($R^2 = 0.104$ for the exhaustive approach and $R^2 = 0.153$ for the heuristic approach) could describe the relation with a plausible fit. The best fit for the relation between network size n and size of the implicant set k could be achieved with a logarithmic function ($y \sim y_{max} \cdot (1 - exp(-k \cdot n)) + Plateau$, Figure 34B).

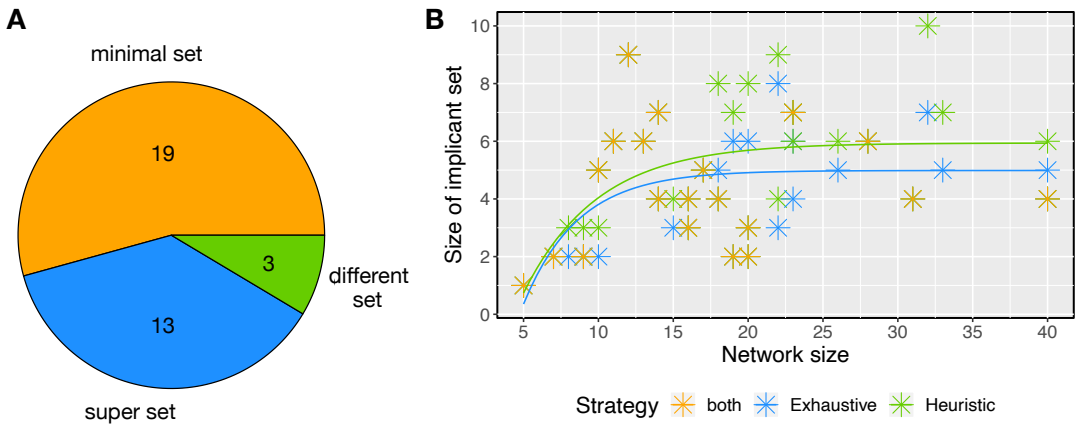

Figure 34: **Implicant sets.** (A) Comparison of the identified sets by the exhaustive and heuristic approach. (B) The general size of the implicant sets is small. The best fit for the relation between network size n and the size of the implicant set k could be achieved by using a logarithmic function $y \sim y_{max} \cdot (1 - exp(-k \cdot n)) + Plateau$ (with $y_{max} = 12, k = 1/12$ and Plateau$= 0$).

3.3.5 *Stable attractors are observable from the implicant sets*

Boolean network models are used to investigate complex mechanistic regulations. In particular, their long-term behaviour plays an important role in the identification of biological phenotypes [196, 421]. Thus, stable attractors are of special interest.
All analysed 35 Boolean network models together have 427 attractors (12.2 on average). This provokes the question if all attractors are biologically meaningful. In general, an attractor is called stable if it can be reached no matter whether the synchronous or asynchronous model simulation is applied [216]. Single state attractors are considered stable [216]. However, not all single state attractors could be found by both synchronous and asynchronous attractor search (Appendix Table 13). In total, 63.45% of attractors can be found by both synchronous as well as asynchronous model simulation (Table 13). In contrast, an evaluation of the attractors which were found starting from the implicant sets (Appendix Table 12) and then applying partial assignment identified an overlap of 90.4% to synchronous model simulations. Note that for these analyses the average effect per network was taken into account since the investigated networks differ strongly in their number of attractors (range from one attractor to 54 attractors).
While common attractors of the synchronous and asynchronous simulations were only single state attractors, synchronous evaluation and simulations from the implicant set also shared multi-states attractors. Detailed analyses of biologically meaningful Boolean networks e.g. of the cell cycle [112] already showed that multi-state attractors are of interest. Thus, the set of identified attractors based on the impli-

cant sets may be more biologically representative than stable attractors identified by synchronous and asynchronous network evaluation.
To find further support for this hypothesis the Boolean network models in which not all attractors could be found were analysed in more detail. By looking at the progression of the partial assignments from the implicant sets to the attractors it was observed that some already defined nodes change their states. This behaviour could not be observed in a partial assignment that identified the complete set of the network's attractors. The synchronous attractor search includes all states of the state space while the partial assignment already excludes states. Therefore, some refinements were applied to increase the state space of the attractor search from the implicant sets:

- Boolean functions are only applied to nodes still undefined
- Boolean functions are applied to all nodes except the implicant nodes
- All values can change by applying Boolean functions. If all nodes are determined then the implicants are reset to their initial value.

Based on the refinements, the set of attractors resulting from the implicant sets could be increased from 90.4% to 93.7%. However, few attractors could still not be found. In order to find reasons for this behaviour, the next step was to compare the interaction graph of these networks with the attractor patterns and the corresponding Boolean functions. This analysis indicates that all missing attractors were extremely fragile and could only be identified by synchronous updating schemes. All of these networks included oscillating states whose equilibrium would be changed by short temporal interferences. These interferences would lead to attractors that can be found based on the implicant set (Figure 35).
Simultaneous state changes do not reflect biological reality [5, 343]. Thus, it can be assumed that even if there are only small variations in time, the oscillating two-states attractors would not exist. They would immediately switch to one of the single state attractors. Consequently, it can be presumed that the presented method to search for attractors based on an implicant set identifies biologically plausible and only stable attractors.

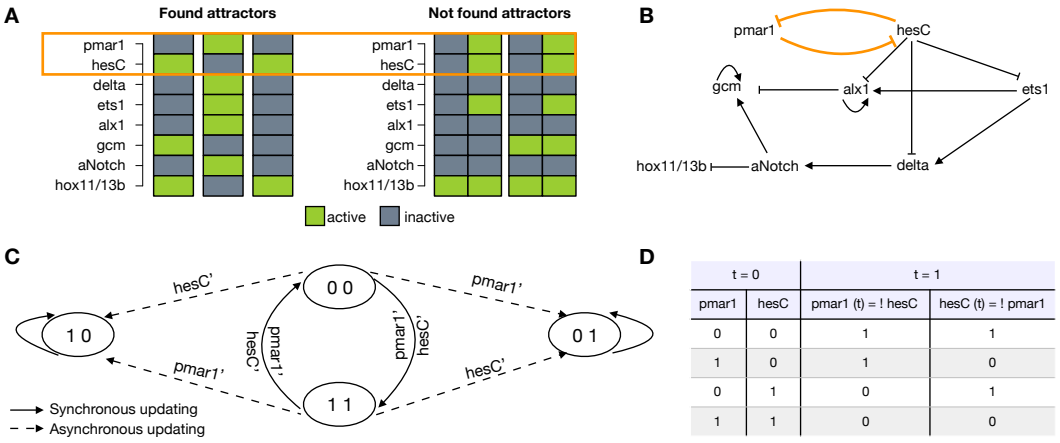

t = 0		t = 1	
pmar1	hesC	pmar1 (t) = ! hesC	hesC (t) = ! pmar1
0	0	1	1
1	0	1	0
0	1	0	1
1	1	0	0

Figure 35: **Unstable attractors.** (A) Two attractor patterns in the Boolean network model of Sun et al. [409] with oscillating states cannot be found by applying partial assignment to the implicant set. Genes that change their state in the two-states attractor are pmar1, hesC and ets1. But only pmar1 and hesC (marked in orange) are mutual inhibitors (see interaction graph of the Boolean network model (B)). The effect on the dynamic can be seen in the state transition graph showing only the two nodes pmar1 and hesC (C). During synchronous updating, the attractor switches between the two states {00} and {11}. However, if a small temporal perturbation takes place and only one node is updated (comparable to asynchronous updating) the system switches to one of the single state attractors. (D) Truth table with synchronous updating of nodes pmar1 and hesC.

3.3.6 *The majority of implicant nodes is low connected but behaves like hub nodes*

The impact of hub nodes on network dynamics is a controversially discussed topic [212]. Some studies describe that it is almost impossible to eliminate the activity of hub nodes by targeted inhibition with small molecules [258, 396]. However, if hub nodes are permanently active their states do not affect the dynamics of a network. Opposed to this opinion there are studies describing hubs as master regulators since their removal correlates with lethal phenotypes [181]. Probably the biggest difference between both observations is that the one side considers the influence of a complete loss of the node while the other side assumes an inhibition.
It has already been shown that it is possible to identify stable attractors based on the implicant sets. Since it is possible to determine the dynamics of a whole Boolean network model based on a small set of implicant nodes, the connection of these implicant nodes was examined in more detail. To ensure that the degree of interactions of the considered proteins within the 35 Boolean network models reflects biology, automatic screening of the protein interaction database BioGRID

[403] was performed. Here, no difference ($p = 1.0$) between the degree of proteins in the Boolean network models and the BioGRID database could be identified. This allows the conclusion that Boolean network models are suitable to evaluate the impact of node degrees on network dynamics.
Within the structure of the considered Boolean network models, 3% of the nodes could be identified as hubs (z-score > 2.5 [141]). Detailed analyses revealed that these hub nodes differ significantly from nodes within the implicant set ($p = 1.5 \cdot 10^{-56}$) namely, the majority of implicant nodes are lowly connected and can still influence the whole network dynamics.
Based on the fact that the majority of implicant nodes are lowly connected, the effect of targeted *in silico* interventions was studied and implicants, hubs and the remaining nodes were compared (Figure 36). It was investigated whether the intervention of different kinds of nodes influences the number of missing attractors. In this context, a pronounced disappearance of attractors can be considered as a strong intervention effect. Furthermore, it was examined whether new additional attractors are created as a result of the intervention. This would indicate the occurrence of side effects. Interestingly, no significant differences could be detected between hubs and implicants concerning their impact as intervention targets. Although the effect size of hub nodes regarding the loss of attractors was more pronounced, these interventions also evoked more side effects (additional attractors, Figure 36). The comparison between the set of implicants and the remaining set of nodes which are neither hubs nor implicants revealed a significantly larger effect for implicant nodes. They produced stronger effects ($p = 0.042$) and a reduced occurrence of side effects ($p = 0.003$).
Based on these findings, the targeted intervention of implicants seems to be a good possibility to achieve sufficient effect size with a reduced risk of side effects.

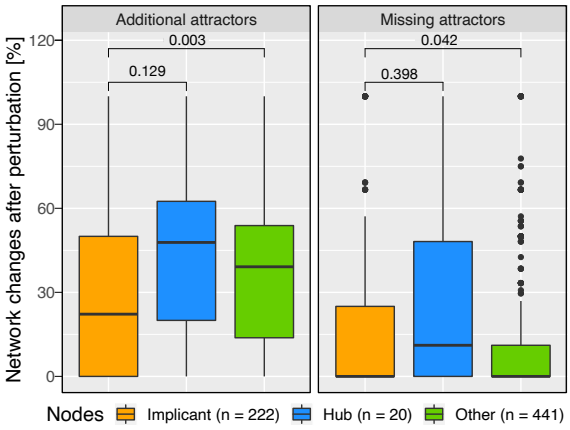

Figure 36: **Impact of interventions.** The impact of targeted interventions like overexpression or knockout experiments differs depending on the kind of perturbed node (implicant, hub or other nodes).

3.3.7 *Lowly connected implicants are suitable for targeted interventions*

On the basis of the previous intervention studies, it could be shown that implicants have a larger impact on dynamics compared to other nodes within the network. At the same time these targets produce fewer side effects (Figure 36). However, so far in this work, the impact of interventions was studied based on mathematical models. In order to investigate whether this behaviour of implicants can be transferred to real biological systems, *in silico* intervention screenings with implicants were performed. The obtained attractor patterns were then compared to laboratory experiments. A special focus was on lowly connected implicant nodes.
The two implicants AKT2 (z-score: 0.98) and TWIST1 (z-score: 0.04) are both parts of the implicant set of the Boolean network model of Cohen et al. [71] describing tumour development. Overexpression of AKT2 in simulations yields an attractor showing EMT and inhibition of apoptosis. Both are characteristics that indicate a tumour promoting role. These assumptions can be supported by the literature. PTEN, an inhibitor of AKT's activity, is frequently lost during tumour development thus leading to activation of AKT [126]. Active AKT is able to phosphorylate caspase-9. Thereby it can inhibit apoptosis [147, 415, 457]. Furthermore, active AKT inhibits GSK3β/Snail signalling and supports EMT [342]. Contrary to the overexpression of AKT2 the simulations of a TWIST1 knockout seems to prevent tumour development. This finding is also in line with laboratory experiments. A knockout of TWIST1 inhibits the expression of EMT markers in breast cancer cell lines and thus metastases in immune-deficient mice [474].
Another example of efficient interventions of less connected implicants can be found in the network of Méndez-López et al. [277] describing EMT. Within this

network, all implicants, Snai2, ESE2 and p16 respectively, are lowly connected (z-score: −0.5; −0.6; 0.7). Simulations revealed the biggest effect for interventions of the implicant Snai2. While the overexpression study of Snai2 yields only an attractor with mesenchymal characteristics, Snai2 knockout simulation resulted in an attractor that loses these mesenchymal characteristics. These findings of the simulation are in line with *in vitro* experiments showing that Snai2 overexpression leads to the mesenchymal appearance of cells within 72 hours [59] while its depletion supports premature cell differentiation [284].
Despite their impact on cancer development effects of less connected nodes can also be found in other pathways. For example, the Boolean network model of Krumsiek et al. [220] describes haematopoiesis. This network contains six low connected implicants. Knockout simulations with each of those implicants led to the disappearance of blood cell lineages without creating additional attractors. The evidence of these results could be confirmed by several *in vitro* experiments [193, 198, 227].
The mentioned examples suggest that besides hubs other characteristics within the network structure should be considered for intervention screenings. The presented methods are able to identify those components of interest.

3.3.8 *Intervention screening for treatment of colorectal cancer patients*

Applying the newly developed methods to screen for intervention targets in already published Boolean network models showed promising results. Likewise, the search for implicants in the CFL1 network identified KRAS as important dynamic influencing regulator. KRAS acquires activating mutations in approximately 90% of pancreatic cancer patients [108, 215, 255, 476] thus supporting the biological evidence of this finding.
In the next step, a new Boolean network model about the crosstalk of Wnt and MAPK signalling in colorectal cancer was developed to search for intervention targets. It comprises 45 nodes. A granular description of its regulatory interactions can be found in Table 9. Both pathways - Wnt and MAPK - are frequently mutated in colorectal cancer leading to progression of the disease [14, 118, 183]. While APC loss of function occurs in 90% of colorectal cancer patients [14], KRAS acquires aberrant activation in approximately 50% of cases [233]. However, having only one of these two mutations is not sufficient to induce a severe phenotype. Only if both mutations are present together, they evoke a severe phenotype with cancerous characteristics [233]. This can be observed in the simulation of cancer progression (Figure 37).

Table 9: Boolean functions of the model about Wnt/MAPK crosstalk in colorectal cancer. All proteins are abbreviated in accordance with the current nomenclature. Logical connectives are depicted by & (=AND), | (=OR), and ! (=NOT).

	Node	Boolean network function	References
Wnt signalling	FZD	MEK | ERK | JNK	FZD is activated by phosphorylation of either mitogen-activated protein kinase kinase (MEK), ERK or JNK [234, 491].
	DVL	FZD	DVL is phosphorylated by FZD [183].
	$GSK3\beta_{cyt}$	!APC | $GSK3\beta_{deg}$	GSK3β is overexpressed in colorectal cancer and has a function apart from the DC [374].
	$GSK3\beta_{deg}$	!PGE2 & !AKT & !ERK & !NF-κB	Phosphorylation of GSK3β by AKT, ERK or prostaglandin E_2 (PGE2) inhibits its activity. NF-κB disrupts the interaction of GSK3β with β-transducin repeat-containing protein (β-TCRP) thus targeting GSK3β for degradation [376, 402, 477, 491].
	$GSK3\beta_{DC}$	AXIN1	Binding to AXIN1 within the DC shelters GSK3β from inhibition by other factors [402].
	APC	APC	APC is lost in early phase of colorectal cancer [118, 183, 465]. Therefore, it was assumed as input.
	AXIN1	DVL	Phosphorylated DVL inhibits the activity of AXIN1 in the DC [183, 287, 491].
	AXIN2	TCF/LEF	Expression of AXIN2 is induced by T-cell factor/lymphoid enhancer-binding factor (TCF/LEF) [234, 468, 491].

Table 9: Boolean functions of the model about Wnt/MAPK crosstalk in colorectal cancer. All proteins are abbreviated in accordance with the current nomenclature. Logical connectives are depicted by & (=AND), | (=OR), and ! (=NOT).

	Node	Boolean network function	References
Wnt signalling	DC	!DVL & $GSK3\beta_{DC}$ & APC & (AXIN1 | AXIN2)	The DC is composed of GSK3β, APC, casein kinase 1 (CK1) and either AXIN1 or AXIN2. Its inactivation is triggered by phosphorylated DVL [118, 183, 287, 465, 491].
	CTNNB1	!DC	The active DC marks cytoplasmic CTNNB1 for proteasomal degradation [118, 183, 287, 465, 491].
	TCF/LEF	CTNNB1 & KRAS & RAC1 & (PAK1 | AKT | MEK | IQGAP1 | TIAM1 | NF-κB | SNAIL1)	Cytoplasmic CTNNB1 translocates into the nucleus where it activates TCF/LEF [183, 287]. Further factors are necessary for nuclear translocation of CTNNB1 such as KRAS or RAC1 [491]. Transcriptional activity of the CTNNB1-TCF/LEF complex can be induced by PAK1, AKT, MEK, IQ motif-containing GTPase-activating protein 1 (IQGAP1), T-lymphoma invasion and metastasis-induction protein (TIAM1), NF-κB and SNAIL1 (snail family transcriptional repressor 1) [43, 49, 111, 183, 368, 405, 482, 491].

Table 9: Boolean functions of the model about Wnt/MAPK crosstalk in colorectal cancer. All proteins are abbreviated in accordance with the current nomenclature. Logical connectives are depicted by & (=AND), | (=OR), and ! (=NOT).

	Node	Boolean network function	References
Wnt/MAPK crosstalk	AKT	(PI3K | PAK1 | SNAIL1) & !PP2A & (NFκB | TCF/LEF | SNAIL1)	TCF/LEF, NF-κB or SNAIL1 are able to induce the transcription of AKT [95, 377, 432]. PI3K or PAK1 activate AKT [377, 482] while SNAIL1 further enhances AKT's activity [432]. in contrast, protein phosphatase 2A (PP2A) dephosphorylates AKT [78].
	IQGAP1	$!GSK3\beta_{deg}$	Inhibition of GSK3β frees IQGAP to regulate RAC1 [410].
	TIAM1	(EGFR | AKT) & !PP2A & (MYC | TCF/LEF)	The transcription of the guanine nucleotide exchange factor TIAM1 is induced by MYC or TCF/LEF [265, 291]. TIAM1 can be activated by the epidermal growth factor receptor (EGFR) or AKT [505] and is inhibited by PP2A [505].
	RAC1	(TIAM1 | IQGAP1 | mTORC1 | PI3K | FZD) & !APC	RAC1 can be activated by TIAM1, mTORC1, PI3K or FZD [142, 478, 480]. IQGAP1 stabilises RAC1 in its active form [458]. APC loss enhances RAC1 expression [291].
	PAK1	RAC1 & !PP2A	RAC1 activates PAK1 while PP2A inhibits it [456, 482].
	JNK	RAC1	RAC1 activates JNK [106].

Table 9: Boolean functions of the model about Wnt/MAPK crosstalk in colorectal cancer. All proteins are abbreviated in accordance with the current nomenclature. Logical connectives are depicted by & (=AND), | (=OR), and ! (=NOT).

	Node	Boolean network function	References
Wnt/MAPK crosstalk	PGE2	COX2 | (SNAIL1 & HDAC2)	Cyclooxygenase-2 (COX2) is the main regulator of the conversion of arachidonic acid into PGE2 [437]. SNAIL1 and histone deacetylase 2 (HDAC2) inhibit 15-hydroxyprostaglandin dehydrogenase thus increasing PGE2 [17].
	HDAC2	!APC & MYC	Loss of APC induces HDAC2 expression by transcriptional regulation of MYC [465, 506].
	ERBB1	HDAC2 | AP1 | TCF/LEF	MYC, activator protein 1 (AP1) or TCF/LEF are inducers of the transcription of the epidermal growth factor receptor gene (ERBB1) [35, 66, 281].
	FAS	NF-κB & !CTNNB1	Active CTNNB1 represses the transcription of NF-κB regulated genes including the Fas cell surface death receptor gene (FAS) [90].
	NF-κB	(RAC1 | ERK | AKT) & HDAC2 & $GSK3\beta_{cyt}$	NF-κB is activated by phosphorylation of RAC1, ERK or AKT [2, 245, 320]. Furthermore, it requires GSK3β to be active [163]. HDAC2 is responsible for nuclear localisation of NF-κB [190].

Table 9: Boolean functions of the model about Wnt/MAPK crosstalk in colorectal cancer. All proteins are abbreviated in accordance with the current nomenclature. Logical connectives are depicted by & (=AND), | (=OR), and ! (=NOT).

	Node	Boolean network function	References
Wnt/MAPK crosstalk	MYC	(ERK | TCF/LEF) & !APC & (!PP2A |CIP2A) & !GSK3β_{deg}	ERK or TCF/LEF induce transcription of MYC in the absence of APC [234, 286, 465]. GSK3β phosphorylates MYC for degradation [136]. If not bound to cancerous inhibitor of PP2A (CIP2A), PP2A degradates MYC [86, 460].
	cJUN	(ERK | TCF/LEF | COX2) & JNK	ERK or TCF/LEF induce the transcription of Jun proto-oncogene (cJUN) [183, 465, 491]. COX2 increases levels of cJUN [238]. JNK enhances the activity of cJun [235].
	cFOS	(TCF/LEF | ERK) & (ERK | RSK1/2)	Fos proto-oncogene (cFOS) expression can be induced by TCF/LEF or ERK [55, 183, 450]. Furthermore, ERK or 90-kDa ribosomal S6 kinase (RSK1/2) phosphorylate cFOS thereby activating it [55, 450].
	AP1	cFOS & cJUN	cFOS and cJUN build the AP1 transcription factor complex [465].
	COX2	AP1 | NF-κB | TCF/LEF	Expression of COX2 can be induced by AP1, NF-κB or TCF/LEF [12, 465].
	SNAIL1	((AXIN2 | ERK | NF-κB) & !GSK3β_{deg}) | (AXIN2 & GSK3β_{deg}	AXIN2, ERK or NF-κB induce the expression of SNAIL1 [240, 467, 468]. GSK3β inhibits SNAIL1 but binding of GSK3β to AXIN2 reduces its activity [468].

Table 9: Boolean functions of the model about Wnt/MAPK crosstalk in colorectal cancer. All proteins are abbreviated in accordance with the current nomenclature. Logical connectives are depicted by & (=AND), | (=OR), and ! (=NOT).

	Node	Boolean network function	References
Wnt/MAPK crosstalk	CDH1	(!SNAIL1 & !HDAC2 & !AKT) | (!SNAIL1 & HDAC2 & AKT) | (!SNAIL1 & !HDAC2 & AKT) | (!SNAIL1 & HDAC2 & !AKT) | (SNAIL1 & !HDAC2 & !AKT) | (SNAIL1 & HDAC2 &!AKT) | (SNAIL1 & !HDAC2 & AKT)	The repression of CDH1 by SNAIL1 further requires HDAC2 and AKT [317, 432, 468].
	Tight junction	CDH1 & (!IQGAP1 | APC | (RAC1 & IQGAP1))	Tight junctions are build by linking CDH1 to surrounding cells [458]. If not bound to RAC1, IQGAP1 disrupts tight junctions [458]. Presence of APC at the cell membrane promotes building of tight junctions [297].
MAPK signalling	EGFR	ERBB1 & PGE2 & !ERK	The gene ERBB1 encodes the EGFR [273]. PGE2 transactivates EGFR [46, 314] while ERK suppresses EGFR [286].
	KRAS	EGFR & !DC	EGFR activates KRAS. Within the DC, GSK3β degradates KRAS [183, 286].
	PI3K	EGFR | KRAS | PGE2	Activity of PI3K can be induced by EGFR, KRAS or PGE2 [307, 314, 465, 505].
	RAF	KRAS & !ERK & !AKT	KRAS phosphorylates RAF [273, 279] while ERK or AKT inhibit RAF [279, 286].
	MEK	RAF	MEK phosphorylates RAF [273, 279, 491].
	SCF	IQGAP1 & RAF & MEK	IQGAP1 is required for the scaffolding (SCF) complex of the MAPK cascade [338].

Table 9: Boolean functions of the model about Wnt/MAPK crosstalk in colorectal cancer. All proteins are abbreviated in accordance with the current nomenclature. Logical connectives are depicted by & (=AND), | (=OR), and ! (=NOT).

	Node	Boolean network function	References
MAPK signalling	ERK	(SCF | PAK1) & !PP2A	The presence of SCF activates ERK [286, 491]. Inhibition of PAK1 evokes an inhibition of ERK [482]. PP2A dephosphorylates ERK [78].
	eIF4F	ERK | mTORC1	Eurkaryotic initiation factor 4F (eIF4F) is a substrate of ERK or mTORC1 [286, 465].
	RSK	PI3K & ERK	ERK phosphorylates RSK [11]. RSK is fully activated by pyruvat dehydrogenase kinase 1 (PDK1), a component of the PI3K complex [11].
	S6K1	mTORC1 & PI3K	mTORC1 phosphorylates S6K [465]. Full activation is achieved by PDK1 [465].
	EBP1	!ERK & !mTORC1	The Erb3-binding protein (EBP1) is inhibited by mTORC1 and ERK [286, 465].
	TSC1/2	$GSK3\beta_{deg}$ & !ERK & !AKT	ERK or AKT inhibit TSC1/2 by phosphorylation [465]. GSK3β activates TSC1/2 [178, 380].
	mTORC1	!TSC1/2	mTORC1 is inhibited by TSC1/2 [465].
	PP2A	!CIP2A	CIP2A inhibits PP2A [78].
	CIP2A	EGFR | MEK | ERK	CIP2A is activated either by EGFR, MEK or ERK [86, 204, 460].

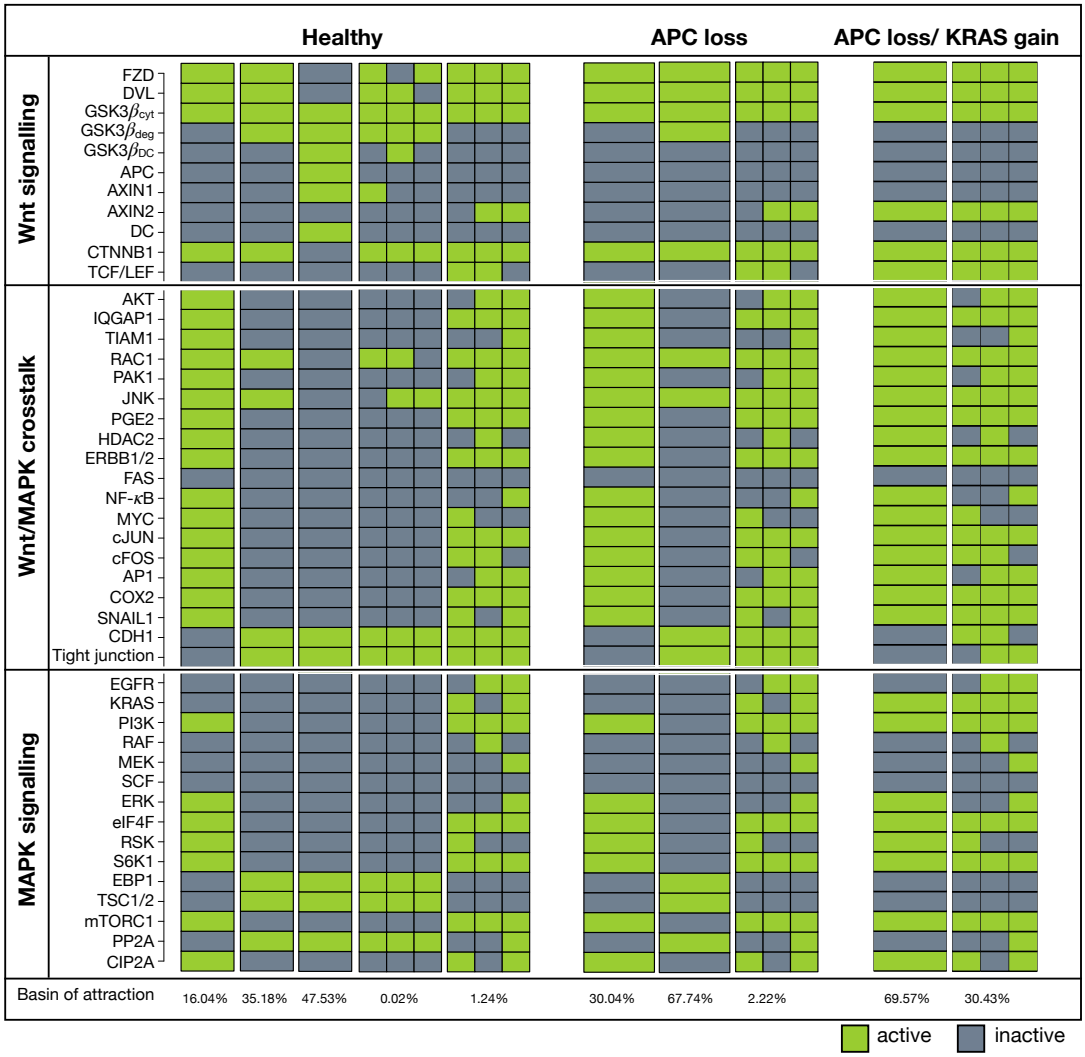

Figure 37: **Progression of colorectal cancer.** Simulations depict the populations of cells in the progression of colorectal cancer. Initially, APC loses its function [14, 183]. Next, KRAS acquires a mutation leading to permanent activation [183, 233]. These changes modify the crosstalk between Wnt and MAPK leading to progression of the disease [233]. Proteins are listed on the left and the state of each component is represented by coloured rectangles.

The simulation of the unperturbed colorectal cancer network revealed a set of attractors (Figure 37). Here, the majority of genes are inactive resembling a healthy, quiescent cell. However, a subpopulation of attractors (16%) shows proliferative traits with active Wnt signalling. Since high levels of Wnt at the intestinal crypts are required for tissue turnover itself [70], this is acceptable behaviour for a healthy state.

When colorectal cancer development takes place, a first step is the functional loss of APC [14]. This condition can be simulated in the model by fixing APC to zero. The consequent simulation yield three attractors (Figure 37). The majority of these attractors (97.8%) shows an accumulation of CTNNB1 without activating further downstream targets like TCF/LEF. Only a minority of the obtained attractors (2.2%) shows activation of RAS signalling partially activating CTNNB1 downstream targets. These two kinds of attractors with active and inactive TCF/LEF can be interpreted as different adenoma states with different prognoses. However, it should be mentioned that RAS cascade is still regulated. This includes the nuclear localisation of CTNNB1 that is required to activate TCF/LEF and could be shown to be absent in adenoma patients [217]. This version of the model may represent familial adenomatous polyposis (FAP) patients who acquire APC loss [14]. However, these patients can live for years without developing cancer [180] thus supporting the idea that single APC loss is not enough to induce severe cancer conditions.
The next step in colorectal cancer progression is the acquisition of an activating KRAS mutation [14, 183]. This was simulated by fixing APC to zero and KRAS to one. The resulting attractors show activation of Wnt and MAPK cascades as well as activation of crosstalk-regulated components (Figure 37). Comparing both attractors, the cyclic three-states attractor represents a milder phenotype since it still contains residual PP2A activity which can be associated with a better prognosis and overall survival [78].
The model simulations of colorectal cancer progression reflect disease progression and could be supported by biological evidence. Therefore, in a next step, the model can be used as a basis to search for promising intervention targets.
The heuristic approach identified seven implicants in the newly established colorectal cancer model namely APC, ERK, TCF/LEF, $GSK3\beta_{deg}$, CIP2A, AKT, and RAC1. Two of them (ERK and TCF/LEF) were identified as network hubs while the majority of the other nodes is less connected to their interactions partners (see Figure 38A). Next, intensive *in silico* screening was performed with the proposed intervention targets (Figure 38B) and model simulations were compared to literature descriptions. Besides APC and $GSK3\beta_{deg}$, all identified implicants had an active state in the simulation of severe colorectal cancer (Figure 37). Therefore, intervention screening was restricted to either knockout or overexpression simulations.
Only APC was excluded from further screening. The finding of APC as implicant is another proof of principle that the established heuristic works. APC is the most altered protein in colorectal cancer and is seen as one of the inducers of colorectal cancer [14, 118, 183]. Since APC is lost in colorectal cancer due to a truncation of the protein [497], a reactivation of this protein was not studied in more detail. However, it should be mentioned that a pre-clinical study with the small molecule truncated APC selective inhibitor (TASIN-1) showed that it is possible to eliminate cells with

APC truncation based on the principle of synthetic lethality [497].
For further screenings, the most severe phenotype with inactive APC and present KRAS was considered. Besides APC, ERK was the second implicant identified by the heuristic approach. A knockout of ERK not only reduced the population of attractors. Besides, it abrogated proliferation and migration by inhibiting MYC and restoring CDH1 at the cell membrane. Moreover, small molecules to target ERK in solid tumours are being tested in clinical trials [127, 408]. These facts present ERK as a promising intervention target.

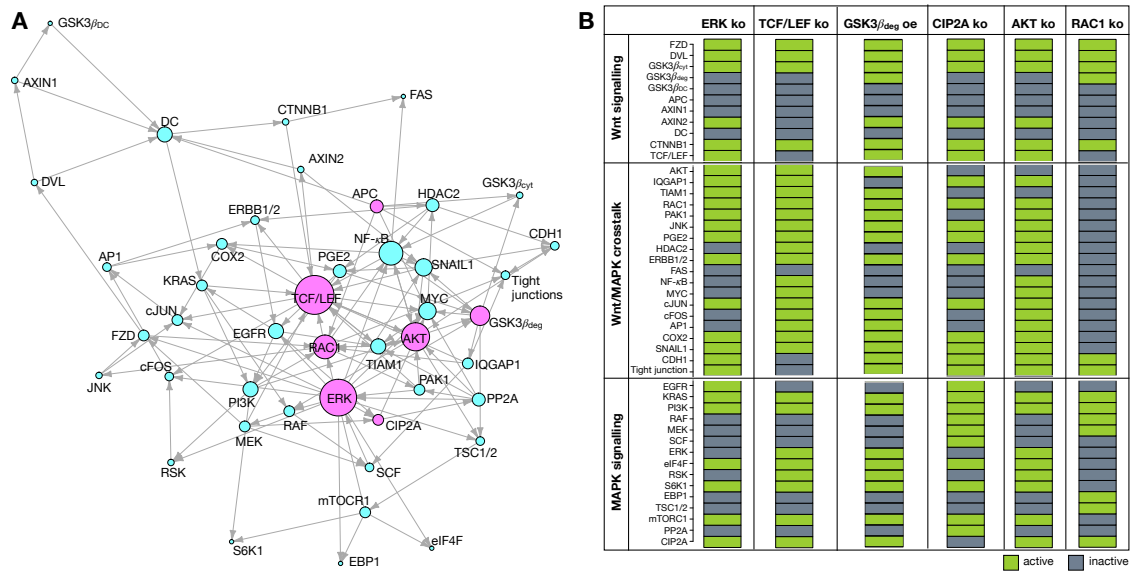

Figure 38: **Implicants within the colorectal cancer model.** (A) Depicted are the regulatory interactions within the colorectal cancer model of Wnt/MAPK crosstalk. Degree of interaction is marked by the sizes of the nodes. Components that were identified as implicants by the heuristic approach are highlighted in pink. (B) Attractors show the long-term behaviour of interventions (knockouts (=ko) and overexpression (=oe)) with implicant nodes. Simulations were performed on the basis of a severe phenotype with inactive APC and active KRAS. Proteins are listed on the left. Their state of activity is represented by coloured rectangles.

Similar to ERK, a knockout of TCF/LEF reduced the population of attractors. However, the obtained attractor neither reduced proliferation nor the migratory potential. This might be explained by the redundant role of ERK on TCF/LEF downstream targets which are permanently active in the attractor. Due to the persistent cancerous characteristics even after a knockout of TCF/LEF, this implicant can be excluded as a target for further studies. Likewise, overexpression of TCF/LEF would make no sense since it is the major target of the Wnt cascade [183, 465] and the aim of the intervention is to silence stable Wnt signalling.

$GSK3\beta_{deg}$ is permanently inactive in the attractors representing the worst phenotype. Thus, reactivation by overexpression of $GSK3\beta_{deg}$ was investigated within the *in silico* simulations. Although the simulations revealed inhibition of proliferation and restoration of tight junctions, these results should be interpreted with caution. Besides its role in the DC, the activity of GSK3β is connected to pro-oncogenic activities [374]. These two opposed mechanisms can be guided by the presence of further proteins like β-casein which prevents the access of GSK3β to the proteasome [466].
The knockout simulations with CIP2A also revealed promising results. It reversed the proliferative phenotype and restored CDH1 at tight junctions. Besides, inhibitors for CIP2A are already approved for lung cancer [248]. These facts make CIP2A a promising target for further studies.
Although a knockout of AKT could inhibit proliferation as well as migration in the simulation, it is not the best target. Clinical trials with AKT inhibitors already indicate resistance mechanisms especially in colorectal cancer patients [395]. This precludes a more detailed study of AKT as an intervention target for these patients.
A knockout of the implicant RAC1 showed promising results in simulations. It induced deactivation of the majority of nodes but still maintained CDH1 at tight junctions. This effect of RAC1 may be explained by the fact that RAC1 is required for the nuclear shuttling of CTNNB1, further activating Wnt downstream targets [491]. However, there are no selective RAC1 inhibitors on the market for the treatment of human beings [32]. Therefore, this treatment strategy is not applicable in clinical trials in anytime soon and was excluded from *in vitro* testing.
Taking all these results into account as well as the availability of small molecule treatments for humans and the fact that their intervention is not yet tested in clinical trials, the most promising targets for further investigation are ERK and CIP2A. Note that ERK is a hub node while CIP2A is less connected to its interaction partners. Furthermore, to include the loss of APC that takes place in 90% of colorectal cancer patients [14], the colorectal cancer cell line SW480 was chosen as a model system since it expresses a truncated form of APC [113]. In order to examine the effects of the proposed targets ERK and CIP2A, both proteins were treated with specific inhibitors.
Loss of APC is reported to be involved in enhanced migration [199] and proliferation [154] as well as deficiencies in cellular adhesion [113]. Therefore, the impact on these processes by inhibiting either ERK, CIP2A or both proteins together was studied in more detail.
First, the impact on proliferation was examined. Both single treatments of the implicants resulted in a 2-fold reduction of the proliferation rate ($p < 0.02$) in comparison to untreated cells. In contrast, the DMSO control which was used as toxicity control did not show any reduction in proliferation ($p > 0.99$). Interestingly,

the combination of inhibition of ERK and CIP2A achieved an even stronger reduction of proliferation by 3.6-fold (p = 0.008). Here, it should be mentioned that the decreased proliferation rate was not induced by increased apoptosis. All treatments showed an apoptosis rate ranging between 0% and 11%.

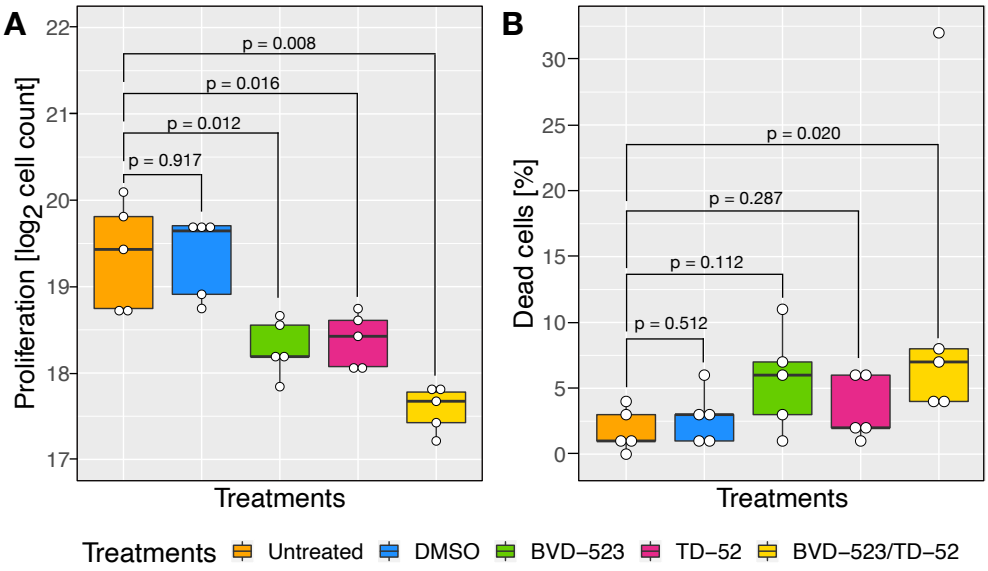

Figure 39: **Inhibition of proliferation without induction of apoptosis by inhibiting ERK (BVD-523) and/or CIP2A (TD-52).** (A) Cell counts after 24 hours post-treatment (n = 5, Wilcoxon test). (B) Percentage of dead cells after 24 hours post-treatment (n = 5, Wilcoxon test).

Next, the migratory potential of cells with inhibited implicants was investigated (Figure 40A). This was done by analysing the potential of wound closure after 48 hours post-treatment in comparison to untreated cells. Cells treated with the ERK inhibitor BVD-523 closed 49% of the wound (p = 0.004) while cells treated with the CIP2A inhibitor TD-52 closed 36% of the wound (p = 0.002). An even stronger effect could be achieved by combining both approaches. Here, only 27% of the wound could be closed within 48 hours post-treatment (p = 0.005). In contrast to the treatments, no significant differences regarding wound closure could be detected for the DMSO control in comparison to untreated cells (p = 0.11).
In silico simulations already indicated a restoration of CDH1 after inhibiting the two implicants ERK and CIP2A (Figure 38B). Since reduced migratory potential can be explained by a restoration of CDH1 at the tight junctions staining for CDH1 was performed 48 hours post-treatment (Figure 40B). Here, restoration of CDH1 at the cell membrane could be observed. This effect was further enhanced by a combination of both treatments. Thus, the restoration of CDH1 at the cell membrane is

a possible explanation for the reduced migratory potential and another support of the model quality.

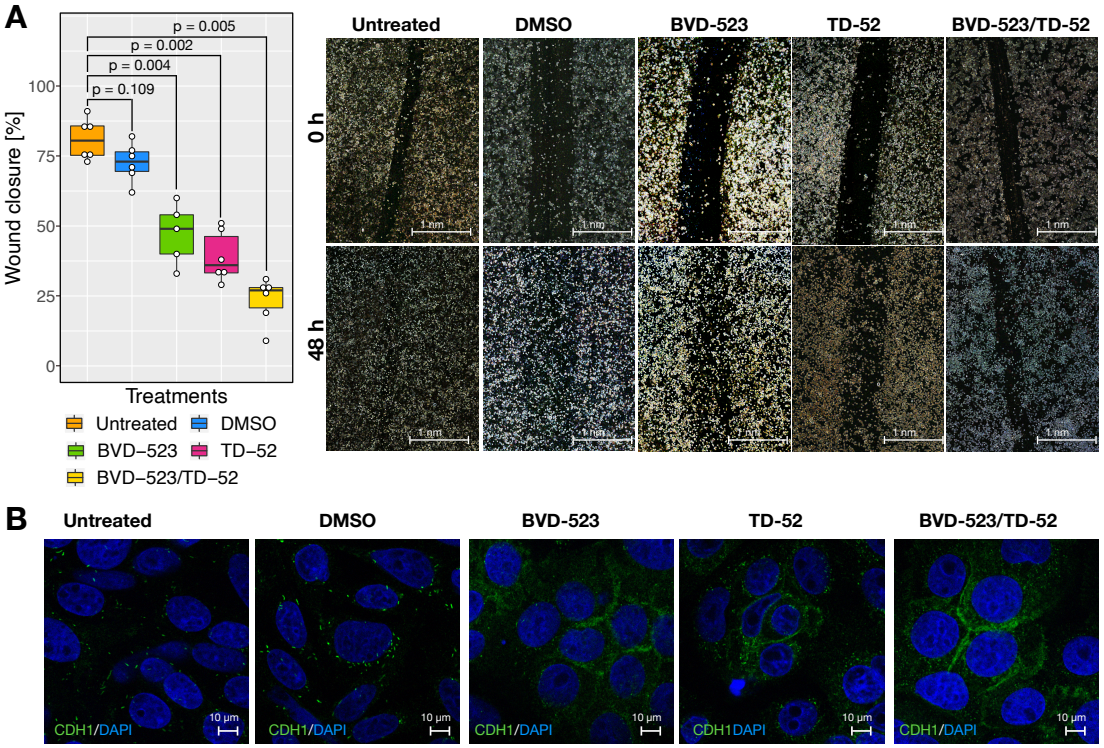

Figure 40: **Inhibition of migratory potential by a restoration of CDH1 at the cell surface.** (A) Reduced potential for wound closure after 48 hours post-treatment (BVD-523: n = 5; otherwise: n = 6). Depicted are the statistical analysis (Wilcoxon test) and a representative picture of each wound. (B) Merged confocal microscope pictures of E-cadherin (CDH1, green) and nuclei (blue) staining showed a restoration of CDH1 at the cell membrane after 48 hours post-treatment. Confocal pictures were kindly provided by A. S. Pfister (Institute of Biochemistry and Molecular Biology, Ulm University).

To sum up, the performed *in vitro* experiments based on identified implicants already show remarkable results in the inhibition of proliferation and infiltration. These results allow two conclusions. First, dynamic characteristics should be given greater attention when choosing treatable candidates. Second, hubs are not the single master regulators in biological processes. This role can be undertaken by lowly connected components which might be easier to target since they are regulated by fewer regulators. Furthermore, the combination of hubs and low connected components seems to be another possible strategy to generate more effective therapies.

3.3.9 *Discussion – Dynamic characteristics in biological networks*

3.3.9.1 *Performance of the algorithms*

Various algorithms have been developed to analyse biological networks [507]. However, to the best of my knowledge, these methods only consider static interactions between nodes as well as qualitative knowledge [258, 507]. Although the heuristic approach considers the degree of a node, it also takes the dynamic and thus time into account. This is the main difference between the presented method and previous network approaches.
The idea to consider temporal dynamical changes for the identification of important network nodes was based on findings that static interactions are not enough to understand resistance mechanisms [396]. In the presented study two algorithms were implemented to search for dynamic-influencing nodes: a heuristic and an exhaustive approach as reference. Exhaustively searching for implicants in a reasonable time is impossible for larger networks [366, 501]. Therefore, a heuristic approach was developed that chooses nodes according to predefined significance values. Certainly, this method only revealed a single set of implicants that is not always the minimal implicant set (Figure 34A). Indeed, it identified the set of implicants much faster than the exhaustive approach. Here, the heuristic approach outperformed the exhaustive search by a factor of up to 1 million. Furthermore, the fact that the heuristic approach identified a superset of the minimal implicant set in 91.4% of cases with only 14% false-positive results underscores its good performance. Taking into account the time that could be saved by the heuristic approach, further analyses can be performed to obtain the most promising results. Besides simulations, this includes a literature search for available inhibitors or inducers. Likewise, this procedure has to be done with the implicants identified by the exhaustive approach since being an implicant does not mean to be a candidate for treatment strategies. Implicants can also be components that are responsible for diseases development. An example of such an implicant is APC which promotes the progression of colorectal cancer [14].

3.3.9.2 *Master regulators of biological processes - hubs versus less connected nodes*

Based on the presented dynamic approach, it could be shown that a small set of implicants is enough to determine the dynamic of the complete network (Figure 34B). This finding is supported by the study of Albert et al. showing that scale-free networks are robust against arbitrary failure even if 80% of nodes fail [6]. Similar set sizes of important nodes in comparison to the number of network nodes could be found by both dynamic approaches (exhaustive median 22.2%, heuristic median 28.6%). However, neither Pearson correlation nor a regression line could describe

the relation of implicant set size and number of network nodes. This indicates that the general implicant set size is small and does not increase linearly with the network size. Albert et al. explain their observations by the fact that coincidences often hit less connected nodes which do not destroy the network integrity [6]. However, by studying the implicant set it could be shown that they do not overlap with network hubs.

The assumption that hub proteins are master regulators of biological processes is based on the finding of Jeong et al. [181]. Studying the protein-protein interaction network of *Saccharomyces cerevisiae* they observed that hubs are more likely to be encoded by essential genes [181]. However, other studies suggest that hubs are not involved in the development of diseases or cancer in humans [132, 258]. A possible explanation for these opposed findings may be that the loss of essential genes leads to abortions in humans. Thus, these alterations are not present in the human population [132].

In silico simulations with implicants as intervention targets already revealed that they perform similar to network hubs (Figure 36). However, in contrast to *in vitro* or *in vivo* studies with inhibitors, the performed simulations with Boolean network models assume a permanent inhibition/overexpression of targets. This could lead to an overestimation of the impact of hubs since reactivation mechanisms are not considered within the performed analysis. Nevertheless, less connected implicants showed similar effects in their ability to alter dynamic behaviours. The fact that these proteins have fewer regulators per se reduces the potential of reactivation mechanisms. In addition, less connected nodes may evoke fewer side effects since they regulate a minority of downstream targets. This assumption is supported by a comparison of drugs that pass clinical trials. Here, Wang et al. [444] could show that drugs targeting non-essential and non-central proteins have higher chances to be approved.

3.3.9.3 *ERK and CIP2A as targets for colorectal cancer patients*

In silico analyses with biologically motivated Boolean network models already indicated a role for implicants as intervention targets or disease drivers. To further support this assumption a new Boolean network model about Wnt/MAPK crosstalk in colorectal cancer was established. Based on this model, ERK and CIP2A were identified as the most promising implicants for interventions (Figure 38A). Both proteins showed anti-tumoral characteristics in knockout simulations (Figure 38B) and small molecules are available for human treatment [127, 248, 408]. Furthermore, their mode of action is specific and resolved [127, 489]. Therefore, their inhibition was further studied *in vitro*. A single treatment of both implicants reduced the number of proliferative cells (Figure 39) as well as their invasive potential (Figure 40).

The two chosen implicants differ in their degree (Figure 38A). While ERK was characterised as a hub, CIP2A had only a few interactions. Nevertheless, they showed similar behaviour after inhibition. These results further support the idea that some less connected proteins are important for dynamics.

Although not observed in this *in vitro* study, inhibition of hubs is associated with resistance mechanisms leading to their reactivation [396, 455]. These resistances are induced by multiple feedback regulations [396]. In line with these findings, Lu et al. showed that highly connected genes have lower changes in expression levels in general [258]. To circumvent resistance mechanisms, the coupling of kinase and phosphatase inhibitors have been suggested [455]. This created the idea to combine ERK and CIP2A inhibitors to treat colorectal cancer cells. In general, both applied intervention strategies have the final goal of decreasing the activity of the hub node ERK. However, they act on different levels. BVD-523 competes with ATP for binding to ERK, thereby reducing ERK's activity [127]. TD-52 blocks CIP2A promoter binding thus increasing PP2A levels [489] which is an inhibitor of ERK phosphorylation [455, 489]. This double intervention may allow to circumventing reactivation mechanisms. Indeed, combining the inhibition of CIP2A and ERK yielded a more pronounced effect than single treatments (Figures 39, 40). Consistent with these findings is the observation that PP2A status affects the response to MAPK inhibitors [197]. Thus, coupling BVD-523 and TD-52 could be a promising treatment strategy for colorectal cancer patients. Another advantage of this approach is that both inhibitors are already being tested in clinical trials for other types of cancer [127, 248, 408].

4

GENERAL DISCUSSION

4.1 Mathematical models for gene regulatory networks and the choice of the right model

Basically, all experiments in life science are conducted in models [122]. In biology or medicine, we are familiar with model organisms like *Mus musculus*, *Drosophila melanogaster* and *Caenorhabditis elegans* as well as with *in vitro* studies of diverse cell lines [115]. But all these models have their limitations and are not directly transferable to human beings [375]. Thus, when choosing a model it has to be carefully assessed if this model is appropriate to tackle the proposed question.
Besides model organisms and cell lines, mathematical models can be applied to study complex biological processes. Here, they can be used to gain an initial understanding of processes and to conduct subsequent laboratory experiments. Therefore, these mathematical models allow experimental costs to be saved and possibly animal experiments to be reduced, as experiments are carried out in a more targeted manner [501].
A variety of dynamic models have been proposed to describe dynamics in GRN, differing in complexity and abstraction [344]. In the scope of this work Boolean network models have been chosen. This choice can be justified primarily by the fact that qualitative statements describing regulatory interactions are sufficient to establish a Boolean network model [7]. Although only rudimentary assumptions can be drawn based on this model type, it is able to give first hints about yet unknown mechanistic regulations to guide further laboratory experiments. This is of particular importance if mechanistic regulations are completely uncertain as it is in the case of CFL1 in pancreatic cancer.
Another point for the choice of Boolean network models concerns the number of expected edges. One of the aims of this thesis was to model complex crosstalk between different signalling cascades. Thus, a high number of edges could already be assumed at the beginning. As a consequence, more complex models like ODE requiring kinetic parameters for each edge were not feasible [344]. In total, the newly developed Boolean network models of colorectal and pancreatic cancer consist of

256 and 130 edges respectively, distributed over 45 and 33 nodes. The NF-κB models reconstructed from expression data are of a similar magnitude. Here, a range of 125 up to 158 dependencies could be found for 22 interacting components. With these sizes, all models are far above the median of 23 edges found for available ODE models (Appendix Table 14) capturing signal transduction pathways on BioModels [229]. This comparison of the established Boolean network models with ODE models further supports that this was the right choice of the model type. In addition, it would not have been possible to determine kinetic parameters for the interactions of NF-κB signalling purely from the totality of all gene expression data.
However, regardless of these reasons, the best proof of the correct choice of the mathematical model type is if it can be confirmed by laboratory experiments [343]. This is the case for the CFL1 as well as for the colorectal cancer model whose assumptions have been confirmed by preliminary laboratory experiments. The assumptions of the IGF-1/Wnt model could be supported by comparison to independent results described in literature as well.
To conclude, the choice to consider Boolean network models is justified on the basis of the available information and the expected model size. Ultimately, however, it is the result of new insights into signalling pathways and the identification of promising intervention targets based on these models that support the choice of model type.

4.2 Data-driven versus literature-based modelling

In the scope of this work, two different methods were applied to establish the Boolean network models. While the Wnt crosstalk models as well as the CFL1 model are based on intensive literature search, the models for NF-κB signalling in the course of ageing are based on time series of gene expression data.
On the one hand, literature-based modelling ensures that evidence is found for every considered interaction. But subjective presumptions by the modeller cannot be excluded. Often controversially described interactions can be found in literature. Reasons for this can be tissue-specific regulations [394] as well as ambiguous regulations [9]. If a comparison by simulating both model variants cannot provide a solution for conflicting descriptions [343], it is up to the modeller to decide which version will be included.
For the CFL1 model controversial regulations were described for cell cycle regulations downstream of CFL1. Regulatory effects were mediated by influencing cell cycle inhibitors [429] or STAT3 [464]. Unfortunately, model simulations including both regulatory possibilities could not exclude one option (Figure 19). In the end, however, laboratory experiments that were conducted based on this contestation were able to exclude a regulation based on cell cycle inhibitors (Figure 20).

While regulations of models based on literature search are finally clarified there are various regulatory possibilities in the reconstruction of Boolean network models from time series. Regardless of the underlying regulation, the resulting attractors, however, show the same long-term behaviour. For NF-κB signalling 1000 independent Boolean network models were reconstructed to ensure that the majority of possible regulations are covered by the reconstruction. However, note that only a small proportion of approximately 20% of all these possible interactions were integrated per individual reconstructed model. In addition, when reconstructing from time series it cannot be guaranteed that all interactions used can be biologically justified. In order to be able to assess this risk, all identified interactions were verified using the protein interaction database STRING [392]. The use of exclusively experimental data and information from curated database ensures that all data considered has biological evidence [411]. All algorithmically reconstructed interactions for the NF-κB signalling could be found as direct or indirect connections in the database. This corroborates the biological relevance of the presented method to reconstruct Boolean network models from gene expression data.
The reconstructions of Boolean network models were performed based on significantly binarizable genes [169]. As a result, 74.4% of all genes included in the gene expression dataset that could be attributed to NF-κB signalling (according to hsa04064 KEGG [192]) were discarded. Initially, this seems to be controversial since changes in NF-κB signalling are described as a hallmark of ageing [256, 423]. However, alterations in NF-κB signalling are mainly reported in case of transcriptional changes and not for cytoplasmic levels of NF-κB components or regulators [156]. Many proteins that are included in the KEGG dataset of NF-κB signalling are part of the cytoplasmic regulation of NF-κB. Thus, changes in expression values are not expected since samples were taken from healthy humans [453]. Moreover, it was not the aim to reconstruct the NF-κB signalling pathway in detail. Rather, the focus was on noticing changes in the process of ageing.
Apart from the restriction the gene set for reconstruction had to be defined due to computational resources [222], this data-driven approach is objective. Although both approaches are able to generate Boolean network models, these networks differ in terms of explanatory power. This is largely due to the different regulatory mechanisms that can be included in a single network obtained by reconstruction [222, 365]. For this reason, only general dynamics were studied with reconstructed Boolean network models [365] while literature-based networks were applied for detailed analyses of signalling pathways.

4.3 Is there a loss of information by binarization?

Initially, the assumption to describe gene regulations only with binary values $(0, 1)$ appears as a big limitation. However, this approximation is common in biology. Here, we categorise genes as overexpressed or repressed and pathways as active or inactive [5]. Even if not called Boolean this procedure is comparable to the principle of binarization of gene expression data. However, in contrast to general thresholds like fold changes [401], the binarization method defines a threshold per gene [169]. This allows for considering small alterations in concentrations of proteins which may be expressed in underrepresented cell types of the whole tissue composition [401] and would be overlooked by a general fold change analysis. A study on inflammatory response has shown that especially genes with small fold changes in gene expression are important for biologically relevant functions [401]. Since NF-κB signalling plays a major role in alterations of immune responses and inflammation [350] small changes in expression values seem to be important.
Furthermore, the concentration curves of components involved in biological reactions can be described by a Hill-function [87]. Since for many values of the Hill-coefficient (especially with increasing values of the Hill-coefficient) the function adopts a sigmoidal shape and can be approximated by a dichotomous step function [131]. Thus, the initial concentration curve is assigned binary values.
In conclusion, binarization of gene expression data does not lead to a loss of information but rather to a different view on the data. This might allow us to identify the effects and dynamics that are overlooked or underestimated by considering expression values alone.

5

SUMMARY

Given the complex nature of biological systems and organisms, the examination of single protein interactions is not enough to understand ageing, the development of diseases or cancer. For this reason, this thesis aimed to explore new relationships between signalling pathways. This was achieved by studying various signalling pathways with Boolean network models.

First, the crosstalk of insulin-like growth factor 1 (IGF-1) and Wingless (Wnt), as well as the signalling pathway of nuclear factor kappa-light chain-enhancer of activated B-cells (NF-κB) were investigated by a literature-based and a data-driven approach. Despite huge differences in the model setups, similar conclusions were drawn from model simulations. Although the process of ageing could only be simulated by crosstalk of IGF-1 and Wnt, it could be shown that Wnt signalling dominates IGF-1 by impairing feedback. Thereby, proteins maintain their activity state. Likewise, proteins that were constantly inactive could be found in the reconstructed NF-κB networks of young and aged phenotype. Network analyses further indicated a loss of redundant protein interactions accompanied by an escalation in error susceptibility with age. These alterations in activity and accumulation of damage can, in turn, be attributed to the development of ageing-associated diseases. In particular, activation of the mammalian target of rapamycin complex 1 (mTORC1) could be identified in the IGF-1/Wnt model, which can be associated with the development of diabetes mellitus type II and the inhibition of autophagy. Likewise, constantly inactive components in the NF-κB model seem to be involved in a decreased inflammatory response and reduced angiogenesis.

The next step in this work was to investigate the role of cofilin-1 (CFL1) in pancreatic cancer. Previously it was already known that CFL1 is highly expressed in pancreatic cancer and correlates with high invasiveness and poor prognosis. However, pathways that contribute to fast cancer progression were still unknown. Based on a Boolean network model newly established in this thesis, it was possible to predict them. Model simulations indicated that Kirsten rat sarcoma (KRAS)

induces an imbalance in actin remodelling leading to overexpression and activation of CFL1. Due to the imbalance in actin remodelling, it seems that the expression of the transcription factor 7-like 2 (TCF7L2) can no longer be suppressed by protein kinase D1 (PRKD1) which leads to an increased expression of TCF7L2 itself and subsequently induces the expression of CFL1. In addition, the activator of CFL1, slingshot (SSH1L), seems to be increasingly expressed by an increased AURKA expression. Thus, CFL1 would not only be present in increased quantities but can also be activated. These model-based assumptions that both AURKA and TCF7L2 are overexpressed in pancreatic cancer patients could be confirmed by gene expression data from pancreatic cancer tissues. Besides the signalling pathway leading to the overexpression and activation of CFL1, the model could also provide an explanation for the involvement of CFL1 in proliferation control and apoptosis inhibition. Here, model simulations suggested that CFL1 regulates cell cycle components based on its impact on the signal transducer and activator of transcription 3 (STAT3). This assumption could be supported by western blots showing reduced protein levels of STAT3. Moreover, STAT3 also seems to be involved in the abrogation of apoptosis in pancreatic cancer cells by inducing the expression of anti-apoptotic proteins. In addition, to reveal the role of CFL1 in pancreatic cancer, the newly established model was used to suggest new therapeutic targets for pancreatic cancer patients with high CFL1 expression. Here, the most promising identified intervention target was CD44 antigen whose in silico inhibition blocked the proliferative phenotype and induced apoptosis.

The last part of this thesis dealt with the identification of dynamic-influencing nodes, called implicants. Here, a new algorithm was established that is able to identify these implicants in a feasible time frame. By studying 35 publically available, biologically motivated Boolean network models, it could be shown that a small set of nodes is sufficient to determine the dynamics of a complete system. Although highly connected components (hubs) are frequently considered to be master regulators of biological processes, the majority of implicants were not static hubs. Furthermore, it could be shown that targeting these implicants reduces the risk for side effects in comparison to targeting static hubs. The superiority of dynamic influencing-targets versus static hubs was confirmed by experimental validation of a newly established Boolean network model depicting the crosstalk of Wnt and mitogen activating protein kinase (MAPK) in colorectal cancer. Based on this model dynamic determining proteins were identified. The two most promising targets, extracellular signal-regulated protein kinase (ERK) and cancerous inhibitor of protein phosphatase 2A (CIP2A) were treated with specific inhibitors. Thereby, it was shown that their inhibition reduced the proliferative and invasive potential of colorectal cancer cells.

6

REFERENCES

[1] ELIXIR a distributed infrastructure for life-science information. http://160.80.34.9/elixir2015/. Accessed: 2020-07-05.

[2] Agarwal, A., Das, K., Lerner, N., Sathe, S., Cicek, M., Casey, G., and Sizemore, N. The AKT/IκB kinase pathway promotes angiogenic/metastatic gene expression in colorectal cancer by activating nuclear factor-κB and β-catenin. *Oncogene 24*, 6 (2005), 1021–1031.

[3] Akutsu, T. *Algorithms for analysis, inference, and control of Boolean networks*. World Scientific Publishing, Singapore, 2018.

[4] Akutsu, T., Miyano, S., and Kuhara, S. Inferring qualitative relations in genetic networks and metabolic pathways. *Bioinformatics 16*, 8 (2000), 727–734.

[5] Albert, I., Thakar, J., Li, S., Zhang, R., and Albert, R. Boolean network simulations for life scientists. *Source Code for Biology and Medicine 3*, 16 (2008).

[6] Albert, R., Jeong, H., and Barabási, A.-L. Error and attack tolerance of complex networks. *Nature 406* (2000), 378–382.

[7] Albert, R., and Thakar, J. Boolean modeling: a logic-based dynamic approach for understanding signaling and regulatory networks and for making useful predictions. *WIREs Systems Biology and Medicine 6*, 5 (2014), 353–369.

[8] Alemeida, M., Han, L., Bellido, T., Manolagas, S. C., and Kousteni, S. Wnt proteins prevent apoptosis of both uncommitted osteoblast progenitors and differentiated osteoblasts by β-catenin-dependent and -independent signaling cascades involving Src/ERK and phosphatidylinositol 3-kinase/AKT. *Journal of Biological Chemistry 280*, 50 (2005), 41342–41351.

[9] Alizad-Rahvar, A. R., and Sadeghi, M. Ambiguity in logic-based models of gene regulatory networks: An integrative multi-perturbation analysis. *PLOS ONE 13*, 11 (2018), e0206976.

[10] Alon, U. Network motifs: theory and experimental approaches. *Nature Reviews Genetics 8*, 6 (2007), 450–461.

[11] Anjum, R., and Blenis, J. The RSK family of kinases: emerging roles in cellular signalling. *Nature Reviews Molecular Cell Biology 9*, 10 (2008), 747–758.

[12] Araki, Y., Okamura, S., Hussain, S. P., Nagashima, M., He, P., Shiseki, M., Miura, K., and Harris, C. C. Regulation of cyclooxygenase-2 expression by the Wnt and Ras pathways. *Cancer Research 63*, 3 (2003), 728–734.

[13] Arlt, A., Müerköster, S. S., and Schäfer, H. Targeting apoptosis pathways in pancreatic cancer. *Cancer Letters 332*, 2 (2013), 346–358.

[14] Armaghany, T., Wilson, J. D., Chu, Q., and Mills, G. Genetic alterations in colorectal cancer. *Gastrointestinal Cancer Research 5*, 1 (2012), 19–27.

[15] Avruch, J., Khokhlatchev, A., Kyriakis, J. M., Luo, Z., Tzivion, G., Vavvas, D., and Zhang, X.-F. Ras activation of the Raf kinase: tyrosine kinase recruitment of the MAP kinase cascade. *Recent Progress in Hormone Research 56* (2001), 127–155.

[16] Azpeitia, E., Weinstein, N., Benítez, M., Mendoza, L., and Alvarez-Buylla, E. R. Finding missing interactions of the *Arabidopsis thaliana* root stem cell niche gene regulatory network. *Frontiers in Plant Science 4*, 110 (2013).

[17] Backlund, M. G., Mann, J. R., Holla, V. R., Shi, Q., Daikoku, T., Dey, S. K., and DuBois, R. N. Repression of 15-hydroxyprostaglandin dehydrogenase involves histone deacetylase 2 and snail in colorectal cancer. *Cancer Research 68*, 22 (2008), 9331–9337.

[18] Badea, L., Herlea, V., Dima, S. O., Dumitrascu, T., and Popescu, I. Combined gene expression analysis of whole-tissue and microdissected pancreatic ductal adenocarcinoma identifies genes specifically overexpressed in tumor epithelia. *Hepato-Gastroenterology 55*, 88 (2008), 2016–2027.

[19] Balcazar Morales, N., and Aguilar de Plata, C. Role of AKT/mTORC1 pathway in pancreatic β-cell proliferation. *Colombia Médica 43*, 3 (2012), 235–243.

[20] Bamburg, J. R. Proteins of the adf/cofilin family: essential regulators of actin dynamics. *Annual Review of Cell and Developmental Biology 15* (1999), 185–230.

[21] Bamburg, J. R., and Bernstein, B. W. Roles of adf/cofilin in actin polymerization and beyond. *F1000 Biology Reports 2*, 62 (2010).

[22] Barabási, A.-L. *Network Science*. Cambridge university press, Cambridge, 2016.

[23] Barabási, A.-L., Gulbahce, N., and Loscalzo, J. Network medicine: A network-based approach to human disease. *Nature Reviews Genetics 12*, 1 (2011), 56–68.

[24] Barabasi, A.-L., and Oltvai, Z. N. Network biology: understanding the cell's functional organization. *Nature Reviews Genetics 5* (2004), 101–113.

[25] Barton-Davis, E. R., Shoturma, D. I., Musaro, A., Rosenthal, N., and Sweeney, H. L. Viral mediated expression of insulin-like growth factor i blocks the aging-related loss of skeletal muscle function. *Proceedings of the National Academy of Sciences 95*, 26 (1998), 15603–15607.

[26] Bates, R. C., Edwards, N. S., Burns, G. F., and Fisher, D. E. A CD44 survival pathway triggers chemoresistance via Lyn kinase and phosphoinositide 3-kinase/Akt in colon carcinoma cells. *Cancer Research 61*, 13 (2001), 5275–5283.

[27] Bauer, A. L., Jackson, T. L., Jiang, Y., and Rohlf, T. Receptor cross-talk in angiogenesis: Mapping environmental cues to cell phenotype using a stochastic, Boolean signaling network model. *Journal of Theoretical Biology 264*, 3 (2010), 838–846.

[28] Ben-Josef, E., George, A., Regine, W. F., Abrams, R., Morgan, M., Thomas, D., Schaefer, P. L., DiPetrillo, T. A., Fromm, M., Small, W. J., Narayan, S., Winter, K., Griffith, K. A., Guha, C., and Williams, T. M. Glycogen synthase kinase 3 beta predicts survival in resected adenocarcinoma of the pancreas. *Clinical Cancer Research 21*, 24 (2015), 5612–5618.

[29] Bera, A., VenkataSubbaRao, K., Manoharan, M. S., Hill, P., and Freeman, J. W. A miRNA signature of chemoresistant mesenchymal phenotype identifies novel molecular targets associated with advanced pancreatic cancer. *PLOS ONE 9*, 9 (2014), e106343.

[30] Bernstein, B. W., and Bamburg, J. R. ADF/cofilin: a functional node in cell biology. *Trends in Cell Biology 20*, 4 (2010), 187–195.

[31] Bewick, V., Cheek, L., and Ball, J. Statistics review 13: Receiver operating characteristic curves. *Critical Care 8*, 6 (2004), 508–512.

[32] Bid, H. K., Roberts, R. D., Manchanda, P. K., and Houghton, P. J. RAC1: an emerging therapeutic option for targeting cancer angiogenesis and metastasis. *Molecular Cancer Therapeutics 12*, 10 (2013), 1925–1934.

[33] Blanchoin, L., and Pollard, T. D. Mechanism of interaction of *Acanthamoeba* actophorin (adf/cofilin) with actin filaments. *Journal of Biological Chemistry 274*, 22 (1999), 15538–15546.

[34] Borneman, A. R., Leigh-Bell, J. A., Yu, H., Bertone, P., Gerstein, M., and Snyder, M. Target hub proteins serve as master regulators of development in yeast. *Genes & Development 20*, 4 (2006), 435–448.

[35] Bottomly, D., Kyler, S. L., McWeeney, S. K., and Yochum, G. S. Identification of β-catenin binding regions in colon cancer cells using ChIP-Seq. *Nucleic Acids Research 38*, 17 (2010), 5735–5745.

[36] Boulter, E., Estrach, S., Garcia-Mata, R., and Féral, C. C. Off the beaten paths: alternative and crosstalk regulation of Rho GTPases. *The FASEB Journal 26*, 2 (2012), 469–479.

[37] Bracho-Valdés, I., Moreno-Alvarez, P., Valencia-Martínez, I., Robles-Molina, E., Chávez-Vargas, L., and Vázquez-Prado, J. mTORC1- and mTORC2-interacting proteins keep their multifunctional partners focused. *IUBMB Life 63*, 10 (2011), 896–914.

[38] Brack, A. S., Conboy, M. J., Roy, S., Lee, M., Kuo, C. J., Keller, C., and Rando, T. A. Increased Wnt signaling during aging alters muscle stem cell fate and increases fibrosis. *Science 317*, 5839 (2007), 807–810.

[39] Bradshaw, R. A., and Dennis, E. A. *Handbook of cell signaling*, 2nd edition ed. Academic press, 2009.

[40] Brandon, M., Howard, B., Lawrence, C., and Laubenbacher, R. Iron acquisition and oxidative stress response in aspergillus fumigatus. *BMC Systems Biology 9*, 19 (2015).

[41] Brandt, D., Gimona, M., Hillmann, M., Haller, H., and Mischak, H. Protein kinase C induces actin reorganization via a Src- and Rho-dependent pathway. *Journal of Biological Chemistry 277*, 23 (2002), 20903–20910.

[42] Bray, F., Ferlay, J., Soerjomataram, I., Siegel, R. L., Torre, L. A., and Jemal, A. Global cancer statistics 2018: Globocan estimates of incidence and mortality worldwide for 36 cancers in 185 countries. *CA: A Cancer Journal for Clinicians 68*, 6 (2018), 394–424.

[43] Briggs, M. W., Li, Z., and Sacks, D. B. IQGAP1-mediated stimulation of transcriptional co-activation by β-catenin is modulated by calmodulin. *Journal of Biological Chemistry 277*, 9 (2002), 7453–7465.

[44] Britten, C. D. PI3K and MEK inhibitor combinations: examining the evidence in selected tumor types. *Cancer Chemotherapy and Pharmacology 71*, 6 (2013), 1395–1409.

[45] Buchadas, A., Vaz, A. S., Honrado, J. P., Alagador, D., Bastos, R., Cabral, J. A., Santos, M., and Vicente, J. R. Dynamic models in research and management of biological invasions. *Journal of Environmental Management 196* (2017), 594–606.

[46] Buchanan, F. G., Wang, D., Bargiacchi, F., and DuBois, R. N. Prostaglandin E2 regulates cell migration via the intracellular activation of the epidermal growth factor receptor. *Journal of Biological Chemistry 278* (2003), 35451–35457.

[47] Buchholz, M., Braun, M., Heidenblut, A., Kestler, H. A., Klöppel, G., Schmiegel, W., Hahn, S. A., Lüttges, J., and Gress, T. M. Transcriptome analysis of microdissected pancreatic intraepithelial neoplastic lesions. *Oncogene 24*, 44 (2005), 6626–6636.

[48] Buffenstein, R. The naked mole-rat: A new long-living model for human aging research. *Journal of Gerontology: Biological Sciences 60A*, 11 (2005), 1369–1377.

[49] Buongiorno, P., Pethe, V. V., Charames, G. S., Esufali, S., and Bapat, B. Rac1 GTPase and the Rac1 exchange factor Tiam1 associate with Wnt-responsive promoters to enhance beta-catenin/TCF-dependent transcription in colorectal cancer cells. *Molecular Cancer 7*, 73 (2008).

[50] Burris, H. A., Moore, M. J., Andersen, J., Green, M. R., Rothenberg, M. L., Modiano, M. R., Cripps, M. C., Portenoy, R. K., Storniolo, A. M., Tarassoff, P., Nelson, R., Dorr, F. A., Stephens, C. D., and Von Hoff, D. D. Improvements in survival and clinical benefit with gemcitabine as first-line therapy for patients with advanced pancreas cancer: a randomized trial. *Journal of Clinical Oncology 15*, 6 (1997), 2403–2413.

[51] Burzynski, S. R. Aging: gene silencing or gene activation? *Medical Hypotheses 64*, 1 (2005), 201–208.

[52] Calzone, L., Tournier, L., Fourquet, S., Thieffry, D., Zhivotovsky, B., Barillot, E., and Zinovyev, A. Mathematical modelling of cell-fate decision in response to death receptor engagement. *PLOS Computational Biology 6*, 3 (2010), e1000702.

[53] Cao, S. X., Dhahbi, J. M., Mote, P. L., and Spindler, S. R. Genomic profiling of short- and long-term caloric restriction effects in the liver of aging mice. *Proceedings of the National Academy of Sciences 98*, 19 (2001), 10630–10635.

[54] Carter, J. H., Douglass, L. E., Deddens, J. A., Colligan, B. M., Bhatt, T. R., Pemberton, J. O., Konicek, S., Hom, J., Marshall, M., and Graff, J. R. Pak-1 expression increases with progression of colorectal carcinomas to metastasis. *Clinical Cancer Research 10*, 10 (2004), 3448–3456.

[55] Casalino, L., De Cesare, D., and Verde, P. Accumulation of Fra-1 in *Ras*-transformed cells depends on both transcriptional autoregulation and MEK-dependent posttranslational stabilization. *Molecular and Cellular Biology 23*, 12 (2003), 4401–4415.

[56] Castellano, E., and Downward, J. RAS interaction with PI3K: more than just another effector pathway. *Genes & Cancer 2*, 3 (2011), 261–274.

[57] Castets, P., Lin, S., Rion, N., Di Fulvio, S., Romanino, K., Guridi, M., Frank, S., Tintignac, L. A., Sinnreich, M., and Rüegg, M. A. Sustained activation of mTORC1 in skeletal muscle inhibits constitutive and starvation-induced autophagy and causes a severe, late-onset myophaty. *Cell Metabolism 17*, 5 (2013), 731–744.

[58] Chaffer, C. L., and Weinberg, R. A. A perspective on cancer cell metastasis. *Science 331*, 6024 (2011), 1559–1564.

[59] Chakrabarti, R., Hwang, J., Blanco, M. A., Wei, Y., Lukačišin, M., Romano, R.-A., Smalley, K., Liu, S., Yang, Q., Ibrahim, T., et al. Elf5 inhibits the epithelial–mesenchymal transition in mammary gland development and breast cancer metastasis by transcriptionally repressing Snail2. *Nature Cell Biology 14*, 11 (2012), 1212–1222.

[60] Chambard, J.-C., Lefloch, R., Pouysségur, J., and Lenormand, P. ERK implication in cell cycle regulation. *Biochimica et Biophysica Acta (BBA) - Molecular Cell Research 1773*, 8 (2007), 1299–1310.

[61] Chen, C., Zhao, S., Karnad, A., and Freeman, J. W. The biology and role of CD44 in cancer progression: therapeutic implications. *Journal of Hematology & Oncology 11*, 64 (2018).

[62] Chen, C.-C., Jeon, S.-M., Bhaskar, P. T., Nogueira, V., Sundararajan, D., Tonic, I., Park, Y., and Hay, N. FoxOs inhibit mTORC1 and activate Akt by inducing the expression of Sestrin3 and Rictor. *Developmental Cell 18*, 4 (2010), 592–604.

[63] Chen, Q., Chao, R., Chen, H., Hou, X., Yan, H., Zhou, S., Peng, W., and Xu, A. Antitumor and neurotoxic effects of novel harmine derivates and structure-activity relationship analysis. *International Journal of Cancer 114*, 5 (2005), 675–682.

[64] Chiu, T. T., Patel, N., Shaw, A. E., Bamburg, J. R., and Klip, A. Arp2/3-and cofilin-coordinated actin dynamics is required for insulin-mediated GLUT4 translocation to the surface of muscle cells. *Molecular Biology of the Cell 21*, 20 (2010), 3529–3539.

[65] Chiu, T. T., Sun, Y., Koshkina, A., and Klip, A. Rac-1 superactivation triggers insulin-independent glucose transporter 4 (GLUT4) translocation that bypasses signaling defects exerted by c-Jun N-terminal kinase (JNK)-and ceramide-induced insulin resistance. *Journal of Biological Chemistry 288*, 24 (2013), 17520–17531.

[66] Chou, C.-W., Wu, M.-S., Huang, W.-C., and Chen, C.-C. HDAC inhibition decreases the expression of EGFR in colorectal cancer cells. *PLOS ONE 6*, 3 (2011), e18087.

[67] Chua, B. T., Volbracht, C., Tan, K. O., Li, R., Victor, C. Y., and Li, P. Mitochondrial translocation of cofilin is an early step in apoptosis induction. *Nature Cell Biology 5*, 12 (2003), 1083–1089.

[68] Clauset, A., Shalizi, C. R., and Newman, M. E. Power-law distributions in empirical data. *SIAM Review 51*, 4 (2009), 661–703.

[69] Clauset, A., Young, M., and Gleditsch, K. S. On the frequency of severe terrorist events. *Journal of Conflict Resolution 51*, 1 (2007), 58–87.

[70] Clevers, H. The intestinal crypt, a prototype stem cell compartment. *Cell 154*, 2 (2013), 274–284.

[71] Cohen, D. P., Martignetti, L., Robine, S., Barillot, E., Zinovyev, A., and Calzone, L. Mathematical modelling of molecular pathways enabling tumour cell invasion and migration. *PLOS Computational Biology 11*, 11 (2015), e1004571.

[72] Collazo, J., Zhu, B., Larkin, S., Martin, S. K., Pu, H., Horbinski, C., Koochekpour, S., and Kyprianou, N. Cofilin drives cell-invasive and metastatic responses to TGF-β in prostate cancer. *Cancer Research 74*, 8 (2014), 2362–2373.

[73] Colloca, G., Di Capua, B., Bellieni, A., Cesari, M., Emanuele, M., Valentini, V., and Calvani, R. Muscoloskeletal aging, sarcopenia and cancer. *Journal of Geriatric Oncology 10*, 3 (2019), 504–509.

[74] Copps, K. D., and White, M. F. Regulation of insulin sensitivity by serine/threonine phosphorylation of insulin receptor substrate proteins IRS1 and IRS2. *Diabetologia 55*, 10 (2012), 2565–2582.

[75] Cormen, T. H., Leiserson, C. E., Rivest, R. L., and Stein, C. *Introduction to Algorithms second edition*. The MIT Press, 2001.

[76] Cornelison, D., and Perdiguero, E. *Muscle Stem Cells: A Model System for Adult Stem Cell Biology*. Springer New York, New York, NY, 2017, pp. 3–19.

[77] Crick, F. Central dogma of molecular biology. *Nature 227*, 5258 (1970), 561–563.

[78] Cristóbal, I., Manso, R., Rincón, R., Caramés, C., Senin, C., Borrero, A., Martínez-Useros, J., Rodriguez, M., Zazo, S., Aguilera, O., et al. PP2A inhibition is a common event in colorectal cancer and its restoration using FTY720 shows promising therapeutic potential. *Molecular Cancer Therapeutics 13*, 4 (2014), 938–947.

[79] Cros, J., Raffenne, J., Couvelard, A., and Poté, N. Tumor heterogeneity in pancreatic adenocarcinoma. *Pathobiology 85* (2018), 64–71.

[80] Cuthbertson, D., Smith, K., Babraj, J., Leese, G., Waddell, T., Atherton, P., Wackerhage, H., Taylor, P. M., and Rennie, M. J. Anabolic signaling deficits underlie amino acid resistance of wasting, aging muscle. *The FASEB Journal 19*, 3 (2005), 422–424.

[81] Cutler, R. G. Redundancy of information content in the genome of mammalian species as a protective mechanism determining aging rate. *Mechanisms of Ageing and Development 2* (1973), 381–408.

[82] Cvijovic, M., Höfer, T., Aćimović, J., Alberghina, L., Almaas, E., Besozzi, D., Blomberg, A., Bretschneider, T., Cascante, M., Collin, O., de Atauri, P., Depner, C., Dickinson, R., Dobrzyknski, M., Fleck, C., Garcia-Ojalvo, J., Gonze, D., Hahn, J., Hess, H. M., Hollmann, S., Krantz, M., Kummer, U., Lundh, T., Martial, G., dos Santos, V. M., Mauer-Oberthür, A., Regierer, B., Skene, B., Stalidzans, E., Stelling, J., Teusink, B., Workman, C. T., and Hohmann, S. Strategies for structuring interdisciplinary education in systems biology: an european perspective. *npj Systems Biology and Applications 2*, 16011 (2016).

[83] Dahlhaus, M., Burkovski, A., Hertwig, F., Müssel, C., Volland, R., Fischer, M., Debatin, K.-M., Kestler, H. A., and Beltinger, C. Boolean modeling identifies Greatwall/MASTL as an important regulator in the AURKA network of neuroblastoma. *Cancer Letters 371*, 1 (2016), 79–89.

[84] Dar, A. A., Belkhiri, A., and El-Rifai, W. The aurora kinase A regulates GSK-3β in gastric cancer cells. *Oncogene 28*, 6 (2009), 866–875.

[85] Davila-Velderrain, J., Villarreal, C., and Alvarez-Buylla, E. R. Reshaping the epigenetic landscape during early flower development: induction of attractor transitions by relative differences in gene decay rates. *BMC Systems Biology 9*, 1 (2015), 20.

[86] De, P., Carlson, J., Leyland-Jones, B., and Dey, N. Oncogenic nexus of cancerous inhibitor of protein phosphatase 2A (CIP2A): an oncoprotein with many hands. *Oncotarget 5*, 13 (2014), 4581–4602.

[87] de Jong, H. Modeling and simulation of genetic regulatory systems: A literature review. *Journal of Computational Biology 9*, 1 (2002), 67–103.

[88] de Magalhães, J. P. How ageing processes influence cancer. *Nature Reviews Cancer 13*, 5 (2013), 357–365.

[89] de Magalhães, J. P., Curado, J., and Church, G. M. Meta-analysis of age-related gene expression profiles identifies common signatures of aging. *Bioinformatics 25*, 7 (2009), 875–881.

[90] Deng, J., Miller, S. A., Wang, H.-Y., Xia, W., Wen, Y., Zhou, B. P., Li, Y., Lin, S.-Y., and Hung, M.-C. β-catenin interacts with and inhibits NF-κB in human colon and breast cancer. *Cancer Cell 2*, 4 (2002), 323–334.

[91] Denicourt, C., and Dowdy, S. F. Cip/Kip proteins: more than just CDKs inhibitors. *Genes & Development 18*, 8 (2004), 851–855.

[92] Dent, P., Yacoub, A., Fisher, P. B., Hagan, M. P., and Grant, S. MAPK pathways in radiation responses. *Oncogene 22*, 37 (2003), 5885–5896.

[93] DesMarais, V., Macaluso, F., Condeelis, J., and Bailly, M. Synergistic interaction between the Arp2/3 complex and cofilin drives stimulated lamellipod extension. *Journal of Cell Science 117*, Pt 16 (2004), 3499–3510.

[94] Dibble, C. C., Asara, J. M., and Manning, B. D. Characterization of rictor phosphorylation sites reveals direct regulation of mTOR complex 2 by S6K1. *Molecular and Cellular Biology 29*, 21 (2009), 5657–5670.

[95] Dihlmann, S., Kloor, M., Fallsehr, C., and von Knebel Doeberitz, M. Regulation of *AKT1* expression by beta-catenin/Tcf/Lef signaling in colorectal cancer cells. *Carcinogenesis 26*, 9 (2005), 1503–1512.

[96] Ding, Q., Xia, W., Liu, J.-C., Yang, J.-Y., Lee, D.-F., Xia, J., Bartholomeusz, G., Li, Y., Pan, Y., Li, Z., Bargou, R. C., Qin, J., Chien-Chen, L., Tsai, F.-J., Tsai, C.-H., and Hung, M.-C. Erk associates with and primes GSK-3β for its inactivation resulting in upregulation of β-catenin. *Molecular Cell 19*, 2 (2005), 159–170.

[97] Donahue, T. R., Tran, L. M., Hill, R., Li, Y., Kovochich, A., Calvopina, J. H., Patel, S. G., Wu, N., Hindoyan, A., Farrell, J. J., Li, X., Dawson, D. W., and Wu, H. Integrative survival-based molecular profiling of human pancreatic cancer. *Clinical Cancer Research 18*, 5 (2012), 1352–1363.

[98] Dong, X., Milholland, B., and Vijg, J. Evidence for a limit to human lifespan. *Nature 538*, 7624 (2016), 257–259.

[99] Döppler, H., Bastea, L. I., Borges, S., Spratley, S. J., Pearce, S. E., and Storz, P. Protein kinase D isoforms differentially modulate cofilin-driven directed cell migration. *PLOS ONE 9*, 5 (2014), e98090.

[100] Downward, J. PI 3-kinase, Akt and cell survival. *Seminars in Cell & Developmental Biology 15*, 2 (2004), 177–182.

[101] Dubash, A. D., Koetsier, J. L., Amargo, E. V., Najor, N. A., Harmon, R. M., and Green, K. J. The GEF Bcr activates RhoA/MAL signaling to promote keratinocyte differentiation via desmoglein-1. *Journal of Cell Biology 202*, 4 (2013), 653–666.

[102] Dubrova, E., and Teslenko, M. A SAT-based algorithm for finding attractors in synchronous Boolean networks. *IEEE/ACM Transactions on Computational Biology and Bioinformatics 8*, 5 (2011), 1393–1399.

[103] Dummler, B., Ohshiro, K., Kumar, R., and Field, J. Pak protein kinases and their role in cancer. *Cancer and Metastasis Reviews 28*, 1-2 (2009), 51–63.

[104] Eiseler, T., Döppler, H., Yan, I. K., Kitatani, K., Mizuno, K., and Storz, P. Protein kinase D1 regulates cofilin-mediated F-actin reorganization and cell motility through slingshot. *Nature Cell Biology 11*, 5 (2009), 545–556.

[105] Enciso, J., Mayani, H., Mendoza, L., and Pelayo, R. Modeling the pro-inflammatory tumor microenvironment in acute lymphoblastic leukemia predicts a breakdown of hematopoietic-mesenchymal communication networks. *Frontiers in Physiology 7*, 349 (2016).

[106] Engström, W., Ward, A., and Moorwood, K. The role of scaffold proteins in JNK signalling. *Cell Proliferation 43*, 1 (2010), 56–66.

[107] Eser, S., Reiff, N., Messer, M., Seidler, B., Gottschalk, K., Dobler, M., Hieber, M., Arbeiter, A., Klein, S., Kong, B., Michalski, C. W., Schlitter, A. M., Esposito, I., Kind, A. J., Rad, L., Schnieke, A. E., Baccarini, M., Alessi, D. R., Rad, R., Schmid, R. M., Schneider, G., and Saur, D. Selective requirement of PI3K/PDK1 signaling for Kras oncogene-driven pancreatic cell plasticity and cancer. *Cancer Cell 23*, 3 (2013), 406–420.

[108] Eser, S., Schnieke, A., Schneider, G., and Saur, D. Oncogenic KRAS signalling in pancreatic cancer. *British Journal of Cancer 111*, 5 (2014), 817–822.

[109] Essers, M. A., de Vries-Smits, L. M., Barker, N., Polderman, P. E., Burgering, B. M., and Korswagen, H. C. Functional interaction between β-catenin and FOXO in oxidative stress signaling. *Science 308*, 5725 (2005), 1181–1184.

[110] Eswaran, J., Soundararajan, M., Kumar, R., and Knapp, S. UnPAKing the class differences among p21-activated kinases. *Trends in Biochemical Sciences 33*, 8 (2008), 394–403.

[111] Fang, D., Hawke, D., Zheng, Y., Xia, Y., Meisenhelder, J., Nika, H., Mills, G. B., Kobayashi, R., Hunter, T., and Lu, Z. Phosphorylation of β-catenin by AKT promotes β-catenin transcriptional activity. *Journal of Biological Chemistry 282* (2007), 11221–11229.

[112] Fauré, A., Naldi, A., Chaouiya, C., and Thieffry, D. Dynamical analysis of a generic Boolean model for the control of the mammalian cell cycle. *Bioinformatics 22*, 14 (2006), e124–e131.

[113] Faux, M. C., Ross, J. L., Meeker, C., Johns, T., Ji, H., Simpson, R. J., Layton, M. J., and Burgess, A. W. Restoration of full-length adenomatous polyposis coli (APC) protein in a colon cancer cell line enhances cell adhesion. *Journal of Cell Science 117* (2004), 427–439.

[114] Fawcett, T. An introduction to ROC analysis. *Pattern Recognition Letters 27*, 8 (2006), 861–874.

[115] Fields, S., and Johnston, M. Whither model organism research? *Science 307*, 5717 (2005), 1885–1886.

[116] Flaig, T. W., Gustafson, D. L., Su, L.-J., Zirrolli, J. A., Crighton, F., Harrison, G. S., Pierson, A. S., Agarwal, R., and Glodé, L. M. A phase I and pharmacokinetic study of silybin-phytosome in prostate cancer patients. *Investigational New Drugs 25*, 2 (2007), 139–146.

[117] Florian, M. C., Nattamai, K. J., Dörr, K., Marka, G., Überle, B., Vas, V., Eckl, C., Andrä, I., Schiemann, M., Oostendorp, R. A. J., Scharffetter-Kochanke, K., Armin, K. H., Zheng, Y., and Geiger, H. A canonical to non-canonical Wnt signalling switch in haematopoietic stem-cell ageing. *Nature 503*, 7476 (2013), 392–396.

[118] Fodde, R. The APC gene in colorectal cancer. *European Journal of Cancer 38*, 7 (2002), 867–871.

[119] Fontana, L. Modulating human aging and age-associated diseases. *Biochimica et Biophysica Acta (BBA) - General Subjects 1790*, 10 (2009), 1133–1138.

[120] Foulquier, S., Daskalopoulos, E. P., Lluri, G., Hermans, K. C. M., Deb, A., and Blasnkesteijn, W. M. Wnt signaling in cardiac and vascular disease. *Pharmacological Reviews 70*, 1 (2018), 68–141.

[121] Franke, T. F. PI3K/Akt: getting it right matters. *Oncogene 27*, 50 (2008), 6473–6488.

[122] Frigg, R., and Hartmann, S. Models in science. In *The Stanford Encyclopedia of Philosophy*, E. N. Zalta, Ed. Metaphysics Research Lab, Stanford University, 2012.

[123] Fritsch, R., de Krijger, I., Fritsch, K., George, R., Reason, B., Kumar, M. S., Diefenbacher, M., Stamp, G., and Downward, J. RAS and RHO families of GTPases directly regulate distinct phosphoinositide 3-kinase isoforms. *Cell 153*, 5 (2013), 1050–1063.

[124] Gai, W.-T., Yu, D.-P., Wang, X.-S., and Wang, P.-T. Anti-cancer effect of ursolic acid activates apoptosis through ROCK/PTEN mediated mitochondrial translocation of cofilin-1 in prostate cancer. *Oncology Letters 12*, 4 (2016), 2880–2885.

[125] García-Gómez, M. L., Azpeitia, E., and Álvarez-Buylla, E. R. A dynamic genetic-hormonal regulatory network model explains multiple cellular behaviors of the root apical meristem of *Arabidopsis thalian*. *PLOS Computational Biology 13*, 4 (2017), e1005488.

[126] Georgescu, M.-M. PTEN tumor suppressor network in PI3K-Akt pathway control. *Genes & Cancer 1*, 12 (2010), 1170–1177.

[127] Germann, U. A., Furey, B. F., Markland, W., Hoover, R. R., Aronov, A. M., Roix, J. J., Hale, M., Boucher, D. M., Sorrell, D. A., Martinez-Botella, G., Fitzgibbon, M., Shapiro, P., Wick, M. J., Samadani, R., Meshaw, K., Groover, A., DeCrescenzo, G., Namchuk, M., Emery, C. M., Saha, S., and Welsch, D. J. Targeting the MAPK signaling pathway in cancer: promising preclinical activity with the novel selective ERK1/2 inhibitor BVD-523 (Ulixertinib). *Molecular Cancer Therapeutics 16*, 11 (2017), 2351–2363.

[128] Gershenson, C., Kauffman, S. A., and Shmulevich, I. The role of redundancy in the robustness of random Boolean networks. *In Artifical Life X, Proceedings of the Tenth International Conference on the Simulation and Synthesis of Living Systems* (2006).

[129] Giacomantonio, C. E., and Goodhill, G. J. A Boolean model of the gene regulatory network underlying mammalian cortical area development. *PLOS Computational Biology 6*, 9 (2010), e1000936.

[130] Gillespie, C. S. Fitting heavy tailed distributions: The powerlaw package. *Journal of Statistical Software 64*, 2 (2015).

[131] Glass, L., and Kauffman, S. A. The logical analysis of continous, non-linear biochemical control networks. *Journal of Theoretical Biology 39*, 1 (1973), 103–129.

[132] Goh, K.-I., Cusick, M. E., Valle, D., Childs, B., Vidal, M., and Barabási, A.-L. The human disease network. *Proceedings of the National Academy of Sciences of the United States of America 104*, 21 (2007), 8685–8690.

[133] Goldspink, G., and Harridge, S. D. R. Growth factors and muscle ageing. *Experimental Gerontology 39*, 10 (2004), 1433–1438.

[134] Goonesekere, N. C. W., Wang, X., Ludwig, L., and Guda, C. A meta analysis of pancreatic microarray datasets yields new targets as cancer genes and biomarkers. *PLOS ONE 9*, 4 (2014), e93046.

[135] Gore, A. J., Deitz, S. L., Palam, L. R., Craven, K. E., and Korc, M. Pancreatic cancer–associated retinoblastoma 1 dysfunction enables TGF-β to promote

proliferation. *The Journal of Clinical Investigation 124*, 1 (2014), 338–352.
[136] Gregory, M. A., Qi, Y., and Hann, S. R. Phosphorylation by glycogen synthase kinase-3 controls c-Myc proteolysis and subnuclear localization. *Journal of Biological Chemistry 278*, 51 (2003), 51606–51612.
[137] Gross, A., Kracher, B., Kraus, J. M., Kühlwein, S. D., Pfister, A. S., Wiese, S., Luckert, K., Pötz, O., Joos, T., Van Daele, D., De Readt, L., and Kühl, Michael, K. H. A. Representing dynamic biological networks with multi-scale probabilistic models. *Communications Biology 2* (2019).
[138] Gruber, J., Yee, Z., and Tolwinski, N. S. Developmental drift and the role of Wnt signaling in aging. *Cancers 8*, 8 (2016), 73.
[139] Guarente, L., and Kenyon, C. Genetic pathways that regulate ageing in model organisms. *Nature 408*, 6809 (2000), 255–262.
[140] Guilluy, C., Garcia-Mata, R., and Burridge, K. Rho protein crosstalk: another social network? *Trends in Cell Biology 21*, 12 (2011), 718–726.
[141] Guimerà, R., and Nunes Amaral, L. A. Functional cartography of complex metabolic networks. *Nature 433* (2005), 895–900.
[142] Gulhati, P., Bowen, K. A., Liu, J., Stevens, P. D., Rychahou, P. G., Chen, M., Lee, E. Y., Weiss, H. L., O'Connor, K. L., Gao, T., and Evers, M. B. mTORC1 and mTORC2 regulate EMT, motility, and metastasis of colorectal cancer via RhoA and Rac1 signaling pathways. *Cancer Research 71*, 9 (2011), 3246–3256.
[143] Guo, S., Rena, G., Cichy, S., He, X., Cohen, P., and Unterman, T. Phosphorylation of serine 256 by protein kinase B disrupts transactivation by FKHR and mediates effects of insulin on insulin-like growth factor-binding protein-1 promoter activity through a conserved insulin response sequence. *Journal of Biological Chemistry 274*, 24 (1999), 17184–17192.
[144] Gupta, S., Bisht, S. S., Kukreti, R., Jain, S., and Brahmachari, S. K. Boolean network analysis of a neurotransmitter signaling pathway. *Journal of Theoretical Biology 244*, 3 (2007), 463–469.
[145] Guridi, M., Kupr, B., Romanino, K., Lin, S., Falcetta, D., Tintignac, L., and Rüegg, M. A. Alterations to mTORC1 signaling in the skeletal muscle differentially affect whole-body metabolism. *Skeletal Muscle 6*, 13 (2016).
[146] Hajian-Tilaki, K. Receiver operating characteristic (ROC) curve analysis for medical diagnostic test evaluation. *Caspian Journal of Internal Medicine 4*, 2 (2013), 627–635.
[147] Hamacher, R., Schmid, R. M., Saur, D., and Schneider, G. Apoptotic pathways in pancreatic ductal adenocarcinoma. *Molecular Cancer 7*, 64 (2008).
[148] Hanahan, D., and Weinberg, R. A. The hallmarks of cancer. *Cell 100*, 1 (2000), 57–70.
[149] Harvey, I., and Bossomaier, T. Time out of joint: attractors in asynchronous random boolean networks. In *Proceedings of the Fourth European Conference on Artificial Life (ECAL97)* (1997), MIT Press, Cambridge, pp. 67–75.
[150] Hawkins, P. T., Eguinoa, A., Qiu, R.-G., Stokoe, D., Cooke, F. T., Walters, R., Wennström, S., Claesson-Welsh, L., Evans, T., Symons, M., and Stephens, L. PDGF stimulates an increase in GTP–Rac via activation of phosphoinositide 3-kinase. *Current Biology 5*, 4 (1995), 393–403.
[151] Hayflick, L. The future of ageing. *Nature 408*, 6809 (2000), 267–269.
[152] He, X., and Zhang, J. Why do hubs tend to be essential in protein networks? *PLOS Genetics 2*, 6 (2006), e88.
[153] Heid, I., Lubeseder-Martellato, C., Sipos, B., Mazur, P. K., Lesina, M., Schmid, R. M., and Siveke, J. T. Early requirement of Rac1 in a mouse model of pancreatic cancer. *Gastroenterology 141*, 2 (2011), 719–730.
[154] Heinen, C. D., Heppner Goss, K., Cornelius, J. R., Babcock, G. F., Knudsen, E. S., Kowalik, T., and Groden, J. The APC tumor suppressor controls entry into S-phase through its ability to regulate the cyclin D/RB pathway. *Gastroenterology 123*, 3 (2002), 751–763.
[155] Helenius, M., Hänninen, M., Lehtinen, S. K., and Salminen, A. Aging-induced up-regulation of nuclear binding activities of oxidative stress responsive NF-κB transcription factor in mouse cardiac muscle. *Journal of Molecular and Cellular Cardiology 28*, 3 (1996), 487–498.
[156] Helenius, M., Hänninen, M., Lehtinen, S. K., and Salminen, A. Changes associated with aging and replicative senescence in the regulation of transcription factor nuclear factor-κB. *Biochemical Journal 318*, Pt 2 (1996), 603–608.
[157] Helikar, T., Kowal, B., McClenathan, S., Bruckner, M., Rowley, T., Madrahimov, A., Wicks, B., Shrestha, M., Limbu, K., and Rogers, J. A. The Cell Collective: toward an open and collaborative approach to systems biology. *BMC Systems Biology 6*, 96 (2012).
[158] Hernández-Negrete, I., Carretero-Ortega, J., Rosenfeldt, H., Hernández-García, R., Calderón-Salinas, J. V., Reyes-Cruz, G., Gutkind, J. S., and Vázquez-Prado, J. P-Rex1 links mammalian target of rapamycin signaling to Rac activation and cell migration. *Journal of Biological Chemistry 282*, 32 (2007), 23708–23715.
[159] Herrmann, F., Gross, A., Zhou, D., Kestler, H. A., and Kühl, M. A Boolean model of the cardiac gene regulatory network determining first and second heart field identity. *PLOS ONE 7*, 10 (2012), e46798.
[160] Hervé, M. *RVAideMemoire: testing and plotting procedures for biostatistics*, 2019. R package version 0.9-71.
[161] Hidalgo, M., Cascinu, S., Kleeff, J., Labianca, R., Löhr, J.-M., Neoptolemos, J., Real, F. X., Van Laethem, J.-L., and Heinemann, V. Addressing the challenges of pancreatic cancer: Future directions for improving outcomes. *Pancreatology 15*, 1 (2015), 8–18.
[162] Hirano, T., Ishihara, K., and Hibi, M. Roles of STAT3 in mediating the cell growth, differentiation and survival signals relayed through the IL-6 family of cytokine receptors. *Oncogene 19*, 21 (2000), 2548–2556.
[163] Hoeflich, K. P., Luo, J., Rubie, E. A., Tsao, M.-S., Jin, O., and Woodgett, J. R. Requirement for glycogen synthase kinase-3β in cell survival and NF-κB activation. *Nature 406*, 6791 (2000), 86–90.
[164] Hong, D., Kurzrock, R., Kim, Y., Woessner, R., Younes, A., Nemunaitis, J., Fowler, N., Zhou, T., Schmidt, J., Jo, M., Lee, S. J., Yamashita, M., Hughes, S. G., Fayad, L., Piha-Paul, S., Nadella, M. V. P., Mohseni, M., Lawson, D., Reimer, C., Blakey, D. C., Xiao, X., Hsu, J., Revenko, A., Monia, B. P., and MacLeod, A. R. AZD9150, a next-generation antisense oligonucleotide inhibitor of STAT3 with early evidence of clinical activity in lymphoma and lung cancer. *Science Translational Medicine 7*, 314 (2015), 314ra185.
[165] Hong, S.-M., Li, A., Olino, K., Wolfgang, C. L., Herman, J. M., Schulick, R. D., Iacobuzio-Donahue, C., Hruban, R. H., and Goggins, M. Loss of E-cadherin expression and outcome among patients with resectable pancreatic adenocarcinomas. *Modern Pathology 24*, 9 (2011), 1237–1247.
[166] Honma, M., Benitah, S. A., and Watt, F. M. Role of LIM kinases in normal and psoriatic human epidermis. *Molecular Biology of the Cell 17*, 4 (2006), 1888–1896.
[167] Hoogeboom, D., and Burgering, B. M. Should I stay or should I go: β-catenin decides under stress. *Biochimica et Biophysica Acta (BBA) - Reviews on Cancer 1796*, 2 (2009), 63–74.
[168] Hopfensitz, M., Müssel, C., Maucher, M., and Kestler, H. A. Attractors in boolean networks: a tutorial. *Computational Statistics 28*, 1 (2013), 19–36.
[169] Hopfensitz, M., Müssel, C., Wawra, C., Maucher, M., Kühl, M., Neumann, H., and Kestler, H. A. Multiscale binarization of gene expression data for reconstructing boolean networks. *IEEE/ACM Transactions on Computational Biology and Bioinformatics (TCBB) 9*, 2 (2012), 487–498.
[170] Howlade, N., Noone, AM, K. M., Miller, D., Bishop, K., Kosary, C., Yu, M., Ruhl, J., Tatalovich, Z., Mariotto, A., Lewis, D., Chen, H., Feuer, E., and (eds), C. K. SEER Cancer Statistics Review, 1975-2014, National Cancer Institute. Bethesda, MD. https://seer.cancer.gov/csr/1975_2014/ *based on November 2016 SEER data submission* (2017).
[171] Hsu, C.-P., Hsu, J.-T., Liao, C.-H., Kang, S.-C., Lin, B.-C., Hsu, Y.-P., Yeh, C.-N., Yeh, T.-S., and Hwang, T.-L. Three-year and five-year outcomes of surgical resection for pancreatic ductal adenocarcinoma: Long-term experiences in one medical center. *Asian Journal of Surgery 41*, 2 (2018), 115–123.
[172] Hu, Z., Klein, J. D., Mitch, W. E., Zhang, L., Martinez, I., and Wang, X. H. MicroRNA-29 induces cellular senescence in aging muscle through multiple signaling pathways. *Aging (Albany NY) 6*, 3 (2014), 160–175.
[173] Huang, C., Yang, G., Jiang, T., Huang, K., Cao, J., and Qiu, Z. Effects of IL-6 and AG490 on regulation of Stat3 signaling pathway and invasion of human pancreatic cancer cells in vitro. *Journal of Experimental & Clinical Cancer Research 29*, 51 (2010).
[174] Huang, J., Dibble, C. C., Matsuzaki, M., and Manning, B. D. The TSC1-TSC2 complex is required for proper activation of mTOR complex 2. *Molecular and Cellular Biology 28*, 12 (2008), 4104–4115.
[175] Huang, J., Wu, S., Wu, C.-L., and Manning, B. D. Signaling events downstream of mammalian target of rapamycin complex 2 are attenuated in cells and tumors deficient for the tuberous sclerosis complex tumor suppressors. *Cancer Research 69*, 15 (2009), 6107–6114.
[176] Ideker, T., Galitski, T., and Hood, L. A new approach to decoding life: systems biology. *Annual Review of Genomics and Human Genetics 2* (2001), 343–372.
[177] Ikonomi, N. The drawback of crosstalk: Wnt and MAPK signalling in colorectal cancer. Master thesis, Medical Faculty, Ulm University, 2019.
[178] Inoki, K., Ouyang, H., Zhu, T., Lindvall, C., Wang, Y., Zhang, X., Yang, Q., Bennett, C., Harada, Y., Stankunas, K., Wang, C.-Y., MacDougald, O. A., You, M., Williams, B. O., and Guan, K.-L. TSC2 integrates Wnt and energy signals via a coordinated phosphorylation by AMPK and GSK3 to regulate cell growth. *Cell 126*, 5 (2006), 955–968.
[179] Irons, D. Logical analysis of the budding yeast cell cycle. *Journal of Theoretical Biology 257*, 4 (2009), 543–559.
[180] Jasperson, K. W., Patel, S. G., and Ahnen, D. J. APC-associated polyposis conditions. In *Gene Reviews* (2017), M. Adam, H. Ardinger, and P. RA, Eds., Seattle WA: University of Washington.

[181] Jeong, H., Mason, S. P., Barabási, A.-L., and Oltvai, Z. N. Lethality and centrality in protein networks. *Nature 411* (2001), 41–42.
[182] Jeong, H., Tombor, B., Albert, R., Oltvai, Z. N., and Barabási, A.-L. The large-scale organization of metabolic networks. *Nature 407*, 6804 (2000), 651–654.
[183] Jeong, W.-J., Ro, E. J., and Choi, K.-Y. Interaction between Wnt/β-catenin and RAS-ERK pathways and an anti-cancer strategy via degradations of β-catenin and RAS by targeting the Wnt/β-catenin pathway. *NPJ Precision Oncology 2*, 5 (2018).
[184] Jho, E.-h., Zhang, T., Domon, C., Joo, C.-K., Freund, J.-N., and Costantini, F. Wnt/β-catenin/Tcf signaling induces the transcription of Axin2, a negative regulator of the signaling pathway. *Molecular and Cellular Biology 22*, 4 (2002), 1172–1183.
[185] Jin, T. The WNT signalling pathway and diabetes mellitus. *Diabetologia 51*, 10 (2008), 1771–1780.
[186] Jin, T., Fantus, I. G., and Sun, J. Wnt and beyond Wnt: multiple mechanisms control the transcriptional property of β-catenin. *Cellular Signalling 20*, 10 (2008), 1697–1704.
[187] Joo, Y.-E., Rew, J.-S., Park, C.-S., and Kim, S.-J. Expression of E-cadherin, alpha-and beta-catenins in patients with pancreatic adenocarcinoma. *Pancreatology 2*, 2 (2002), 129–137.
[188] Joseph, G. A., Wang, S. X., Jacobs, C. E., Zhou, W., Kimble, G. C., Tse, H. W., Eash, J. K., Shavlakadze, T., and Glass, D. J. Partial inhibition of mTORC1 in aged rats counteracts the decline in muscle mass and reverses molecular signaling associated with sarcopenia. *Molecular and Cellular Biology 39*, 19 (2019), e00141–19.
[189] Juiz, N. A., Iovanna, J., and Dusetti, N. Pancreatic cancer heterogeneity can be explained beyond the genome. *Frontiers in Oncology 9* (2019), 246.
[190] Kaler, P., Sasazuki, T., Shirasawa, S., Augenlicht, L., and Klampfer, L. HDAC2 deficiency sensitizes colon cancer cells to TNFα-induced apoptosis through inhibition of NF-κB activity. *Experimental Cell Research 314*, 7 (2008), 1507–1518.
[191] Kamran, M. Z., Patil, P., and Gude, R. P. Role of $STAT_3$ in cancer metastasis and translational advances. *BioMed Research International 2013*, 421821 (2013).
[192] Kanehisa, M., and Goto, S. KEGG: kyoto encyclopedia of genes and genomes. *Nucleic Acids Research 28*, 1 (2000), 27–30.
[193] Karsunky, H., Zeng, H., Schmidt, T., Zevnik, B., Kluge, R., Schmid, K. W., Dührsen, U., and Möröy, T. Inflammatory reactions and severe neutropenia in mice lacking the transcriptional repressor Gfi1. *Nature Genetics 30*, 3 (2002), 295–300.
[194] Katsha, A., Arras, J., Soutto, M., Belkhiri, A., and El-Rifai, W. AURKA regulates JAK2–STAT3 activity in human gastric and esophageal cancers. *Molecular Oncology 8*, 8 (2014), 1419–1428.
[195] Kauffman, S. A. Metabolic stability and epigenesis in randomly constructed genetic nets. *Journal of Theoretical Biology 22*, 3 (1969), 437–467.
[196] Kauffman, S. A. *The Origins of order: Self-Organization and Selection in Evolution*. Oxford: Oxford University Press, 1993.
[197] Kauko, O., O'Connor, C., Kulesskiy, E., Sangodkar, J., Aakula, A., Izadmehr, S., Yetukuri, L., Yadav, B., Padzik, A., Laajala, T. D., Haapaniemi, P., Momeny, M., Varila, T., Ohlmeyer, M., Aittokallio, T., Wennerberg, K., Goutham, N., and Westermarck, J. PP2A inhibition is a druggable MEK inhibitor resistance mechanism in KRAS-mutant lung cancer cells. *Science Translational Medicine 10*, 450 (2018).
[198] Kawada, H., Ito, T., Pharr, P. N., Spyropoulos, D. D., Watson, D. K., and Ogawa, M. Defective megakaryopoiesis and abnormal erythroid development in Fli-1 gene-targeted mice. *International Journal of Hematology 73*, 4 (2001), 463–468.
[199] Kawasaki, Y., Sato, R., and Akiyama, T. Mutated APC and Asef are involved in the migration of colorectal tumour cells. *Nature Cell Biology 5* (2003), 211–215.
[200] Kenyon, C., Chang, J., Gensch, E., Rudner, A., and Tabtiang, R. A C. elegans mutant that lives twice as long as wild type. *Nature 366*, 6454 (1993), 461–464.
[201] Kenyon, C. J. The genetics of ageing. *Nature 464*, 7288 (2010), 504–512.
[202] Kervizic, G., and Corcos, L. Dynamical modeling of the cholesterol regulatory pathway with Boolean networks. *BMC Systems Biology 2*, 99 (2008).
[203] Kestler, H. A., and Kühl, M. From individual Wnt pathways towards a Wnt signalling network. *Philosophical Transactions of the Royal Society B 363*, 1495 (2008), 1333–1347.
[204] Khanna, A., Okkeri, J., Bilgen, T., Tiirikka, T., Vihinen, M., Visakorpi, T., and Westermarck, J. ETS1 mediates MEK1/2-dependent overexpression of cancerous inhibitor of protein phosphatase 2A (CIP2A) in human cancer cells. *PLOS ONE 6*, 3 (2011), e17979.
[205] Kikuchi, A., Yamamoto, H., Sato, A., and Matsumoto, S. New insights into the mechanisms of Wnt signaling pathway activation. *International Review of Cell and Molecular Biology 291* (2011), 21–71.
[206] Kim, D., Rath, O., Kolch, W., and Cho, K.-H. A hidden oncogenic positive feedback loop caused by crosstalk between Wnt and ERK pathways. *Oncogene 26*, 31 (2007), 4571–4579.
[207] Kim, E. K., Yun, S. J., Ha, J. M., Kim, Y. W., Jin, I. H., Yun, J., Shin, H. K., Song, S. H., Kim, J. H., Lee, J. S., Kim, C. D., and S, B. S. Selective activation of Akt1 by mammalian target of rapamycin complex 2 regulates cancer cell migration, invasion, and metastasis. *Oncogene 30*, 26 (2011), 2954–2963.
[208] Kim, J. W., Lee, J. E., Kim, M. J., Cho, E.-G., Cho, S.-G., and Choi, E.-J. Glycogen synthase kinase 3β is a natural activator of mitogen-activated protein kinase/extracellular signal-regulated kinase kinase kinase 1 (MEKK1). *Journal of Biological Chemistry 278*, 16 (2003), 13995–14001.
[209] Kim, M.-J., Jang, S.-J., and Yu, E. Loss of E-cadherin and cytoplasmic-nuclear expression of β-catenin are the most useful immunoprofiles in the diagnosis of solid-pseudopapillary neoplasm of the pancreas. *Human Pathology 39*, 2 (2008), 251–258.
[210] Kimura, K. D., Tissenbaum, H. A., Liu, Y., and Ruvkun, G. daf-2, an insulin receptor-like gene that regulates longevity and diapause in *Caenorhabditis elegans*. *Science 277*, 5328 (1997), 942–946.
[211] Kirchhoff, S. *Zellbasierte Hochdurchsatzanalysen identifizieren eine zentrale, wachstumsregulierende Rolle von Cofilin-1 im humanen Pankreaskarzinom*. PhD thesis, Philipps Universität, Marburg, 2013.
[212] Kitano, H. Computational systems biology. *Nature 420*, 6912 (2002), 206–210.
[213] Kitano, H. Systems biology: A brief overview. *Science 295*, 5560 (2002), 1662–1664.
[214] Klamt, S., Saez-Rodriguez, J., Lindquist, J. A., Simeoni, L., and Gilles, E. D. A methodology for the structural and functional analysis of signaling and regulatory networks. *BMC Bioinformatics 7*, 56 (2006).
[215] Kleeff, J., Korc, M., Apte, M., La Vecchia, C., Johnson, C. D., Biankin, A. V., Neale, R. E., Tempero, M., Tuveson, D. A., Hruban, R. H., and Neoptolemos, J. P. Pancreatic cancer. *Nature Reviews Disease Primers 2*, 16022 (2016).
[216] Klemm, K., and Bornholdt, S. Stable and unstable attractors in Boolean networks. *Physical Review E, Statistical, Nonlinear and Soft Matter Physics 72*, 5 Pt 2 (2005), 055101.
[217] Kobayashi, M., Honma, T., Matsuda, Y., Suzuki, Y., Narisawa, R., Ajioka, Y., and Asakura, H. Nuclear translocation of beta-catenin in colorectal cancer. *British Journal of Cancer 82*, 10 (2000), 1689–1693.
[218] Kohno, H., Tanaka, T., Kawabata, K., Hirose, Y., Sugie, S., Tsuda, H., and Mori, H. Silymarin, a naturally occurring polyphenolic antioxidant flavonoid, inhibits azoxymethane-induced colon carcinogenesis in male F344 rats. *International Journal of Cancer 101*, 5 (2002), 461–468.
[219] Kokash, N. An introduction to heuristic algorithms. *Department of Informatics and Telecommunications* (2005).
[220] Krumsiek, J., Marr, C., Schroeder, T., and Theis, F. J. Hierarchical differentiation of myeloid progenitors is encoded in the transcription factor network. *PLOS ONE 6*, 8 (2011), e22649.
[221] Kuro-o, M., Matsumura, Y., Aizawa, H., Kawaguchi, H., Suga, T., Utsugi, T., Ohyama, Y., Kurabayashi, M., Kaname, T., Kume, E., Iwasaki, H., Iida, A., Shiraki-Iida, T., Nishikawa, S., Nagai, R., and Nabeshima, Y.-i. Mutation of the mouse klotho gene leads to a syndrome resembling ageing. *Nature 390*, 6655 (1997), 45–51.
[222] Lähdesmäki, H., Shmulevich, I., and Yli-Harja, O. On learning gene regulatory networks under the Boolean network model. *Machine Learning 52*, 1-2 (2003), 147–167.
[223] Lamberts, S. W. J., van den Beld, A. W., and Van Der Lely, A.-J. The endocrinology of aging. *Science 278*, 5337 (1997), 419–424.
[224] Lan, T., Chen, Y., Sang, J., Wu, Y., Wang, Y., Jiang, L., and Tao, Y. Type II cGMP-dependent protein kinase inhibits EGF-induced MAPK/JNK signal transduction in breast cancer cells. *Oncology Reports 27*, 6 (2012), 2039–2044.
[225] Larrea, M. D., Liang, J., Da Silva, T., Hong, F., Shao, S. H., Han, K., Dumont, D., and Slingerland, J. M. Phosphorylation of p27Kip1 regulates assembly and activation of cyclin D1-Cdk4. *Molecular and Cellular Biology 28*, 20 (2008), 6462–6472.
[226] Larrea, M. D., Wander, S. A., and Slingerland, J. p27 as Jekyll and Hyde: regulation of cell cycle and cell motility. *Cell Cycle 8*, 21 (2009), 3455–3461.
[227] Laslo, P., Spooner, C. J., Warmflash, A., Lancki, D. W., Lee, H.-J., Sciammas, R., Gantner, B. N., Dinner, A. R., and Singh, H. Multilineage transcriptional priming and determination of alternate hematopoietic cell fates. *Cell 126*, 4 (2006), 755–766.
[228] Le Grand, F., and Rudnicki, M. A. Skeletal muscle satellite cells and adult myogenesis. *Current Opinion in Cell Biology 19*, 6 (2007), 628–633.
[229] Le Novère, N., Bornstein, B., Broicher, A., Courtot, M., Donizelli, M., Dharuri, H., Li, L., Sauro, H., Schilstra, M., Shapiro, B., Snoep, J. L., and Hucka, M. BioModels Database: a free, centralized database of curated, published, quantitative kinetic models of biochemical and cellular systems. *Nucleic*

Acids Research 34, Database issue (2006), D689–D691.

[230] Lederman, R. J., Mendelsohn, F. O., Anderson, R. D., Saucedo, J. F., Tenaglia, A. N., Hermiller, J. B., Hillegass, W. B., Rocha-Singh, K., Moon, T. E., Whitehouse, M., Annex, B. H., and investigators, T. Therapeutic angiogenesis with recombinant fibroblast growth factor-2 for intermittent claudication (the TRAFFIC study): a randomised trial. *THE LANCET 359*, 9329 (2002), 2053–2058.

[231] Lee, E.-K., Cho, H., and Kim, C.-W. Proteomic analysis of cancer stem cells in human prostate cancer cells. *Biochemical and Biophysical Research Communications 412*, 2 (2011), 279–285.

[232] Lee, K., and Esselman, W. J. Inhibition of PTPs by H_2O_2 regulates the activation of distinct MAPK pathways. *Free Radical Biology and Medicine 33*, 8 (2002), 1121–1132.

[233] Lee, S.-K., Hwang, J.-H., and Choi, K.-Y. Interaction of the Wnt/β-catenin and RAS-ERK pathways involving co-stabilization of both β-catenin and RAS plays important roles in the colorectal tumorigenesis. *Advances in Biological Regulation 68* (2018), 46–54.

[234] Lemieux, E., Cagnol, S., Beaudry, K., Carrier, J., and Rivard, N. Oncogenic KRAS signalling promotes the Wnt/β-catenin pathway through LRP6 in colorectal cancer. *Oncogene 34*, 38 (2015), 4914–4927.

[235] Li, G., Ying, L., Wang, H., Wei, S.-S., Chen, J., Chen, Y.-H., Xu, W.-P., Jie, Q.-Q., Zhou, Q., Li, Y.-G., et al. Rac1b enhances cell survival through activation of the JNK2/c-JUN/Cyclin-D1 and AKT2/MCL1 pathways. *Oncotarget 7*, 14 (2016), 17970–17985.

[236] Li, H., Malhotra, S., and Kumar, A. Nuclear factor-kappa B signaling in skeletal muscle atrophy. *Journal of Molecular Medicine 86*, 10 (2008), 1113–1126.

[237] Li, H., Ung, C. Y., Ma, X. H., Li, B. W., Low, B. C., Cao, Z. W., and Chen, Y. Z. Simulation of crosstalk between small GTPase RhoA and EGFR-ERK signaling pathway via MEKK1. *Bioinformatics 25*, 3 (2009), 358–364.

[238] Li, H., Zhu, F., Boardman, L. A., Wang, L., Oi, N., Liu, K., Li, X., Fu, Y., Limburg, P. J., Bode, A. M., et al. Aspirin prevents colorectal cancer by normalizing EGFR expression. *EBioMedicine 2*, 5 (2015), 447–455.

[239] Li, P., Nijhawan, D., Budihardjo, I., Srinivasula, S. M., Ahmad, M., Alnemri, E. S., and Wang, X. Cytochrome c and dATP-dependent formation of Apaf-1/caspase-9 complex initiates an apoptotic protease cascade. *Cell 91*, 4 (1997), 479–489.

[240] Li, S., Lu, J., Chen, Y., Xiong, N., Li, L., Zhang, J., Yang, H., Wu, C., Zeng, H., and Liu, Y. MCP-1-induced ERK/GSK-3β/Snail signaling facilitates the epithelial–mesenchymal transition and promotes the migration of MCF-7 human breast carcinoma cells. *Cellular & Molecular Immunology 14* (2017), 621–630.

[241] Li, X.-P., Zhang, X.-W., Zheng, L.-Z., and Guo, W.-J. Expression of CD44 in pancreatic cancer and its significance. *International Journal of Clinical & Experimental Pathology 8*, 6 (2015), 6724–6731.

[242] Likić, V. A., McConville, M. J., Lithgow, T., and Bacic, A. Systems biology: The next frontier for bioinformatics. *Advances in Bioinformatics 2010*, 268925 (2010).

[243] Lin, A., Piao, H.-l., Zhuang, L., Sarbassov, D. D., Ma, L., and Gan, B. FoxO transcription factors promote AKT Ser473 phosphorylation and renal tumor growth in response to pharmacologic inhibition of the PI3K–AKT pathway. *Cancer Research 74*, 6 (2014), 1682–1693.

[244] Lin, G., Brownsey, R. W., and MacLeod, K. M. Complex regulation of PKCβ2 and PDK-1/AKT by ROCK2 in diabetic heart. *PLOS ONE 9*, 1 (2014), e86520.

[245] Lin, G., Tang, Z., Ye, Y.-B., and Chen, Q. NF-κB activity is downregulated by KRAS knockdown in SW620 cells via the RAS-ERK-IκBα pathway. *Oncology Reports 27*, 5 (2012), 1527–1534.

[246] Ling, X., and Arlinghaus, R. B. Knockdown of STAT3 expression by RNA interference inhibits the induction of breast tumors in immunocompetent mice. *Cancer Research 65*, 7 (2005), 2532–2536.

[247] Liu, A., Chen, S., Cai, S., Dong, L., Liu, L., Yang, Y., Guo, F., Lu, X., He, H., Chen, Q., Hu, S., and Qiu, H. Wnt5a through noncanonical Wnt/JNK or Wnt/PKC signaling contributes to the differentiation of mesenchymal stem cells into type II alveolar epithelial cells *in vitro*. *PLOS ONE 9*, 3 (2014), e90229.

[248] Liu, C.-Y., Huang, T.-T., Huang, C.-T., Hu, M.-H., Wang, D.-S., Wang, W.-L., Tsai, W.-C., Lee, C.-H., Lau, K.-Y., Yang, H.-P., Chen, M.-H., Shiau, C.-W., Tseng, L.-M., and Chen, K.-F. EGFR-independent Elk1/CIP2A signalling mediates apoptotic effect of an erlotinib derivative TD52 in triple-negative breast cancer cells. *European Journal of Cancer 72* (2017), 112–123.

[249] Liu, H., Fergusson, M. M., Castilho, R. M., Liu, J., Cao, L., Chen, J., Malide, D., Rovira, I. I., Schimel, D., Kuo, C. J., Gutkind, J. S., Hwang, P. M., and Finkel, T. Augmented Wnt signaling in a mammalian model of accelerated aging. *Science 317*, 5839 (2007), 803–806.

[250] Liu, J., Chen, B., Lu, Y., Guan, Y., and Chen, F. JNK-dependent Stat3 phosphorylation contributes to Akt activation in response to arsenic exposure. *Toxicological Sciences 129*, 2 (2012), 363–371.

[251] Liu, L., and Rando, T. A. Manifestations and mechanisms of stem cell aging. *The Journal of Cell Biology 193*, 2 (2011), 257–266.

[252] Liu, L., Wang, Y., and Yu, Q. The PI3K/Akt signaling pathway exerts effects on the implantation of mouse embryos by regulating the expression of RhoA. *International Journal of Molecular Medicine 33*, 5 (2014), 1089–1096.

[253] Liu, Z., Chu, S., Yao, S., Li, Y., Fan, S., Sun, X., Su, L., and Liu, X. CD74 interacts with CD44 and enhances tumorigenesis and metastasis via RHOA-mediated cofilin phosphorylation in human breast cancer cells. *Oncotarget 7*, 42 (2016), 68303–68313.

[254] Logan, C. Y., and Nusse, R. The Wnt signaling pathway in development and disease. *Annual Review of Cell and Developmental Biology 20* (2004), 781–810.

[255] Logsdon, C. D., and Lu, W. The significance of Ras activity in pancreatic cancer initiation. *International Journal of Biological Sciences 12*, 3 (2016), 338–346.

[256] López-Otín, C., Blasco, M. A., Partridge, L., Serrano, M., and Kroemer, G. The hallmarks of aging. *Cell 153*, 6 (2013), 1194–1217.

[257] Louderbough, J. M., and Schroeder, J. A. Understanding the dual nature of CD44 in breast cancer progression. *Molecular Cancer Research 9*, 12 (2011), 1573–1586.

[258] Lu, X., Jain, V. V., Finn, P. W., and Perkins, D. L. Hubs in biological interaction networks exhibit low changes in expression in experimental asthma. *Molecular Systems Biology 3*, 98 (2007).

[259] Luo, J. The role of glycogen synthase kinase 3β (GSK3β) in tumorigenesis and cancer chemotherapy. *Cancer Letters 273*, 2 (2009), 194–200.

[260] Machesky, L. M. Lamellipodia and filopodia in metastasis and invasion. *FEBS Letters 582*, 14 (2008), 2102–2111.

[261] MacLachlan, T. K., and Giordano, A. TRAF2 expression in differentiated muscle. *Journal of Cellular Biochemistry 71*, 4 (1998), 461–466.

[262] MacLean, D., and Studholme, D. J. A Boolean model of the *Pseudomonas syringae* hrp regulon predicts a tightly regulated system. *PLOS ONE 5*, 2 (2010), e9101.

[263] Mai, Z., and Liu, H. Boolean network-based analysis of the apoptosis network: Irreversible apoptosis and stable surviving. *Journal of Theoretical Biology 259*, 4 (2009), 760–769.

[264] Maimaiti, Y., Tan, J., Liu, Z., Guo, Y., Yan, Y., Nie, X., Huang, B., Zhou, J., and Huang, T. Overexpression of cofilin correlates with poor survival in breast cancer: A tissue microarray analysis. *Oncology Letters 14*, 2 (2017), 2288–2294.

[265] Malliri, A., Rygiel, T. P., van der Kammen, R. A., Song, J.-Y., Engers, R., Hurlstone, A. F., Clevers, H., and Collard, J. G. The Rac activator *Tiam1* is a Wnt-responsive gene that modifies intestinal tumor development. *Journal of Biological Chemistry 281*, 1 (2006), 543–548.

[266] Manolagas, S. C., and Almeida, M. Gone with the Wnts: β-catenin, T-cell factor, forkhead box O, and oxidative stress in age-dependent diseases of bone, lipid, and glucose metabolism. *Molecular Endocrinology 21*, 11 (2007), 2605–2614.

[267] Mao, Z., and Zhang, W. Role of mTOR in glucose and lipid metabolism. *International Journal of Molecular Sciences 19*, 7 (2018), 2043.

[268] Marques-Pita, M., and Rocha, L. M. Canalization and control in automata networks: body segmentation in *Drosophila melanogaster*. *PLOS ONE 8*, 3 (2013), e55946.

[269] Martinez-Sanchez, M. E., Mendoza, L., Villarreal, C., and Alvarez-Buylla, E. R. A minimal regulatory network of extrinsic andintrinsic factors recovers observed patterns of CD4+ T cell differentiation and plasticity. *PLOS Computational Biology 11*, 6 (2015), e1004324.

[270] Martins, R., Lithgow, G. J., and Link, W. Long live FOXO: unraveling the role of FOXO proteins in aging and longevity. *Aging Cell 15*, 2 (2016), 196–207.

[271] Mbodj, A., Junion, G., Brun, C., Furlong, E. E., and Thieffry, D. Logical modelling of *Drosophila* signalling pathways. *Molecular BioSystems 9*, 9 (2013), 2248–2258.

[272] McCubrey, J. A., Steelman, L. S., Bertrand, F. E., Davis, N. M., Sokolosky, M., Abrams, S. L., Montalto, G., D'Assoro, A. B., Libra, M., Nicoletti, F., Maestro, R., Basecke, J., Rakus, D., Gizak, A., Demidenko, Z., Cocco, L., Martelli, A. M., and Cervello, M. GSK-3 as potential target for therapeutic intervention in cancer. *Oncotarget 5*, 10 (2014), 2881–2911.

[273] McCubrey, J. A., Steelman, L. S., Chappell, W. H., Abrams, S. L., Franklin, R. A., Montalto, G., Cervello, M., Libra, M., Candido, S., Malaponte, G., Mazzarino, M. C., Fagone, P., Nicoletti, F., Bäsecke, J., Mijatovic, S., Maksimovic-Ivanic, D., Milella, M., Tafuri, A., Chiarini, F., Evangelisti, C., Cocco, L., and Martelli, A. M. Ras/Raf/MEK/ERK and PI3K/PTEN/Akt/mTOR cascade inhibitors: how mutations can result in therapy resistance and how to overcome resistance. *Oncotarget 3*, 10 (2012), 1068–1111.

[274] McCubrey, J. A., Steelman, L. S., Chappell, W. H., Abrams, S. L., Montalto, G., Cervello, M., Nicoletti, F., Fagone, P., Malaponte, G., Mazzarino, M. C., Candido, S., Massima, L., Bäsecke, J., Mijatovic, S., Maksimovic-Ivanic, D., Milella, M., Tafuri, A., Cocco, L., Evangelisti, C., Francesca, C., and Martelli, A. M. Mutations and deregulation of Ras/Raf/MEK/ERK and PI3K/PTEN/Akt/mTOR cascades which alter therapy response. *Oncotarget 3*, 9 (2012), 954–987.

[275] Medvedev, Z. A. Possible role of repeated nucleotide sequences in DNA in the evolution of life spans of differentiated cells. *Nature 237*, 5356 (1972), 453–454.

[276] Méndez, A., and Mendoza, L. A network model to describe the terminal differentiation of B cells. *PLOS Computational Biology 12*, 1 (2016), e1004696.

[277] Méndez-López, L. F., Davila-Velderrain, J., Domínguez-Hüttinger, E., Enríquez-Olguín, C., Martínez-García, J. C., and Alvarez-Buylla, E. R. Gene regulatory network underlying the immortalization of epithelial cells. *BMC Systems Biology 11*, 24 (2017).

[278] Mendoza, L., and Xenarios, I. A method for the generation of standardized qualitative dynamical systems of regulatory networks. *Theoretical Biology and Medical Modelling 3*, 13 (2006).

[279] Mendoza, M. C., Er, E. E., and Blenis, J. The Ras-ERK and PI3K-mTOR pathways: cross-talk and compensation. *Trends in Biochemical Sciences 36*, 6 (2011), 320–328.

[280] Meyer, P., Maity, P., Burkovski, A., Schwab, J., Müssel, C., Singh, K., Ferreira, F. F., Krug, L., Maier, H. J., Wlaschek, M., Wirth, T., Kestler, H. A., and Scharffetter-Kochanek, K. A model of the onset of the senescence associated secretory phenotype after DNA damage induced senescence. *PLOS Computational Biology 13*, 12 (2017), e1005741.

[281] Miao, F., Zhang, M., Zhao, Y., Li, X., Yao, R., Wu, F., Huang, R., Li, K., Miao, S., Ma, C., et al. RHBDD1 upregulates EGFR via the AP-1 pathway in colorectal cancer. *Oncotarget 8*, 15 (2017), 25251–25260.

[282] Miranti, C. K., Ohno, S., and Brugge, J. S. Protein kinase C regulates integrin-induced activation of the extracellular regulated kinase pathway upstream of Shc. *Journal of Biological Chemistry 274*, 15 (1999), 10571–10581.

[283] Missiou, A., Rudolf, P., Stachon, P., Wolf, D., Varo, N., Aichele, P., Colberg, C., Hoppe, N., Ernst, S., Münkel, C., Walter, C., Sommer, B., Hilgendorf, I., Nakano, H., Bode, C., and Zirlik, A. TRAF5 deficiency accelerates atherogenesis in mice by increasing inflammatory cell recruitment and foam cell formation. *Circulation Research 107*, 6 (2010), 757–766.

[284] Mistry, D. S., Chen, Y., Wang, Y., Zhang, K., and Sen, G. L. SNAI2 controls the undifferentiated state of human epidermal progenitor cells. *Stem Cells 32*, 12 (2014), 3209–3218.

[285] Mitchell, L., Hobbs, G. A., Aghajanian, A., and Campbell, S. L. Redox regulation of Ras and Rho GTPases: mechanism and function. *Antioxidants & Redox Signaling 18*, 3 (2013), 250–258.

[286] Morkel, M., Riemer, P., Bläker, H., and Sers, C. Similar but different: distinct roles for KRAS and BRAF oncogenes in colorectal cancer development and therapy resistance. *Oncotarget 6*, 25 (2015), 20785–20800.

[287] Mukherjee, A., Dhar, N., Stathos, M., Schaffer, D. V., and Kane, R. S. Understanding how Wnt influences destruction complex activity and β-catenin dynamics. *iScience 6* (2018), 13–21.

[288] Munshi, A., and Ramesh, R. Mitogen-activated protein kinases and their role in radiation response. *Genes & Cancer 4*, 9-10 (2013), 401–408.

[289] Müssel, C., Hopfensitz, M., and Kestler, H. A. BoolNet – an R package for generation, reconstruction and analysis of Boolean networks. *Bioinformatics 26*, 10 (2010), 1378–1380.

[290] Müssel, C., Schmid, F., Blätte, T. J., Hopfensitz, M., Lausser, L., and Kestler, H. A. BiTrinA—multiscale binarization and trinarization with quality analysis. *Bioinformatics 32*, 3 (2016), 465–468.

[291] Myant, K. B., Cammareri, P., McGhee, E. J., Ridgway, R. A., Huels, D. J., Cordero, J. B., Schwitalla, S., Kalna, G., Ogg, E.-L., Athineos, D., Timpson, P., Vidal, M., Murray, G. I., Greten, F. R., Anderson, K. I., and Sansom, O. J. ROS production and NF-κB activation triggered by RAC1 facilitate WNT-driven intestinal stem cell proliferation and colorectal cancer initiation. *Cell Stem Cell 12*, 6 (2013), 761–773.

[292] Naito, A. T., Shiojima, I., Komuro, I., and Kühl, M. Wnt signaling and aging-related heart disorders. *Circulation Research 107*, 11 (2010), 1295–1303.

[293] Nakano, H., Oshima, H., Chung, W., Williams-Abbott, L., Ware, C. F., Yagita, H., and Okumura, K. TRAF5, an activator of NF-κB and putative signal transducer for the lymphotoxin-β receptor. *Journal of Biological Chemistry 271*, 25 (1996), 14661–14664.

[294] Nakano, H., Sakon, S., Koseki, H., Takemori, T., Tada, K., Matsumoto, M., Munechika, E., Sakai, T., Shirasawa, T., Akiba, H., Kobata, T., Santee, S. M., Ware, C. F., Rennert, P. D., Taniguchi, M., Yagita, H., and Okumura, K. Targeted disruption of *Traf5* gene causes defects in CD40- and CD27-mediated lymphocyte activation. *Proceedings of the National Academy of Sciences of the United States of America 96*, 17 (1999), 9803–9808.

[295] Nambiar, D., Prajapati, V., Agarwal, R., and Singh, R. P. *In vitro* and *in vivo* anticancer efficacy of silibinin against human pancreatic cancer BxPC-3 and PANC-1 cells. *Cancer Letters 334*, 1 (2013), 109–117.

[296] Narumiya, S., Tanji, M., and Ishizaki, T. Rho signaling, ROCK and mDia1, in transformation, metastasis and invasion. *Cancer and Metastasis Reviews 28*, 1-2 (2009), 65–76.

[297] Näthke, I. Cytoskeleton out of the cupboard: colon cancer and cytoskeletal changes induced by loss of APC. *Nature Reviews Cancer 6*, 12 (2006), 967–974.

[298] Neoptolemos, J. P., Kleeff, J., Michl, P., Costello, E., Greenhalf, W., and Palmer, D. H. Therapeutic developments in pancreatic cancer: current and future perspectives. *Nature Reviews Gastroenterology & Hepatology 15*, 6 (2018), 333–348.

[299] Niccoli, T., and Partridge, L. Ageing as a risk factor for disease. *Current Biology 22*, 17 (2012), R741–R752.

[300] Nicholas, N. S., Pipili, A., Lesjak, M. S., Ameer, S. M., Geh, J. L., Healy, C., Ross, A. D. M., Parsons, M., Nestle, F. O., Lacy, K. E., and Wells, C. M. PAK4 suppresses PDZ-RhoGEF activity to drive invadopodia maturation in melanoma cells. *Oncotarget 7*, 43 (2016), 70881–70897.

[301] Niehrs, C. The complex world of WNT receptor signalling. *Nature Reviews Molecular Cell Biology 13*, 12 (2012), 767–779.

[302] Nikonova, A. S., Astsaturov, I., Serebriiskii, I. G., Dunbrack, R. L., and Golemis, E. A. Aurora A kinase (AURKA) in normal and pathological cell division. *Cellular and Molecular Life Sciences 70*, 4 (2013), 661–687.

[303] Nishimura, S., Tsuda, H., Kataoka, F., Arao, T., Nomura, H., Chiyoda, T., Susumu, N., Nishio, K., and Aoki, D. Overexpression of cofilin 1 can predict progression-free survival in patients with epithelial ovarian cancer receiving standard therapy. *Human Pathology 42*, 4 (2011), 516–521.

[304] Nishita, M., Wang, Y., Tomizawa, C., Suzuki, A., Niwa, R., Uemura, T., and Mizuno, K. Phosphoinositide 3-kinase-mediated activation of cofilin phosphatase slingshot and its role for insulin-induced membrane protrusion. *Journal of Biological Chemistry 279*, 8 (2004), 7193–7198.

[305] Nitulescu, G. M., Van De Venter, M., Nitulescu, Ungurianu, A., Juzenas, P., Peng, Q., Olaru, O. T., Grădinaru, D., Tsatsakis, A., Tsoukalas, D., Spandidos, D. A., and Margina, D. The Akt pathway in oncology therapy and beyong (review). *International Journal of Oncology 53*, 6 (2018), 2319–2331.

[306] Ohuchida, K., Mizumoto, K., Ohhashi, S., Yamaguchi, H., Konomi, H., Nagai, E., Yamaguchi, K., Tsuneyoshi, M., and Tanaka, M. *Twist*, a novel oncogene, is upregulated in pancreatic cancer: clinical implication of *Twist* expression in pancreatic juice. *International Journal of Cancer 120*, 8 (2007), 1634–1640.

[307] Oikonomou, E., Koustas, E., Goulielmaki, M., and Pintzas, A. BRAF vs RAS oncogenes: Are mutations of the same pathway equal? Differential signalling and therapeutic implications. *Oncotarget 5* (2014), 11752–11777.

[308] Okamoto, M., Inoue, K., Iwamura, H., Terashima, K., Soya, H., Asashima, M., and Kuwabara, T. Reduction in paracrine Wnt3 factors during aging causes impaired adult neurogenesis. *The FASEB Journal 25*, 10 (2011), 3570–3582.

[309] Olfert, I. M., Baum, O., Hellsten, Y., and Egginton, S. Advances and challenges in skeletal muscle angiogenesis. *American Journal of Physiology Heart and Circulatory Physiology 310*, 3 (2016), H326–H336.

[310] Orlando, D. A., Lin, C. Y., Bernard, A., Wang, J. Y., Socolar, J. E., Iversen, E. S., Hartemink, A. J., and Haase, S. B. Global control of cell-cycle transcription by coupled CDK and network oscillators. *Nature 453* (2008), 944–947.

[311] Ortiz-Gutiérrez, E., García-Cruz, K., Azpeitia, E., Castillo, A., de la Paz Sánchez, M., and Álvarez-Buylla, E. R. A dynamic gene regulatory network model that recovers the cyclic behavior of *Arabidopsis thaliana* cell cycle. *PLOS Computational Biology 11*, 9 (2015), e1004486.

[312] Osorio, F., Soria-Valles, C., Santiago-Fernández, O., Freije, J., and López-Otín, C. NF-κB signaling as a driver of ageing. In *International Review of Cell and Molecular Biology*, vol. 326. Elsevier, 2016, pp. 133–174.

[313] Ougolkov, A. V., Fernandez-Zapico, M. E., Bilim, V. N., Smyrk, T. C., Chari, S. T., and Billadeau, D. D. Aberrant nuclear accumulation of glycogen synthase kinase-3β in human pancreatic cancer: Association with kinase activity and tumor dedifferentiation. *Clinical Cancer Research 12*, 17 (2006), 5074–5081.

[314] Pai, R., Soreghan, B., Szabo, I. L., Pavelka, M., Baatar, D., and Tarnawski, A. S. Prostaglandin E2 transactivates EGF receptor: A novel mechanism for promoting colon cancer growth and gastrointestinal hypertrophy. *Nature Medicine 8* (2002), 289–293.

[315] Partridge, L. The new biology of ageing. *Philosophical Transactions of the Royal Society B: Biological Sciences 365*, 1537 (2010), 147–154.

[316] Pei, H., Li, L., Fridley, B. L., Jenkins, G. D., Kalari, K. R., Lingle, W., Petersen, G., Lou, Z., and Wang, L. FKBP51 affects cancer cell response to

chemotherapy by negatively regulating Akt. *Cancer Cell 16*, 3 (2009), 259–266.
[317] Peinado, H., Ballestar, E., Esteller, M., and Cano, A. Snail mediates E-cadherin repression by the recruitment of the Sin3A/Histone deacetylase 1 (HDAC1)/HDAC2 complex. *Molecular and Cellular Biology 24*, 1 (2004), 306–319.
[318] Peng, X.-c., Gong, F.-m., Zhao, Y.-w., Zhou, L.-x., Xie, Y.-w., Liao, H.-l., Lin, H.-j., Li, Z.-y., Tang, M.-h., and Tong, A.-p. Comparative proteomic approach identifies PKM2 and cofilin-1 as potential diagnostic, prognostic and therapeutic targets for pulmonary adenocarcinoma. *PLOS ONE 6*, 11 (2011), e27309.
[319] Perez-Roger, I., Kim, S.-H., Griffiths, B., Sewing, A., and Land, H. Cyclins D1 and D2 mediate Myc-induced proliferation via sequestration of p27Kip1 and p21Cip1. *The EMBO Journal 18*, 19 (1999), 5310–5320.
[320] Perona, R., Montaner, S., Saniger, L., Sanchez-Perez, I., Bravo, R., and Lacal, J. C. Activation of the nuclear factor-κB by Rho, CDC42, and Rac-1 proteins. *Genes & Development 11*, 4 (1997), 463–475.
[321] Pettee, K. M., Dvorak, K. M., Nestor-Kalinoski, A. L., and Eisenmann, K. M. An mDia2/ROCK signaling axis regulates invasive regress from epithelial ovarian cancer spheroids. *PLOS ONE 9*, 2 (2014), e90371.
[322] Pollard, T. D. Regulation of actin filament assembly by Arp2/3 complex and formins. *Annual Review Biophysics and Biomolecular Structure 36* (2007), 451–477.
[323] Posadas, I., Pérez-Martínez, F. C., Guerra, J., Sánchez-Verdú, P., and Ceña, V. Cofilin activation mediates Bax translocation to mitochondria during excitotoxic neuronal death. *Journal of Neurochemistry 120*, 4 (2012), 515–527.
[324] R Development Core Team. *R: A Language and Environment for Statistical Computing*. R Foundation for Statistical Computing, Vienna, Austria, 2008. ISBN 3-900051-07-0.
[325] Radu, M., Semenova, G., Kosoff, R., and Chernoff, J. PAK signalling during the development and progression of cancer. *Nature Reviews Cancer 14*, 1 (2014), 13–25.
[326] Rao, T. P., and Kühl, M. An updated overview on Wnt signaling pathways: a prelude for more. *Circulation Research 106*, 12 (2010), 1798–1806.
[327] Rau, C.-S., Yang, J. C.-S., Chen, Y.-C., Wu, C.-J., Lu, T.-H., Tzeng, S.-L., Wu, Y.-C., and Hsieh, C.-H. Lipopolysaccharide-induced microRNA-146a targets CARD10 and regulates angiogenesis in human umbilical vein endothelial cells. *Toxicological Sciences 140*, 2 (2014), 315–326.
[328] Rauhala, H. E., Teppo, S., Niemelaä, S., and Kallioniemi, A. Silencing of the ARP2/3 complex disturbs pancreatic cancer cell migration. *Anticancer Research 33*, 1 (2013), 45–52.
[329] Reif, K., Nobes, C. D., Thomas, G., Hall, A., and Cantrell, D. A. Phosphatidylinositol 3-kinase signals activate a selective subset of Rac/Rho-dependent effector pathways. *Current Biology 6*, 11 (1996), P1445–1455.
[330] Reya, T., and Clevers, H. Wnt signalling in stem cells and cancer. *Nature 434*, 7035 (2005), 843–850.
[331] Richardson, A., Liu, F., Adamo, M. L., Van Remmen, H., and Nelson, J. F. The role of insulin and insulin-like growth factor-I in mammalian ageing. *Best Practice & Research Clinical Endocrinology & Metabolism 18*, 3 (2004), 393–406.
[332] Ríos, O., Frias, S., Rodríguez, A., Kofman, S., Merchant, H., Torres, L., and Mendoza, L. A Boolean network model of human gonadal sex determination. *Theoretical Biology and Medical Modelling 12*, 26 (2015).
[333] Robin, X., Turck, N., Hainard, A., Tiberti, N., Lisacek, F., Sanchez, J.-C., and Müller, M. pROC: an open-source package for R and S+ to analyze and compare ROC curves. *BMC bioinformatics 12*, 77 (2011).
[334] Robine, J.-M., and Allard, M. The oldest human. *Science 279*, 5358 (1998), 1831.
[335] Rodrik-Outmezguine, V. S., Chandarlapaty, S., Pagano, N. C., Poulikakos, P. I., Scaltriti, M., Moskatel, E., Baselga, J., Guichard, S., and Rosen, N. mTOR Kinase inhibition causes feedback-dependent biphasic regulation of AKT signaling. *Cancer Discovery 1*, 3 (2011), 248–259.
[336] Rommel, C., Bodine, S. C., Clarke, B. A., Rossman, R., Nunez, L., Stitt, T. N., Yancopoulos, G. D., and Glass, D. J. Mediation of IGF-1-induced skeletal myotube hypertrophy by PI(3)K/AKT/mTOR and PI(3)K/Akt/GSK3 pahtways. *Nature Cell Biology 3*, 11 (2001), 1009–1013.
[337] Rosso, S. B., Sussman, D., Wynshaw-Boris, A., and Salinas, P. C. Wnt signaling through Dishevelled, Rac and JNK regulates dendritic development. *Nature Neuroscience 8*, 1 (2005), 34–42.
[338] Roy, M., Li, Z., and Sacks, D. B. IQGAP1 is a scaffold for mitogen-activated protein kinase signaling. *Molecular and Cellular Biology 25*, 18 (2005), 7940–7952.
[339] Rubinfeld, H., and Seger, R. The ERK cascade: a prototype of MAPK signaling. *Molecular Biotechnology 31*, 2 (2005), 151–174.
[340] Rubinsztein, D. C., Mariño, G., and Kroemer, G. Autophagy and aging. *Cell 146*, 5 (2011), P682–695.
[341] Rubio-Escudero, C., Harari, O., Cordón, O., and Zwir, I. Modeling genetic networks: Comparison of static and dynamic models. In *Evolutionary Computation, Machine Learning and Data Mining in Bioinformatics* (2007), E. Marchiori, J. H. Moore, and J. C. Rajapakse, Eds., vol. LNCS 4447 of *5th European Conference, EvoBIO 2007*, Springer, pp. 79–89.
[342] Rychahou, P. G., Kang, J., Gulhati, P., Doan, H. Q., Chen, L. A., Xiao, S.-Y., Chung, D. H., and Evers, B. M. Akt2 overexpression plays a critical role in the establishment of colorectal cancer metastasis. *Proceedings of the National Academy of Sciences 105*, 51 (2008), 20315–20320.
[343] Saadatpour, A., and Albert, R. Boolean modeling of biological regulatory networks: A methodology tutorial. *Methods 62*, 1 (2013), 3–12.
[344] Saadatpour, A., and Albert, R. A comparative study of qualitative and quantitative dynamic models of biological regulatory networks. *EPJ Nonlinear Biomedical Physics 4*, 5 (2016).
[345] Saadatpour, A., Albert, R., and Reluga, T. C. A reduction method for Boolean network models proven to conserve attractors. *SIAM Journal on Applied Dynamical Systems 12*, 4 (2013), 1997–2011.
[346] Saadatpour, A., Wang, R.-S., Liao, A., Liu, X., Loughran, T. P., Albert, I., and Albert, R. Dynamical and structural analysis of a T cell survival network identifies novel candidate therapeutic targets for large granular lymphocyte leukemia. *PLOS Computational Biology 7*, 11 (2011), e1002267.
[347] Saci, A., Cantley, L. C., and Carpenter, C. L. Rac1 regulates the activity of mTORC1 and mTORC2 and controls cellular size. *Molecular Cell 42*, 1 (2011), 50–61.
[348] Sahin, Ö., Fröhlich, H., Löbke, C., Korf, U., Burmester, S., Majety, M., Mattern, J., Schupp, I., Chaouiya, C., Thieffry, D., Poustka, A., Wiemann, S., Beissbarth, T., and Arlt, D. Modeling ERBB receptor-regulated G1/S transition to find novel targets for *de novo* trastuzumab resistance. *BMC Systems Biology 3*, 1 (2009).
[349] Sahu, R. P., and Srivastava, S. K. The role of STAT-3 in the induction of apoptosis in pancreatic cancercells by benzyl isothiocyanate. *Journal of the National Cancer Institute 101*, 3 (2009), 176–193.
[350] Salminen, A., and Kaarniranta, K. NF-κB signaling in the aging process. *Journal of Clinical Immunology 29*, 4 (2009), 397–405.
[351] Salminen, A., and Kaarniranta, K. AMP-activated protein kinase (AMPK) controls the aging process via an integrated signaling network. *Ageing Research Reviews 11*, 2 (2012), 230–241.
[352] Samaga, R., and Klamt, S. Modeling approaches for qualitative and semi-quantitative analysis of cellular signaling networks. *Cell Communication and Signaling 11*, 43 (2013).
[353] Samm, N., Werner, K., Rückert, F., Saeger, H. D., Grützmann, R., and Pilarsky, C. The role of apoptosis in the pathology of pancreatic cancer. *Cancers 3*, 1 (2011), 1–16.
[354] Sankar, M., Osmont, K. S., Rolcik, J., Gujas, B., Tarkowska, D., Strnad, M., Xenarios, I., and Hardtke, C. S. A qualitative continuous model of cellular auxin and brassinosteroid signaling and their crosstalk. *Bioinformatics 27*, 10 (2011), 1404–1412.
[355] Satoh, M., Takano, S., Sogawa, K., Noda, K., Yoshitomi, H., Ishibashi, M., Mogushi, K., Takizawa, H., Otsuka, M., Shimizu, H., Miyazaki, M., and Nomura, F. Immune-complex level of cofilin-1 in sera is associated with cancer progression and poor prognosis in pancreatic cancer. *Cancer Science 108*, 4 (2017), 795–803.
[356] Saxena, M., Dykes, S. S., Malyarchuk, S., Wang, A. E., Cardelli, J. A., and Pruitt, K. The sirtuins promote Dishevelled-1 scaffolding of TIAM1, Rac activation and cell migration. *Oncogene 34*, 2 (2015), 188–198.
[357] Scaffidi, C., Fulda, S., Srinivasan, A., Friesen, C., Li, F., Tomaselli, K. J., Debatin, K.-M., Krammer, P. H., and Peter, M. E. Two CD95 (APO-1/Fas) signaling pathways. *The EMBO Journal 17*, 6 (1998), 1675–1687.
[358] Scarpa, A., Capelli, P., Mukai, K., Zamboni, G., Oda, T., Iacono, C., and Hirohashi, S. Pancreatic adenocarcinomas frequently show p53 gene mutations. *American Journal of Pathology 142*, 5 (1993), 1534–1543.
[359] Schaible, R., Scheuerlein, A., Dańko, M. J., Gampe, G., and Martínez, D. E. Constant mortality and fertility over age in hydra. *Proceedings of the National Academy of Sciences of the United States of America 112*, 51 (2015), 15701–15706.
[360] Schlieman, M., Fahy, B., Ramsamooj, R., Beckett, L., and Bold, R. Incidence, mechanism and prognostic value of activated AKT in pancreas cancer. *British Journal of Cancer 89*, 11 (2003), 2110–2115.

[361] Schlupf, J., and Steinbeisser, H. IGF antagonizes the Wnt/β-Catenin pathway and promotes differentiation of extra-embryonic endoderm. *Differentiation 87*, 5 (2014), 209–219.

[362] Scholz, A., Heinze, S., Detjen, K. M., Peters, M., Welzel, M., Hauff, P., Schirner, M., Wiedenmann, B., and Rosewicz, S. Activated signal transducer and activator of transcription 3 (STAT3) supports the malignant phenotype of human pancreatic cancer. *Gastroenterology 125*, 3 (2003), 891–905.

[363] Schulte, G., Schambony, A., and Bryja, V. β-arrestins–scaffolds and signalling elements essential for WNT/Frizzled signalling pathways? *British Journal of Pharmacology 159*, 5 (2010), 1051–1058.

[364] Schwab, J., Burkovski, A., Siegle, L., Müssel, C., and Kestler, H. A. ViSiBooL—visualization and simulation of Boolean networks with temporal constraints. *Bioinformatics 33*, 4 (2016), 601–604.

[365] Schwab, J., Siegle, L., Kühlwein, S., Kühl, M., and Kestler, H. Stability of signaling pathways during aging—a Boolean network approach. *Biology 6*, 4 (2017), 46.

[366] Schwab, J. D., and Kestler, H. A. Automatic screening for perturbations in Boolean networks. *Frontiers in Physiology 9*, 431 (2018).

[367] Schwab, J. D., Kühlwein, S. D., Ikonomi, N., Kühl, M., and Kestler, H. A. Concepts in Boolean network modeling: What do they all mean? *Computational and Structural Biotechnology 18* (2020), 571–582.

[368] Schwitalla, S., Fingerle, A. A., Cammareri, P., Nebelsiek, T., Göktuna, S. I., Ziegler, P. K., Canli, O., Heijmans, J., Huels, D. J., Moreaux, G., Rupec, R. A., Gerhard, M., Schmid, R., Barker, N., Clevers, H., Lang, R., Neumann, J., Kirchner, T., Taketo, M. M., van den Brink, G. R., Jansom, O. J., Arkan, M. C., and Greten, F. R. Intestinal tumorigenesis initiated by dedifferentiation and acquisition of stem-cell-like properties. *Cell 152*, 1-2 (2013), 25–38.

[369] Selvaraj, N., Budka, J. A., Ferris, M. W., Jerde, T. J., and Hollenhorst, P. C. Prostate cancer ETS rearrangements switch a cell migration gene expression program from RAS/ERK to PI3K/AKT regulation. *Molecular Cancer 13*, 61 (2014).

[370] Semenova, G., and Chernoff, J. Targeting PAK1. *Biochemical Society Transactions 45*, 1 (2017), 79–88.

[371] Serrano, M., and Blasco, M. A. Cancer and ageing: convergent and divergent mechanisms. *Nature Reviews Molecular Cell Biology 8*, 9 (2007), 715–722.

[372] Seufferlein, T., Bachet, J., Van Cutsem, E., Rougier, P., and Group, E. G. W. Pancreatic adenocarcinoma: ESMO–ESDO clinical practice guidelines for diagnosis, treatment and follow-up. *Annals of Oncology 23*, suppl_7 (2012), vii33–vii40.

[373] Shah, A. N., Summy, J. M., Zhang, J., Park, S. I., Parikh, N. U., and Gallick, G. E. Development and characterization of gemcitabine-resistant pancreatic tumor cells. *Annals of Surgical Oncology 14*, 12 (2007), 3629–3637.

[374] Shakoori, A., Ougolkov, A., Yu, Z. W., Zhang, B., Modarressi, M. H., Billadeau, D. D., Mai, M., Takahashi, Y., and Minamoto, T. Deregulated GSK3β activity in colorectal cancer: Its association with tumor cell survival and proliferation. *Biochemical and Biophysical Research Communications 334*, 4 (2005), 1365–1373.

[375] Shanks, N., Greek, R., and Greek, J. Are animal models predictive for humans? *Philosophy, Ethics, and Humanities in Medicine 4*, 2 (2009).

[376] Shao, J., Jung, C., Liu, C., and Sheng, H. Prostaglandin E2 stimulates the β-catenin/T Cell factor-dependent transcription in colon cancer. *Journal of Biological Chemistry 280*, 28 (2005), 26565–26572.

[377] Shen, H.-M., and Tergaonkar, V. NFκB signaling in carcinogenesis and as a potential molecular target for cancer therapy. *Apoptosis 14*, 4 (2009), 348–363.

[378] Shi, Y. Mechanisms of caspase activation and inhibition during apoptosis. *Molecular Cell 9*, 3 (2002), 459–470.

[379] Shimizu, T., Kagawa, T., Inoue, T., Nonaka, A., Takada, S., Aburatani, H., and Taga, T. Stabilized β-catenin functions through TCF/LEF proteins and the Notch/RBP-Jκ complex to promote proliferation and suppress differentiation of neural precursor cells. *Molecular and Cellular Biology 28*, 24 (2008), 7427–7441.

[380] Shimobayashi, M., and Hall, M. N. Making new contacts: the mTOR network in metabolism and signalling crosstalk. *Nature Reviews Molecular Cell Biology 15*, 3 (2014), 155–162.

[381] Shin, S., Wolgamott, L., Yu, Y., Blenis, J., and Yoon, S.-O. Glycogen synthase kinase (GSK)-3 promotes p70 ribosomal protein S6 kinase (p70S6K) activity and cell proliferation. *Proceedings of the National Academy of Sciences 108*, 47 (2011), E1204–1213.

[382] Shishkin, S., Eremina, L., Pashintseva, N., Kovalev, L., and Kovaleva, M. Cofilin-1 and other ADF/Cofilin superfamily members in human malignant cells. *International Journal of Molecular Sciences 18*, 10 (2017).

[383] Shmulevich, I., Dougherty, E. R., Kim, S., and Zhang, W. Probabilistic boolean networks: a rule-based uncertainty model for gene regulatory networks. *Bioinformatics 18*, 2 (2002), 261–274.

[384] Shravah, J., Wang, B., Pavlovic, M., Kumar, U., Chen, D. D., Luo, H., and Ansley, D. M. Propofol mediates signal transducer and activator of transcription 3 activation and crosstalk with phosphoinositide 3-kinase/AKT. *JAK-STAT 3*, 2 (2014), e29554.

[385] Siegel, R. L., Miller, K. D., and Jemal, A. Cancer statistics, 2018. *CA: A Cancer Journal for Clinicians 68*, 1 (2018), 7–30.

[386] Siegle, L. A Boolean network of the IGF and Wnt signalling in ageing. Bachelor thesis, Medical Faculty, Ulm University, 2014.

[387] Siegle, L., Schwab, J. D., Kühlwein, S. D., Lausser, L., Tümpel, S., Pfister, A. S., Kühl, M., and Kestler, H. A. A Boolean network of the crosstalk between IGF and Wnt signaling in aging satellite cells. *PLOS ONE 13*, 3 (2018), e0195126.

[388] Singh, R. P., Dhanalakshmi, S., Tyagi, A. K., Chan, D. C. F., Agarwal, C., and Agarwal, R. Dietary feeding of silibinin inhibits advance human prostate carcinoma growth in athymic nude mice and increases plasma insulin-like growth factor-binding protein-3 levels. *Cancer Research 62*, 11 (2002), 3063–3069.

[389] Singh, R. P., Mallikarjuna, G. U., Sharma, G., Dhanalakshmi, S., Tyagi, A. K., Chan, D. C. F., Agarwal, C., and Agarwal, R. Oral silibinin inhibits lung tumor growth in athymic nude mice and forms a novel chemocombination with doxorubicin targeting nuclear factor κB-mediated inducible chemoresistance. *Clinical Cancer Research 10*, 24 (2004), 8641–8647.

[390] Sit, S.-T., and Manser, E. Rho GTPases and their role in organizing the actin cytoskeleton. *Journal of Cell Science 124*, 5 (2011), 679–683.

[391] Smith, G. R., and Shanley, D. P. Modelling the response of FOXO transcription factors to multiple post-translational modifications made by ageing-related signalling pathways. *PLOS ONE 5*, 6 (2010), e11092.

[392] Snel, B., Lehmann, G., Bork, P., and Huynen, M. A. STRING: a web-server to retrieve and display the repeatedly occurring neighbourhood of a gene. *Nucleic Acids Research 28*, 18 (2000), 3442–3444.

[393] So, J. Y., Smolarek, A. K., Salerno, D. M., Maehr, H., Uskokovic, M., Liu, F., and Suh, N. Targeting CD44-STAT3 signaling by Gemini vitamin D analog leads to inhibition of invasion in basal-like breast cancer. *PLOS ONE 8*, 1 (2013), e54020.

[394] Sonawane, A. R., Platig, J., Fagny, M., Chen, C.-Y., Paulson, J. N., Lopes-Ramos, C. M., DeMeo, D. L., Quackenbush, J., Glass, K., and Kuijjer, M. L. Understanding tissue-specific gene regulation. *Cell Reports 21*, 4 (2017), 1077–1088.

[395] Song, M., Bode, A. M., Dong, Z., and Lee, M.-H. AKT as a therapeutic target for cancer. *Cancer Research 79*, 6 (2019), 1019–1031.

[396] Song, Q., Sun, X., Guo, H., and Yu, Q. Concomitant inhibition of receptor tyrosine kinases and downstream AKT synergistically inhibited growth of KRAS/BRAF mutant colorectal cancer cells. *Oncotarget 8*, 3 (2017), 5003–5015.

[397] Soosairajah, J., Maiti, S., Sarmiere, P., Moussi, N., Sarcevic, B., Sampath, R., Bamburg, J. R., and Bernard, O. Interplay between components of a novel LIM kinase–slingshot phosphatase complex regulates cofilin. *The EMBO Journal 24*, 3 (2005), 473–486.

[398] Spalding, A. C., Watson, R., Davis, M. E., Kim, A. C., Lawrence, T. S., and Ben-Josef, E. Inhibition of protein kinase Cβ by enzastaurin enhances radiation cytotoxicity in pancreatic cancer. *Clinical Cancer Research 13*, 22 Pt 1 (2007), 6827–6833.

[399] Spratley, S. J., Bastea, L. I., Döppler, H., Mizuno, K., and Storz, P. Protein kinase D regulates cofilin activity through p21-activated kinase 4. *Journal of Biological Chemistry 286*, 39 (2011), 34254–34261.

[400] Sridharan, S., Layek, R., Datta, A., and Venkatraj, J. Boolean modeling and fault diagnosis in oxidative stress response. *BMC Genomics 13*, S4 (2012).

[401] St. Laurent, G., Shtokalo, D., Tackette, M. R., Yang, Z., Vyatkin, Y., Milos, P. M., Seilheimer, B., McCaffrey, T. A., and Kapranov, P. On the importance of small changes in RNA expression. *Methods 63*, 1 (2013), 18–24.

[402] Stamos, J. L., and Weis, W. I. The β-catenin destruction complex. *Cold Spring Harbor Perspectives in Biology 5*, 1 (2013), a007898.

[403] Stark, C., Breitkreutz, B.-J., Reguly, T., Boucher, L., Breitkreutz, A., and Tyers, M. BioGRID: a general repository for interaction datasets. *Nucleic Acids Research 34*, Database issue (2006), D535–D539.

[404] Steed, E., Elbediwy, A., Vacca, B., Dupasquier, S., Hemkemeyer, S. A., Suddason, T., Costa, A. C., Beaudry, J.-B., Zihni, C., Gallagher, E., Pierreux, C. E., Balda, M. S., and Karl, M. MarvelD3 couples tight junctions to the MEKK1–JNK pathway to regulate cell behavior and survival. *Journal of Cell Biology 204*, 5 (2014), 821–838.

[405] Stemmer, V. d., De Craene, B., Berx, G., and Behrens, J. Snail promotes Wnt target gene expression and interacts with β-catenin. *Oncogene 27* (2008), 5075–5080.

[406] Subramaniam, V., Vincent, I. R., and Jothy, S. Upregulation and dephosphorylation of cofilin: modulation by CD44 variant isoform in human colon cancer

cells. *Experimental and Molecular Pathology 79*, 3 (2005), 187–193.
[407] Sugahara, K. N., Hirata, T., Hayasaka, H., Stern, R., Murai, T., and Miyasaka, M. Tumor cells enhance their own CD44 cleavage and motility by generating hyaluronan fragments. *The Journal of Biological Chemistry 281*, 9 (2006), 5861–5868.
[408] Sullivan, R. J., Infante, J. R., Janku, F., Wong, D. J. L., Sosman, J. A., Keedy, V., Patel, M. R., Shapiro, G. I., Mier, J. W., Tolcher, A. W., Wang-Gillam, A., Sznol, M., Flaherty, K., Buchbinder, E., Carvajal, R. D., Varghese, A. M., Lacouture, M. E., Ribas, A., Patel, S. P., DeCrescenzo, G. A., Emery, C. M., Groover, A. L., Saha, S., Varterasian, M., Welsch, D. J., Hyman, D. M., and Li, B. T. First-in-class ERK1/2 inhibitor Ulixertinib (BVD-523) in patients with MAPK mutant advanced solid tumors: results of a phase I dose-escalation and expansion study. *Cancer Discovery 8*, 2 (2018), 184–195.
[409] Sun, M., Cheng, X., and Socolar, J. E. Regulatory logic and pattern formation in the early sea urchin embryo. *Journal of Theoretical Biology 363* (2014), 80–92.
[410] Sun, T., Rodriguez, M., and Kim, L. Glycogen synthase kinase 3 in the world of cell migration. *Development, Growth & Differentiation 51*, 9 (2009), 735–742.
[411] Szklarczyk, D., Gable, A. L., Lyon, D., Junge, A., Wyder, S., Huerta-Cepas, J., Simonovic, M., Doncheva, N. T., Morris, J. H., Bork, P., Jensen, L. J., and von Mering, C. STRING v11: protein–protein association networks with increased coverage, supporting functional discovery in genome-wide experimental datasets. *Nucleic Acids Research 47*, D1 (2019), D607–D613.
[412] Taira, N., Mimoto, R., Kurata, M., Yamaguchi, T., Kitagawa, M., Miki, Y., and Yoshida, K. DYRK2 priming phosphorylation of c-Jun and c-Myc modulates cell cycle progression in human cancer cells. *The Journal of Clinical Investigation 122*, 3 (2012), 859–872.
[413] Tan, J., Geng, L., Yazlovitskaya, E. M., and Hallahan, D. E. Protein kinase B/Akt-dependent phosphorylation of glycogen synthase kinase-3β in irradiated vascular endothelium. *Cancer Research 66*, 4 (2006), 2320–2327.
[414] Tang, Q., Ji, Q., Tang, Y., Chen, T., Pan, G., Hu, S., Bao, Y., Peng, W., and Yin, P. Mitochondrial translocation of cofilin-1 promotes apoptosis of gastric cancer BGC-823 cells induced by ursolic acid. *Tumor Biology 35*, 3 (2014), 2451–2459.
[415] Tang, Q.-F., Sun, J., Yu, H., Shi, X.-J., Lv, R., Wei, H.-C., and Yin, P.-H. The Zuo Jin Wan formula induces mitochondrial apoptosis of cisplatin-resistant gastric cancer cells via cofilin-1. *Evidence-Based Complementary and Alternative Medicine 2016*, 8203789 (2016).
[416] Tania, N., Condeelis, J., and Delstein-Keshet, L. Modeling the synergy of Cofilin and Arp2/3 in lamellipodial protrusive activity. *Biophysical Journal 105*, 9 (2013), 1946–1955.
[417] Tao, S., Tang, D., Morita, Y., Sperka, T., Omrani, O., Lechel, A., Sakk, V., Kraus, J., Kestler, H. A., Kühl, M., and Rudolph, K. L. Wnt activity and basal niche position sensitize intestinal stem and progenitor cells to DNA damage. *The EMBO Journal 34*, 5 (2015), 624–640.
[418] Terai, K., and Matsuda, M. Ras binding opens c-Raf to expose the docking site for mitogen-activated protein kinase kinase. *EMBO Reports 6*, 3 (2005), 251–255.
[419] Tetsu, O., and McCormick, F. β-Catenin regulates expression of cyclin D1 in colon carcinoma cells. *Nature 398*, 6726 (1999), 422–426.
[420] Thakar, J., Pathak, A. K., Murphy, L., Albert, R., and Cattadori, I. M. Network model of immune responses reveals key effectors to single and co-infection dynamics by a respiratory bacterium and a gastrointestinal helminth. *PLOS Computational Biology 8*, 1 (2012), e1002345.
[421] Thomas, R., and Kaufman, M. Multistationarity, the basis of cell differentiation and memory. II. Logical analysis of regulatory networks in terms of feedback circuits. *Chaos: An Interdisciplinary Journal of Nonlinear Science 11*, 1 (2001), 180–195.
[422] Tian, H., Biehs, B., Chiu, C., Siebel, C. W., Wu, Y., Costa, M., de Sauvage, F. J., and Klein, O. D. Opposing activities of Notch and Wnt signaling regulate intestinal stem cells and gut homeostasis. *Cell Reports 11*, 1 (2005), 33–42.
[423] Tilstra, J. S., Clauson, C. L., Niedernhofer, L. J., and Robbins, P. D. NF-κB in aging and disease. *Aging and Disease 2*, 6 (2011), 449–465.
[424] Timpson, P., McGhee, E. J., Morton, J. P., von Kriegsheim, A., Schwarz, J. P., Karim, S. A., Doyle, B., Quinn, J. A., Carragher, N. O., Edward, M., Olson, M. F., Frame, M. C., Brunton, V. G., Sansom, O. J., and Anderson, K. I. Spatial regulation of RhoA activity during pancreatic cancer cell invasion driven by mutant p53. *Cancer Research 71*, 3 (2011), 747–757.
[425] Todd, R. G., and Helikar, T. Ergodic sets as cell phenotype of budding yeast cell cycle. *PLOS ONE 7*, 10 (2012), e45780.
[426] Tomczyk, S., Fischer, K., Austad, S., and Galliot, B. Hydra, a powerful model for aging studies. *Invertebrate Reproduction & Development 59*, S1 (2015), 11–16.
[427] Torii, S., Yamamoto, T., Tsuchiya, Y., and Nishida, E. ERK MAP kinase in G1 cell cycle progression and cancer. *Cancer Science 97*, 8 (2006), 697–702.
[428] Toyonaga, T., Nakano, K., Nagano, M., Zhao, G., Yamaguchi, K., Kuroki, S., Eguchi, T., Chijiiwa, K., Tsuneyoshi, M., and Tanaka, M. Blockade of constitutively activated Janus kinase/signal transducer and activator of transcription-3 pathway inhibits growth of human pancreatic cancer. *Cancer Letters 201*, 1 (2003), 107–116.
[429] Tsai, C.-H., Chiu, S.-J., Liu, C.-C., Sheu, T.-J., Hsieh, C.-H., Keng, P. C., and Lee, Y.-J. Regulated expression of cofilin and the consequent regulation of p27(kip1) are essential for G(1) phase progression. *Cell Cycle 8*, 15 (2009), 2365–2374.
[430] van Amerongen, R. Alternative Wnt pathways and receptors. *Cold Spring Harbor Perspectives in Biology 4*, 10 (2012), a007914.
[431] Veliz-Cuba, A., and Stigler, B. Boolean models can explain bistability in the *lac* operon. *Journal of Computational Biology 18*, 6 (2011), 783–794.
[432] Villagrasa, P., Díaz, V., Viñas-Castells, R., Peiró, S., Del Valle-Pérez, B., Dave, N., Rodríguez-Asiain, A., Casal, J. I., Lizcano, J., Duñach, M., and García de Herreros, A. Akt2 interacts with Snail1 in the E-cadherin promoter. *Oncogene 31* (2012), 4022–4033.
[433] Volpi, E., Nazemi, R., and Fujita, S. Muscle tissue changes with aging. *Current Opinion in Clinical Nutrition and Metabolic Care 7*, 4 (2004), 405–410.
[434] von Burstin, J., Eser, S., Paul, M. C., Seidler, B., Brandl, M., Messer, M., von Werder, A., Schmidt, A., Mages, J., Pagel, P., Schnieke, A., Schmid, R. M., Schneider, G., and Saur, D. E-Cadherin regulates metastasis of pancreatic cancer in vivo and is suppressed by a SNAIL/HDAC1/HDAC2 repressor complex. *Gastroenterology 137*, 1 (2009), 361–371.e5.
[435] von Maltzahn, J., Bentzinger, C. F., and Rudnicki, M. A. Wnt7a-Fzd7 signalling directly activates the Akt/mTOR anabolic growth pathway in skeletal muscle. *Nature Cell Biology 14*, 2 (2012), 186–191.
[436] Wander, S. A., Zhao, D., and Slingerland, J. M. p27: a barometer of signaling deregulation and potential predictor of response to targeted therapies. *Clinical Cancer Research 17*, 1 (2011), 12–18.
[437] Wang, D., and DuBois, R. N. The role of COX-2 in intestinal inflammation and colorectal cancer. *Oncogene 29*, 6 (2010), 781–778.
[438] Wang, F., Wu, D., Fu, H., He, F., Xu, C., Zhou, J., Li, D., Li, G., Xu, J., Wu, Q., Chen, J., Su, L., Wang, W., and Zhang, S. Cofilin 1 promotes bladder cancer and is regulated by TCF7L2. *Oncotarget 8*, 54 (2017), 92043–92054.
[439] Wang, H., Tao, L., Jin, F., Gu, H., Dai, X., Ni, T., Feng, J., Ding, Y., Xiao, W., Qian, Y., and Liu, Y. Cofilin 1 induces the epithelial-mesenchymal transition of gastric cancer cells by promoting cytoskeletal rearrangement. *Oncotarget 8*, 24 (2017), 39131–39142.
[440] Wang, J., Nikhil, K., Viccaro, K., Chang, L., Jacobsen, M., Sandusky, G., and Shah, K. Aurora A-Twist1 axis promotes highly aggressive phenotypes in pancreatic carcinoma. *Journal of Cell Science 130*, 6 (2017), 1078–1093.
[441] Wang, L.-h., Xiang, J., Yan, M., Zhang, Y., Zhao, Y., Yue, C.-f., Xu, J., Zheng, F.-m., Chen, J.-n., Kang, Z., Chen, T.-s., Xing, D., and Liu, Q. The mitotic kinase aurora-A induces mammary cell migration and breast cancer metastasis by activating the Cofilin-F-actin pathway. *Cancer Research 70*, 22 (2010), 9118–9128.
[442] Wang, W., Eddy, R., and Condeelis, J. The cofilin pathway in breast cancer invasion and metastasis. *Nature Reviews Cancer 7*, 6 (2007), 429–440.
[443] Wang, W., Mouneimne, G., Sidani, M., Wyckoff, J., Chen, X., Makris, A., Goswami, S., Bresnick, A. R., and Condeelis, J. S. The activity status of cofilin is directly related to invasion, intravasation, and metastasis of mammary tumors. *The Journal of Cell Biology 173*, 3 (2006), 395–404.
[444] Wang, X., Thijssen, B., and Yu, H. Target essentiality and centrality characterize drug side effects. *PLOS Computational Biology 9*, 7 (2013), e1003119.
[445] Wang, Y., Kuramitsu, Y., Kitagawa, T., Baron, B., Yoshino, S., Maehara, S.-I., Maehara, Y., Oka, M., and Nakamura, K. Cofilin-phosphatase slingshot-1L (SSH1L) is over-expressed in pancreatic cancer (PC) and contributes to tumor cell migration. *Cancer Letters 360*, 2 (2015), 171–176.
[446] Wang, Y., Kuramitsu, Y., Ueno, T., Suzuki, N., Yoshino, S., Iizuka, N., Zhang, X., Oka, M., and Nakamura, K. Differential expression of up-regulated cofilin-1 and down-regulated cofilin-2 characteristic of pancreatic cancer tissues. *Oncology Reports 26*, 6 (2011), 1595–1599.
[447] Wang, Z., Wang, M., and Carr, B. I. Involvement of receptor tyrosine phosphatase DEP-1 mediated PI3K-cofilin signaling pathway in Sorafenib-induced cytoskeletal rearrangement in hepatoma cells. *Journal of Cellular Physiology 224*, 2 (2010), 559–565.
[448] Watanabe, S., Sato, K., Hasegawa, N., Kurihara, T., Matsutani, K., Sanada, K., Hamaoka, T., Fujita, S., and Iemitsu, M. Serum C1q as a novel biomarker of sarcopenia in older adults. *The FASEB Journal 29*, 3 (2015), 1003–1010.
[449] Watson, R. L., Spalding, A. C., Zielske, S. P., Morgan, M., Kim, A. C., Bommer, G. T., Eldar-Finkelman, H., Giordano, T., Feron, E. R., Hammer, G. D., Lawrence, T. S., and Ben-Josef, E. GSK3β and β-catenin modulate radiation cytotoxicity in pancreatic cancer. *Neoplasia 12*, 5 (2010), 357–365.
[450] Wee, P., and Wang, Z. Epidermal growth factor receptor cell proliferation signaling pathways. *Cancers 9*, 5 (2017), 52.
[451] Weinberg, R. A. The retinoblastoma protein and cell cycle control. *Cell 81*, 3 (1995), 323–330.
[452] Weinberg, R. A. *The biology of cancer*, vol. Second edition. Garland science, 2013.

[453] Welle, S., Brooks, A. I., Delehanty, J. M., Needler, N., and Thornton, C. A. Gene expression profile of aging in human muscle. *Physiological Genomics 14*, 2 (2003), 149–159.

[454] Werner, H. M., Mills, G. B., and Ram, P. T. Cancer systems biology: a peek into the future of patient care? *Nature Reviews Clinical Oncology 11*, 3 (2014), 167–176.

[455] Westermarck, J. Targeted therapies don't work for a reason; the neglected tumor suppressor phosphatase PP2A strikes back. *The FEBS Journal 285*, 22 (2018), 4139–4145.

[456] Westphal, R. S., Coffee, R. L., Marotta, A., Pelech, S. L., and Wadzinski, B. E. Identification of kinase-phosphatase signaling modules composed of p70 S6 kinase-protein phosphatase 2A (PP2A) and p21-activated kinase-PP2A. *Journal of Biological Chemistry 274*, 2 (1999), 687–692.

[457] Westphal, S., and Kalthoff, H. Apoptosis: Targets in pancreatic cancer. *Molecular Cancer 2*, 6 (2003).

[458] White, C. D., Brown, M. D., and Sacks, D. B. Iqgaps in cancer: a family of scaffold proteins underlying tumorigenesis. *FEBS Letters 583*, 12 (2009), 1817–1824.

[459] White, M. C., Holman, D. M., Boehm, J. E., Peipins, L. A., Grossman, M., and Henley, S. J. Age and cancer risk: A potentially modifiable relationship. *American Journal of Preventive Medicine 46*, 3 (2014), S7–S15.

[460] Wiegering, A., Pfann, C., Uthe, F. W., Otto, C., Rycak, L., Mäder, U., Gasser, M., Waaga-Gasser, A.-M., Eilers, M., and Germer, C.-T. CIP2A influences survival in colon cancer and is critical for maintaining Myc expression. *PLOS ONE 8*, 10 (2013), e75292.

[461] Wijnhoven, B., Dinjens, W., and Pignatelli, M. E-cadherin—catenin cell—cell adhesion complex and human cancer. *British Journal of Surgery 87*, 8 (2000), 992–1005.

[462] Wolkenhauer, O., Auffray, C., Jaster, R., Steinhoff, G., and Dammann, O. The road from systems biology to systems medicine. *Pediatric Research 73*, 4 (2013), 502–507.

[463] Wu, D., and Pan, W. GSK3: a multifaceted kinase in Wnt signaling. *Trends in Biochemical Sciences 35*, 3 (2010), 161–168.

[464] Wu, Q., Jiang, Y., Cui, S., Wang, Y., and Wu, X. The role of cofilin-l in vulvar squamous cell carcinoma: A marker of carcinogenesis, progression and targeted therapy. *Oncology Reports 35*, 5 (2016), 2743–2754.

[465] Wu, W. K., Wang, X. J., Cheng, A. S., Luo, M. X., Ng, S. S., To, K. F., Chan, F. K., Cho, C. H., Sung, J. J., and Yu, J. Dysregulation and crosstalk of cellular signaling pathways in colon carcinogenesis. *Critical Reviews in Oncology/Hematology 86*, 3 (2013), 251–277.

[466] Wu, Y., Deng, J., Rychahou, P. G., Qiu, S., Evers, B. M., and Zhou, B. P. Stabilization of Snail by NF-κB is required for inflammation-induced cell migration and invasion. *Cancer Cell 15*, 5 (2009), 416–428.

[467] Wu, Y.-d., and Zhou, B. TNF-α/NF-κB/Snail pathway in cancer cell migration and invasion. *British Journal of Cancer 102*, 4 (2010), 639–644.

[468] Wu, Z.-Q., Brabletz, T., Fearon, E., Willis, A. L., Hu, C. Y., Li, X.-Y., and Weiss, S. J. Canonical Wnt suppressor, Axin2, promotes colon carcinoma oncogenic activity. *Proceedings of the National Academy of Sciences 109*, 28 (2012), 11312–11317.

[469] Wullschleger, S., Loewith, R., and Hall, M. N. TOR signaling in growth and metabolism. *Cell 124*, 3 (2006), 471–484.

[470] Wullschleger, S., Loewith, R., Oppliger, W., and Hall, M. N. Molecular organization of target of rapamycin complex 2. *Journal of Biological Chemistry 280*, 35 (2005), 30697–30704.

[471] Xiao, Y. A tutorial on analysis and simulation of boolean gene regulatory network models. *Current Genomics 10*, 7 (2009), 511–525.

[472] Xie, X., and Guan, K.-L. The ribosome and TORC2: collaborators for cell growth. *Cell 144*, 5 (2011), P640–642.

[473] Xiong, A., Yang, Z., Shen, Y., Zhou, J., and Shen, Q. Transcription factor STAT3 as a novel molecular target for cancer prevention. *Cancers 6*, 2 (2014), 926–957.

[474] Xu, Y., Lee, D.-K., Feng, Z., Xu, Y., Bu, W., Li, Y., Liao, L., and Xu, J. Breast tumor cell-specific knockout of Twist1 inhibits cancer cell plasticity, dissemination, and lung metastasis in mice. *Proceedings of the National Academy of Sciences 114*, 43 (2017), 11494–11499.

[475] Yamaguchi, H., and Condeelis, J. Regulation of the actin cytoskeleton in cancer cell migration and invasion. *Biochimica et Biophysica Acta (BBA)-Molecular Cell Research 1773*, 5 (2007), 642–652.

[476] Yan, Y., and Ouellette, M. M. Rac1 GTPase in pancreatic cancer. *Aging 7*, 9 (2015), 609–610.

[477] Yang, C.-C., and Wolf, D. A. Inflamed Snail speeds metastasis. *Cancer Cell 15*, 5 (2009), 355–357.

[478] Yang, H. W., Shin, M.-G., Lee, S., Kim, J.-R., Park, W. S., Cho, K.-H., Meyer, T., and Do Heo, W. Cooperative activation of PI3K by Ras and Rho family small GTPases. *Molecular Cell 47*, 2 (2012), 281–290.

[479] Yang, Z.-L., Miao, X., Xiong, L., Zou, Q., Yuan, Y., Li, J., Liang, L., Chen, M., and Chen, S. CFL1 and Arp3 are biomarkers for metastasis and poor prognosis of squamous cell/adenosquamous carcinomas and adenocarcinomas of gallbladder. *Cancer Investigation 31*, 2 (2013), 132–139.

[480] Yao, Q., An, Y., Hou, W., Cao, Y.-N., Yao, M.-F., Ma, N.-N., Hou, L., Zhang, H., Liu, H.-J., and Zhang, B. LRP6 promotes invasion and metastasis of colorectal cancer through cytoskeleton dynamics. *Oncotarget 8*, 65 (2017), 109632–109645.

[481] Yap, C. T., Simpson, T. I., Pratt, T., Price, D. J., and Maciver, S. K. The motility of glioblastoma tumour cells is modulated by intracellular cofilin expression in a concentration-dependent manner. *Cell Motility and the Cytoskeleton 60*, 3 (2005), 153–165.

[482] Ye, D. Z., and Field, J. PAK signaling in cancer. *Cellular Logistics 2*, 2 (2012), 105–116.

[483] Yin, F., Jiang, T., and Cadenas, E. Metabolic triad in brain aging: mitochondria, insulin/IGF-1 signalling and JNK signalling. *Biochemical Society Transactions 41*, 1 (2013), 101–105.

[484] Yin, H., Price, F., and Rudnicki, M. A. Satellite cells and the muscle stem cell niche. *Physiological Reviews 93*, 1 (2013), 23–67.

[485] Yochum, Z. A., Cades, J., Mazzacurati, L., Neumann, N. M., Khetarpal, S. K., Chatterjee, S., Wang, H., Attar, M. A., Huang, E. H.-B., Chatley, S. N., Nugent, K., Somasundaram, A., Engh, J. A., Ewald, A. J., Cho, Y.-J., Rudin, C. M., Tran, P. T., and Burns, T. F. A first-in-class TWIST1 inhibitor with activity in oncogene-driven lung cancer. *Molecular Cancer Research 15*, 12 (2017), 1764–1776.

[486] Yokoyama, N., and Malbon, C. C. Dishevelled-2 docks and activates Src in a Wnt-dependent manner. *Journal of Cell Science 122*, 24 (2009), 4439–4451.

[487] Yoon, M.-K., Mitrea, D. M., Ou, L., and Kriwacki, R. W. Cell cycle regulation by the intrinsically disordered proteins p21 and p27. *Biochemical Society Transactions 40*, 5 (2012), 981–988.

[488] Yousefi, M. R., and Dougherty, E. R. Intervention in gene regulatory networks with maximal phenotype alteration. *Bioinformatics 29*, 14 (2013), 1758–1767.

[489] Yu, H.-C., Hung, M.-H., Chen, Y.-L., Chu, P.-Y., Wang, C.-Y., Chao, T.-T., Liu, C.-Y., Shiau, C.-W., and Chen, K.-F. Erlotinib derivate inhibits hepatocellular carcinoma by targeting CIP2A to reactivate protein phosphatase 2A. *Cell Death & Disease 5* (2014), e1359.

[490] Yun, M.-S., Kim, S.-E., Jeon, S. H., Lee, J.-S., and Choi, K.-Y. Both ERK and Wnt/β-catenin pathways are involved in Wnt3a-induced proliferation. *Journal of Cell Science 118*, 2 (2005), 313–322.

[491] Zeller, E., Hammer, K., Kirschnick, M., and Braeuning, A. Mechanisms of RAS/β-catenin interactions. *Archives of Toxicology 87*, 4 (2013), 611–632.

[492] Zeng, G., Germinaro, M., Micsenyi, A., Monga, N. K., Bell, A., Sood, A., Malhotra, V., Sood, N., Midda, V., Monga, D. K., Kokkinakis, D. M., and Monga, S. P. S. Aberrant Wnt/β-catenin signaling in pancreatic adenocarcinoma. *Neoplasia 8*, 4 (2006), 279–289.

[493] Zhai, G. G., Malhotra, R., Delaney, M., Latham, D., Nestler, U., Zhang, M., Mukherjee, N., Song, Q., Robe, P., and Chakravarti, A. Radiation enhances the invasive potential of primary glioblastoma cells via activation of the Rho signaling pathway. *Journal of Neuro-Oncology 76*, 3 (2006), 227–237.

[494] Zhan, T., Rindtorff, N., and Boutros, M. Wnt signaling in cancer. *Oncogene 36*, 11 (2017), 1461–1473.

[495] Zhang, J., Gao, Z., Yin, J., Quon, M. J., and Ye, J. S6K directly phosphorylates IRS-1 on Ser-270 to promote insulin resistance in response to TNF-α signaling through IKK2. *Journal of Biological Chemistry 283*, 51 (2008), 35375–35382.

[496] Zhang, J., Zhang, L.-L., Shen, L., Xu, X.-M., and Yu, H.-G. Regulation of AKT gene expression by cisplatin. *Oncology Letters 5*, 3 (2013), 756–760.

[497] Zhang, L., Theodoropoulos, P. C., Eskiocak, U., Wang, W., Moon, Y.-A., Posner, B., Williams, N. S., Wright, W. E., Bum Kim, S., Nijhawan, D., De Brabander, J. K., and Shay, J. W. Selective targeting of mutant adenomatous polyposis coli (APC) in colorectal cancer. *Science Translational Medicine 8*, 361 (2016), 361ra140.

[498] Zhang, X., Tang, N., Hadden, T. J., and Rishi, A. K. Akt, FoxO and regulation of apoptosis. *Biochimica et Biophysica Acta (BBA)-Molecular Cell Research 1813*, 11 (2011), 1978–1986.

[499] Zhao, Z., Rahman, M. A., Chen, Z. G., and Shin, D. M. Multiple biological functions of Twist1 in various cancers. *Oncotarget 8*, 12 (2017), 20380–20393.

[500] Zheng, H.-C. The molecular mechanisms of chemoresistance in cancers. *Oncotarget 8*, 35 (2017), 59950–59964.

[501] Zhou, D., Müssel, C., Lausser, L., Hoffensitz, M., Kühl, M., and Kestler, H. A. Boolean networks for modeling and analysis of gene regulation. Ulmer Informatik-Berichte, Fakultät für Ingenieurwissenschaften und Informatik Universität Ulm, 2009.

[502] Zhou, H., and Huang, S. Role of mTOR signaling in tumor cell motility, invasion and metastasis. *Current Protein and Peptide Science 12*, 1 (2011), 30–42.

[503] Zhou, J., Ning, Z., Wang, B., Yun, E., Zhang, T., Pong, R., Fazli, L., Gleave, M., Zeng, J., Fan, J., Wang, X., L, L., Hsieh, J.-T., He, D., and K, W. DAB2IP loss

confers the resistance of prostate cancer to androgen deprivation therapy through activating STAT3 and inhibiting apoptosis. *Cell Death & Disease 6*, 10 (2015), e1955.

[504] Zhou, T., Wang, C.-H., Yan, H., Zhang, R., Zhao, J.-B., Qian, C.-F., Xiao, H., and Liu, H.-Y. Inhibition of the Rac1-WAVE2-Arp2/3 signaling pathway promotes radiosensitivity via downregulation of cofilin-1 in U251 human glioma cells. *Molecular Medicine Reports 13*, 5 (2016), 4414–4420.

[505] Zhu, G., Fan, Z., Ding, M., Zhang, H., Mu, L., Ding, Y., Zhang, Y., Jia, B., Chen, L., Chang, Z., and Wu, W. An EGFR/PI3K/AKT axis promotes accumulation of the Rac1-GEF Tiam1 that is critical in EGFR-driven tumorigenesis. *Oncogene 34* (2015), 5971–5082.

[506] Zhu, P., Martin, E., Mengwasser, J., Schlag, P., Janssen, K.-P., and Göttlicher, M. Induction of HDAC2 expression upon loss of APC in colorectal tumorigenesis. *Cancer Cell 5*, 5 (2004), 455–463.

[507] Zhu, X., Gersten, M., and Snyder, M. Getting connected: analysis and principles of biological networks. *Genes & Development 21* (2007), 1010–1024.

[508] Zhu, Y., Tian, Y., Du, J., Hu, Z., Yang, L., Liu, J., and Gu, L. Dvl2-dependent activation of Daam1 and RhoA regulates Wnt5a-induced breast cancer cell migration. *PLOS ONE 7*, 5 (2012), e37823.

[509] Zielinski, R., Przytycki, P. F., Zheng, J., Zhang, D., Przytycka, T. M., and Capala, J. The crosstalk between EGF, IGF, and Insulin cell signaling pathways - computational and experimental analysis. *BMC Systems Biology 3*, 88 (2009).

[510] Zinzalla, V., Stracka, D., Oppliger, W., and Hall, M. N. Activation of mTORC2 by association with the ribosome. *Cell 144*, 5 (2011), 757–768.

[511] Zou, H., Li, Y., Liu, X., and Wang, X. An APAF-1· cytochrome C multimeric complex is a functional apoptosome that activates procaspase-9. *Journal of Biological Chemistry 274*, 17 (1999), 11549–11556.

7

APPENDIX

Table 10: Identified dependencies in the young phenotype networks. If a protein is an input of another, there is a 1 in the column of the corresponding protein row. Otherwise it is labeled with 0. In total, there are 158 dependencies. The table was modified from Schwab, Siegle, Kühlwein et al. [365], licensed under CC BY 4.0, https://creativecommons.org/licenses/by/4.0/.

	TAB1	CHUK	CSNK2A2	ERC1	CARD10	IRAK1	LBP	LTA	LTBR	PLCG2	PRKCB	PRKCQ	PTGS2	BTK	TNF	TRAF1	TRAF3	TRAF5	TNFSF11	BCL10	CD14	CD40
TAB1	1	1	1	1	1	1	1	1	1	1	1	1	0	1	1	1	1	1	0	1	1	1
CHUK	0	1	1	1	1	1	1	0	1	1	1	1	0	0	1	1	1	1	0	1	0	1
CSNK2A2	0	0	0	0	0	0	0	0	0	0	0	0	0	0	1	1	0	0	0	0	0	0
ERC1	0	0	0	0	0	0	1	0	0	0	0	0	0	0	0	0	1	0	0	0	0	0
CARD10	0	0	0	0	0	0	0	0	0	0	0	0	0	0	0	0	0	1	0	1	0	0
IRAK1	0	0	1	1	0	0	0	0	0	0	1	0	0	0	0	0	0	0	0	0	0	0
LBP	0	0	0	0	0	0	0	0	0	1	0	0	0	0	0	0	0	0	0	0	0	0
LTA	1	1	1	1	1	1	1	1	1	1	1	1	0	1	1	1	1	1	0	1	1	1
LTBR	0	0	0	0	0	0	1	0	0	0	0	0	0	0	0	0	1	0	0	0	0	0
PLCG2	0	1	1	1	1	1	1	0	1	1	1	1	0	0	1	1	1	1	0	1	0	1
PRKCB	0	0	0	0	0	0	0	0	0	0	0	0	0	0	1	1	0	0	0	0	0	0
PRKCQ	0	0	0	0	1	0	0	0	0	0	0	0	0	0	0	0	0	0	0	0	0	0
PTGS2	0	0	0	0	0	0	0	0	0	0	0	1	0	0	0	0	0	0	0	0	0	0
BTK	1	1	1	1	1	1	1	1	1	1	1	1	0	1	1	1	1	1	0	1	1	1
TNF	0	0	0	0	0	0	0	0	1	0	0	0	0	0	0	0	0	0	0	0	0	0
TRAF1	0	0	0	0	0	0	0	0	0	0	0	0	0	0	0	0	0	1	0	1	0	0
TRAF3	0	0	0	0	0	0	0	0	0	1	0	0	0	0	0	0	0	0	0	0	0	0
TRAF5	0	1	0	0	0	0	0	0	0	0	0	0	0	0	0	0	0	0	0	0	0	0
TNFSF11	0	0	0	0	0	0	0	0	0	0	0	1	0	0	0	0	0	0	0	0	0	0
BCL10	1	1	1	1	1	1	1	1	1	1	1	1	0	1	1	1	1	1	0	1	1	1
CD14	1	1	1	1	1	1	1	1	1	1	1	1	0	1	1	1	1	1	0	1	1	1
CD40	1	0	0	0	0	0	0	1	0	0	0	0	0	1	0	0	0	0	0	0	1	0

Table 11: Identified dependencies in the aged phenotype networks. If a protein is an input of another, there is a 1 in the column of the corresponding protein row. Otherwise it is labeled with 0. In total there are 125 dependencies. The table was modified from Schwab, Siegle, Kühlwein et al. [365], licensed under CC BY 4.0, https://creativecommons.org/licenses/by/4.0/.

	TAB1	CHUK	CSNK2A2	ERC1	CARD10	IRAK1	LBP	LTA	LTBR	PLCG2	PRKCB	PRKCQ	PTGS2	BTK	TNF	TRAF1	TRAF3	TRAF5	TNFSF11	BCL10	CD14	CD40
TAB1	0	0	0	0	0	0	0	1	0	0	0	0	0	0	0	0	0	0	0	0	0	0
CHUK	0	1	0	1	0	0	0	1	1	0	0	0	1	0	1	1	1	0	1	1	0	1
CSNK2A2	0	0	0	1	0	0	0	1	1	0	0	0	0	0	1	0	1	0	1	1	0	1
ERC1	0	0	0	0	0	0	0	0	0	0	1	1	0	0	0	0	0	0	0	0	0	0
CARD10	0	0	0	0	0	0	0	0	0	0	0	0	0	0	0	0	0	0	0	0	0	0
IRAK1	0	0	0	0	0	0	0	0	0	0	0	0	0	0	0	0	0	0	0	0	0	0
LBP	1	1	1	1	0	0	0	1	1	0	1	1	1	1	1	1	1	0	1	1	0	1
LTA	1	1	1	0	0	0	0	1	1	0	1	1	1	1	1	1	0	0	0	1	0	0
LTBR	0	1	1	1	0	0	1	1	1	0	1	1	1	0	0	0	0	0	0	0	1	0
PLCG2	0	0	0	0	0	0	0	0	0	0	0	0	0	0	0	0	0	0	0	0	0	0
PRKCB	0	0	0	0	0	0	0	0	0	0	0	0	0	0	0	0	1	0	1	0	0	1
PRKCQ	0	0	0	0	0	0	0	0	0	0	0	0	0	0	0	0	1	0	1	0	0	1
PTGS2	0	1	0	1	0	0	0	1	1	0	0	0	1	0	1	1	1	0	1	1	0	1
BTK	1	1	1	1	0	0	0	1	1	0	1	1	1	1	1	1	1	0	1	1	0	1
TNF	0	0	1	0	0	0	0	0	0	0	0	0	0	0	0	0	0	0	0	0	0	0
TRAF1	0	1	0	0	0	0	0	0	1	0	0	0	1	0	0	1	0	0	0	1	0	0
TRAF3	0	0	0	1	0	0	0	0	0	0	0	0	0	0	0	0	0	0	0	0	0	0
TRAF5	0	0	0	0	0	0	0	0	0	0	0	0	0	0	0	0	0	0	0	0	0	0
TNFSF11	0	1	1	1	0	0	1	1	1	0	1	1	1	0	0	0	0	0	0	0	1	0
BCL10	0	0	1	1	0	0	1	0	1	0	1	1	0	0	1	0	1	0	1	0	1	1
CD14	0	0	0	0	0	0	0	0	0	0	0	0	0	0	0	0	1	0	1	0	0	1
CD40	0	0	0	1	0	0	0	0	0	0	0	0	0	0	0	0	0	0	0	0	0	0

Table 12: Implicant sets of exhaustive approach and heuristic approach. Identical implicant sets are highlighted in bold while supersets are depicted in blue.

network	set of implicants exhaustive approach	set of implicants heuristic approach
Azpeitia et al. 2013 [16]	k=7: **{SHR, SCR, JKD, MGP, miRNA165, Auxin, CLE}**, {SHR, JKD, MGP, miRNA165, Auxin, CLE, SYS}	k=7: **{SHR, Auxin, CLE, SCR, miRNA165, JKD, MGP}**
Brandon et al. 2015 [40]	k=3: {LIP, Iron, Superoxide}	k=4: {Iron, Superoxide, HapX, CccA}
Calzone et al. 2010 [52]	k=6: **{TNF, FADD, FASL, cIAP, ROS, NFkB}**, {TNF, FADD, FASL, cIAP, MPT, cFLIP}, {TNF, FADD, FASL, cIAP, MPT, CASP8}, {TNF, FADD, FASL, cIAP, MPT, NFkB}	k=6: **{TNF, FADD, FASL, NFkB, MPT, cIAP}**
Cohen et al. 2015 [71]	k=7: {DNAdamage, ECM, p73, p53, CTNNB1, SNAI1, p63}, {DNAdamage, ECM, p73, p53, CTNNB1, SNAI1, NICD}, {DNAdamage, ECM, p53, CTNNB1, TWIST1, miR34, NICD}, {DNAdamage, ECM, p53, CTNNB1, TWIST1, NICD, AKT2}, {DNAdamage, ECM, p53, CTNNB1, SNAI1, miR34, NICD}, {DNAdamage, ECM, p53, CTNNB1, SNAI1, miR200, NICD}, {DNAdamage, ECM, p53, CTNNB1, SNAI1, NICD, AKT2}	k=10: {DNAdamage, ECM, p53, TWIST1, NICD, CTNNB1, AKT1, miR203, TGFbeta, SNAI1}
Dahlhaus et al. 2016 [83]	k=6: {CentrosomeMat, AURKAActive, GSK3b, AJUBA, MTCanAct, STMNCanAct}, {SpindleAssembly, AURKAActive, GSK3b, AJUBA, MTCanAct, STMNCanAct}	k=7: {GSK3b, AJUBA, MTCanAct, STMNCanAct, Cytokinesis, AURKAActive, CentrosomeMat}
Davila-Velderrain et al. 2015 [85]	k=6: **{AG, AP1, AP3, LFY, WUS, UFO}**, {AG, AP3, EMF1, TFL1, WUS, UFO}, {AG, AP3, LFY, TFL1, WUS, UFO}	k=6: **{UFO, LFY, AG, WUS, AP1, AP3}**

Table 12: Implicant sets of exhaustive approach and heuristic approach. Identical implicant sets are highlighted in bold while supersets are depicted in blue.

network	set of implicants exhaustive approach	set of implicants heuristic approach
Enciso et al. 2016 [105]	k=5: {FoxO3aH, Gfi1H, Cx43M, lTLR, IL1}	k=6: {Cx43M, lTLR, IL1, Gfi1H, FoxO3aM, FoxO3aH}
Fauré et al. 2006 [112]	k=5: {CycD, Rb, CycA, p27, CycB}, **{CycD, CycE, CycA, p27, CycB}**	k=5: **{CycD, CycB, CycA, p27, CycE}**
Garciá - Gómez et al. 2017 [125]	k=4: **{MIR166, AUX, SHR, SCR}**, {PHB, AUX, SHR, SCR}	k=4: **{SHR, SCR, AUX, MIR166}**
Giacomantonio et al. 2010 [129]	k=1: **{Fgf8}**	k=1: **{Fgf8}**
Gupta et al. 2007 [144]	k=3: **{tyrosinehydroxylase, glutamate, dopamine}**, {tyrosinehydroxylase, glutamate, COMT},	k=3: **{tyrosinehydroxylase, dopamine, glutamate}**
Herrmann et al. 2012 [159]	k=3: {GATAs, Tbx5, exogenCanWntI}, {Nkx25, Tbx5, exogenCanWntI}	k=4: {exogenCanWntI, Tbx5, exogenBMP2I, Nkx25}
Irons 2009 [179]	k=5: {SMBF, Clb2, SFF, Cdc20, B}, {SMBF, Clb2, SFF, FEAR, B}, {SMBF, Clb2, SFF, Cdc14, B}, {SMBF, Clb2, SFF, B, M}, {SMBF, Clb2, SFF, B, CD}	k=8: {Clb2, SMBF, Cdc20, CKI, CD, S, B, SFF}
Klamt et al. 2006 [214]	k=4: {CD45, CD8, TCRlig, TCRbind}, {CD45, CD8, TCRlig, cCbl}, **{CD45, CD8, TCRlig, ZAP70}**, {CD45, CD8, TCRlig, Lck}, {CD45, CD8, TCRlig, PAGCsk}	k=4: **{CD45, CD8, TCRlig, ZAP70}**
Krumsiek et al. 2011 [220]	k=6: {GATA2, GATA1, EKLF, CEBPa, PU1, EgrNab}, {GATA2, GATA1, EKLF, CEBPa, PU1, Gfi1}, {GATA2, GATA1, Fli1, CEBPa, PU1, EgrNab}, **{GATA2, GATA1, Fli1, CEBPa, PU1, Gfi1}**	k=6: **{GATA1, Fli1, PU1, GATA2, CEBPa, Gfi1}**
MacLean et al. 2010 [262]	k=2: {GacSGacA, HrpRS}, **{GacSGacA, HrpL}**	k=2: **{GacSGacA, HrpL}**
Mai et 2009 [263]	k=5: {TNF, GF, IkB, Cas6, p53}, {TNF, GF, IkB, p53, Cas3}, {TNF, GF, Cas6, NFkB, p53}, {TNF, GF, NFkB, p53, Cas3}	k=6: {TNF, GF, p53, IkB, IAP, Cas3}
Marques-Pita et al. 2013 [268]	k=5: **{nWG, nhh, SLP, wg, PTC}**	k=5: **{nWG, nhh, SLP, PTC, wg}**
Martinez-Sanchez et al. 2015 [269]	k=9: **{TBET, IFNG, GATA3, IL2, IL4, IL21, FOXP3, TGFB, IL10}**	k=9: **{IL21, TGFB, IFNG, IL2, GATA3, IL10, TBET, IL4, FOXP3}**
Méndez et al. 2016 [276]	k=8: {CD40L, IL4, Ag, IL2, IL21,Irf4, Bcl6, Pax5}	k=9: {CD40L, IL4, Ag, IL2, IL21, Blimp1, Irf4, Pax5, Bcl6}
Méndez-López et al. 2017 [277]	k=2: {Snai2, p16}	k=3: {Snai2, ESE2, p16}
Mendoza et al. 2006 [278]	k=7: {IFNb, TCR, IL18, IL12, GATA3, Tbet, SOCS1}, {IFNb, TCR, IL18, IL12, GATA3, Tbet, STAT1}, **{IFNb, TCR, IL18, IL12, GATA3, Tbet, JAK1}**	k=7: **{IFNb, TCR, IL18, IL12, GATA3, Tbet, JAK1}**
Meyer et al. 2017 [280]	k=4: {NFkB, IRAK, IL6, AP1}, {NFkB, IRAK, ERK1/2, AP1}, {NFkB, IRAK, IL6, MKP1}, {NFkB, IRAK, ERK1/2, MKP1}	k=5: {NFkB, IRAK, IL6, cFOS, AP1}
Orlando et al. 2008 [310]	k=2: {MBF, SBF}, {MBF, YOX1}, **{SBF, CLN3}**, {YOX1, CLN3}	k=2: **{SBF, CLN3}**
Ortiz-Gutiérrez et al. 2015 [311]	k=4: **{SCF, RBR, E2Fa, MYB3R14}**, {RBR, E2Fa, E2Fc, MYB3R14}, {RBR, E2Fa, E2Fe, MYB3R14}, {RBR, E2Fa, MYB3R14, APCC}	k=4: **{RBR, E2Fa, MYB3R14, SCF}**
Ríos et al. 2015 [332]	k=6: {SRY, SOX9, UGR, GATA4, WNT4, RSPO1}, {SRY, WNT4, CTNNB1, UGR, SOX9, GATA4}, {SRY, SOX9, UGR, GATA4, RSPO1, CTNNB1}, {SRY, SOX9, UGR, NR5A1, WNT4, RSPO1},{SRY, WNT4, CTNNB1, UGR, SOX9, NR5A1}	k=7: {WNT4, SOX9, CTNNB1, UGR, GATA4, NR0B1, SRY}
Saadatpour et al. 2011 [346]	k=4: {Apoptosis, Ceramide, CTLA4, P2}, {Apoptosis, Ceramide, TCR, P2}, **{Apoptosis, S1P, TCR, P2}**, {Apoptosis, S1P, CTLA4, P2}	k=4: **{Apoptosis, TCR, S1P, P2}**
Sahin et al. 2009 [348]	k=2: **{IGF1R, EGF}**	k=2: **{EGF, IGF1R}**
Sankar et al. 2011 [354]	k=3: {AUXIAA, StimAux, StimBR}, **{AuxREs, StimAux, StimBR}**	k=3: **{StimAux, StimBR, AuxREs}**
Siegle et al. 2018 [387]	k=4: {Wnt, Rho, IGF, mTORC2}	k=6 {Wnt, IGF, GSK3b, Rho, IRS, mTORC2}
Sridharan et al. 2012 [400]	k=2: {Stress, ROS}, **{Stress, ARE}**	k=2: **{Stress, ARE}**
Sun et al. 2014 [409]	k=2: {pmar1, gcm}, {hesC, gcm}	k=3: {hesC, alx1, gcm}
Thakar et al. 2012 *B. bronchiseptica*[420]	k=5: {IgG, BC, IFNgI, PIC, Bb}, {IgG, BC, IFNgI, IL10I, Bb}	k=7: {Bb, DCI, BC, IgG, IgA, IL4II, MPI}
Todd et al. 2012 [425]	k=6: {SpindleCP, Size, BuddingCP, Start, Sic1, Clb2}	k=8: {SpindleCP, Size, BuddingCP, Start, Clb2, SMBF, Swi5, Sic1}
Yousefi et al. 2013 [488]	k=2: {RET1, MART1}	k=3: {MART1, WNT5A, RET1}

Table 13: Attractors for synchronous and asynchronous evaluation and attractors detected from implicant sets.

network	synchronous evaluation	asynchronous evaluation	implicant sets
Azpeitia et al. 2013 [16]	20x single-state, 4x two-states	20x single-state, 4x two-states	20x single-state, 4x two-states
Brandon et al. 2015 [40]	2x two-, 2x nine-states	not feasible	2x two-, 2x nine-states
Calzone et al. 2010 [52]	22x single-state, 14x two-, 6x four-, 12x eight-states	22x single-state	22x single-state
Cohen et al. 2015 [71]	9x single-state, 3x two-states, 3x four-states	9x single-state	9x single-state, 1x two-, 2x four-states
Dahlhaus et al. 2016 [83]	16x single-state, 36x three-states	16x single, 8x 112-, 8x 224-states	16x single-state, 16x three-states
Davila-Velderrain et al. 2015 [85]	10x single-state	10x single-state	10x single-state
Enciso et al. 2016 [105]	2x single-state, 4x two-states	2x single-state, 2x four-states	2x single-state, 2x two-states
Fauré et al. 2006 [112]	1x single-state, 1x seven-states	1x single, 1x 112-states	1x single, 1x seven-states
Garciá - Gómez et al. 2017 [125]	10x single-state, 4x two-states	10x single-state	10x single-state
Giacomantonio et al. 2010 [129]	2x single-state	2x single-state	2x single-state
Gupta et al. 2007 [144]	2x single-state, 2x four-states	2x single-state, 1x 2048-, 1x 15872-states	2x single-state, 2x four-states
Herrmann et al. 2012 [159]	3x single-state	3x single-state	3x single-state
Irons 2009 [179]	1x eleven-states	237600-states	1x eleven-states
Klamt et al. 2006 [214]	8x single-state, 1x six-states	8x single-state	8x single-state, 1x six-states
Krumsiek et al. 2011 [220]	6x single-state, 2x two-states	6x single-state	6x single-state, 2x two-states
MacLean et al. 2010 [262]	2x single-state	2x single-state	2x single-state
Mai et al. 2009 [263]	4x three-, 13x four-, 4x five-, 7x six-states	3x 32-, 2x 64-, 1x 4096-states	1x three-, 8x four-, 2x five-, 4x six-states
Marques-Pita et al. 2013 [268]	10x single-state	10x single-state	10x single-state
Martinez-Sanchez et al. 2015 [269]	13x single-state	13x single-state	13x single
Méndez et al. 2016 [276]	45x single-state	43x single-state	45x single-state
Méndez-López et al. 2017 [277]	3x single-state	3x single-state	3x single-state
Mendoza et al. 2006 [278]	33x single-state	32x single-state	33x single-state
Meyer et al. 2017 [280]	15x single-state, 2x three-, 2x nine-states	12x single-state, 1x 1408-, 1x 2854- states	15x single-state, 2x nine-states
Orlando et al. 2008 [310]	1x single-state, 1x five-states	1x single-state	1x single-state, 1x five-states
Ortiz-Gutiérrez et al. 2015 [311]	1x eleven-states	2x twelve, 1x 400-states, 1x 253696-states	1x eleven-states
Ríos et al. 2015 [332]	3x single-state	3x single-state	3x single-state
Saadatpour et al. 2011 [346]	1x single-state, 2x four-states	1x single-state, 2x four-states	1x single-state, 2x four-states
Sahin et al. 2009 [348]	3x single-state	3x single-state	3x single-state
Sankar et al. 2011 [354]	2x two-, 2x six-, 4x nine-, 1x 23-states	2x twelve-, 1x 400, 1x 253696-states	2x six-, 1x nine-, 1x twelve-states
Siegle et al. 2018 [387]	4x single-state, 1x three-states	4x single-state	4x single-state
Sridharan et al. 2012 [400]	1x single-state, 1x seven-states, 1x ten-states	1x single-state, 1x 262144-states	1x single-state, 1x ten-states
Sun et al. 2014 [409]	3x single-state, 2x two-states	3x single-state	3x single-state
Thakar et al. 2012 *B. bronchiseptica*[420]	3x single-state, 1x two-states	3x single-state	3x single-state
Todd et al. 2012 [425]	8x single-state, 4x two, 4x three-, 8x six-states	8x single, 1x 60-, 1x 108-, 1x 240-, 1x 432-, 1x 2304-, 1x 4352, 1x 9216-, 1x 17408-states	8x single-state, 4x two-, 8x six-states
Yousefi et al. 2013 [488]	4x single-state	4x single-state	4x single-state

Table 14: Comparison of available Boolean network models and Ordinary differential equation models.

Regulation	Analysed characeristics	Boolean network models	Ordinary differential equation models.
Gene regulation	Analysed networks	38	83
	Median nodes	18.5	16
	Median edges	50.5	20
	Maximal number of nodes	131	622
	Maximal number of edges	302	806
Signal transduction	Analysed networks	42	176
	Median nodes	42.5	24
	Median edges	100	23
	Maximal number of nodes	321	460
	Maximal number of edges	1100	850
Metabolism	Analysed networks	4	110
	Median nodes	20.5	34
	Median edges	35	29
	Maximal number of nodes	34	1748
	Maximal number of edges	43	1826
Wnt	Analysed networks	2	9
	Median nodes	19	53
	Median edges	45	62
	Maximal number of nodes	23	53
	Maximal number of edges	52	103

STATUTORY DECLARATION

I hereby declare that I wrote the present dissertation with the topic:
Modelling pathway crosstalk and dynamics with qualitative models
independently and used no other aids that those cited. In each individual case, I have clearly identified the source of the passages that are taken word for word or paraphrased from other works.
I also hereby declare that I have carried out my scientific work according to the principles of good scientific practice in accordance with the current „Satzung der Universität Ulm zur Sicherung guter wissenschaftlicher Praxis“ [Rules of the University of Ulm for Assuring Good Scientific Practice].

Ulm, 20.07.2020

Silke Daniela Kühlwein